NASA CONTRACT REPORT 154364

Ku-BAND MULTIPLE BEAM ANTENNA

(NASA-CR-154364) KU-BAND MULTIPLE BEAM ANTENNA Final Report (TRW Defense and Space Systems Group) 187 p HC A09/MF A01 CSCL 17B

N81-15180

Unclas
G3/32 29616

C.C. CHEN AND C.F. FRANKLIN

TRW
DEFENSE AND SPACE SYSTEMS GROUP

ONE SPACE PARK, REDONDO BEACH, CALIFORNIA 90278

CONTRACT NO. NAS1-14814
DECEMBER 1980

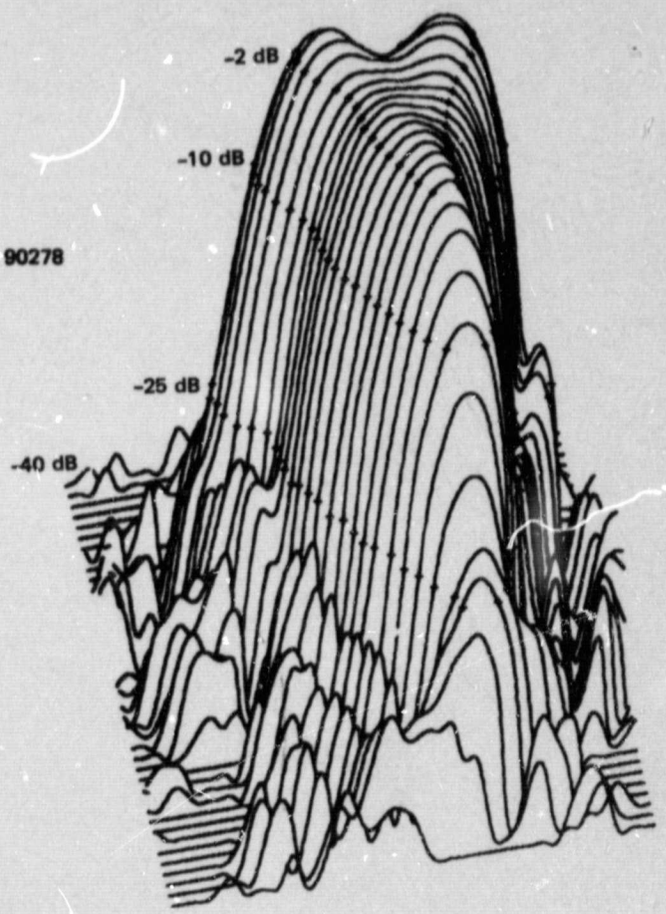

NASA
National Aeronautics and Space Administration

Langley Research Center
Hampton, Virginia 23665

NASA CONTRACT REPORT 154364

Ku-BAND MULTIPLE BEAM ANTENNA

C.C. CHEN AND C.F. FRANKLIN

TRW
DEFENSE AND SPACE SYSTEMS GROUP

ONE SPACE PARK, REDONDO BEACH, CALIFORNIA 90278

CONTRACT NO. NASI-14814
DECEMBER 1980

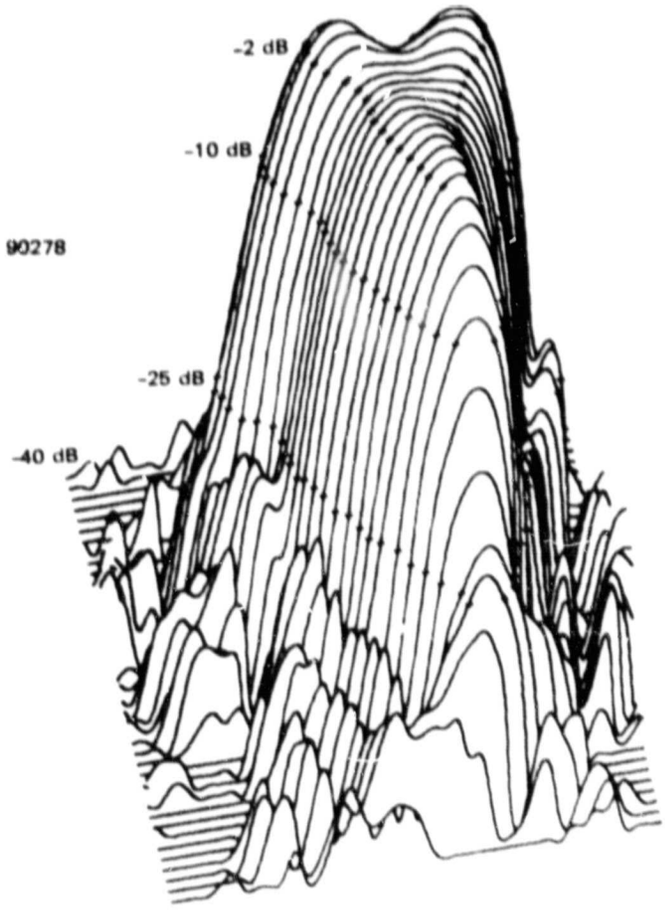

NASA
National Aeronautics and
Space Administration

Langley Research Center
Hampton, Virginia 23665

ACKNOWLEDGMENTS

This report describes the results of a Ku-Band Multiple Beam Antenna Study conducted by TRW Inc., Redondo Beach, California for NASA/LARC at Hampton, Virginia, under Contract NAS1-14914. The technical monitor for this program was Mr. W.F. Croswell. The program manager and principal investigators for this effort were C.C. Chen and J.W. Duncan.

The personnel participating in this program included:

C.F. Franklin
C.J. Frank
S.J. Hamada
R.P. Winnen
W.C. Wong
R.A. Young
L.J. McGuire

Many other individuals participated in obtaining the design and test data and their assistance is greatly appreciated.

CONTENTS

CONTENTS (Continued)

ILLUSTRATIONS

ILLUSTRATIONS (Continued)

ILLUSTRATIONS (Continued)

ILLUSTRATIONS (Continued)

ILLUSTRATIONS (Continued)

ILLUSTRATIONS (Continued)

ILLUSTRATIONS (Continued)

1. INTRODUCTION AND SUMMARY

The purpose of this study is to demonstrate the frequency reuse capability of a Ku-band multiple beam antenna which provides contiguous low sidelobe spot beams for point-to-point communications between any two points within the continental United States (CONUS), or regional coverage beams for direct broadcast systems. The study is divided into two parts. The first is to design, develop, and test a spot beam antenna in the 14/12 GHz band which provides contiguous overlapping beams covering CONUS, and two discrete beams covering Hawaii and Alaska. Two-reflector antennas are required for providing contiguous coverage of CONUS. Each is comprised of one offset parabolic reflector, one flat polarization diplexer, and two separate planar array feeds. This antenna system provides contiguous spot beam coverage of CONUS, utilizing 15 beams.

The second part of the study is to design, develop, and demonstrate a shaped contoured beam antenna system which provides contiguous four-time zone coverage of CONUS from a single offset parabolic reflector incorporating one flat polarization diplexer and two separate planar array feeds. The beams which illuminate the eastern time zone and the mountain time zone are horizontally polarized, while the beams which illuminate the central time zone and the pacific time zone are vertically polarized. Frequency reuse is achieved by amplitude and polarization isolation.

Section 2 deals with the spot beam antenna development. New design concepts in low sidelobe synthesis, cross-polarization suppression, and polarization diplexing for multiple beam feeds are presented in Sections 2.2. Implementation of the standarized nine-horn array feeds for providing contiguous coverage of CONUS, and separate Alaska and Hawaii beams is presented in Sections 2.3 and 2.4. Results of far field measurements follows in Section 2.5. All the design techniques are unique and represent the most advanced state-of-art technologies. Each spot beam is generated by a nine-horn array feed. All 17 spot beam feeds are physically identical. They are assembled by three basic standarized components: square horn, 3-way power divider, and 90 degree twist. The nine-horn array feed has

achieved -38 dB sidelobes when it is placed at the reflector focus compared with the -33 dB performance obtained from a corrugated feed in the past. In addition, the cross-polarization radiation of this nine-horn feed can be suppressed well below the noise level (-50 dB or more) by incorporating simple septum polarizers inside the radiating horns. The polarization diplexer improves the cross-polarization radiation and permits overlapping of two orthogonally polarized beams; one emerges from the vicinity of prime focus, while the other from the secondary focus located at the opposite side of the diplexer. Each spot beam feed can be operated from 11.7 to 14.5 GHz with a VSWR of less than 1.2:1 and insertion loss of less than 0.2 dB. The contiguous coverage of low sidelobe spot beam demonstrates that each spot beam can utilize one half the available frequency bandwidth.

Section 3 deals with the contoured beam antenna development. Selection of the reflector/feed geometries imposes constraints on the gain and sidelobe performance. An illustration of a step-by-step design procedure in determining the optimum reflector feed dimensions is given. Rosenbrock pattern search technique was employed to optimize the coverage gain and determine the amplitude and phase of a 25-element feed. The correlation between the measured and calculated results is excellent throughout the entire bandwidth. The 25 element array feed is a masterpiece of fine art which provides extremely low sidelobe contoured beams over a wide band of frequencies.

The design and development of this multiple beam antenna are aimed towards future applications for direct broadcast and point-to-point communications. The technology and hardware developed in this study can be applied directly or with slight modification to 30/20 GHz and even higher frequency communication antenna systems.

For point-to-point communications, the 14/12 GHz band provides several advantages which make it a natural extension of the present 6/4 GHz band for satellite use. Since the interference from terrestrial users is considerably less at 14/12 GHz, it is possible to locate earth terminals near metropolitan areas, thereby eliminating a large portion of the very costly ground links. The rain attenuation at 14/12 GHz, which is significant, can be accommodated through additional link margins, diversity techniques, multilevel power amplifiers, or variable data rates to provide acceptable

outage statistics. Another major advantage of the 14/12 GHz band is the narrower beam achievable from a given size reflector on a satellite. This eases the requirement for deploying large aperture spacecraft antennas to provide a limited coverage beam.

Dual-polarization operation can be implemented at 14/12 GHz in the manner now employed for satellites at 6/4 GHz in order to double the available bandwidth and satellite capacity, even though the rain depolarization effects are more severe. However, to properly exploit the capability of the 14/12 GHz band it is necessary to develop further techniques of frequency reuse through isolated multiple spot beams. These methods have the potential for increasing the utilization of the available bandwidth, and therefore the achievable satellite capacity, by an order of magnitude. This would allow the implementation of satellite designs which fully utilized the spectrum/orbit resources in the 14/12 GHz band before any extensive movement toward higher frequencies.

The development of both spot beam and contoured beam antennas has successfully demonstrated the system concepts set forth in the proposal and has achieved the expected design performance. A number of accomplishments in this program are significant, and represent the most advanced state-of-the-art in multiple beam antenna design. They are:

1) Low sidelobe synthesis. A -38 dB sidelobe design was accomplished by a nine-horn feed compared to the -33 dB state-of-the-art design using a corrugated horn.

2) Suppression of cross-polarized radiation. This is a new concept for eliminating the cross-polarization field components in an offset reflector configuration by a cluster of elliptically polarized feed elements. This new feed design will provide low sidelobes with nearly cross- polarization free radiation.

3) Polarization diplexer. The concept of using a wire grid subreflector as a polarization diplexer has been successfully verified. This diplexer not only improves the far field cross-polarization, but also serves as a means for overlapping the beams in the desired coverage area.

4) Contoured beam synthesis. A step-by-step contoured beam design procedure has been established. The implication of selecting the appropriate physical reflector/feed dimensions have been fully illustrated.

5) Contiguous coverage of spot or contoured beams. The system concepts for contiguous coverage of CONUS with either high gain spot beam or contoured beam have been fully demonstrated.

6) Broadband array feed design. The design and development of an extremely low sidelobe array feed operating from 11.5 to 15 GHz with VSWR of less than 1.2:1 has been fully proven. The measured gain contours are in excellent agreement with the theoretically calculated gain contours.

During the course of this study, it has been found that the measureable sidelobe level is limited by the reflector surface tolerance, radome curtain, and test environments including the reflector/feed supports. Since the beam isolation is extremely sensitive to both near-in as well as far-out sidelobe levels, the beam isolation measurements were seriously impaired by those limiting factors.

2. SPOT BEAM ANTENNA

2.1 OBJECTIVE

The primary objective of this Ku-band multiple beam antenna study is to design, develop, and test a brassboard antenna which provides multiple spot beams for contiguous coverage of CONUS, and two separate spot beams for Hawaii and Alaska. The contiguous coverage of CONUS with low sidelobe spot beams maximizes the frequency reuse and represents the most difficult task in the multiple beam antenna design. The success of this design implies that there should be no difficulties in providing point-to-point communications between any two points within CONUS.

The specific tasks to be performed in the spot beam study were

1) Design, develop, and test a 14/12 GHz multiple beam antenna which provides contiguous coverage of CONUS with low sidelobe spot beams, and also provides two separate beams for Alaska and Hawaii.

2) Maximize frequency reuse via a combination of frequency plan, polarization orthogonality, and spatial isolation through low sidelobe beams.

3) Build and test a brassboard model antenna to:

   a) Prove the design concept for providing contiguous spot beam coverage

   b) Evaluate the antenna performance characteristics

   c) Establish achievable gain, bandwidth, and beam isolation

   d) Determine the key technology and the key elements of antenna hardware

   e) Prove feasibility of a flight model antenna.

The performance goals for an experimental 14/12 GHz communication link system for the contiguous coverage of CONUS were agreed upon between TRW and NASA Langley Research Laboratory, based on cost and complexity considerations. These are listed in Figure 2.1-1. The performance requirements for the CONUS spot beam antenna are intended primarily for the breadboard demonstration of the design concept only, not for a fully operational system.

FREQUENCY	11.7 TO 12.2 GHZ FOR DOWNLINK 14.0 TO 14.5 GHZ FOR UPLINK
POLARIZATION	ORTHOGONAL LINEAR
COVERAGE	CONTIGUOUS CONUS, ALASKA AND HAWAII
NUMBER OF BEAMS	ABOUT 25 BEAMS
BEAM ISOLATION	28 DB BETWEEN ANY TWO BEAMS
BEAM EFFICIENCY	≥ 90 PERCENT WITHIN 2.8 TIMES HALF POWER BEAMWIDTH IN THE MAIN BEAM
SIDELOBE LEVEL	≥ 32 DB BELOW BEAM PEAK
CROSS POLARIZATION	≥ 28 DB BELOW PRINCIPAL POLARIZATION LEVEL
BEAM CROSS-OVER LEVEL	≤7 DB BELOW MAIN BEAM PEAK FOR DOWNLINK ≤9 DB FOR UPLINK
FEED CIRCUIT LOSS	≤ 0.30 DB
INPUT VSWR	≤ 1.2:1
REFLECTOR DIAMETER	200 CM APPROXIMATELY
POWER HANDLING CAPACITY	100 WATTS AVERAGE POWER

Figure 2.1-1. Spot Beam Antenna Design Specifications

2.2 DESIGN ANALYSIS

This section defines the system configuration and addresses problems and solutions to meet the expected requirements by using offset reflector antennas. Detailed analysis is performed to determine the optimum reflector/feed configuration, gain, sidelobes, beam cross-over level, and beam isolation.

2.2.1 System Design Concept

The analytical study of CONUS coverage with contiguous spot beams is performed assuming a geosynchronous satellite position of 98 degrees west longitude. A map projection of the United States as viewed from the satellite is used to study the spot beam coverage. An offset reflector antenna with a projected aperture diameter of approximately 200 cm was chosen in the early phase of the study because of the availability at TRW of a paraboloid mold with focal length of 249 cm. The half-power beamwidth of a single spot beam is about 1 degree at the frequency of 11.95 GHz. Since the CONUS coverage as viewed from a synchronous orbit extends approximately over a 3 x 6 degree field of view, superposition of a 1 degree beam on the CONUS coverage map indicates that a total of 15 beams is adequate to

achieve full CONUS coverage. A -6 dB contoured beam map is illustrated in Figure 2.2-1. The beams in the center row are elongated to reduce the beam crossover level. Accordingly, the peak gain of these elliptical beams will be slightly lower than the circular beams, but this will significantly improve coverage gain in the vicinity of three beam crossover.

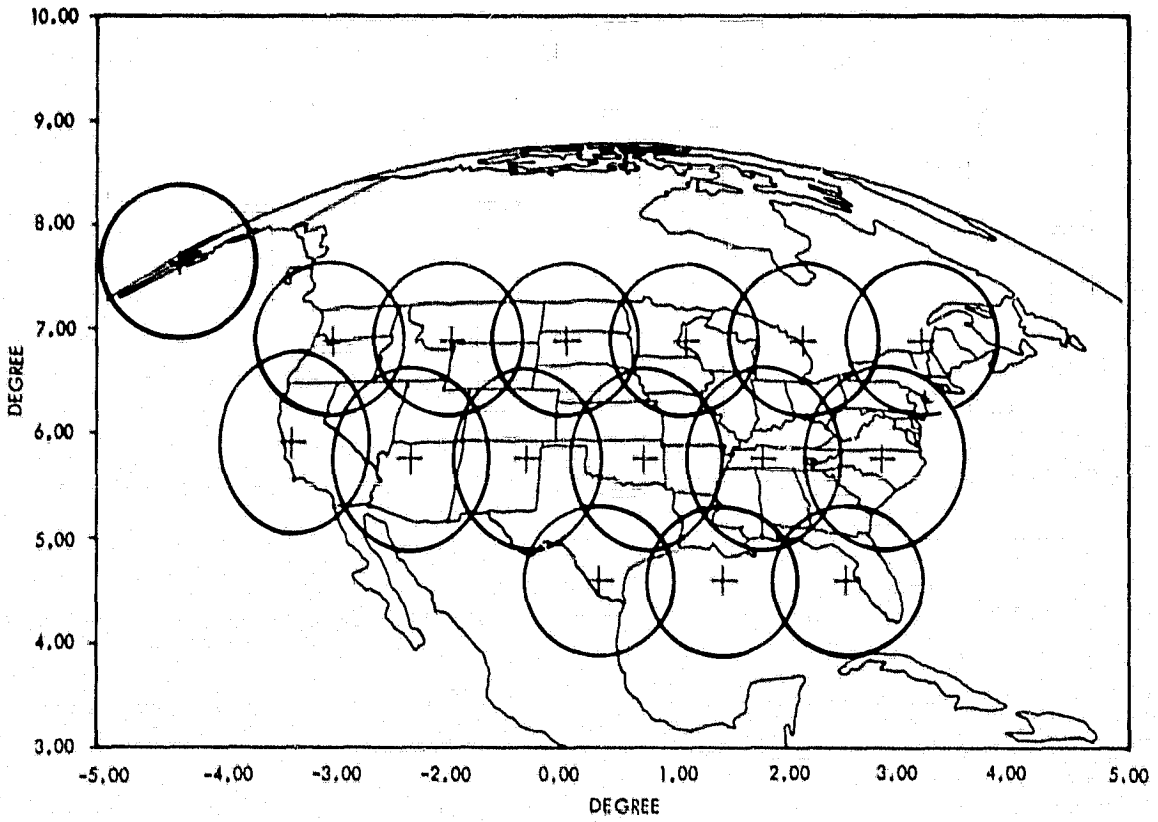

Figure 2.2-1. Contiguous Spot Beam Antenna Coverage of CONUS (-6 dB Contour)

The communication link capacity of a synchronous satellite which provides contiguous spot beam coverage over CONUS can be maximized by a combination of frequency separation, polarization orthogonality, and spatial isolation of low sidelobe beams.

An arrangement of contiguous low sidelobe beams with alternate frequency or polarization for maximal frequency reuse is shown in Figure 2.2-2. Both uplink and downlink frequency bands are subdivided into even or odd channels within the allocated frequency band. All beams in the same

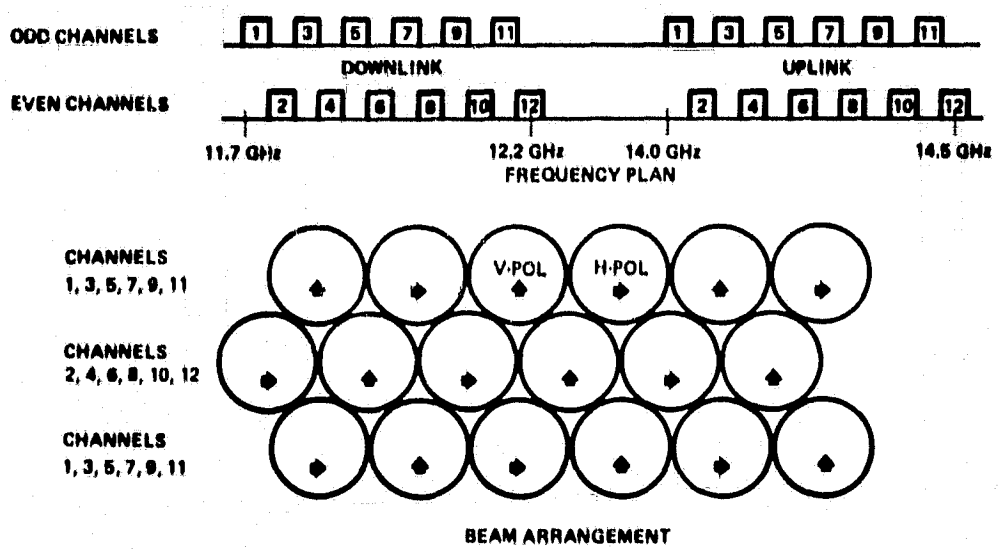

Figure 2.2-2. Frequency and Polarization Allocation for Contiguous Spot Beam Coverage

row transmit either even or odd frequency channels. Beams in the adjacent rows are isolated by frequency separation. Beams of one polarization in a row are interlaced with beams of the orthogonal polarization. Therefore, each beam is isolated from all the adjacent beams by either polarization orthogonality or frequency separation. All the co-polarization, co-channel beams are spaced approximately two beamwidths apart. Isolation between these co-polarized, co-channel beams is accomplished by sidelobe control. As a result, each beam can utilize one-half the available bandwidth for both uplink and downlink communications. This means that the same frequency spectrum can be reused for every other beam in a high capacity communication system.

The main concerns in antenna design for providing this type of coverage are:

1) Total number of antennas required for providing contiguous beam coverage and the complexity of each antenna

2) Gain variation within each spot beam coverage area, or gain in the vicinity of the common crossover point of three-beam clusters

3) Beam-to-beam isolation between co-polarized beams and orthogonally polarized beams in the low gain area

4) Total number of beams required to cover CONUS and the growth potential for more users and more traffic.

Contiguous spot beams having -3 dB crossover can be obtained by a single offset reflector, or lens, with multiple feeds at the expense of approximately 3 dB spillover loss and -17 dB sidelobes. Sidelobe levels can be improved by increasing the feed diameter resulting in higher taper illumination of the reflector aperture and lower sidelobes. However, increasing the size of the feed results in increased spacing between two adjacent beams. For a -35 dB sidelobe design, the beam spacing approaches two beamwidths, even if the multiple feed elements are closely packed in the focal plane of an offset reflector. As a result, four conventional offset reflectors or lenses would be required for providing contiguous spot beam coverage. During this study, however, a new concept was developed which utilizes a wire grid subreflector as a polarization diplexer in an offset reflector to combine or separate two orthogonally polarized signals. With this concept, the contiguous beam coverage was accomplished by only two reflectors.

2.2.2 Offset Reflector Antenna Analysis

The geometry of an offset parabolic reflector antenna is shown in Figure 2.2-3. The basic reflector parameters are: focal length F, projected

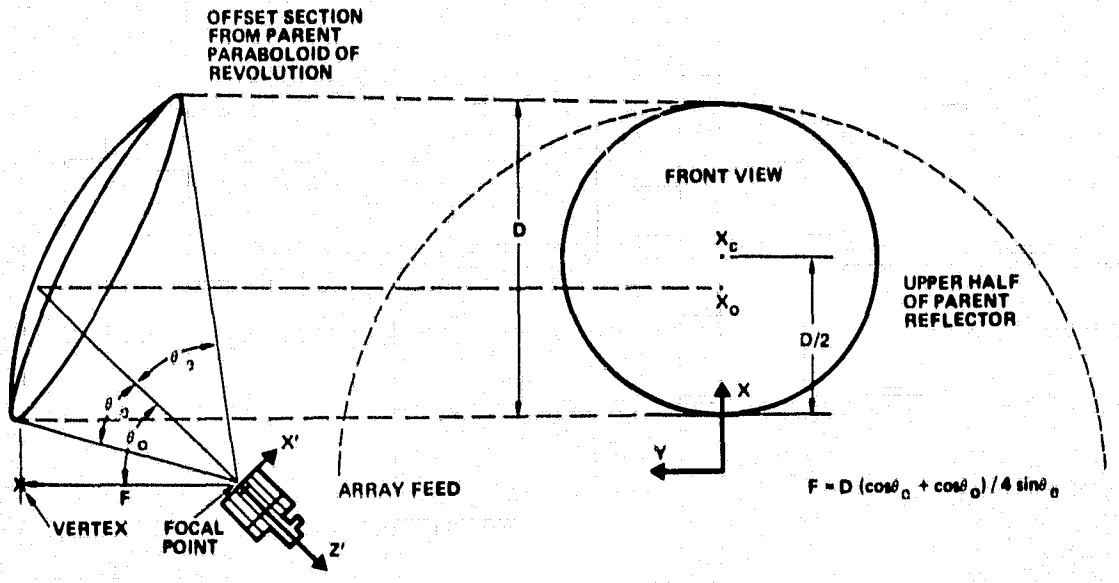

Figure 2.2-3. Geometry of the Offset Reflector with Array Feed

aperture diameter D, feed offset angle θ_o, and half of the reflector subtended angle θ_e. The intersection of a circular cone with a half cone angle of θ_e around the array feed axis, and a parent paraboloid with focal length F, define the boundary of an offset reflector. This offset reflector is an ellipse but the projected aperture on a plane perpendicular to the paraboloid axis is circular. The disadvantages of an offset reflector configuration are; asymmetric reflector/feed geometry, limited scanning capability, and cross-polarized radiation. The advantage is that there is no aperture blockage. The avoidance of aperture blockage as well as scattering from the reflector/feed supporting structure is essential for extremely low sidelobe applications.

The asymmetric reflector feed configuration occupies more space and is more difficult to install on a spacecraft than the symmetrical configuration. In some cases, however, it could turn out to be an advantage for a three-axis stabilized spacecraft if two offset reflectors are symmetrically mounted on the opposite sides of the spacecraft in a clam shell type configuration as shown in Figure 2.2-4 before being deployed into the on-orbit configuration. This configuration permits the feed assembly to be placed close to the spacecraft platform, thus reduces the loss in waveguide run to the feed. The off-axis scan capability is mainly limited by the coma lobes which are caused by the phase aberration due to the displacement of the feed in the plane of scan. This phase aberration depends upon the focal length to projected aperture diameter ratio and the reflector offset angle. These undesirable coma lobes or sidelobe lobes can be suppressed by using multi-element feed techniques. In addition, in case of dual linear polarization operation, the cross-polarized radiation due to asymmetric reflector surface imposes limitations on the frequency reuse. Fortunately this cross-polarization problem also can be resolved by using either a multi-element polarization compensated feed or a polarization grid subreflector. All the problems associated with an offset reflector antenna will be resolved in the following subsections.

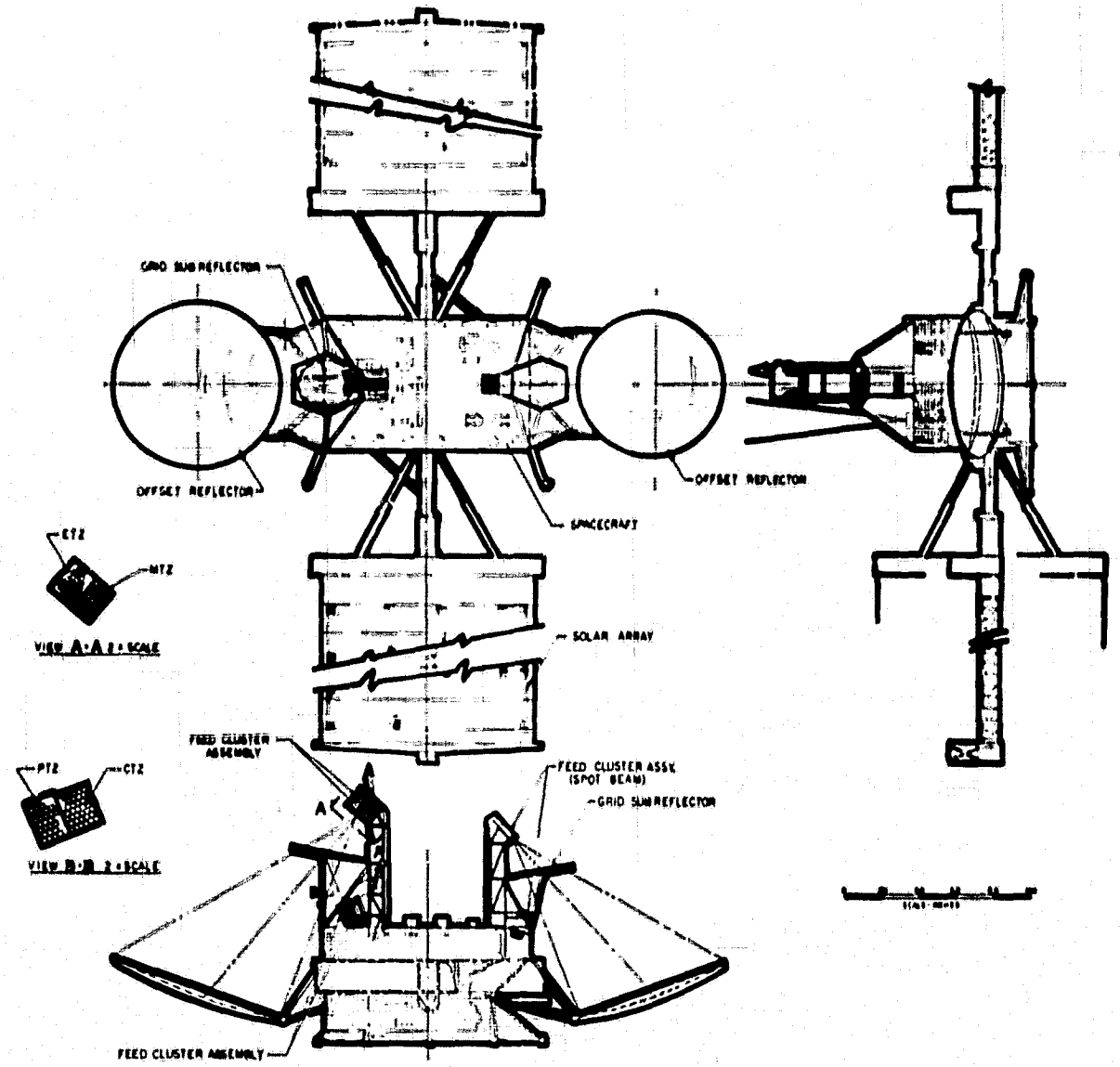

Figure 2.2-4. Conceptual Satellite Configuration

The computer software used in evaluating the far field radiation pattern characteristics of an offset reflector is based on the vector Kirchhoff theory of physical optics in which the scattered field E_s from the reflector is given by

$$\bar{E}_s(\theta,\phi) = -\frac{j}{4\pi\mu\varepsilon}\int_s \left[(\bar{K}\cdot\nabla)\,\nabla + k^2\,\bar{K}\right]\frac{e^{-jkR}}{R}\,ds \qquad (2.1)$$

and

$$\bar{K} = \sum_{n=1}^{N} (2\hat{n} \times \bar{H}_n) \tag{2.2}$$

$$\bar{H}_n = \sqrt{\frac{\epsilon}{\mu}}\ \hat{k} \times \bar{E}_n \tag{2.3}$$

where $\bar{K}$ is the surface current induced on the reflector, $\bar{E}_n$ and $\bar{H}_n$ are the incident fields emerging from the nth feed horn and $\hat{n}$ and $\hat{R}$ are the unit vectors associated with the normal of the local reflecting surface and the direction of wave propagation.

The incident field from the n^{th} horn is assumed to have an arbitrary amplitude, phase, and polarization described by

$$\bar{E}_n(\rho,\theta',\phi') = \frac{e^{-jk\rho}}{\rho} \left\{ \sum_{m=0}^{M'} \left[A_m(\theta') \sin m\phi' + B_m(\theta') \cos m\phi' \right] \hat{\theta}' + \sum_{m=0}^{M'} \left[C_m(\theta') \sin m\phi' + D_m(\theta') \cos m\phi' \right] \hat{\phi}' \right\} \tag{2.4}$$

where ρ is the distance from the nth feed to the reflector surface, (θ',ϕ') are the spherical coordinates of the tilted array feed and A_m, B_m, C_m, and D_m are the Fourier expansion coefficients of the nth feed at a discrete set of ϕ' angles. These coefficients can be obtained from either measured data or calculated patterns. Substituting equations (2.2) through (2.4) into (2.1), the final scattered field E_s obtained by W. Wong[1] is again expressed in terms of Fourier coefficients F_m, G_m, H_m, and K_m

$$E_s(\theta,\phi) = E_\theta \hat{\theta} + E_\phi \hat{\phi}$$

$$= \sum_{m=0}^{M} \left[F_m(\theta) \sin m\phi + G_m(\theta) \cos m\phi \right] \hat{\theta}$$

$$+ \sum_{m=0}^{M} \left[H_m(\theta) \sin m\phi + K_m(\theta) \cos m\phi \right] \hat{\phi} \tag{2.5}$$

The principal polarization and cross-polarization of the far zone radiated field are defined by the two orthogonal field components tangent to a spherical surface

$$E_p = \frac{-E_\theta \cos\phi \cos\theta + E_\phi \sin\phi}{1 - \sin^2\theta \cos^2\phi} \qquad (2.6)$$

$$E_c = \frac{-E_\theta \sin\phi - E_\phi \cos\theta \cos\phi}{1 - \sin^2\theta \cos^2\phi} \qquad (2.7)$$

Since the earth's field of view as seen from synchronous orbit is typically less than 9 degrees in radius, equations (2.6) and (2.7) may be approximated by the components actually measured on the antenna range. This is equivalent to

$$E_p = -E_\theta \cos\phi + E_\phi \sin\phi \qquad (2.8)$$

$$E_c = -E_\theta \sin\phi - E_\phi \cos\phi \qquad (2.9)$$

The OFFSET computer code based on the above equations has been experimentally validated in the past. It is extremely accurate not only in the main beam region, but also in the far sidelobe region as well.

2.2.3 Low Sidelobe Pattern Synthesis

The far field radiation pattern of an offset reflector can be predicted accurately because the radiating aperture is free from feed blockage. The sidelobe level of these reflector antennas depends strongly on the feed illumination on the reflector surface.

Two types of feed are commonly used for low sidelobe applications: the corrugated conical horn and the dual-mode conical horn. Both of these horns will provide low sidelobe rotationally symmetrical primary patterns around the feed axis. They have been used for high efficiency as well as for low sidelobes. A -33 dB sidelobe with 70 percent aperture efficiency at 30 GHz has been reported by Rudge.[2] However, when these feeds are

displaced from the focal point to scan a beam more than four beamwidths away from the reflector boresight, both gain and sidelobe performance degrade rapidly because of the lack of amplitude and phase control in a single feed aperture. To resolve this problem, a multihorn array feed is used to synthesize a low sidelobe pattern. The most commonly used array feed configurations are the seven-horn cluster and the nine-horn cluster. The feeds may be circular or square in shape, depending on the feed network, feed size, and the primary pattern characteristics.

The techniques used to synthesize a low sidelobe spot beam or contoured beam in an offset reflector configuration with a cluster of feeds are of interest to most antenna engineers, particulary for an off-axis scanned beam. Unfortunately, most of the synthesis techniques use numerical optimization of the relative amplitude and phase of each element in the feed cluster and provide very little physical insight to the resulting antenna performance. Since suppression of sidelobes at some angles may result in spurious lobes at some other angles, it is better to examine the radiation mechanism of this feed cluster thoroughly before proceeding to design an antenna.

The pattern synthesis of a three-element array feed in an offset reflector is illustrated in Figure 2.2-5. The feed horns, in general, may be laterally displaced from the focal point in the azimuth plane. They are adjacent to each other. Assume that mutual coupling between these horns is negligible. Each horn generates a secondary radiation pattern with high coma lobes in the plane of displacement. Note that (1) the sidelobe structures of all three horns are similar, (2) three main beams are roughly separated by one beamwidth (3) the first and third inner sidelobes of the two edge horns are approximately out of phase with the second inner sidelobe of the center horn, and (4) superposition of these three patterns would result in an extremely low sidelobe composite pattern when the amplitude of the two edge horns is reduced by -8 dB relative to the amplitude excitation of the center horn. Nearly perfect sidelobe cancellation occurs when the feed parameters are properly chosen. This sidelobe cancellation scheme applies not only to a one-dimensional array feed but also to a two-dimensional array feed for a spot beam as well as contoured beam design.

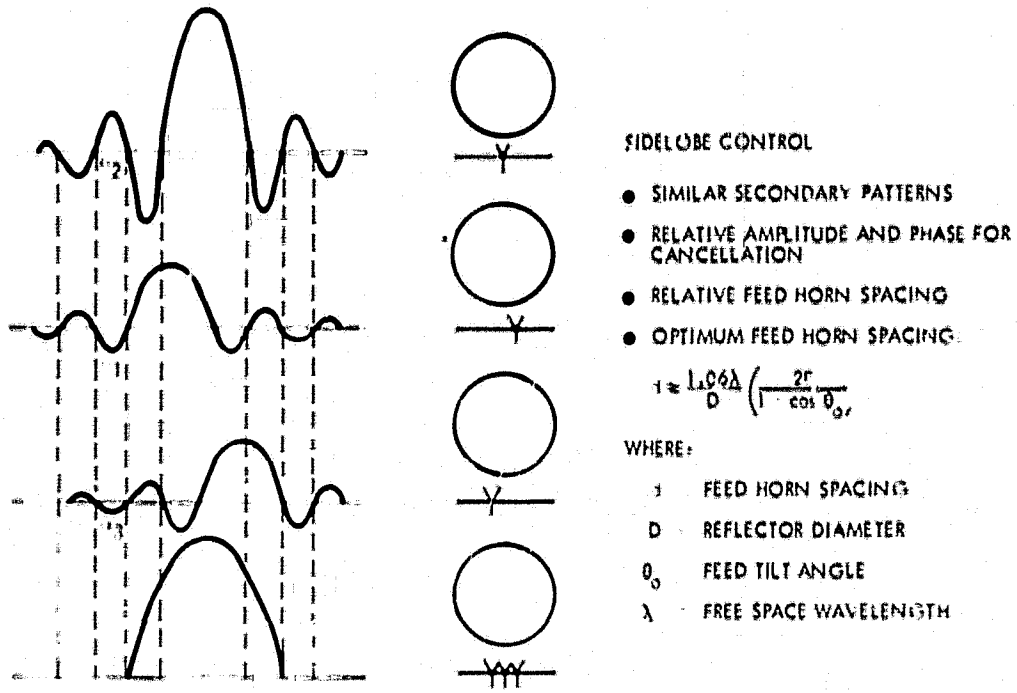

Figure 2.2-5. Sidelobe Cancellation Technique

The most important factors in obtaining a low sidelobe beam are:

- Similarity in individual secondary radiation patterns
- Relative spacing between feed horns
- Relative amplitude and phase of the feeds.

All three factors are essential in sidelobe cancellation.

Pattern similarity can be met easily as long as the feed horns are identical and adjacent to each other. Spacing between the feed horns is dependent on the reflector geometry such as reflector focal length F, projected reflector aperture diameter D, and reflector offset angle θ_o. The spacing can be determined approximately by

$$d = \frac{1.06\lambda}{D} \cdot \left(\frac{2F}{1 + \cos\theta_o}\right) \qquad (2.10)$$

where λ is the free space wavelength or, more precisely, by aligment of the individual secondary patterns as shown in Figure 2.2-5 for cancellation in the sidelobe region. The desired amplitude and phase of a multielement

array feed can be provided by the feed network. The phase variable can be eliminated if the feed position in the offset configuration is properly chosen. Particularly in broadband operation, it is desirable to have a co-phasal output at the feed aperture. This can be accomplished by placing the feed aperture in the offset reflector focal plane (a plane passing through the focal point and perpendicular to the offset feed axis).

Assume the amplitude of the center horn is normalized to unity. It would seem that the amplitude of one of the edge horns could be arbitrary as long as the amplitude of the horn on the opposite side is selected so that the summation of the first and third sidelobes of these two edge horns is equal in amplitude and out of phase with the second sidelobe of the center horn. However, this arbitrary amplitude selection of one edge horn would result in cancellation of sidelobes on one side of the main beam while sidelobes on the opposite side of the main beam could remain. In order to suppress sidelobes on both sides of the main beam so that the array feed has a symmetrical amplitude distribution with respect to the center horn, the amplitude ratio x, of these two edge horns must be approximated by

$$x = \frac{a_2}{a_1 + a_3} \tag{2.11}$$

where a_1, a_2, and a_3 are the amplitude coefficients of the first, second, and third sidelobes of the three consecutive horns.

The foregoing principle of sidelobe cancellation can be extended to the case of a two-dimensional array feed such as the seven-horn and the nine-horn. In this study, a nine-horn array of square pyramidal horns were chosen because of the fabrication simplicity for a linearly polarized feed.

2.2.4 Spot Beam Reflector Feed Configuration

An offset parabolic reflector with 2 meter projected aperture diameter was selected for the optimization analysis. This reflector can be fabricated from an existing Intelsat V reflector mold which has a focal length of 249.02 cm. The geometry of this reflector antenna is shown in Figure 2.2-6. The lower edge of the reflector is about 91.44 cm above the vertex

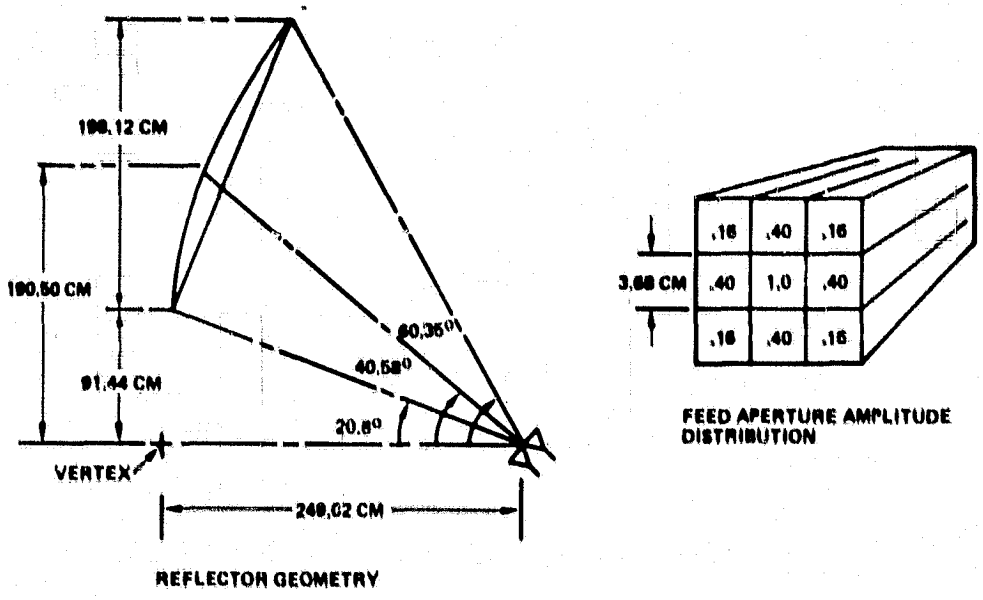

Figure 2.2-6. CONUS Spot Beam Antenna Configuration

of the parent reflector. This avoids possible blockage from polarization grid which may be inserted later in between the feed and the offset reflector. A nine-horn feed cluster is employed to provide a low sidelobe beam near the reflector boresight as well as for the east and west coast beams. The principle of sidelobe cancellation is used to determine the optimum spacing between the feed horns from the approximate Equation (2.10) the spacing is equal to 3.81 cm. The half-power beamwidth of a square pyramidal horn is approximately 35.0 degrees in the E-plane and 49.5 degrees in the H-plane at 11.95 GHz. Therefore, a theoretical primary horn pattern of the form

$$\bar{E} = \hat{\theta} \cos^{7.3}(\pi-\theta) \cos\phi + \hat{\phi} \cos^{3.6}(\pi-\theta) \sin\phi \qquad (2.12)$$

is used in the analysis. Figures 2.2-7a and b illustrate the secondary pattern of three adjacent horns equally spaced with the center horn displaced 11.43 cm off the focal point in the azimuth plane. All the sidelobes are almost coincident to each other at 3.81 cm spacing between feed horns. If an amplitude distribution of 0.4, 1.0, 0.4 as determined by Equation (2.11) is applied to the three-element array feed, an extremely low sidelobe pattern is obtained. In principle, a 40 dB sidelobe pencil

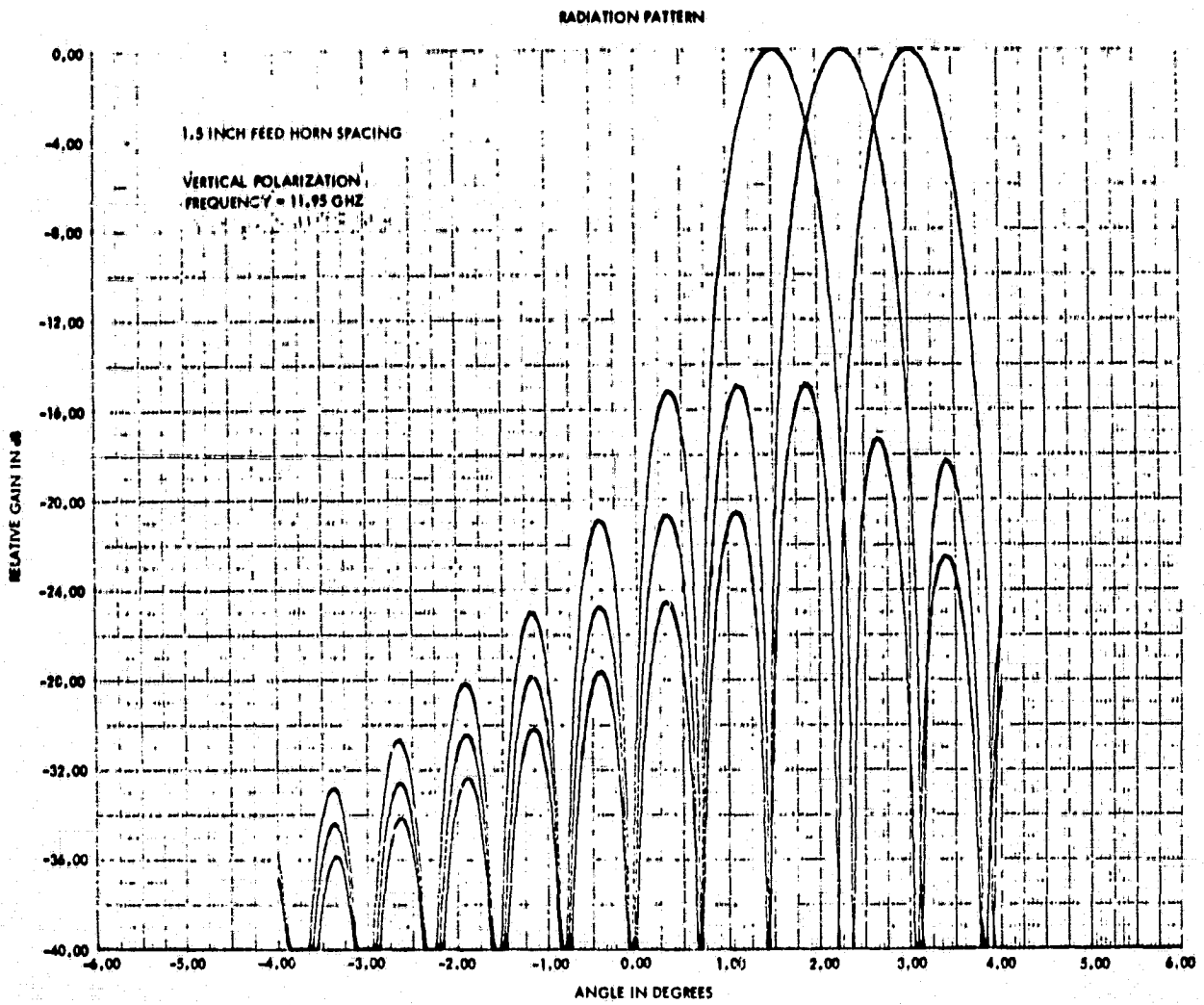

Figure 2.2-7a. Far Field Patterns of Three Adjacent Feeds Laterally Displaced from the Focal Point

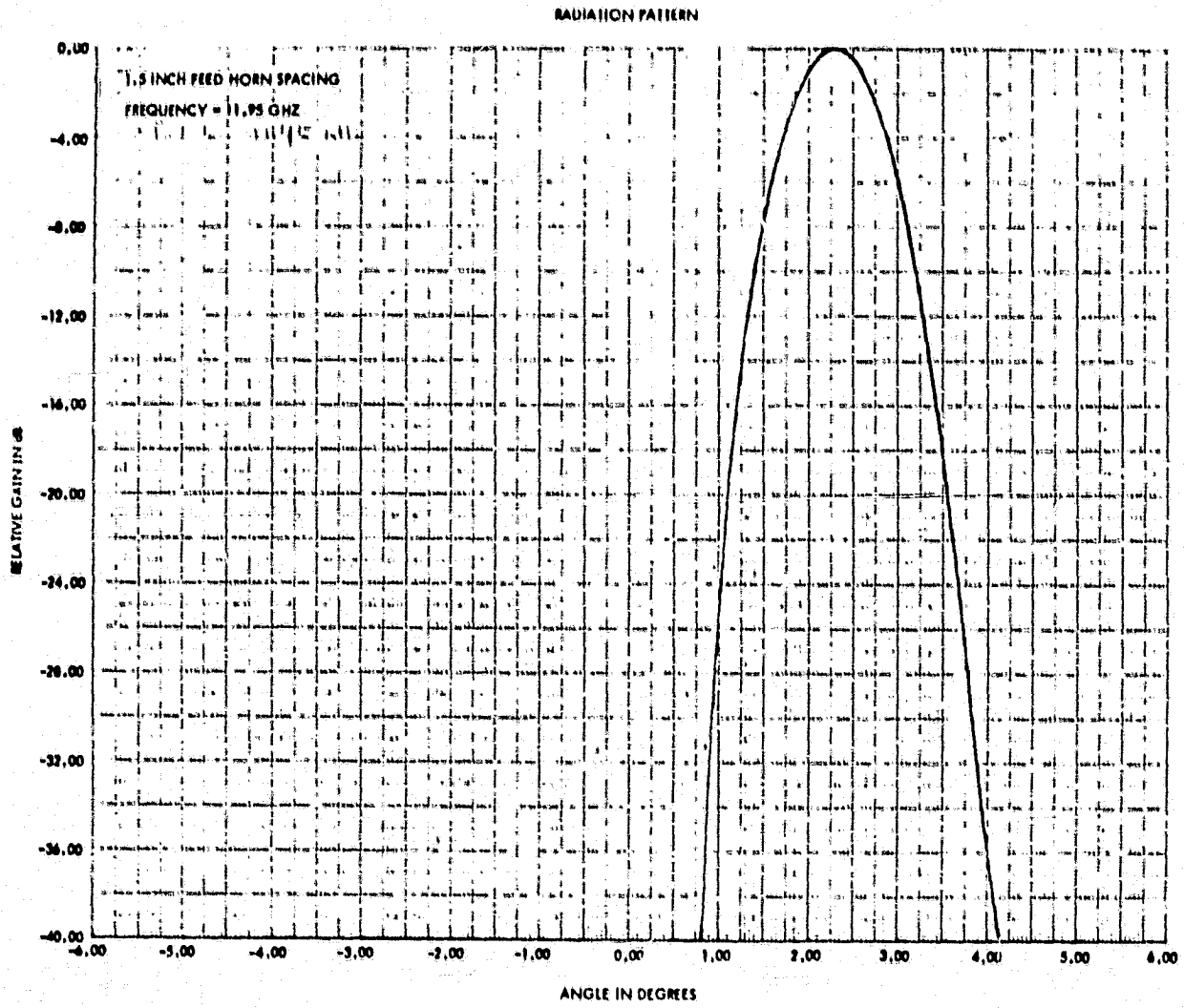

Figure 2.2-7b. Far Field Pattern of a 9-Horn Feed Cluster (3.81 cm Feed Horn Spacing)

beam can be achieved with a perfect reflector surface. However, the actual sidelobe level is always limited by the reflector surface roughness and the test environment, including scattering from the antenna range and reflector support.

The nine-horn array feed was designed to operate in both the uplink and downlink frequency bands. As a compromise, and to emphasise the downlink sidelobe performance, a 3.68 cm spacing between the feed horn was chosen for development instead of the 3.81 cm optimum spacing at 11.95 GHz. Further, reduction of this spacing would degrade the sidelobe performance of an off-axis beam at 11.7 GHz. For the rest of this section, the 3.68 cm square horn is used in the analysis.

Figures 2.2-8a and b shows the principal and cross-polarization gain contours of the nine-horn array feed. Figure 2.2-9 shows a typical off-axis scan beam. It is noted that a sidelobe above -40 dB appears in the azimuth plane which is due to the imperfect sidelobe cancellation resulting from the reduction of horn spacing from 3.81 cm to 3.68 cm. Figure 2.2-10 shows a sequence of scanned beams in the azimuth plane. The co-polarized beams are generated by an array of multiple nine-horn feeds. The orthogonally polarized beams are generated by a separate antenna or by another set of nine-horn feeds with a polarization grid subreflector placed between the prime focus and the reflector. The crossover point between two orthogonally polarized beams is about 3.5 dB below the main beam peaks. Figure 2.2-11 shows the loss in gain as a function of scanned angle off the reflector boresight.

The cross-polarized radiation level of an offset reflector depends largely on the focal length to projected reflector diameter ratio F/D, and the reflector offset angle θ_o. For the reflector configuration shown in Figure 2.2-6, the peak cross-polarization is about 29.8 dB below the main beam in the azimuth plane (ϕ = 90 degree plane). The principal and cross-polarization patterns of three adjacent co-polarized beams in the azimuth plane are shown in Figure 2.2-12. Also, the principal and cross-polarization pattern of a boresight beam in the ϕ = 45 degree plane is shown in Figure 2.2-13. It is noted that the cross-polarization level of a typical beam is about -26.3 dB below the principal polarization signal at the -3.5 dB beam crossover point between two adjacent beams in a row, and

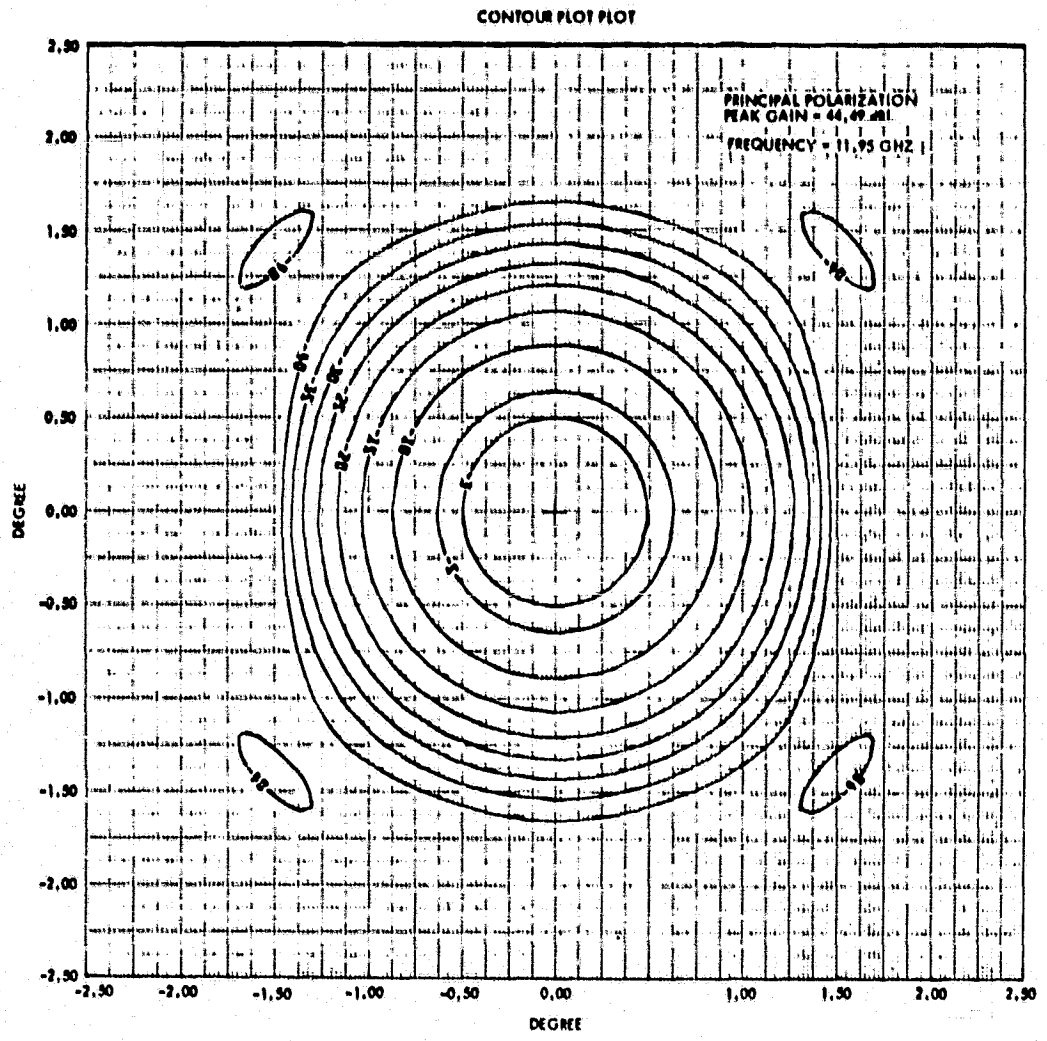

Figure 2.2-8a. Principal Polarization Contour of a Boresight Beam — 11.95 GHz

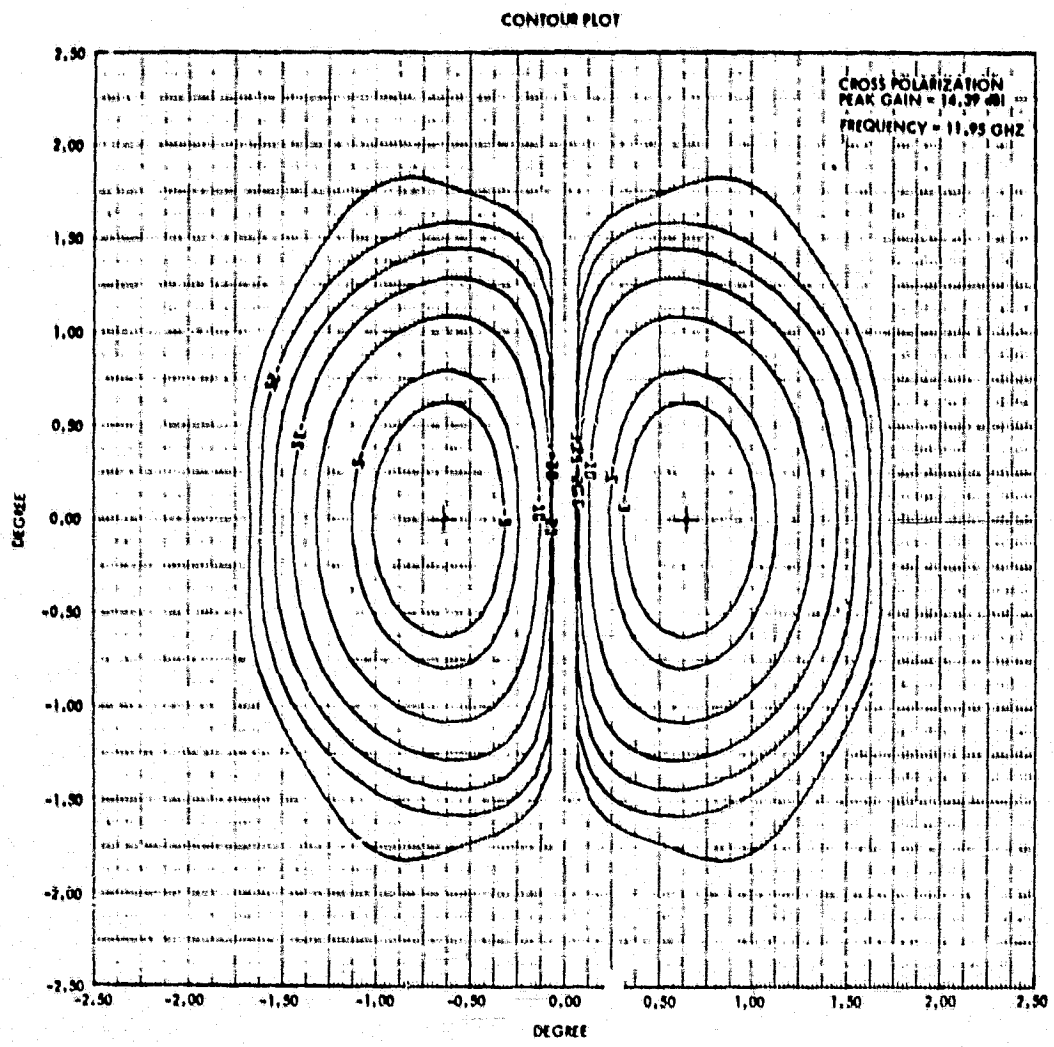

Figure 2.2-8b. Cross-Polarization Contour of a Boresight Beam — 11.95 GHz

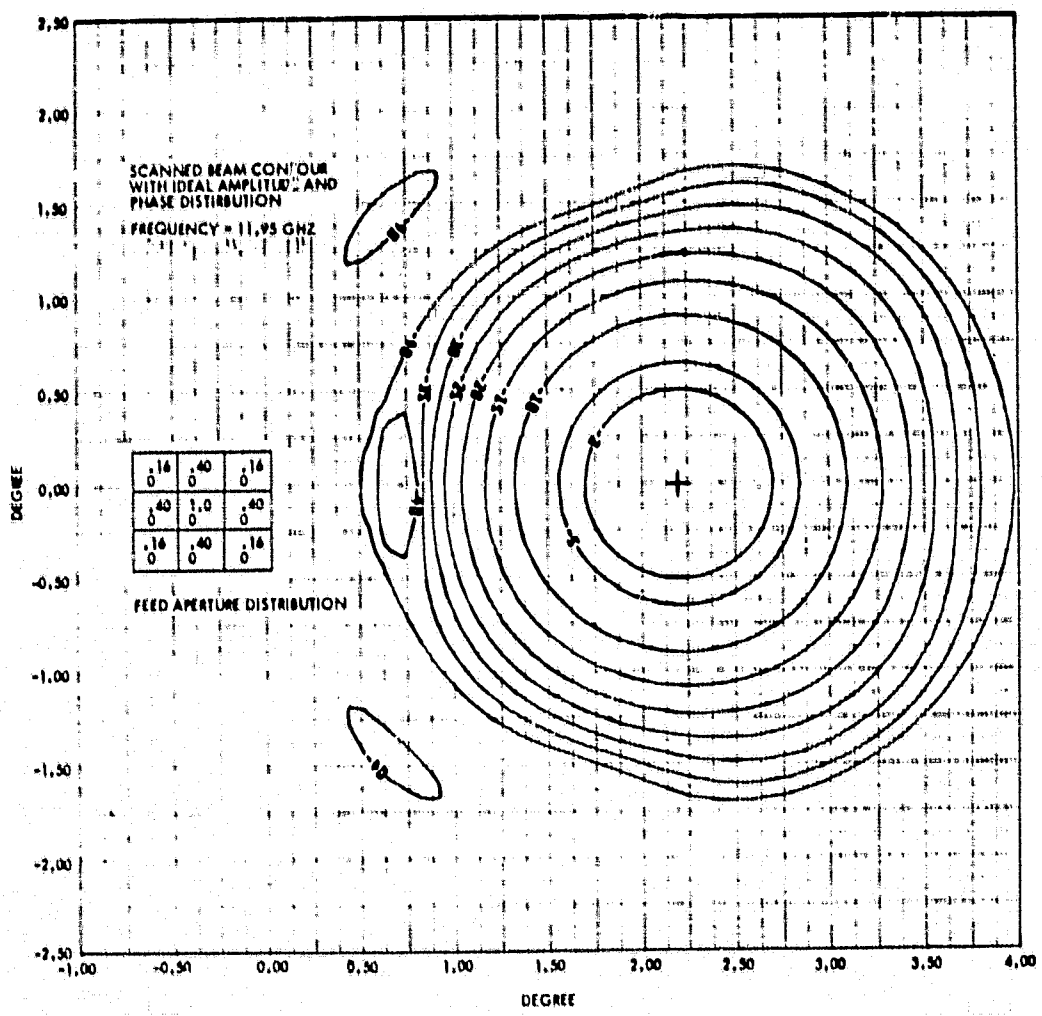

Figure 2.2-9. Typical Off-Axis Beam Contour — 11.95 GHz

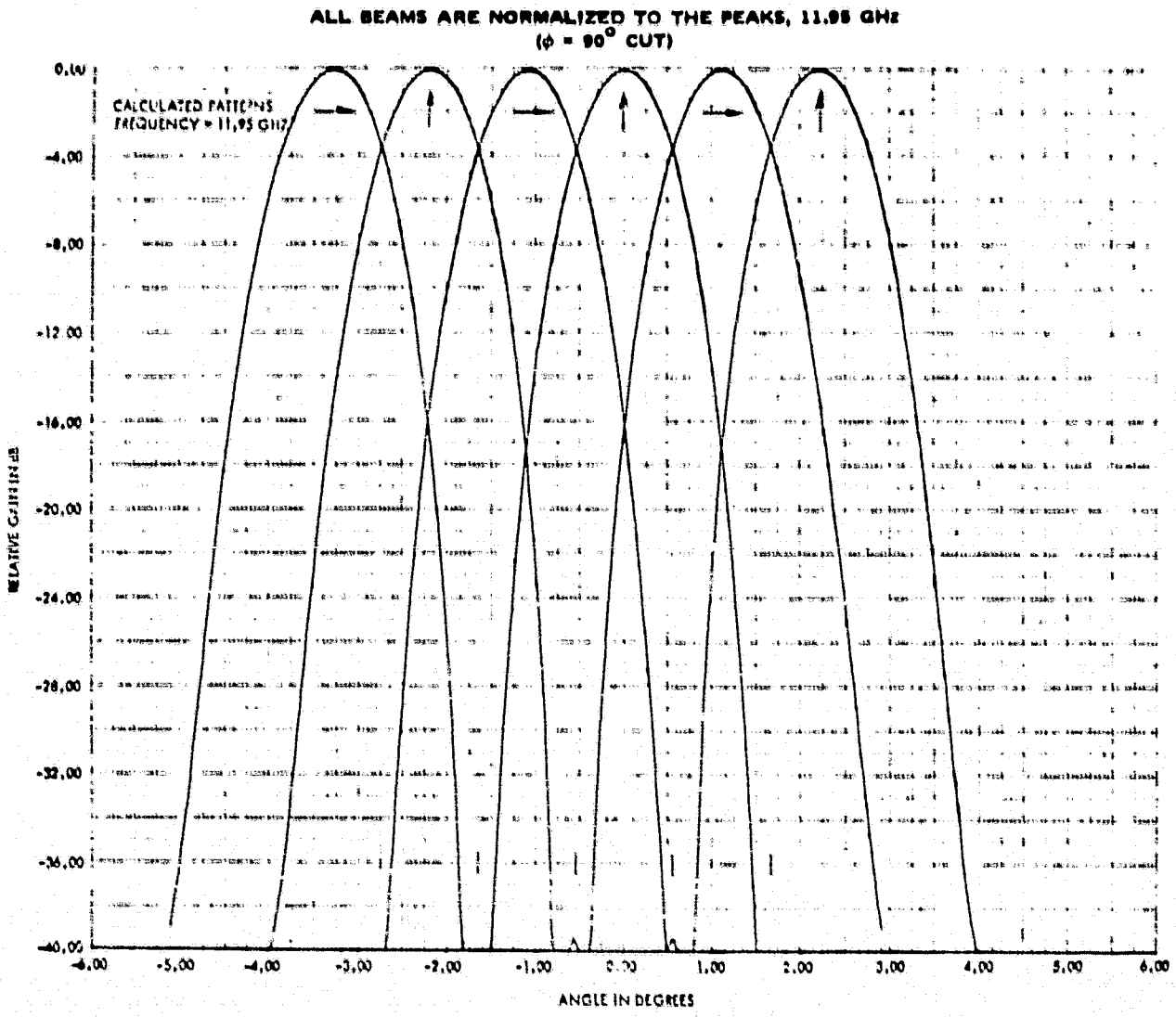

Figure 2.2-10. Beam Crossover Level of Contiguous Spot Beams

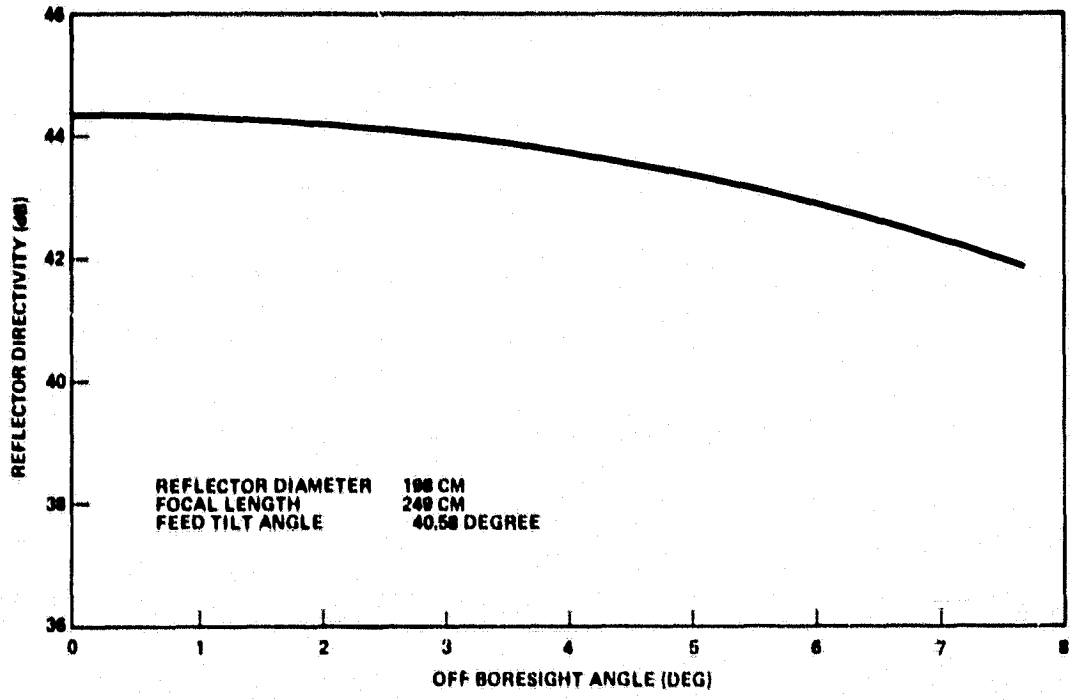

Figure 2.2-11. Gain Loss as a Function of Scanned Angle

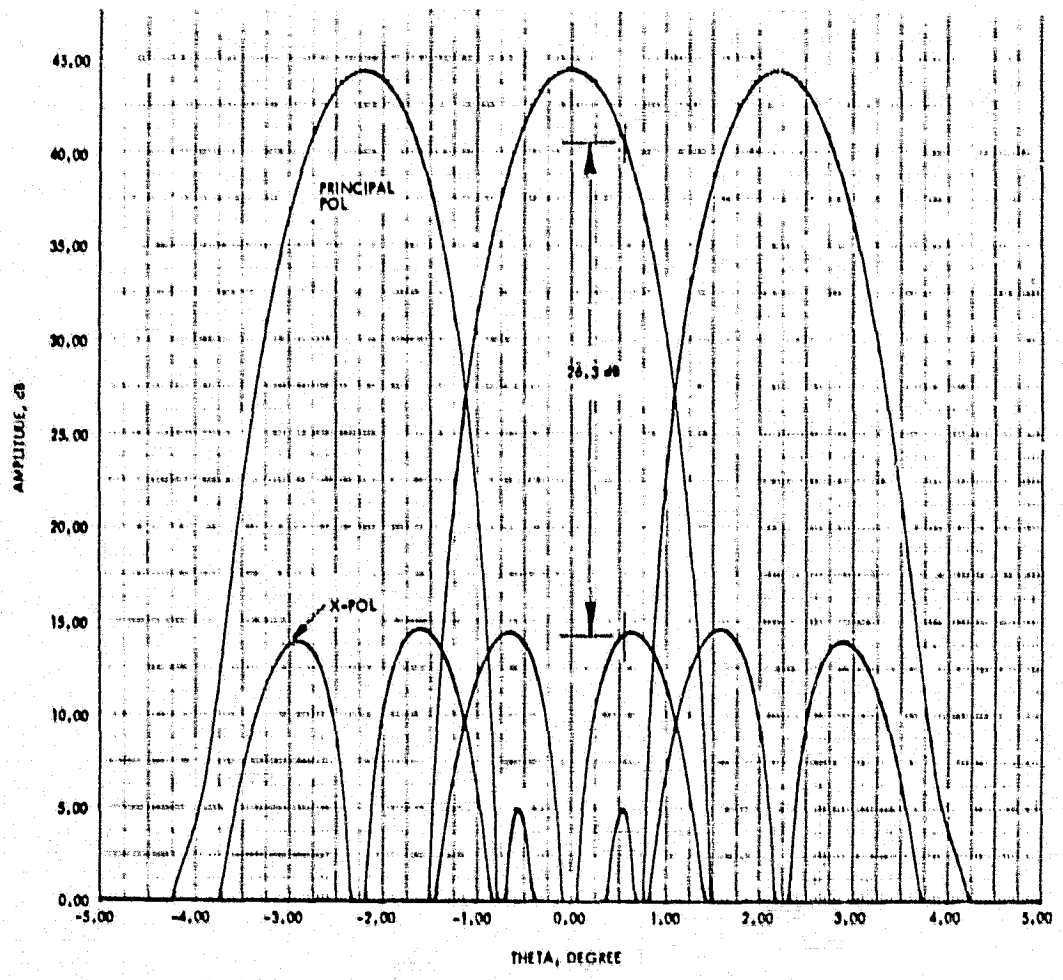

Figure 2.2-12. Principal and Cross-Polarization Patterns in the Azimuth Plane (ϕ = 90° Plane), 11.95 GHz

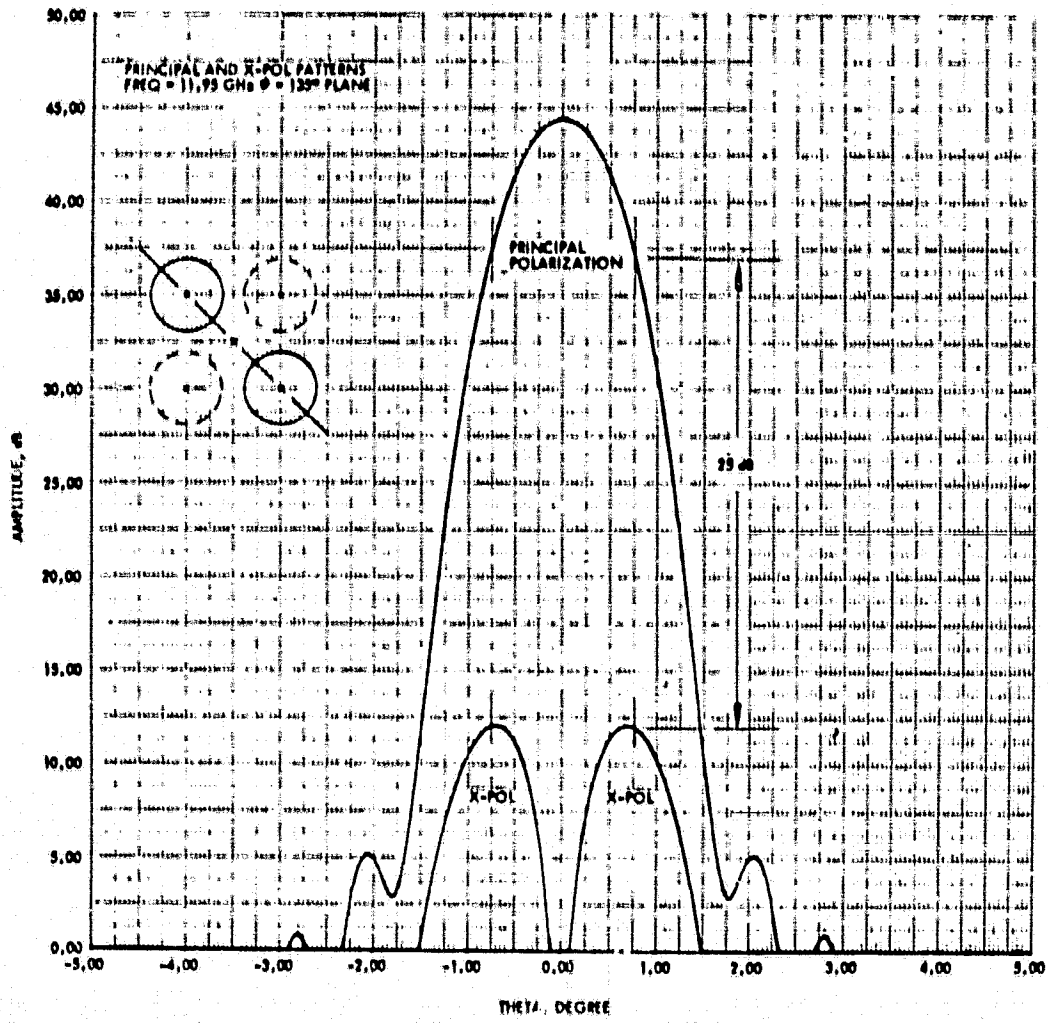

Figure 2.2-13. Principal and Cross-Polarization Patterns (ϕ = 45° Cut)

about -25 dB below the principal polarization signal at the center of four spot beams. The cross-polarization components are usually in phase quadrature with the principal polarization components. Therefore, the polarization of each beam varies from linear at the peak of a beam to an elliptical polarization in the region of cross-polarization lobes. Figure 2.2-14 shows the far field polarization characteristics of a typical circular spot beam.

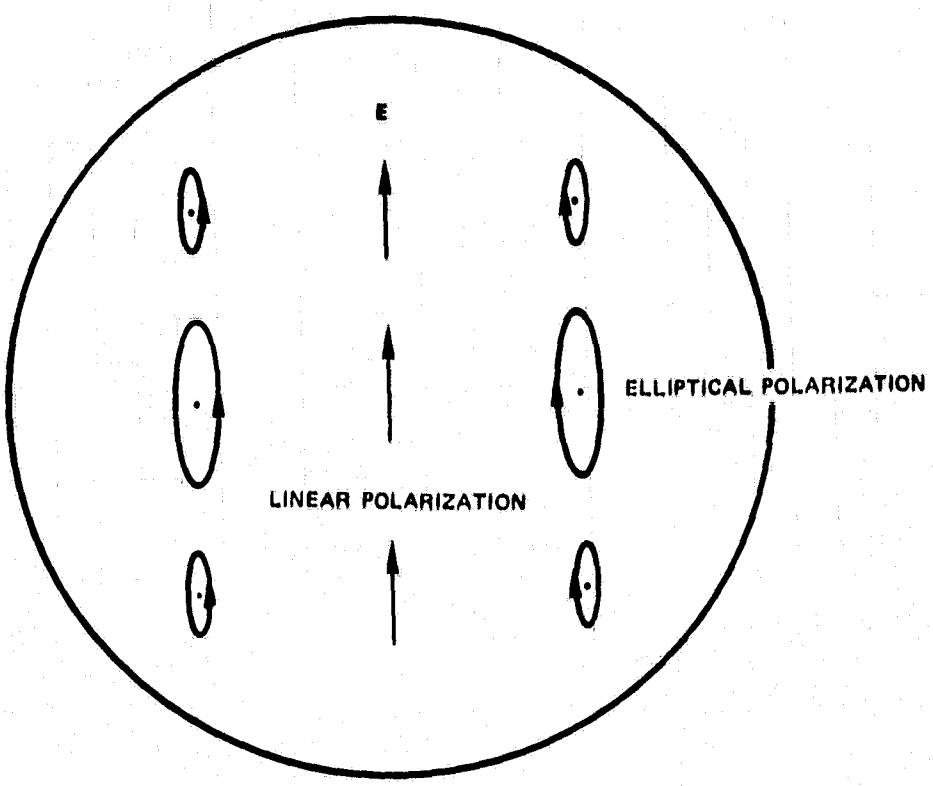

Figure 2.2-14. Far-Field Polarization Characteristics of a Circular Spot Beam

2.2.5 Suppression of Cross-Polarization

Obviously the above design does not meet the 30 dB isolation requirement in the vicinity of beam crossover point due to the cross-polarized radiation. Further increase in focal length will result in a large feed, long waveguide run with little improvement in cross-polarized radiation. One remedy is to use a polarization compensated feed which would substantially reduce the cross-polarized radiation. The cross-polarized radiation

which arises as a consequence of the reflector asymmetry reveals that the peak values of these two lobes appear in the vicinity of -4 dB down from the peak of the main beam. They are equal in amplitude, 180 degrees out of phase from each other, and in phase-quadrature (±90 degrees) relative to the main beam. Essentially they are similar to the difference mode patterns in the azimuth plane emerging from a monopulse feed. This fact indicates that either a nine-horn or seven-horn array feed with azimuth difference mode excitation of an orthogonally polarized field component can be employed effectively to suppress these two cross-polarization lobes. Particulary, the difference pattern of a nine-horn feed can be adjusted to closely resemble the cross-polarization pattern of a conventional offset reflector as shown in Figures 2.2-8b or 2.2-12. An illustration of these far-field difference pattern contours produced by a nine-horn feed is given in Figure 2.2-15. Superposition of this feed excitation with the conventional low sidelobe feed excitation shown in Figure 2.2-16 will result into an almost cross-polarization free far field radiation. It is interesting to note that the resulting feed aperture distribution shown in Figure 2.2-16 appears to be similar to the far field polarization of an uncompensated feed system shown in Figure 2.2-14. The cancellation of cross-polarization takes place when the polarization compensated primary field is reflected off the main reflector surface. The incident cross-polarization components are out of phase with the induced cross-polarization components caused by the asymmetric reflector surface. This cancellation principal can also be applied to the case a seven-horn array feed.

The polarization compensated feed can be implemented by adding thin diaphrams or septums inside the horns on the left and right columns of the nine-horn feed. The edge of these septums should be parallel to the diagonal plane of the square horns similar to that of the polarizer designs. The opposite phase relation for difference mode excitation, can be obtained by placing these septums in the opposite corner of the horns shown in Figure 2.2-17. Since the cross-polarization component usually is 20 to 30 dB below the principal polarization component, this level of cross-polarization can be easily excited by septum or wire polarizers with little perturbation to the low sidelobe performance.

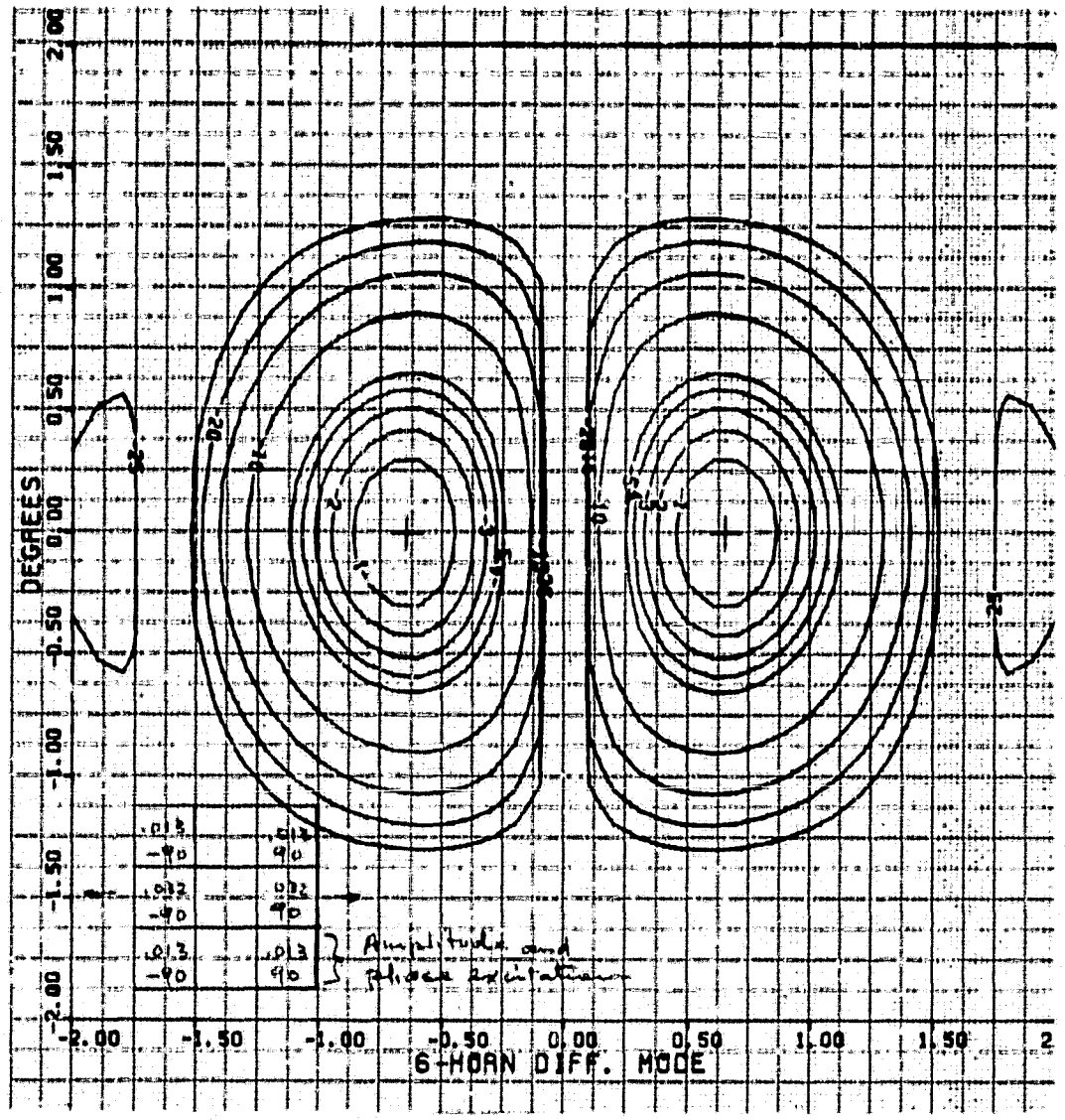

Figure 2.2-15. Far-Field Gain Contours Obtained from Six-Horn Difference Mode Excitation

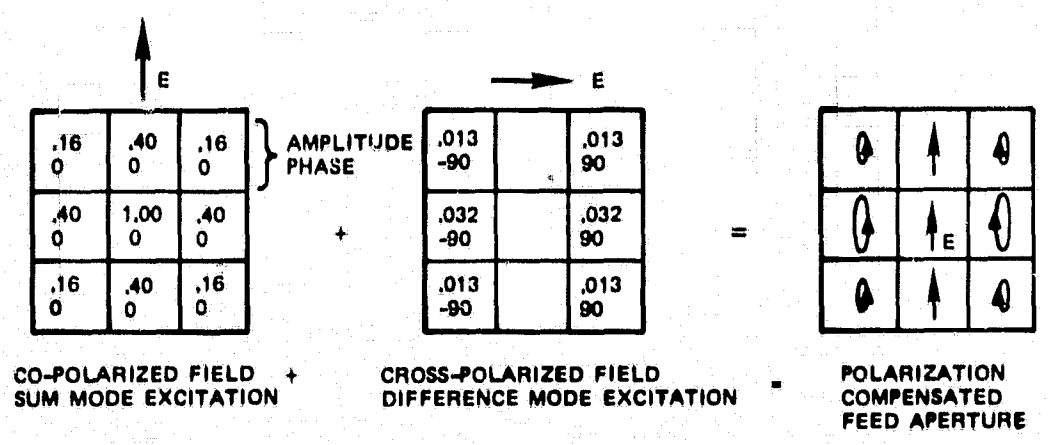

Figure 2.2-16. Polarization Compensated Feed Aperture Distribution

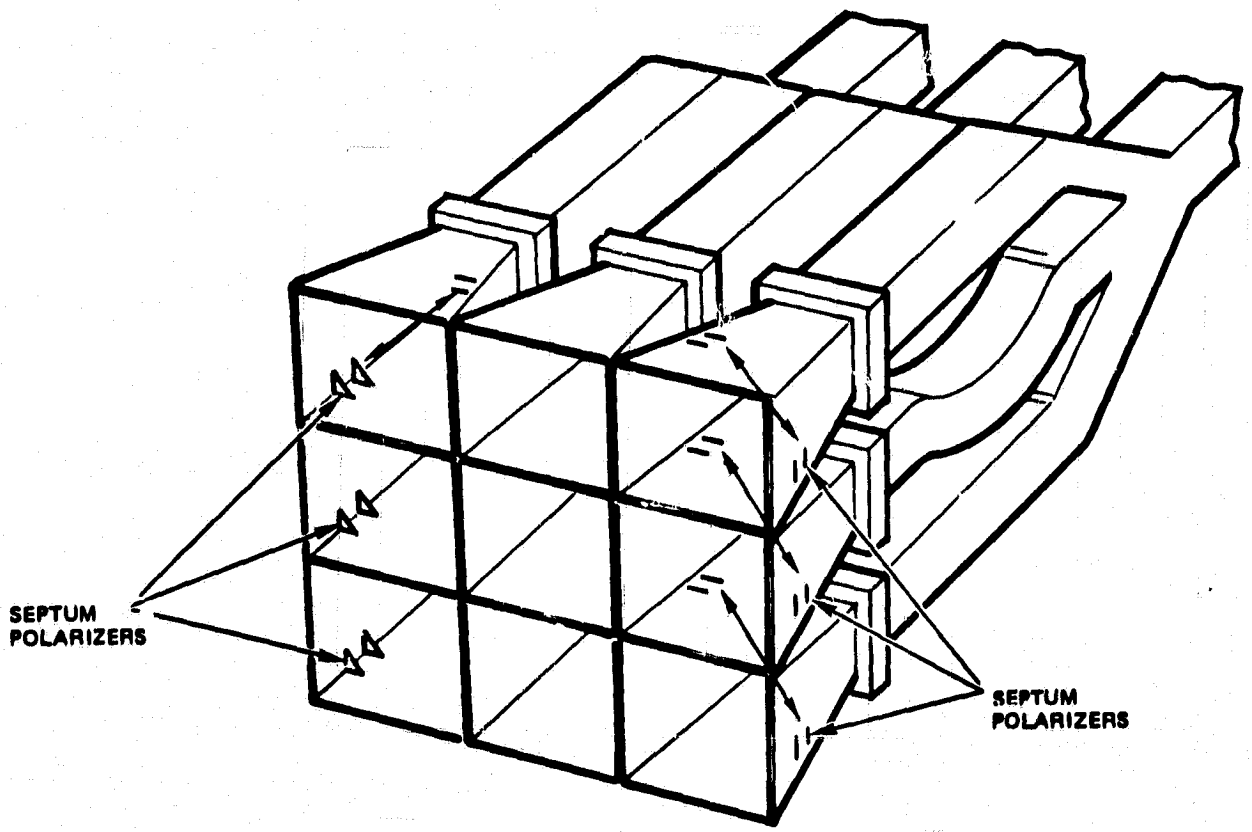

Figure 2.2-17. Polarization Compensated Feed – Cross-Polarized Fields are Excited by Septum Polarizers Inside the Horns

2.2.6 Gridded Reflector Antenna

Both sidelobe and cross-polarization radiation problems can be resolved by the sidelobe and cross-polarization cancellation techniques with nine-horn or seven-horn array feed. Unfortunately, because of the physical size of the nine-horn feed cluster, it is not possible to pack them close enough to provide overlapping beams. Hence four reflectors would be required to provide contiguous CONUS coverage.

Two approaches were evaluated in attempting to reduce the number of reflectors from four to two. The first approach utilizes two wire-gridded reflectors stacked front-to-back so that physically they do not occupy much more space than a single offset reflector and feed system. We call this the dual-gridded reflector approach. The second approach employs a gridded

subreflector used as a polarization diplexer incorporated with two separate sets of array feeds. The polarization diplexer splits and combines two orthogonally polarized signals to and from the two separated sets of feeds located on both sides of the diplexer. We call this the offset reflector with polarization grid subreflector approach.

Dual-Gridded Offset Reflector

Figure 2.2-18 shows a dual-gridded reflector configuration. This design concept was first investigated by Wilkinson[3] and was employed by RCA in their SATCOM system for 6/4 GHz domestic communication. In this configuration, two orthogonally polarized wire grid reflector are used to share the same aperture. One is placed in front of the other, but each has a different focal point. This permits the two orthogonally polarized feed assemblies to be placed with adequate separation in the vicinity of their respective focal points. The space occupied by the four reflectors is essentially the same as the space occupied by two separate side by side reflectors.

Each feed that illuminates this dual-gridded reflector system will produce a co-polarized beam and one pair of cross-polarized beams approximately 30 dB below the co-polarized beam, as shown in Figure 2.2-19. Separation between co-polarized and cross-polarized beams is determined by the relative feed position with respect to the focal points of their vertical and horizontal grid reflectors. In this case, the focal points of the dual-gridded reflector are chosen so that all the cross-polarized beams fall outside the United States.

This four-reflector antenna system provides contiguous spot beam coverage of CONUS with excellent polarization linearity in the CONUS coverage area. The drawbacks of this dual-grid reflector antenna are: the surface tolerance of the front wire grid is extremely difficult to maintain because of the lack of a rigid backup structure. All the spacers and supporting brackets in the back are deterimants to the gain and sidelobe performance of the reflector, particularly for a 2 meter diameter reflector operating at 14/12 GHz. Tight fabrication tolerance and precise alignment requirements between the two gridded reflectors result in a substantial increase in weight and cost.

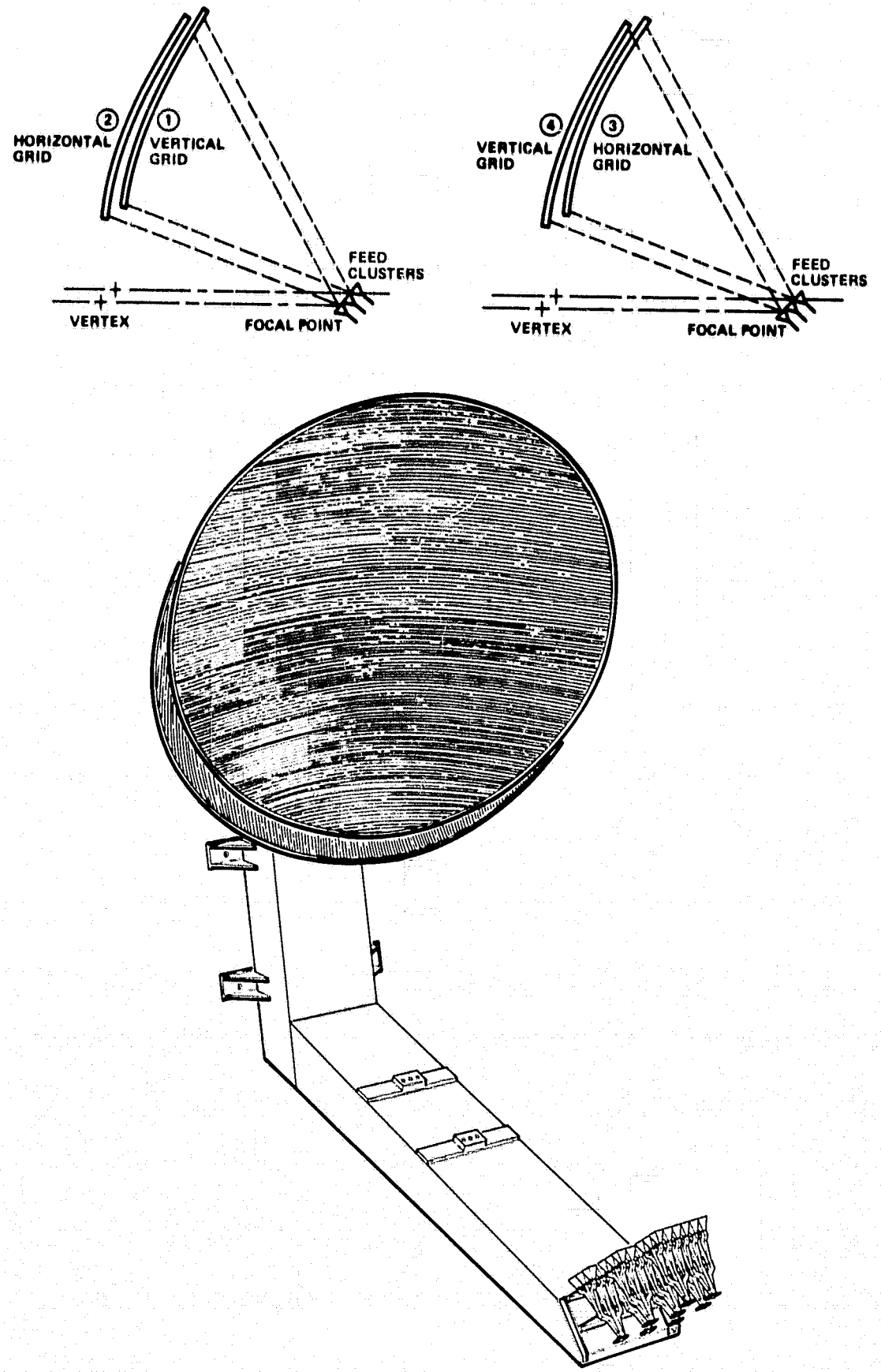

Figure 2.2-18. Dual-Gridded Offset Reflector Approach

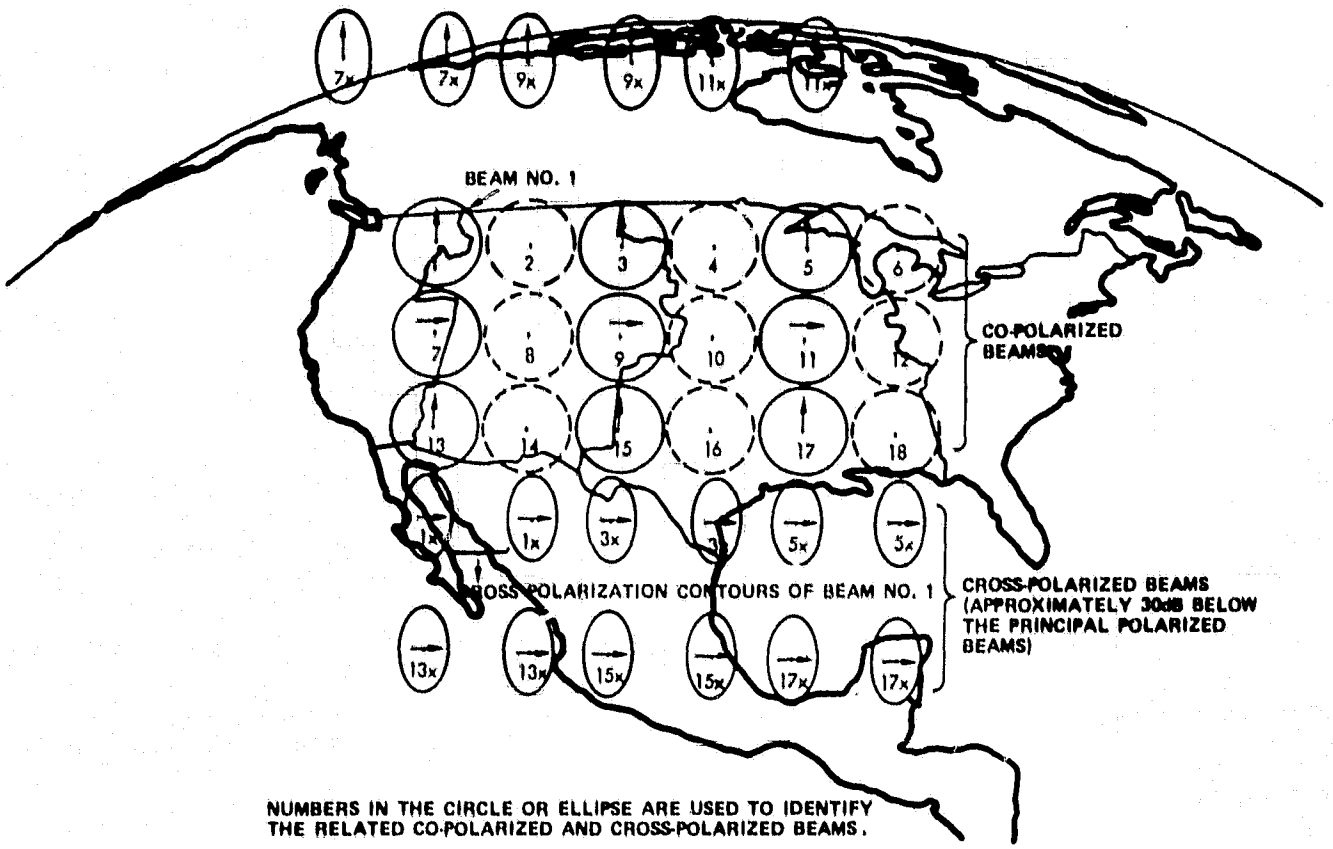

Figure 2.2-19. Principal and Cross-Polarized Beam Distribution of a Dual-Gridded Reflector System

Polarization Grid Subreflector

Alternatively, suppression of cross-polarization can be achieved by using a wire grid subreflector as a polarization diplexer. This polarization diplexer is inserted between the prime focus and the offset paraboloidal reflector so that an orthogonally polarized feed may be placed on the opposite side of the prime focus, as shown in Figure 2.2-20. This second set of feeds can be a cluster of spot beam feeds, contoured beam feeds, or a scanning beam feed using a variable power dividing feed network. In general, the polarization diplexer can be a hyperbolic surface with a family of grids specially designed so that the illumination of an offset paraboloid will produce a pure linear polarization in the far field of a reflector antenna. The theory and design of the special grid reflector has been published by Dragone.[4] Further investigation and experimentation of this new concept will be beneficial for future satellite communications.

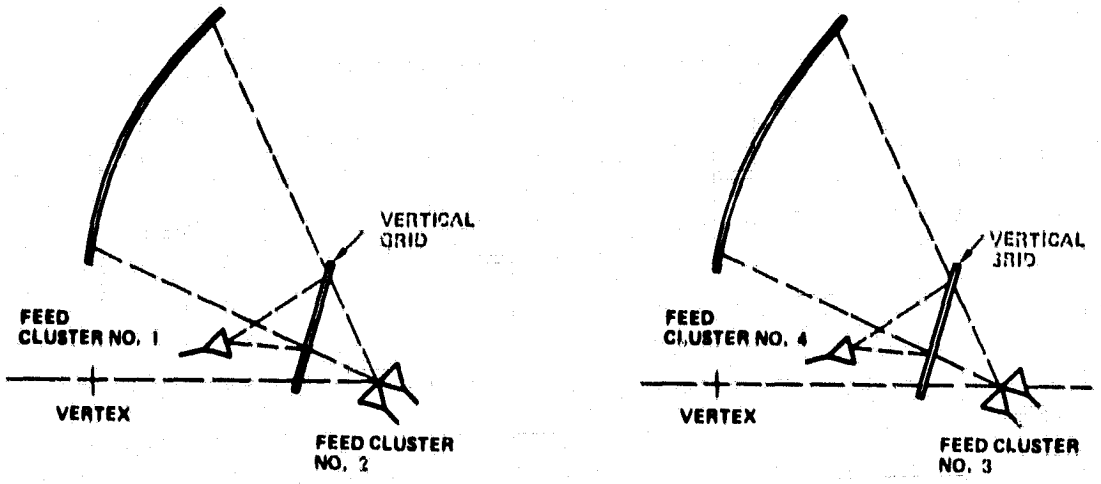

Figure 2.2-20. Wire Grid Subreflector Approach

In this work, we simply used a flat plate, so that the nine-horn spot beam array feed can be utilized in a front-fed as well as a Cassegrain-fed geometry to obtain a contiguous spot beam coverage. The advantages of using this polarization diplexer are:

- To suppress the cross-polarization radiation
- To permit overlapping two orthogonally polarized beams in the same coverage area
- To provide a combination of multiple fixed and scanning beams within a single reflector antenna
- To ease the polarization alignment and feed packaging problem
- To reduce the weight and cost.

The far field radiation characteristics of an offset paraboloid with a polarization grid geometry has been investigated by Chu.[5] Results of his analysis indicate that more than 10 dB reduction of the peak cross-polarization is obtained, based on the assumptions that both the reflector and polarization grid are located in the far zone of the radiation from a primary feed. A more rigorous analysis of scattering by the polarization grid, including the Kevlar-honeycomb Kevlar sandwich structure located in the near field region of a multi-element array feed, has been carried out by W. Wong[1] at TRW. Using the reflector geometry shown in Figure 2.2-20 a 4 dB reduction is achieved with the peak of cross-polarization roughly 34

dB below the peak of the main beam. This result has been substantiated by the far field measurements which will be presented in Section 2.5. In addition, the analysis has been extended to calculate the cross-polarization characteristics of off-axis scanned beams compared with those of a dual-polarized reflector system. Results of this calculation are presented in Figure 2.2-21. It is noted that the cross-polarization performance of a dual-polarized reflector is superior to that of a grid subreflector. However, when the beam is scanned more than five beamwidths away from the reflector axis, the cross-polarization of the second approach becomes lower than the first approach. Further investigation of these off-axis scan polarization characteristics is needed to obtain better understanding of the problem.

SCAN ANGLE (DEGREES)	TYPE OF REFLECTOR	P-POLARIZATION (DBI)	CROSS-POLARIZATION (DBI)	CROSS-POLARIZATION BELOW PEAK (DB)	ISOLATION (DB)
0	SOLID REFLECTOR	44.34	14.25	30.09	25.0
	WIRE SUB-REFLECTOR	44.44	8.91	35.53	30.4
	WIRE REFLECTOR	44.3	-27.18	>60.0	55.0
5	SOLID REFLECTOR	43.37	16.47	26.9	22.9
	WIRE SUB-REFLECTOR	43.37	14.05	29.32	29.0
	WIRE REFLECTOR	43.34	12.72	30.62	29.8

Figure 2.2-21. Computed Cross-Polarization Characteristics of Offset Reflector

Polarization Grid Analysis

A TRW computer program STRIP has been used to analyze the transmissivity of the wire grid reflector surface. The paraboloidal surface analyzed is a honeycomb sandwich shell consisting of a two-layer Kevlar face sheet, a 6.35 mm thick honeycomb core, and a second two-layer Kevlar sheet. The copper strips are sandwiched between two 1.27 mm Kevlar sheets placed on the inner face of the reflector surface. The STRIP program analysis indicates that a 30 strip-per-inch shell will give a transmission loss of less than 0.03 dB for a plane wave with polarization perpendicular to the strips, and a return loss of 20 dB for a plane wave with polarization parallel to the strips.

A detailed analysis of the wire grid or parallel plate grating is given by C.C. Chen[6] in a TRW Internal Technical Memo. A simplified version of this program was used to calculate the scattering from a finite flat plate. The scattered field is then used to analyze the far field principal and cross-polarization characteristics of the antenna.

2.2.7 Contiguous Coverage Antennas

Two gridded reflector antenna concepts were discussed and evaluated in Section 2.2.6. The offset reflector with wire grid subreflector configuration was selected for further investigation and development.

Two identical reflector antennas and four sets of feeds (Figure 2.2-20) are used to provide contiguous spot beam coverage; one provides eight spot beams and the other nine spot beams. Each antenna consists of a solid surface parabolic reflector, one flat wire grid subreflector for polarization diplexing, and two orthogonally polarized feed clusters located on both sides of the diplexing reflector. Feed clusters 1 and 2 consist of five vertically polarized feeds, including Hawaii, and three horizontally polarized feeds which illuminate approximately one half the CONUS beams as shown in Figure 2.2-22. The shaded areas are within the -6

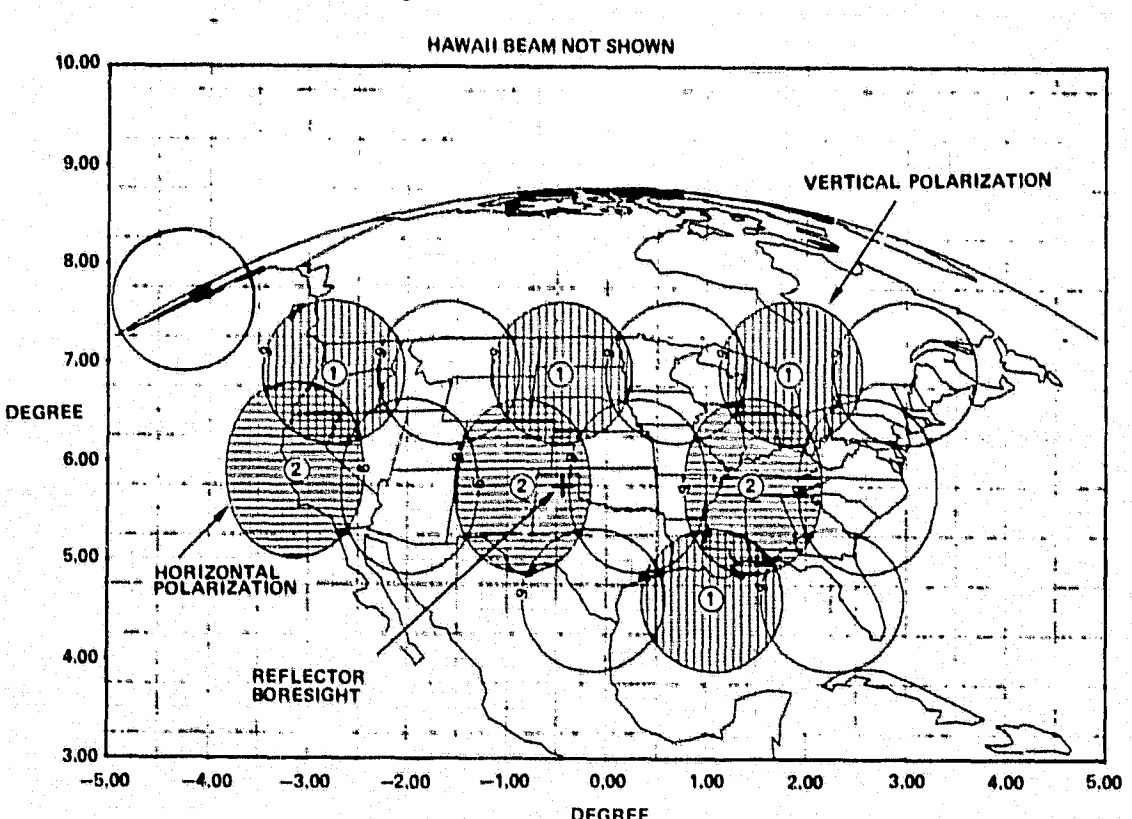

Figure 2.2-22. 17 Beam Arrangement (-6 dB Contour)

each beam. The beams in the center row are designed to provide an elliptical cross-section so that the gain at the three beam crossover can be maintained less than 6 dB below the main beam peak of each beam. Each spot beam is produced by a nine-horn array feed. For simplicity in design, all eight feeds including the Hawaiian feed, are physically identical except for the elliptical beam feeds which were achieved by changing the septum spacing slightly in the three-way power divider. Figure 2.2-23 shows calculated gain contours of four co-polarized circular beams produced by feed cluster 1. They operate at the same frequencies; therefore, the amplitude isolation between these beams is important in determining the co-polarized beam isolation. Figure 2.2-24 shows the calcuated elliptical beam gain contours (in the center row of CONUS coverage) produced by feed cluster 2. The elliptical beams are isolated from the circular spot beams by frequency separation. It is noted that a minimum of 30 dB isolation can be achieved between any two co-polarized beams based on the calculated results from a perfect reflector surface.

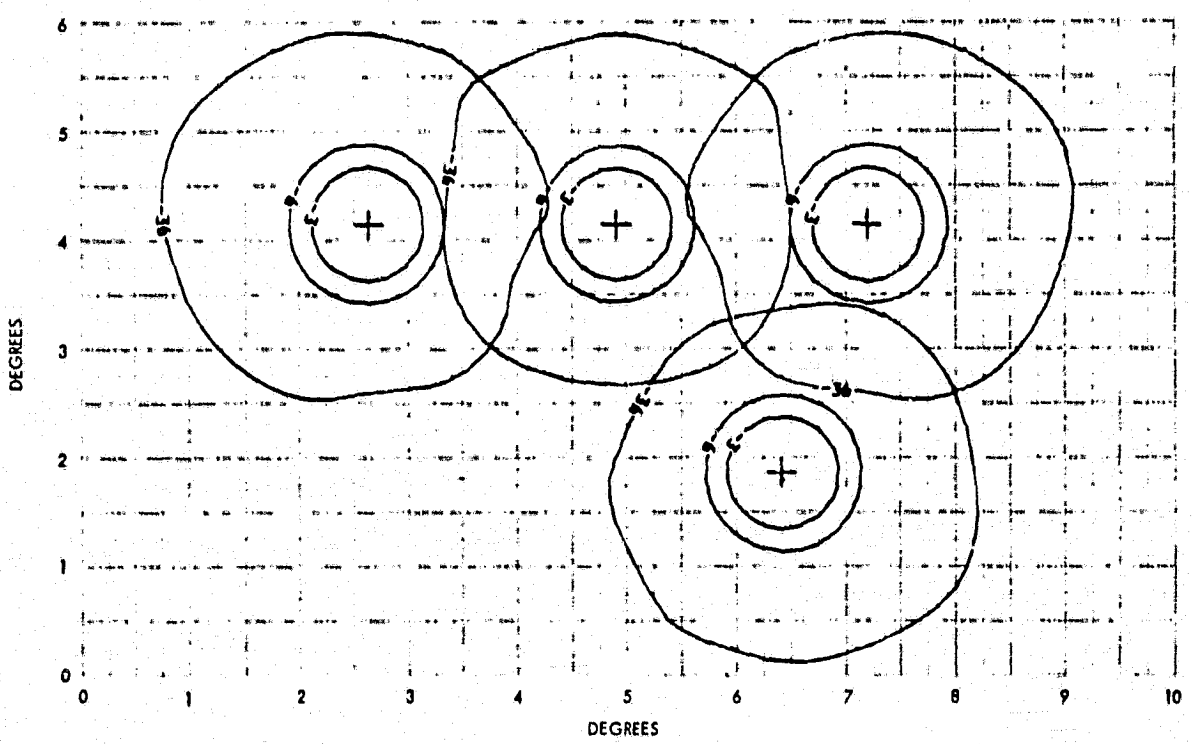

Figure 2.2-23. Beam Isolation Between Four Co-polarized Beams Produced by Feed Cluster Number 1

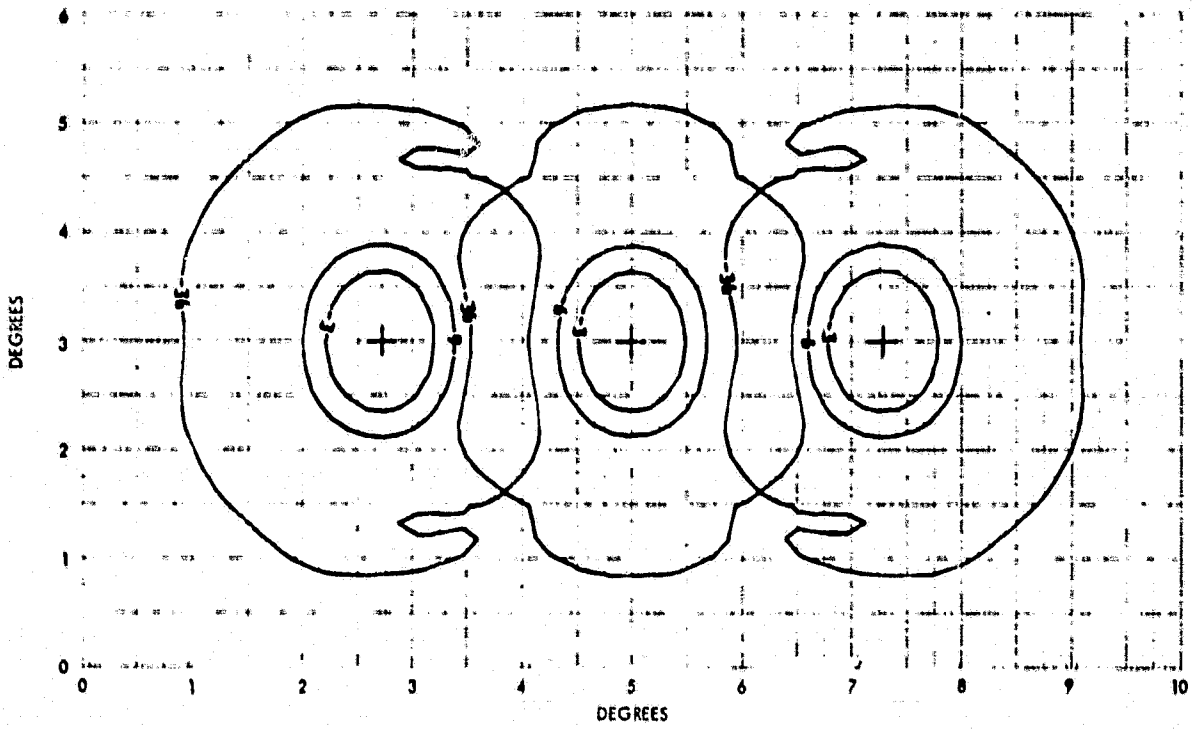

Figure 2.2-24. Beam Isolation Between Three Co-polarized Beams Produced by Feed Cluster Number 2

The second antenna was designed to provide the other half of the CONUS coverage. The beam arrangement and performance of this antenna are given in Figures 2.2-25 through 2.2-27.

2.2.8 Reflector Surface Irregularities

The effects of reflector surface roughness on the sidelobe level are extremely important in a multiple beam communication system which requires a number of beams operating at the same frequency. The interference signal increases with the number of beams. The surface irregularities can be classified into two categories: systematic errors and random errors. Systematic errors are caused by either thermal expansion or mechanical stress which distorts the reflector surface from the ideal parabolic shape. This error usually results in beam broadening, beam shoulders, or high sidelobes near the main beam region. Random errors are usually caused by manufacturing imperfections which form random irregular bumps on the reflector surface. These random errors usually raise the far out sidelobe level. These undesirable radiations are the main source of interference which impair beam isolation in a multiple beam communication system.

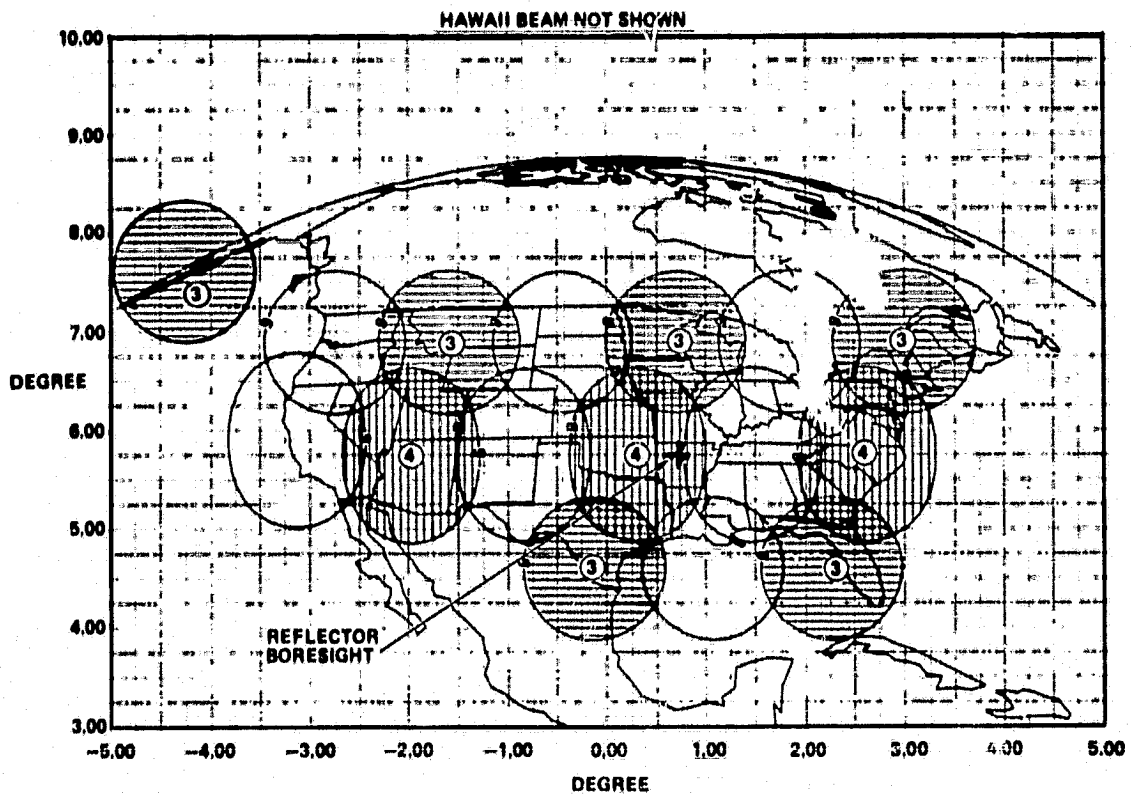

Figure 2.2-25. 17 Beam Arrangement (-6 dB Contour)

The effects of reflector surface roughness on the peak gain are well known. However, the effects on the sidelobe level are difficult to predict accurately because, in most cases, the reflector surfaces under test are not measured as they are difficult to measure precisely and so analysis is used instead. The analysis of reflector surface error for a front-fed circular reflector has been given by Rudge.[7] He modeled the surface error as a distribution of bumps on the reflector surface. These bumps introduce rms phase error 2σ in the aperture field. Since the bumps used to describe the reflector surface are first order approximations only, the resulting sidelobe predictions are not accurate. TRW's reflector distortion analysis program, developed by W. Wong,[1] uses a much more accurate mathematical model. First, the measured reflector surface data is processed by computer to generate the 2σ phase errors at a set of discrete points around the center of the reflector aperture. This data is then input to the OFFSET program to calculate the far field radiation of the reflector. These errors vary sinusoidally in the radial direction of the aperture and have the form

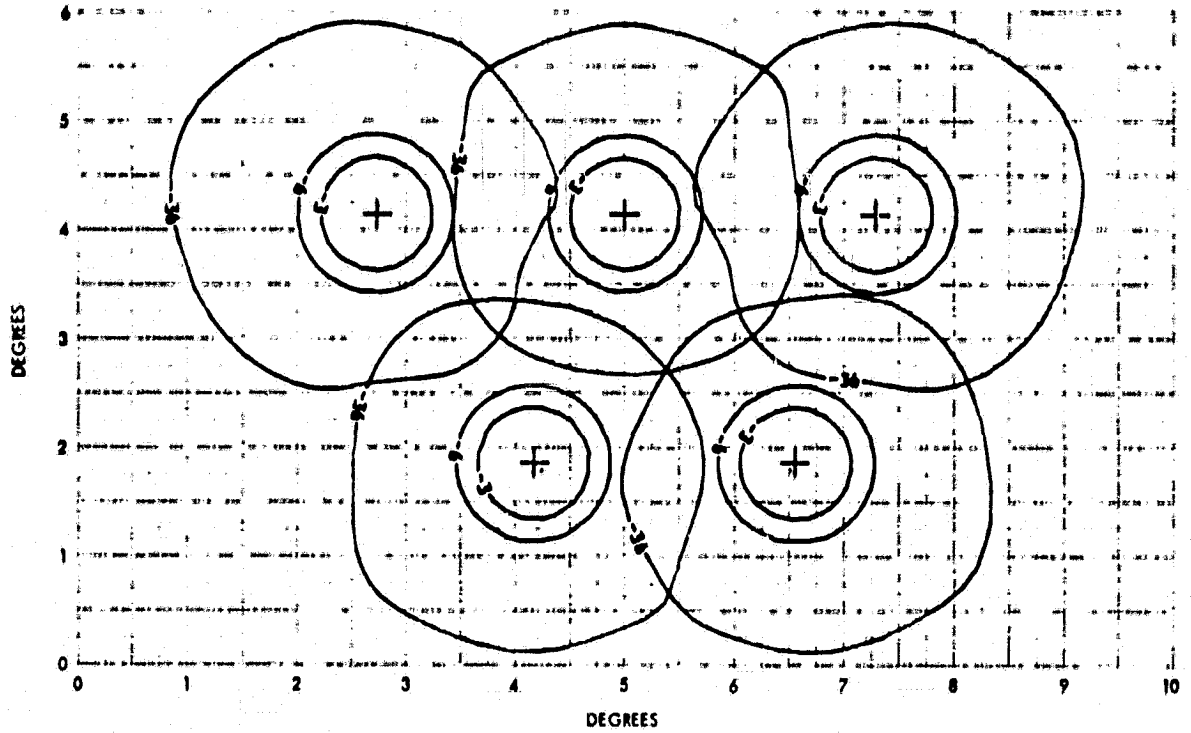

Figure 2.2-26. Beam Isolation Between Five Co-polarized Beams Produced by Feed Cluster Number 3

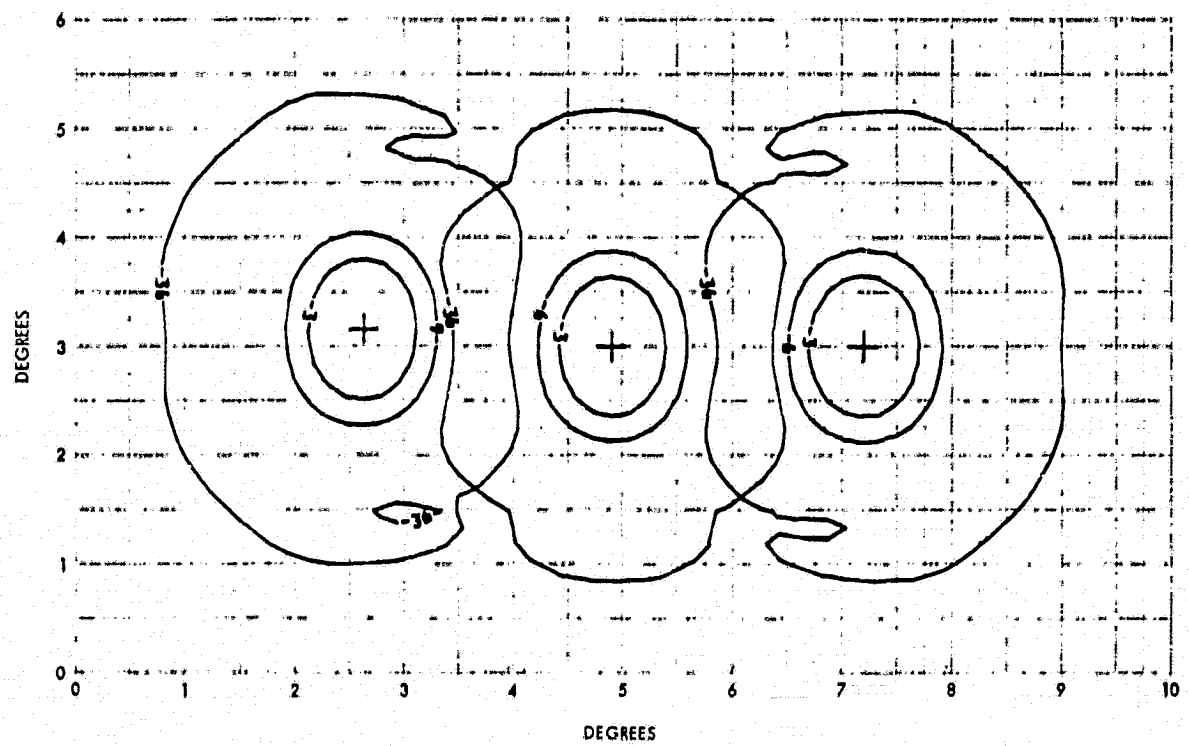

Figure 2.2-27. Beam Isolation Between Three Co-polarized Beams Produced by Feed Cluster Number 4

$$\psi(r) = \exp\left[-j2\pi A/\lambda \cdot \sin(n\pi r)\right]$$

where

A = magnitude of phase distortion

n = number of distortion cycles

r = normalized radial variable, r = 1 at the reflector edge.

Analysis shows that the levels and locations of the sidelobes are determined by the harmonic contents of the reflector distortion. The lower harmonic components affect the near in sidelobes, while the higher harmonic components affect the far out sidelobes. The thermal and mechanical stress distortions are manifested in lower harmonic components and the random surface irregularities are manifested in higher haromic components. In general, the magnitude of the low harmonic contents is greater than the magnitude of the high harmonic contents.

Figure 2.2-28 shows the measured deviation from a perfect parabolic surface in thousandth of an inch on a 2-meter diameter offset reflector. The surface rms error is approximately 10 mils. Figure 2.2-29 shows comparison of the calculated E- and H-plane patterns from a perfect parabolic reflector, and the same calculation when the measured surface errors are introduced in the calculation. The main effects, as expected, show up in the near-in sidelobes where they may severely impair beam isolation in a contiguous beam arrangement.

2.2.9 Beam Isolation

Beam isolation is defined as the ratio of the desired signal received from the desired beam to the total undesired signal received from all the other beams operating at the same frequency at a specific ground terminal located in the (θ,ϕ) direction of the spacecraft antenna coordinates. The desired signal is the carrier signal and the undesired signal is the interference which is an algebraic summation of all co-polarized and cross-polarized radiation recieved by the ground terminal. More specifically, the isolation can be expressed as

$$\text{Beam isolation } (\theta,\phi) = \frac{S_1(\theta,\phi)}{\sum_{n=1}^{N} S_n(\theta,\phi) - S_1(\theta,\phi)} = \frac{S_1(\theta,\phi)}{I_1(\theta,\phi)}$$

where N is the total number of beams in a multibeam antenna system.

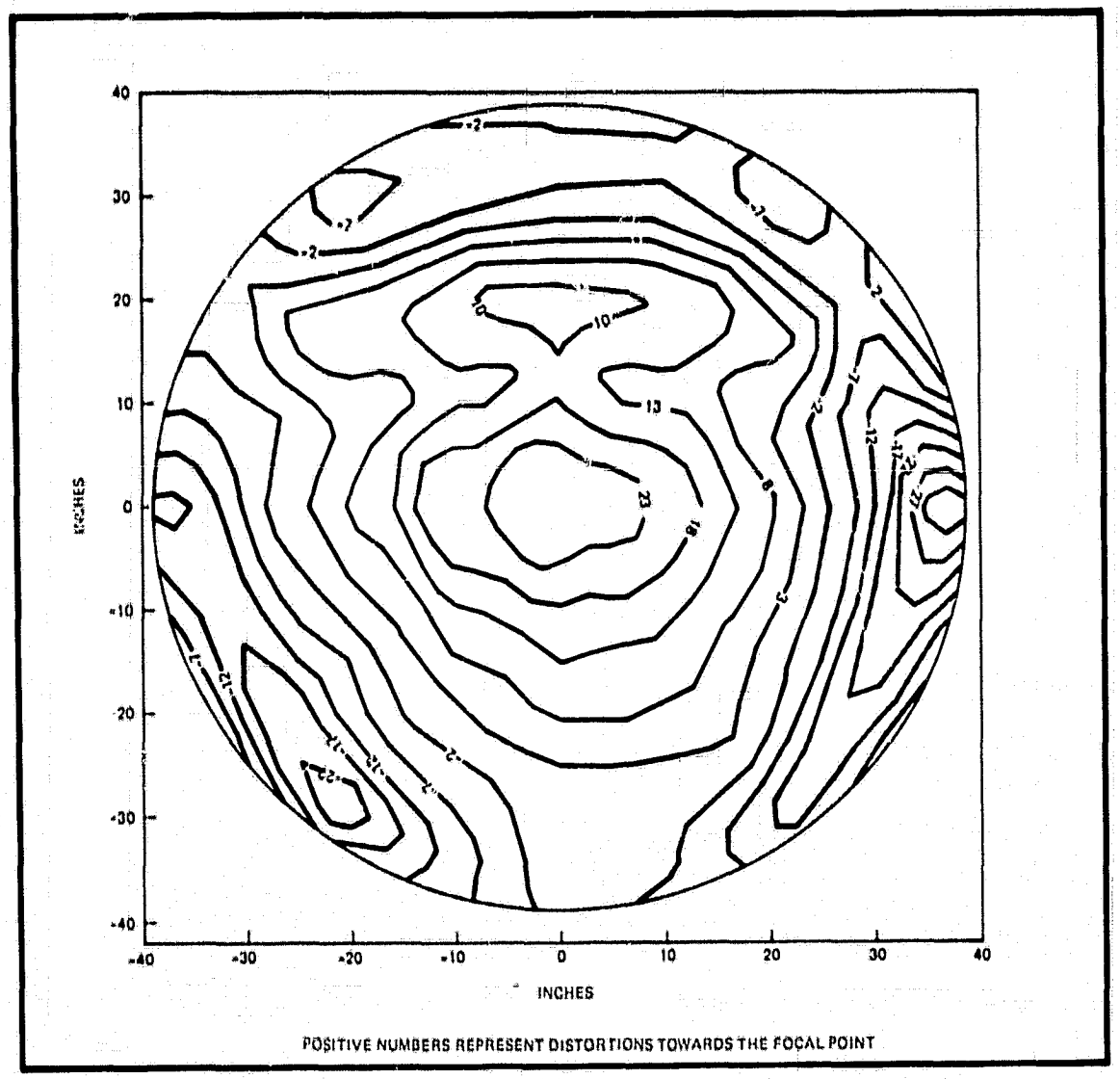

Figure 2.2-28. Measured Surface Error Contour in 1/1000 Inch on 78-Inch Reflector Diameter: 78 Inches (200 cm)
Focal Length: 98.04 inches (249 cm)

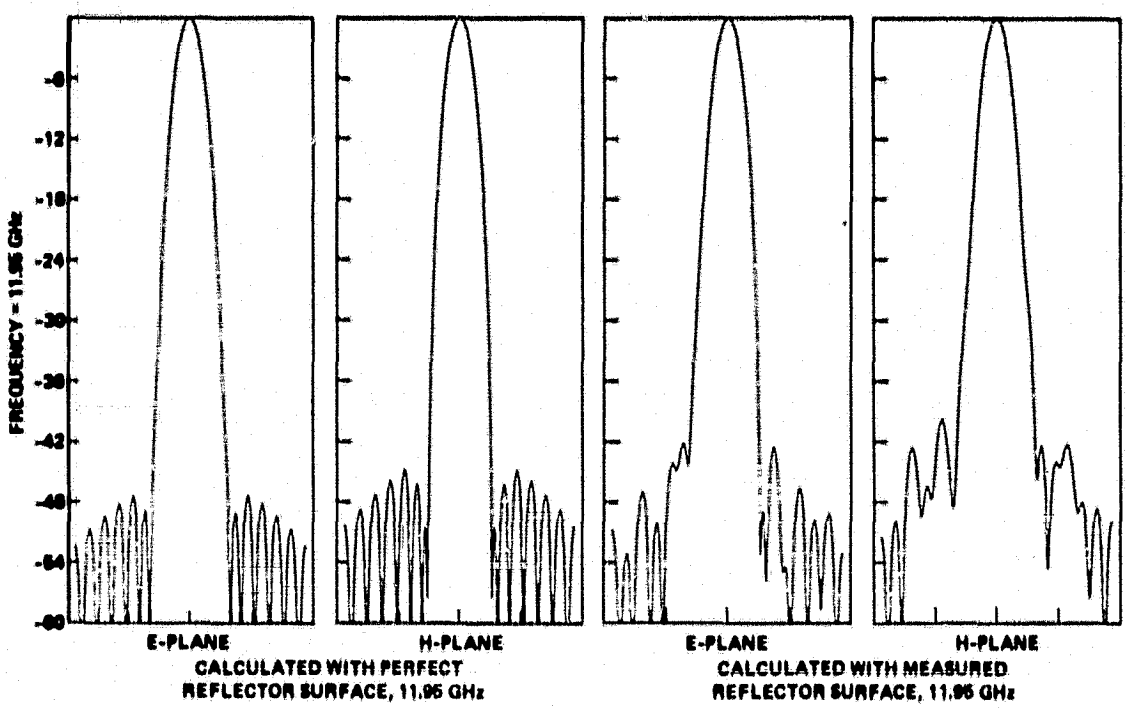

Figure 2.2-29. Effect of Surface Roughness on Sidelobe Level

There are two principal sources of interference: co-polarized sidelobes and cross-polarized lobes. The cross-polarization components in an offset reflector can be predicted accurately. They are insensitive to the reflector surface roughness, but extremely sensitive to mechanical alignment. Therefore they can be controlled. However, the scattered sidelobes are difficult to control. The random phase error due to manufacturing surface imperfections, and scattering from the antenna supports and multipath range reflection contribute to far out sidelobes and, in general, raise the noise floor level. This type of interference is more likely directly proportional to the number of beams operating at the same frequency. In a 17-beam antenna system, this noise alone would contribute 9 dB degradation to beam isolation, not even taking into account the near-in sidelobe interference from thermal and mechanical stress distortion of the reflector.

2.3 SPOT BEAM FEED DEVELOPMENT

2.3.1 Feed Concepts

During the design analysis and tradeoff study phase of the program, a nine-horn array feed was configured to yield the desired circular and elliptical beam shapes for multiple beam CONUS coverage. The element voltage excitation coefficients determined by the low sidelobe pattern synthesis are:

Circular Beam			Elliptical Beam		
0.16	0.40	0.16	0.26	0.64	0.26
0.40	1.0	0.40	0.40	1.0	0.40
0.16	0.40	0.16	0.26	0.64	0.26

All nine elements are fed in phase. The feed should be capable of operating over both 14/12 GHz bands in either vertical or horizontal polarization with a VSWR of less than 1.2:1.

To satisfy the above requirements, combinations of waveguide components grouped into four prospective feed circuit configurations were evaluated. The first configuration considered was made up of two stages of E-plane septum power dividers, as shown in Figure 2.3-1, to achieve the 1 to 9 power split. This type of parallel feed eases the design difficulties in providing cophasal outputs at the feed aperture. Septum power dividers are inherently broadband. However, in cascading two or more of these reactive devices, small values of power mismatch in the feed circuit could lead to resonance and produce significant power amplitude variations at the input port of the feed. In addition, a means of rotating the polarization 90 degrees between two dividers in cascade is required in matching the input and output port field polarizations.

The second configuration shown in Figure 2.3-2 is obtained by substituting all the septum dividers with top wall directional couplers. In this configuration, the reflected energy due to impedance mismatch at the aperture or in the power divider will be absorbed into the loaded terminals. A 90 degree phase delay at the two coupled ports helps to compensate for path differences between the center and the two outer ports. The needed tight coupling over the 20 percent bandwidth is attained at the cost of increased component size and weight.

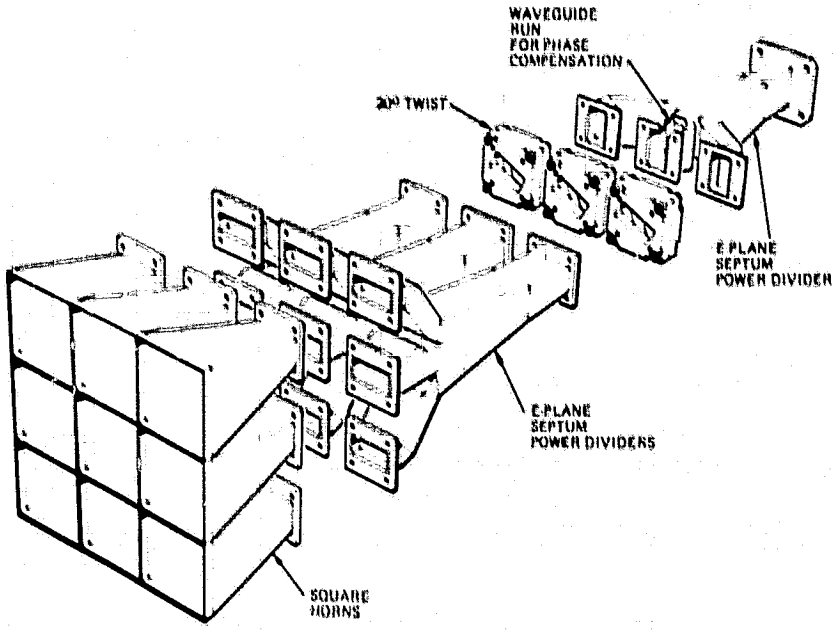

Figure 2.3-1. Spot Beam Antenna Feed Configuration Number 1

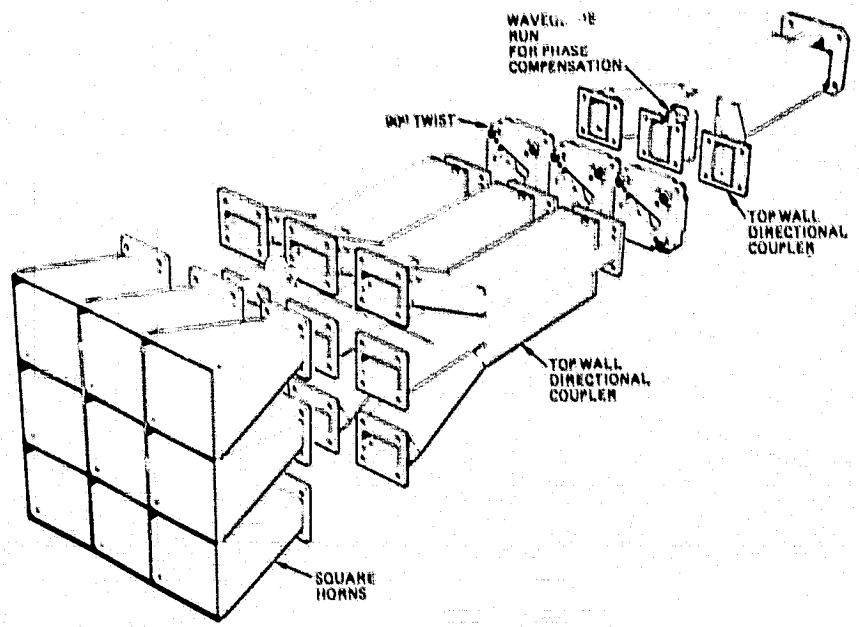

Figure 2.3-2. Spot Beam Antenna Feed Configuration Number 2

The third configuration depicted in Figure 2.3-3 eliminates the problem of cross-polarized adjoining junctions by replacing the input divider of the first configuration with a sidewall coupler.

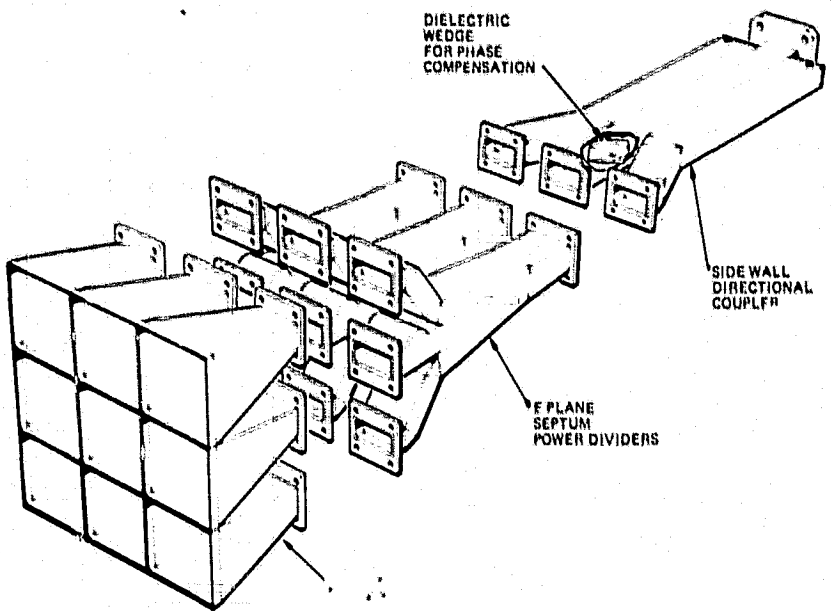

Figure 2.3-3. Spot Beam Antenna Feed Configuration Number 3

The last configuration shown in Figure 2.3-4 eliminates the crossed waveguide problem and the externally mounted horn radiator by using an E-plane septum divider as an input to an H-plane septum divider. Proper phasing, matching, and power division are extremely difficult to obtain in this particular design concept.

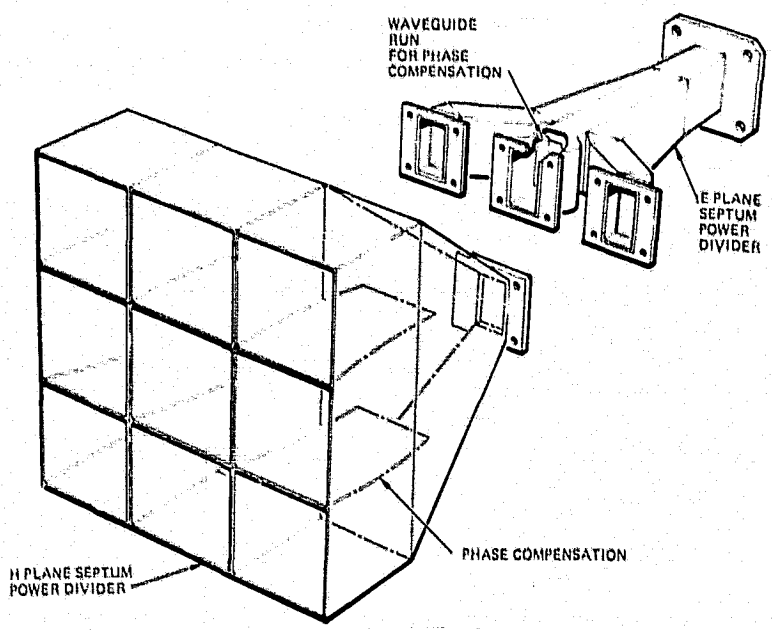

Figure 2.3-4. Spot Beam Antenna Feed Configuration Number 4

Before the final feed configuration (Figure 2.3-1) was selected each of these feed concepts was evaluated by fabricating and testing of the appropriate feed components to determining the feasibilities of these feeds for wideband operation.

2.3.2 Feed Hardware Development

The following is a list of feed hardware needed for the four feed configurations described above:

1) Horn

   Square horn
   Circular Horn

2) 3-Way power divider

   Sidewall coupler
   Topwall coupler
   E-plane septum power divider
   H-plane septum power divider

3) Step transformer (for impedance matching)

4) 90 degree twist (for polarization rotation)

5) Phasing section (for cophasal operation)

   U-bend
   Mitered corners
   Dielectric phase shifter.

In the early stage of horn design, consideration was given to the use of circular horns to improve the E-plane and H-plane pattern symmetry. The use of this type of horn would require a rectangular-to-circular transition. Also, polarization alignment would be difficult. The circular horn was dropped in favor of the square horn.

Three sizes of square aperture horns, 2.54, 3.0, and 3.7 cm, were fabricated. The small horns were used to illuminate a 152 cm diameter reflector used as a transmit source antenna for the far field test. The other horns were designed for use in two reflector geometries, one with an optimum focal length of 202 cm, the other with an existing Intelsat V

reflector mold which employs a focal length of 249 cm. VSWR measurements of these horns are shown in Figures 2.3-5a, b, and c. The radiation patterns for the 3.7 cm horn is given in Figures 2.3-6a, b, c, and d.

In a sidewall directional coupler, power division is accomplished by power coupling through a series of slots machined in the sidewalls of the main branch line. Slot dimensions, numbers, and spacing determine the coupling value, match, and bandwidth. Figure 2.3-7 shows a breadboard branch line coupler. The measured results shown in Figure 2.3-8 indicate that the bandwidth is too narrow to satisfy the requirements. Although the bandwidth could have been broadened by increasing the number of slots, this would result in increased size and insertion loss. Also, it is difficult to compensate a phase shift of 90 degree between main guide and coupled guide ports over the entire 14/12 GHz band. Consequently this design was eliminated from futher consideration.

In an E-plane divider, a thin conducting plate (septum) is inserted across a waveguide perpendicular to the electric field. This will divide the waveguide into multiple heights of the respective branches with the power divided in proportion to the branches. The height of each branch being less than that of the main waveguide will produce a different impedance.

The design of a septum power divider was completed by a three-step process. The first step was to obtain the proper power ratios to each of the branches. The second step was to minimize branch VSWR. The third step was to phase match each of the branches. The initial E-plane power divider was a three-way device. The power was proportioned to yield three branches of the proper distribution for use in the elliptical beam feed (outer ports are 4 dB lower than the center port). Each branch was tapered to the main waveguide dimensions. Figures 2.3-9a and b, illustrates the coupling response and the impedance match of the device with respect to frequency. The ease with which the desired power was split and the potential for minimum component size in the E-septum divider established it as the choice for use in the feed circuit.

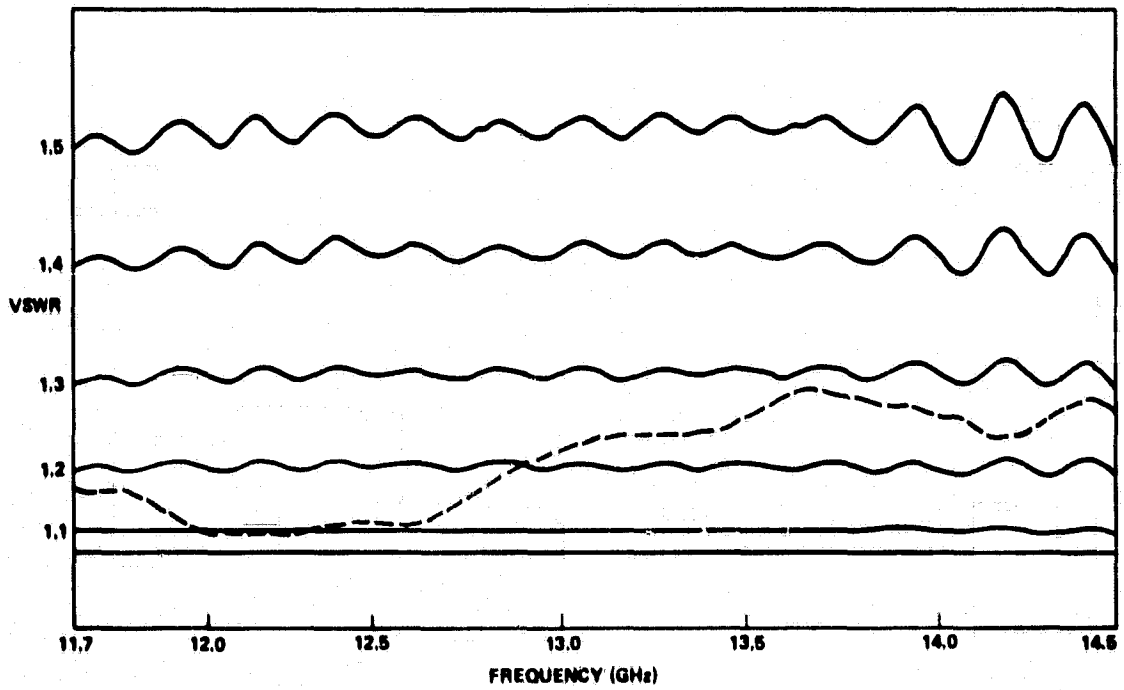

Figure 2.3-5a. VSWR of 2.5 cm Square Aperture Horn

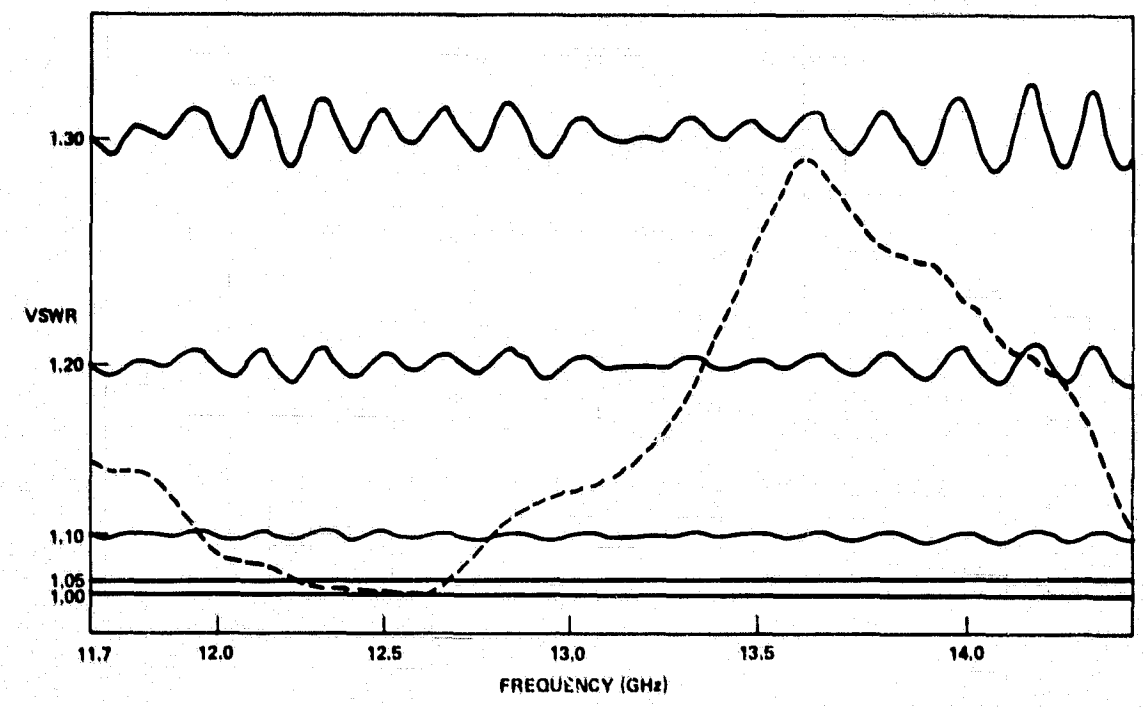

Figure 2.3-5b. VSWR of 3.0 cm Square Aperture Horn

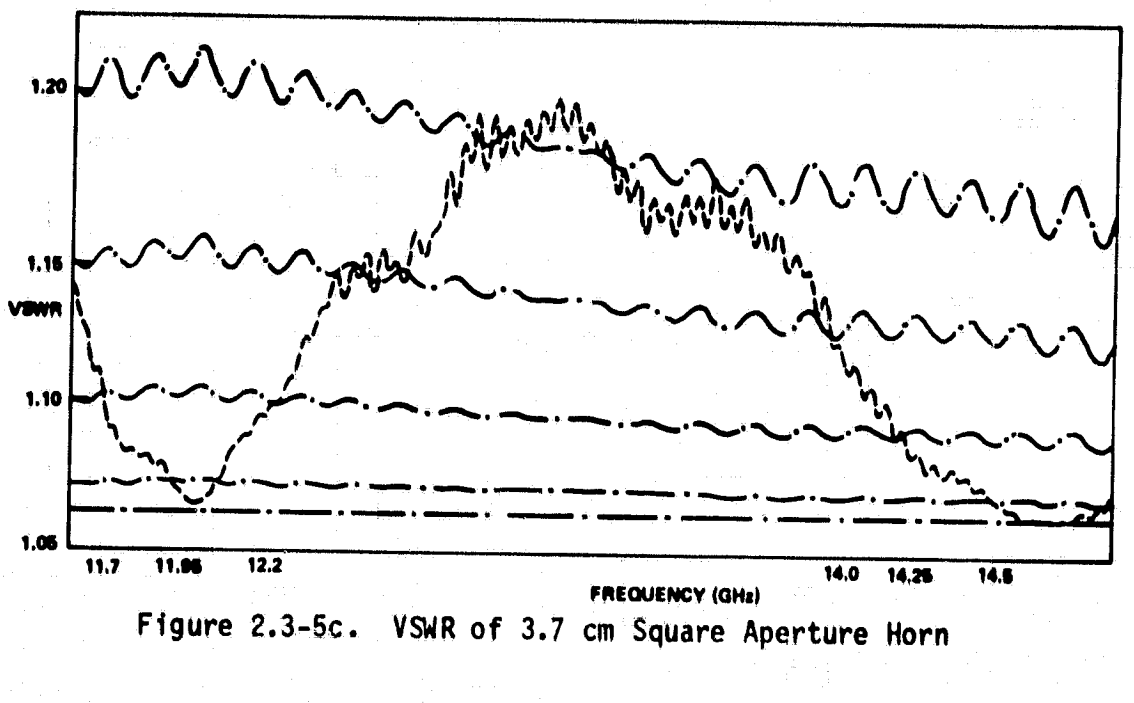

Figure 2.3-5c. VSWR of 3.7 cm Square Aperture Horn

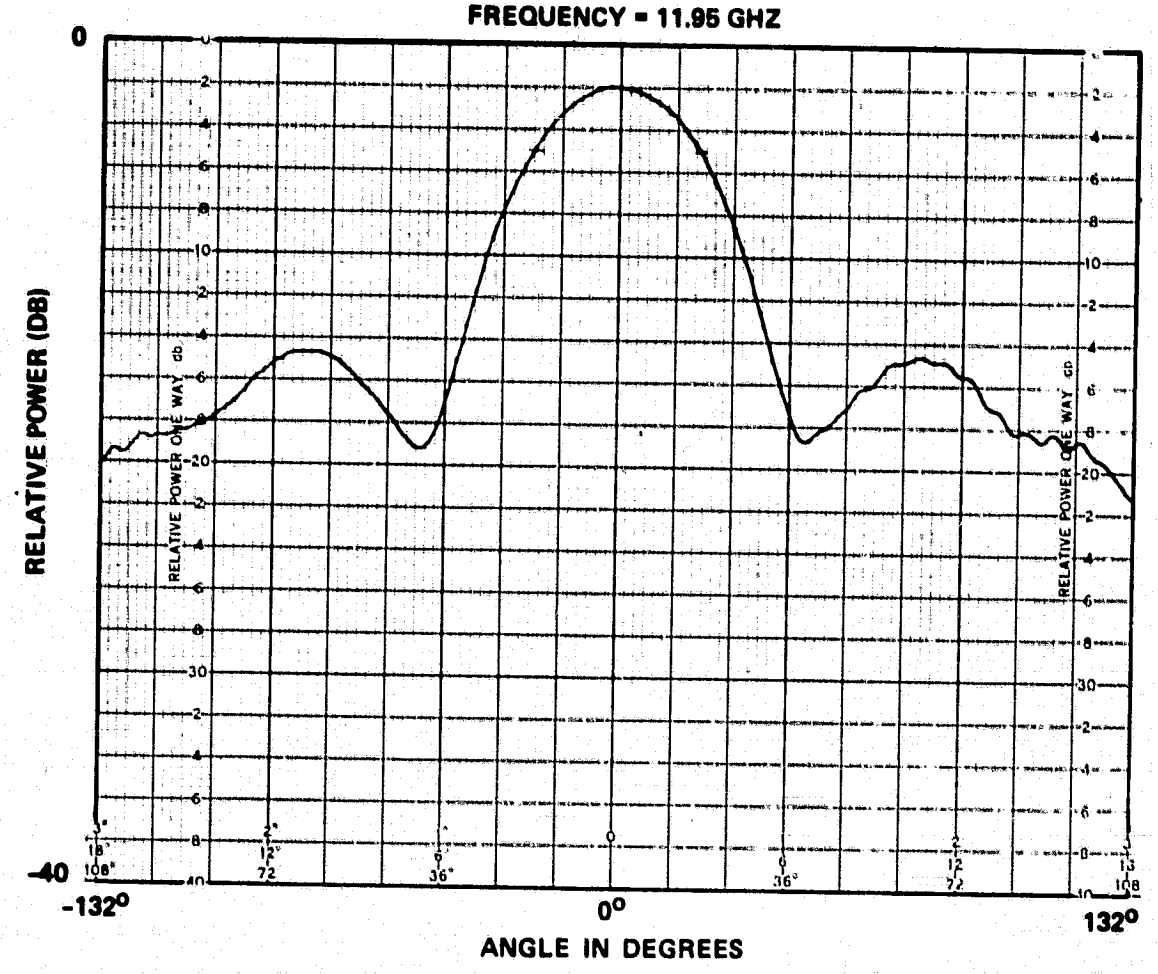

Figure 2.3-6a. E-Plane Radiation Pattern for 3.7 cm Square Aperture Horn

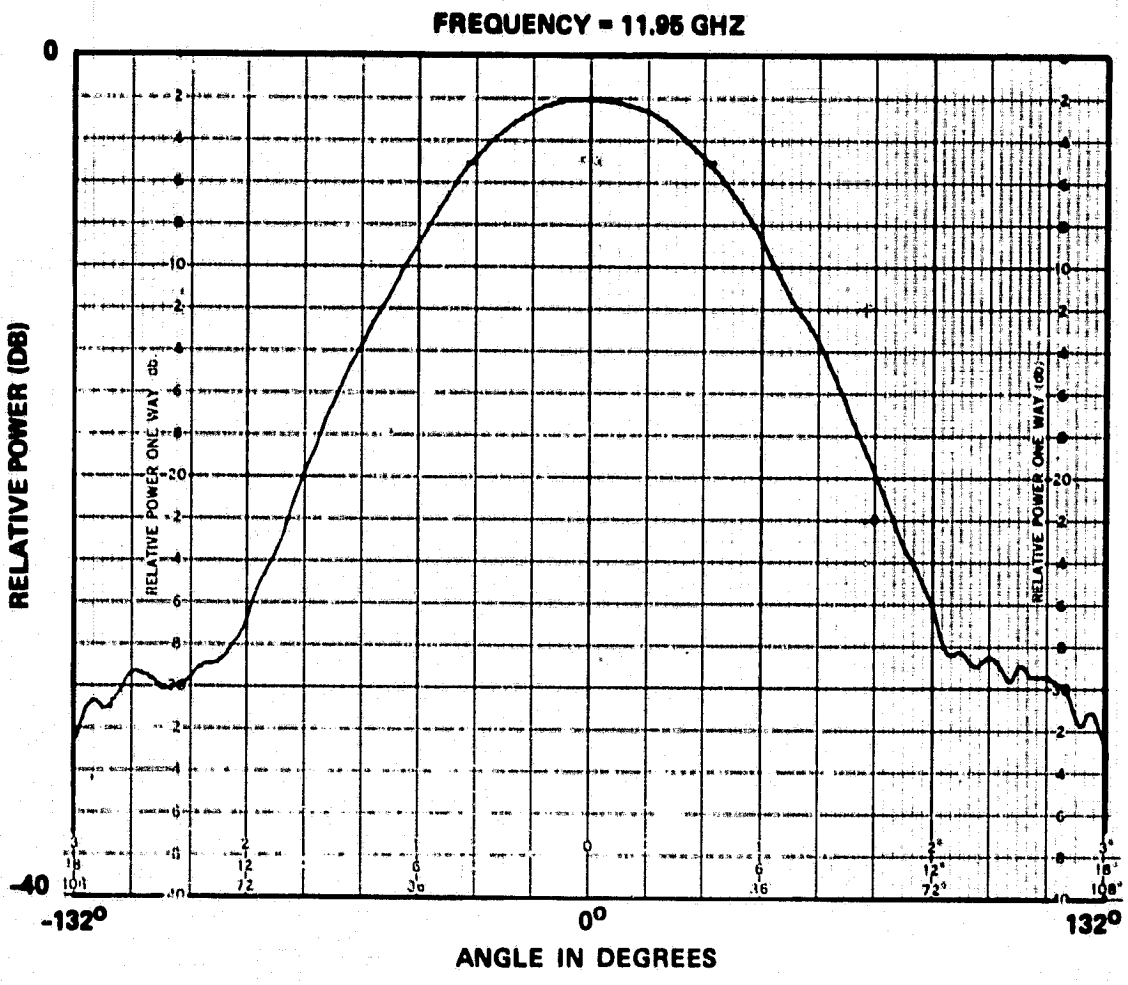

Figure 2.3-6b. H-Plane Radiation Pattern for 3.7 cm Square Aperature Horn

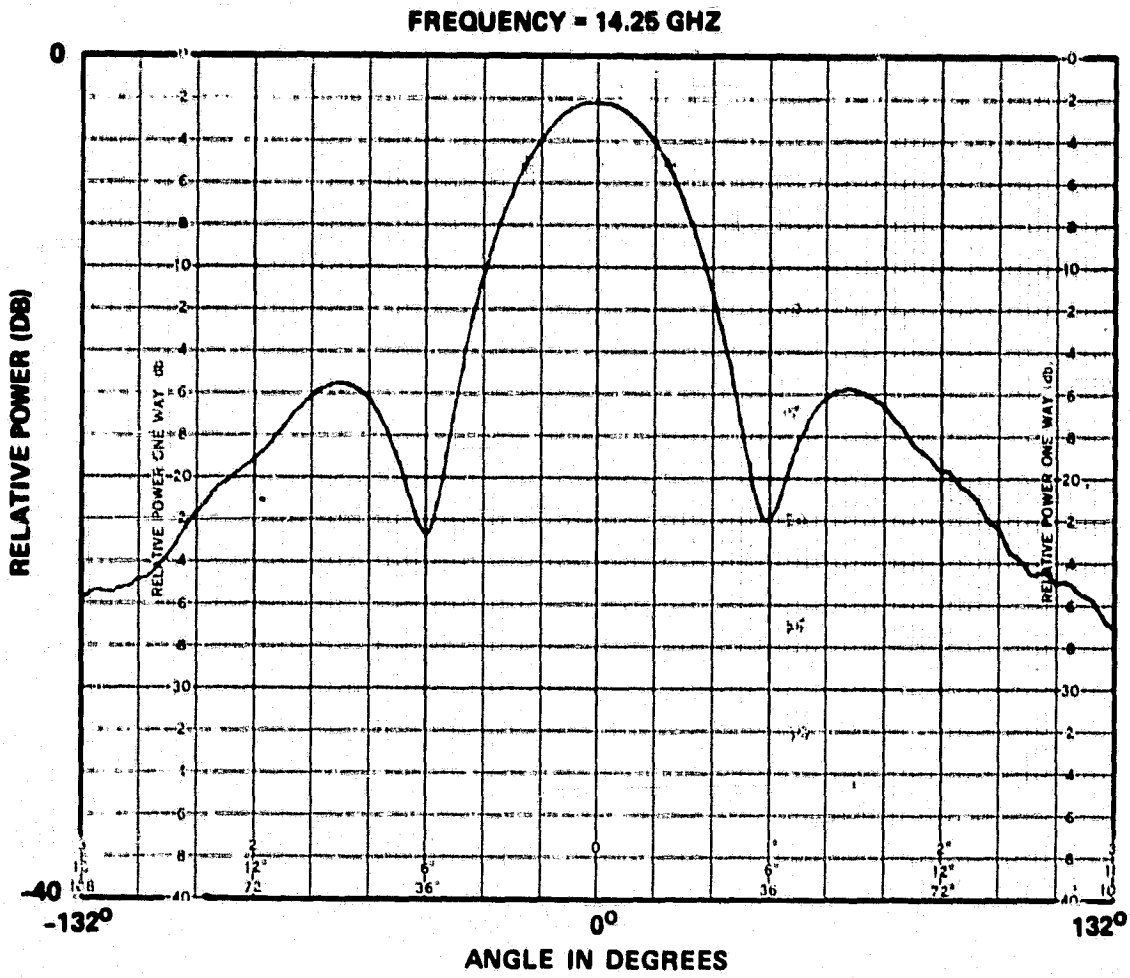

Figure 2.3-6c. E-Plane Radiation Pattern for 3.7 cm Square Aperature Horn

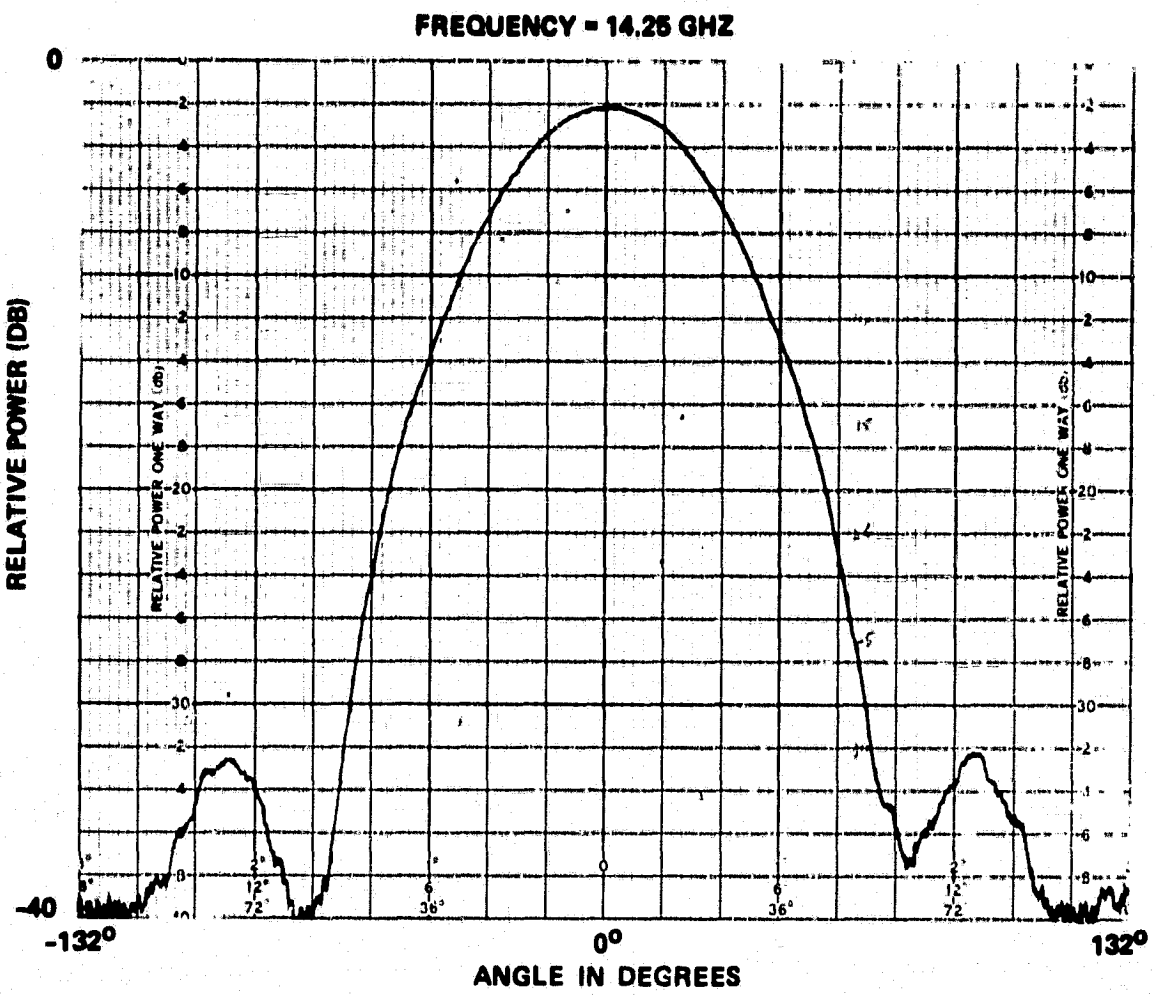

Figure 2.3-6d. H-Plane Radiation Pattern for 3.7 cm Square Aperture Horn

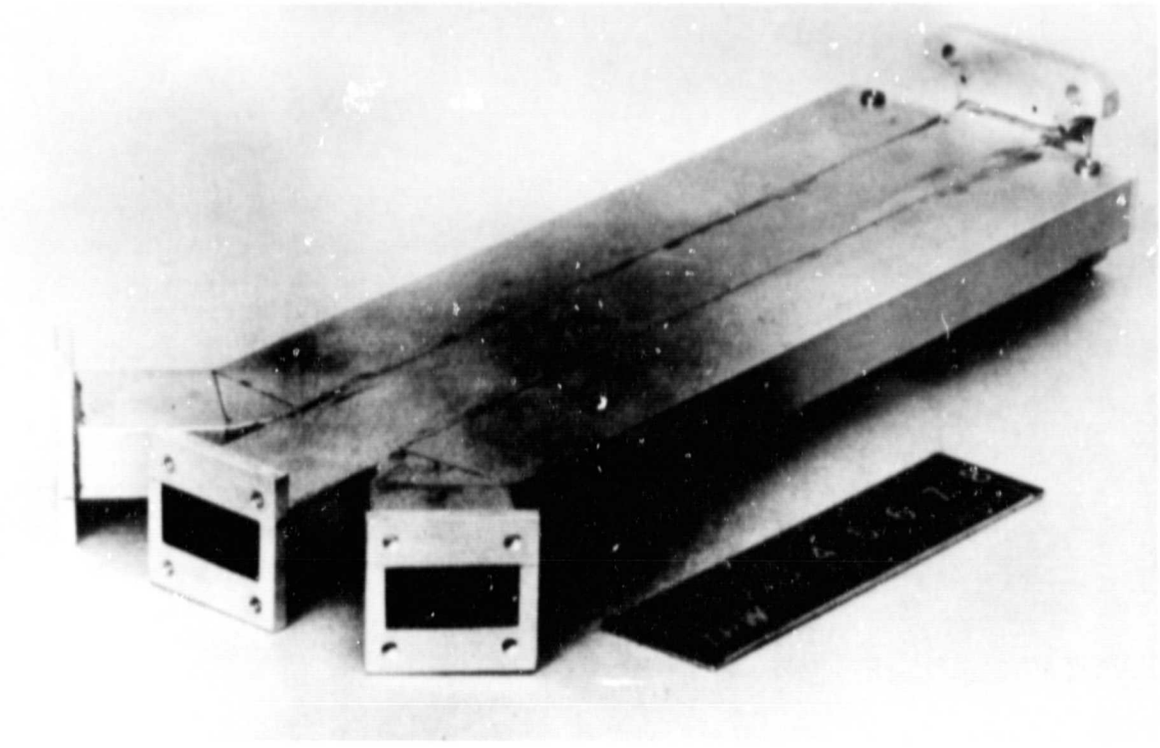

141872-77

Figure 2.3-7. First Breadboard Three-Way Septum Power Divider

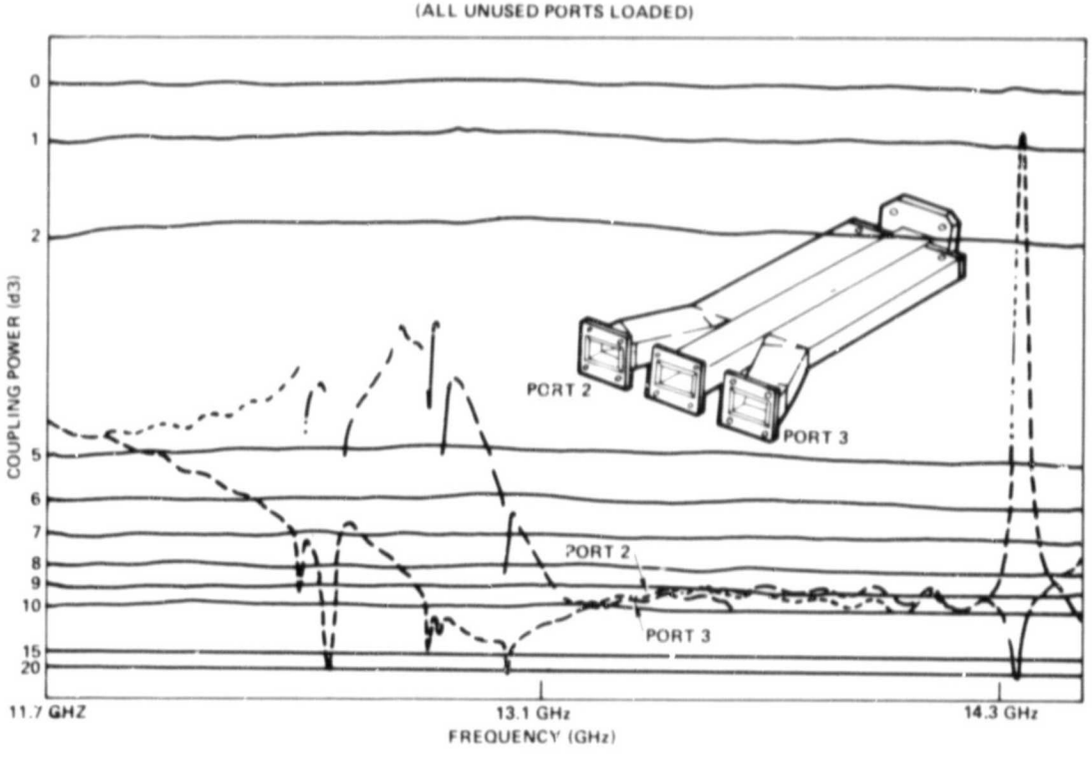

Figure 2.3-8. Coupling Performance of 8 dB Double Sidewall Directional Coupler

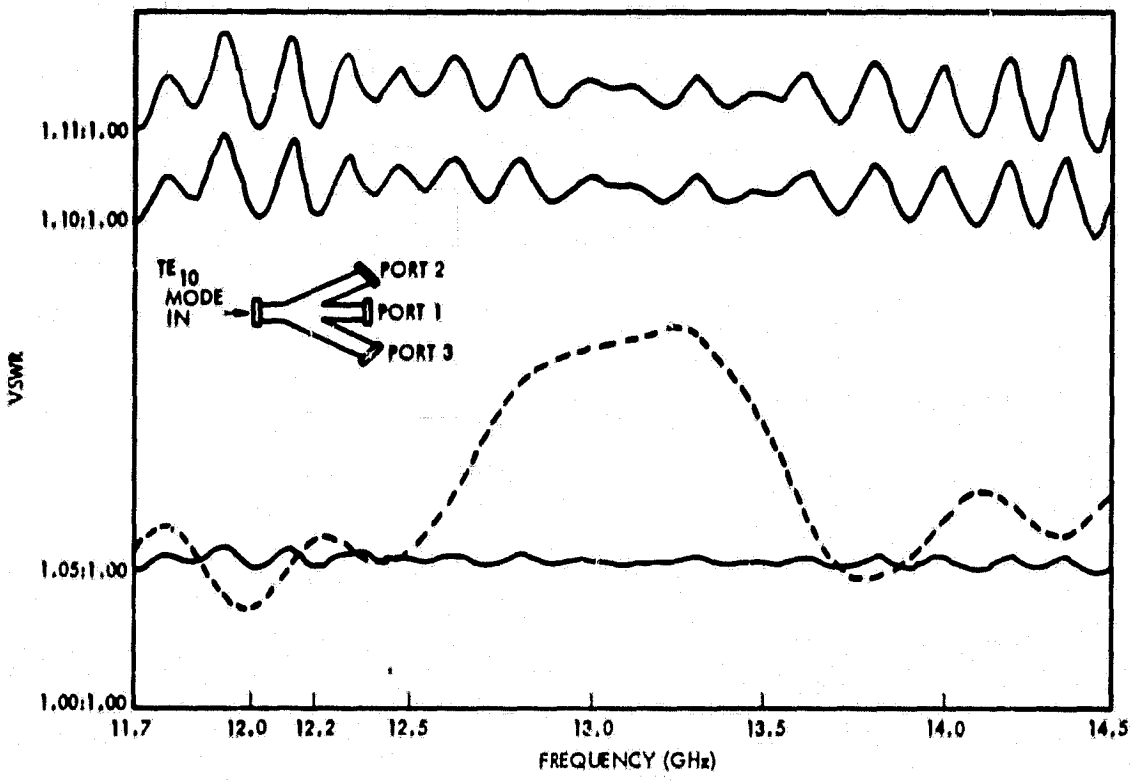

Figure 2.3-9a. VSWR of 4 dB Septum Power Divider (with Tapered Transformers)

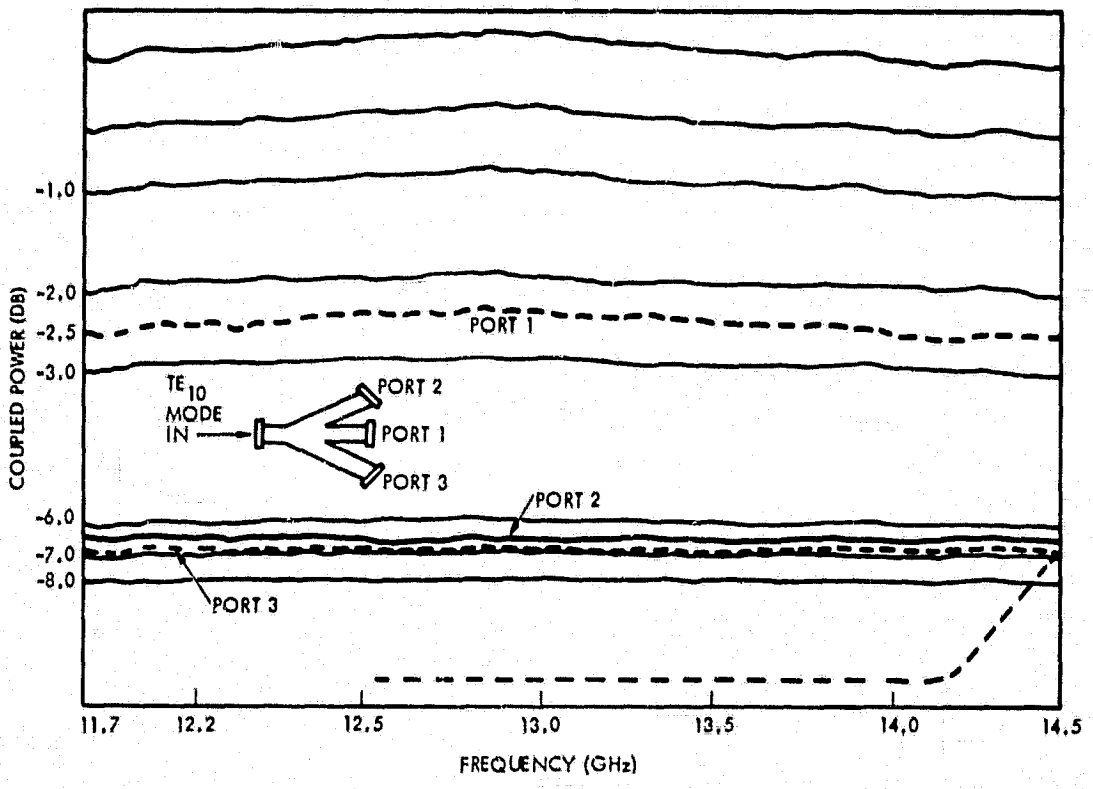

Figure 2.3-9b. Coupling Performance of 4 dB Septum Power Divider (with Tapered Transformers)

Based on the bandwidth and simplicity consideration the two-stage septum power divider network was chosen as the final feed network to be used. This feed circuit required 4 and 8 dB three-way dividers, a 90-degree twist for polarization matching, and a feed horn radiator.

The 4 and 8 dB power division was accomplished by proper placement of the septums in the main guide path. The impedance was transformed to match that of the standard size waveguide. This was done by a tapered line in one case and a series of step transformations in another case. While both yielded satisfactory results, the step transformer greatly reduced the overall divider length and thus provided lower waveguide ohmic loss. Care must be taken in matching a divider. Measuring the VSWR at the input of the feed masks any reflections taking place in the coupled ports. Thus, each port must be matched independently. Once the coupling and VSWR tasks were resolved, attention was given to phase matching each of the ports.

The path lengths to the outer output ports of the divider are longer than those to the center port. To eliminate this difference, several phase compensation sections were examined. A dielectric filled waveguide and a short mitered U-bend phase shifter were fabricated and tested. Both sections exhibited narrow bandwidth. The bandwidth of the dielectric device was narrowed by phase dispersion with respect to frequency. The U-bend exhibited large VSWRs at a few in-band frequencies. Phasing of either transmit or receive, but not both, could be accomplished. At the cost of increasing the divider size, the center port was arched to increase its length. The arch was made up of a 90 degree bend and two 45 degree mitered corners. The 45 degree mitered corners were also used in the outer ports arms. The VSWR of the 45 degree mitered corner, the center arm phasing section, and the outer port arm are shown in Figures 2.3-10a, b, and c.

Figure 2.3-11 shows the progression in power divider components. First, a divider using a tapered matching transformer was fabricated. Next, the tapered sections were replaced by a series of approximately 1/4 wavelength steps. The step lengths differ from 1/4 wavelength because of the length correction for discontinuity capacitances. The final stage was to electroform the step transformer divider.

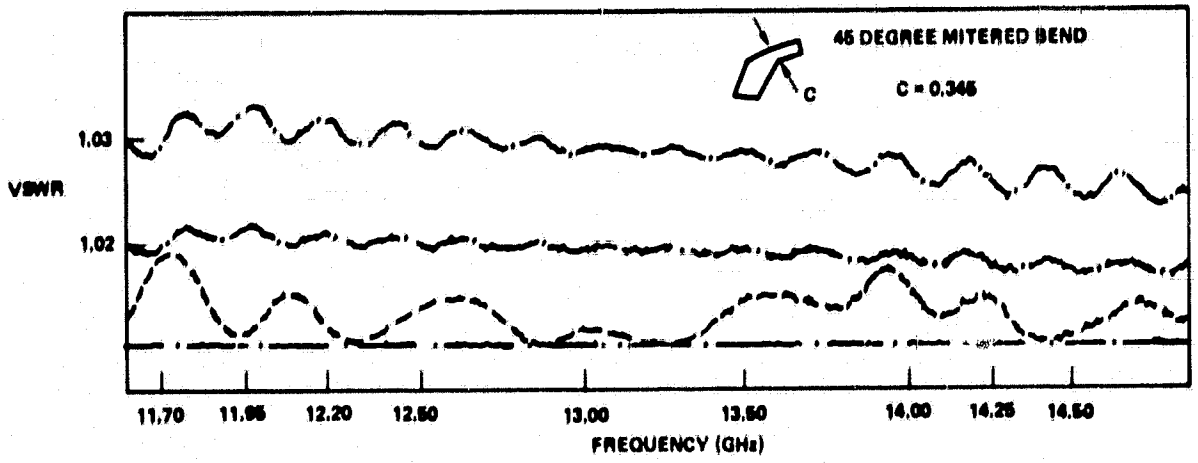

Figure 2.3-10a. VSWR of 45 Degree Mitered Bend (Used in 3-Way Power Dividers)

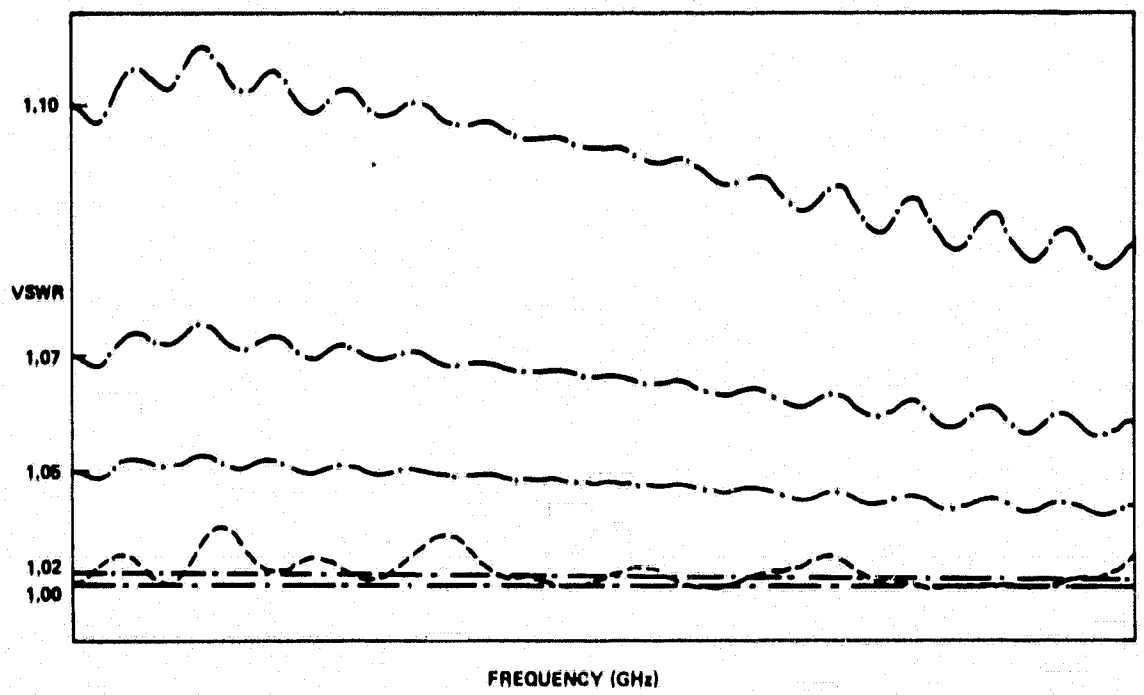

Figure 2.3-10b. VSWR of Center Arm Phase Compensation Section (Used in 3-Way Power Dividers)

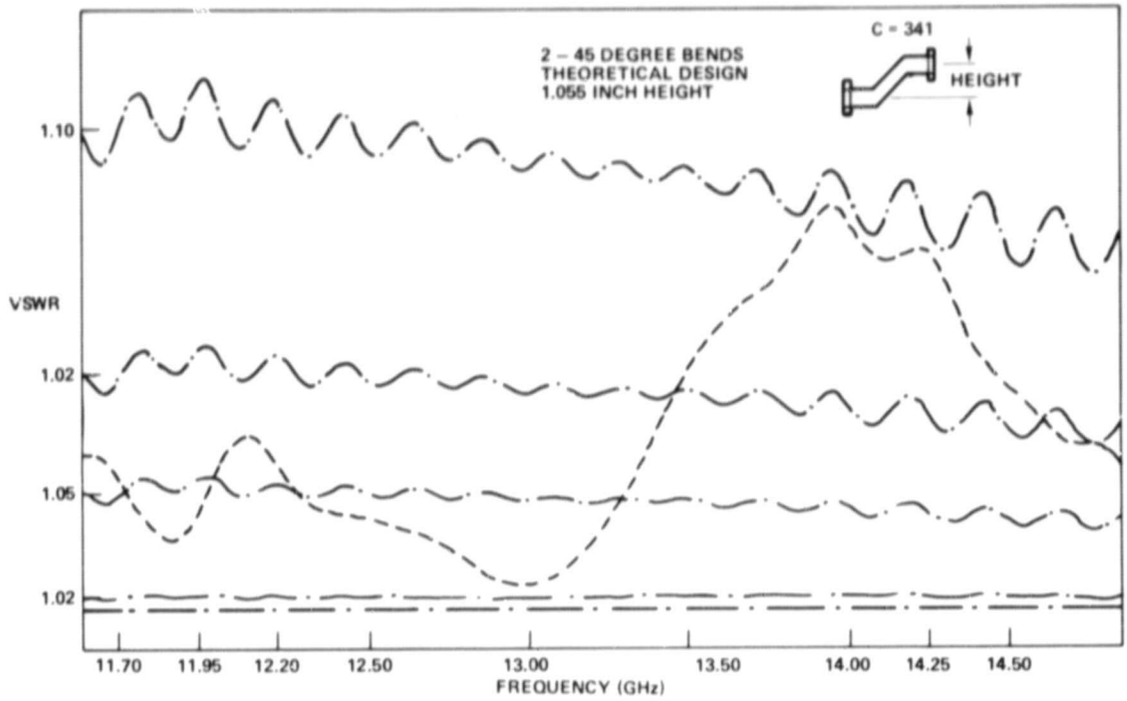

Figure 2.3-10c. VSWR of Side Port in 3-Way Power Dividers (Stepped Transformer not Included)

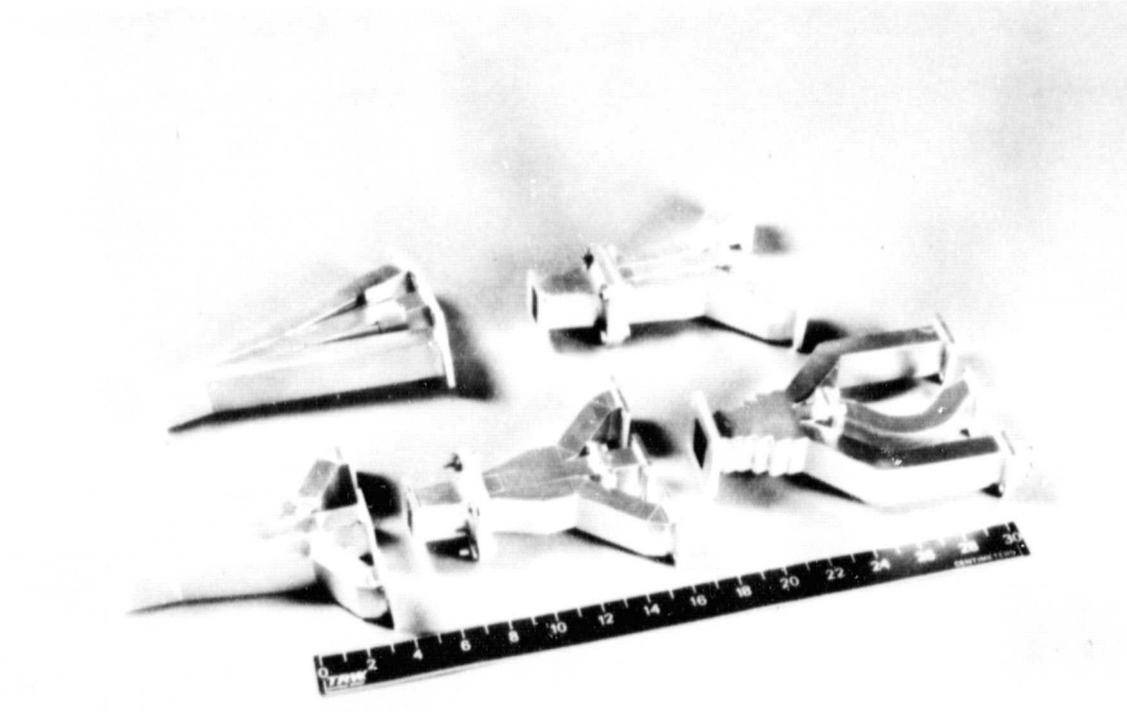

144931-78

Figure 2.3-11. Breadboard Three-Way Power Divider

To match the waveguide openings between the input and output power dividers, a 90-degree waveguide step twist was fabricated. The step twist was made up of three adjoining straight rectangular waveguide sections twisted about their common axis at their junction faces according to a binomial rule. These angles of rotation are proportioned 1:2:1. The twist faces are separated by approximately 1/4 wavelength. VSWRs for three 90 degree breadboard twists are plotted in Figure 2.3-12.

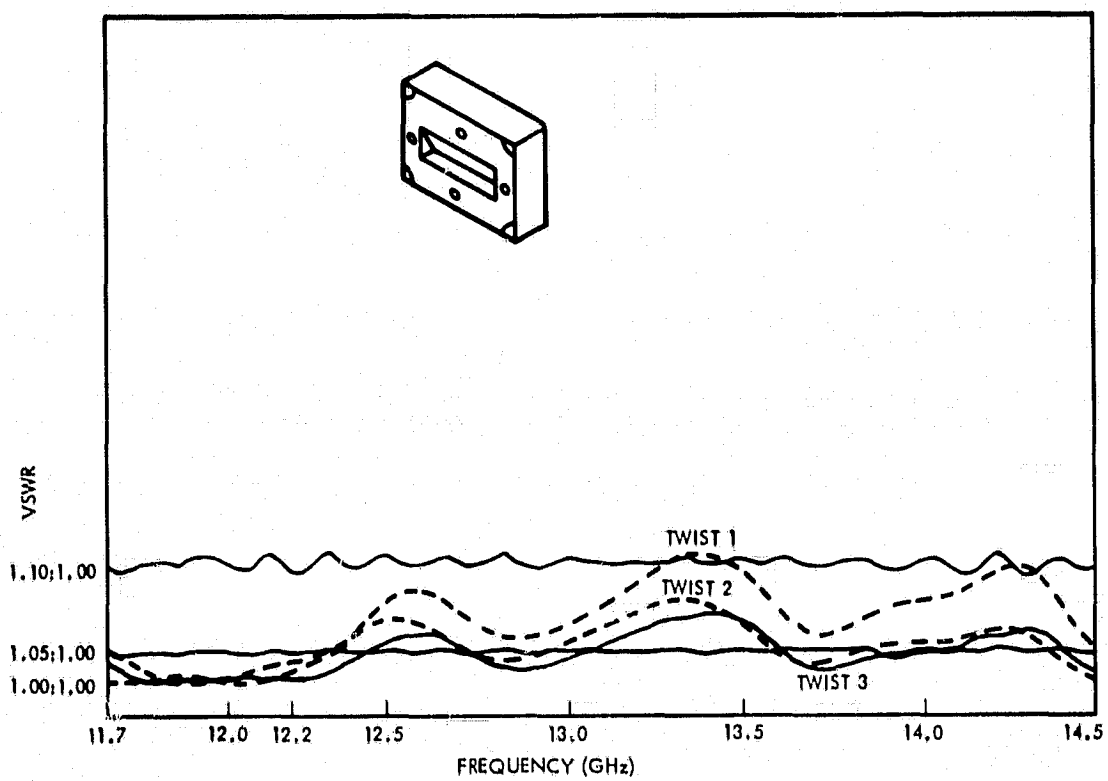

Figure 2.3-12. VSWR of 90 Degree Waveguide Twist

2.3.3 Feed Assembly and Test

A picture of the first breadboard feed is shown in Figure 2.3-13. Individual components used in the assembly were:

- Nine waveguide horns (machined and soldered)
- Four electroformed 8 dB E-plane set power dividers
- Three 90 degree waveguide twists (machined and broached)
- Four phasing sections (machined and soldered)
- Four input step transformers (machined and soldered).

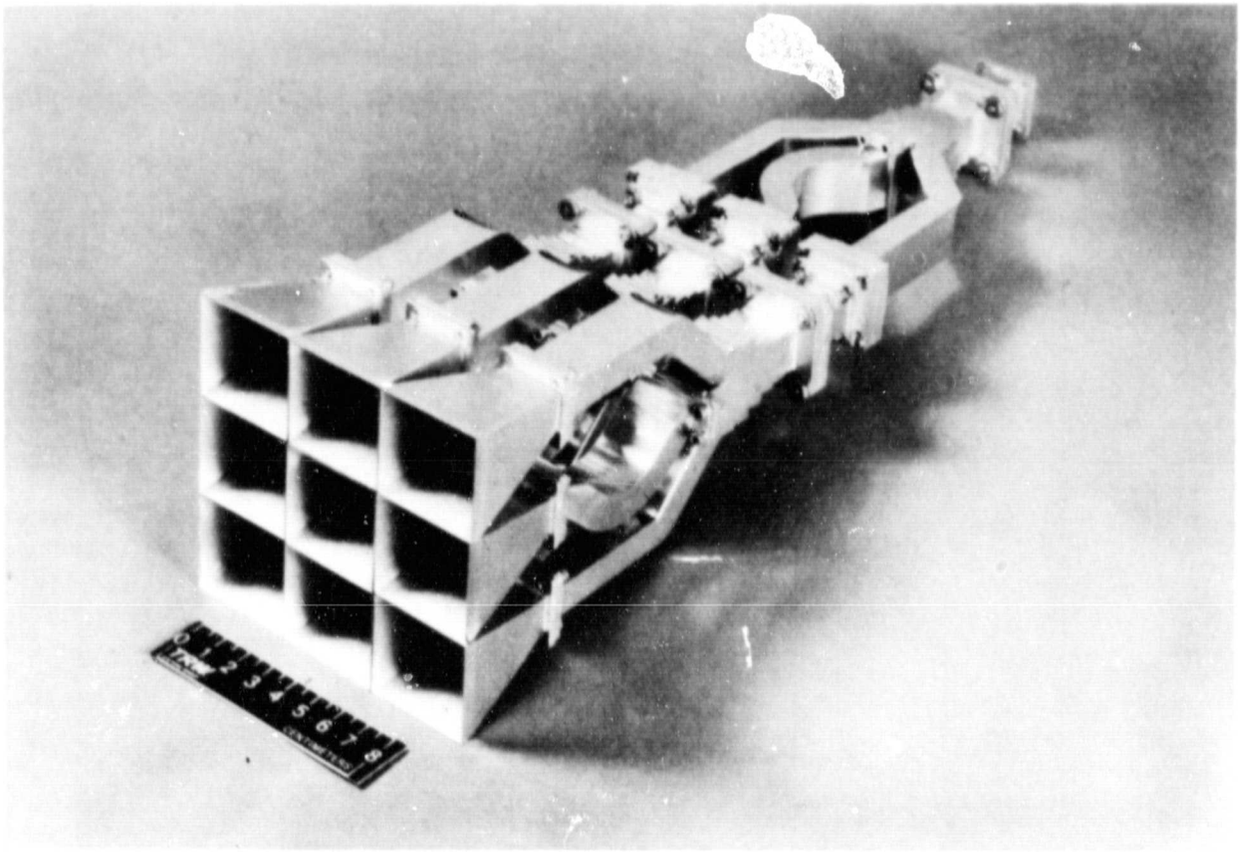

145227-78

Figure 2.3-13. First Breadboard of Nine-Horn Array Feed

The measured performance of four typical individual electroformed 8 dB power dividers is shown in Figures 2.3-14a and b. Test results on an integral unit, which consist of VSWR, coupling, insertion loss, and phase measurements, are shown in Figures 2.3-15a, b, and c. E-plane and H-plane primary feed patterns were taken in an anechoic chamber. Comparison of the measured primary patterns for a brassboard circular spot beam feed and theoretically calculated patterns are presented in Figures 2.3-16a, b, c, and d.

PERFORMED ON FOUR ELECTROFORMED 8 DB

E-PLANE SEPTUM POWER DIVIDERS WITH PHASING SECTION INCORPORATED

FREQUENCY (GHZ)	VSWR	COUPLING (RELATIVE TO CENTER PORT)		PATH LENGTH (DEGREES) (RELATIVE TO CENTER PORT)	
		PORT 2	PORT 3	PORT 2	PORT 3
		POWER DIVIDER NUMBER 1			
11.7	1.05	8.23	8.30	-1.04	-1.08
11.95	1.05	8.04	8.07	-0.78	-0.80
12.2	1.07	8.19	8.17	-0.40	-0.22
14.0	1.02	8.10	8.34	-0.29	+1.20
14.25	1.04	8.30	8.64	-1.06	+0.77
14.5	1.03	8.19	8.72	-3.31	-1.54
		POWER DIVIDER NUMBER 2			
11.7	1.07	7.92	7.78	+3.07	+1.90
11.95	1.07	7.93	7.85	+2.68	+1.16
12.2	1.03	7.97	7.89	+2.68	+0.58
14.0	1.01	8.14	8.0	+3.24	+0.05
14.25	1.03	8.28	8.11	+3.10	-0.86
14.5	1.02	8.42	8.08	+2.24	-2.71

Figure 2.3-14a. Measurements of VSWR, Coupling, and Path Length

PERFORMED ON FOUR ELECTROFORMED 8 DB

E-PLANE SEPTUM POWER DIVIDERS WITH PHASING SECTION INCORPORATED

FREQUENCY (GHZ)	VSWR	COUPLING (RELATIVE TO CENTER PORT)		PATH LENGTH (DEGREES) (RELATIVE TO CENTER PORT)	
		PORT 2	PORT 3	PORT 2	PORT 3
		POWER DIVIDER NUMBER 3			
11.7	1.07	7.96	8.03	+1.91	+0.71
11.95	1.06	7.91	7.98	+2.44	+1.36
12.2	1.06	8.16	8.16	+2.66	+1.24
14.0	1.02	8.22	8.28	+3.33	-0.21
14.25	1.05	8.33	8.3	+2.08	-1.71
14.5	1.02	8.29	8.12	+1.11	-3.12
		POWER DIVIDER NUMBER 4			
11.7	1.06	8.09	8.09	+1.3	+0.87
11.95	1.05	7.95	7.97	+1.76	+0.61
12.2	1.06	8.05	8.06	+2.22	+0.95
14.0	1.02	8.08	8.12	+1.97	+0.31
14.25	1.04	8.21	8.26	+2.24	+0.43
14.5	1.03	8.30	8.37	+0.78	-1.17

Figure 2.3-14b. Measurements of VSWR, Coupling, and Path Length

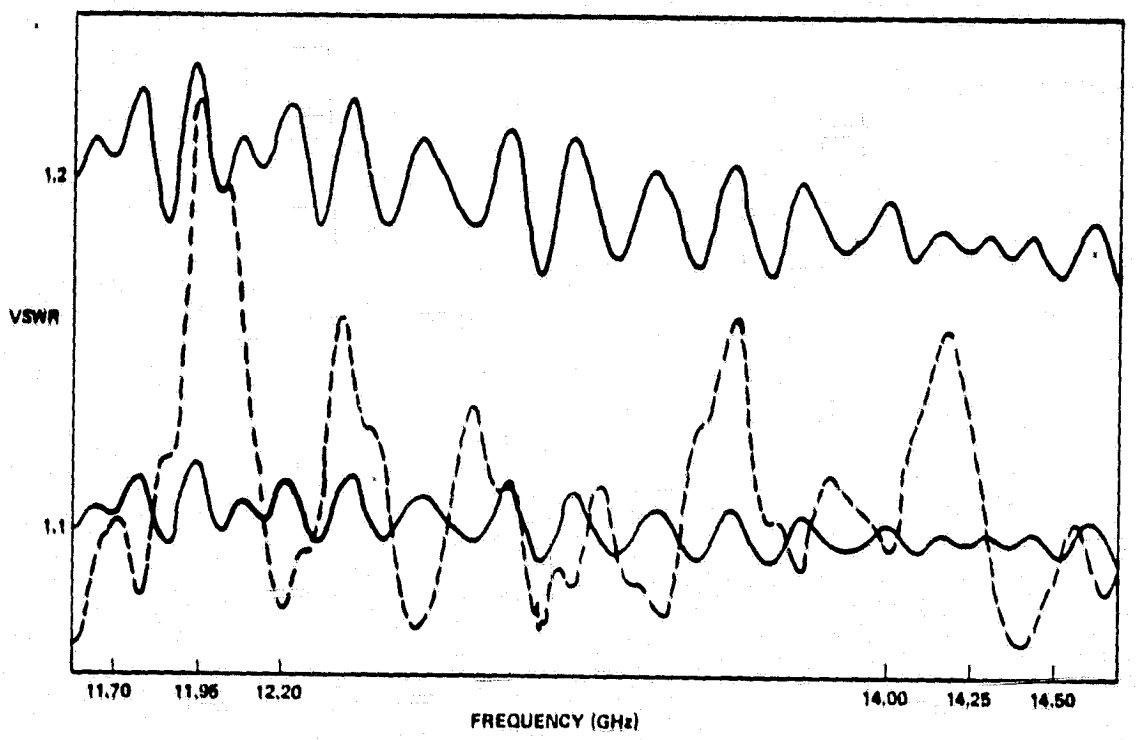

Figure 2.3-15a. VSWR of Breadboard 9-Horn Feed Cluster

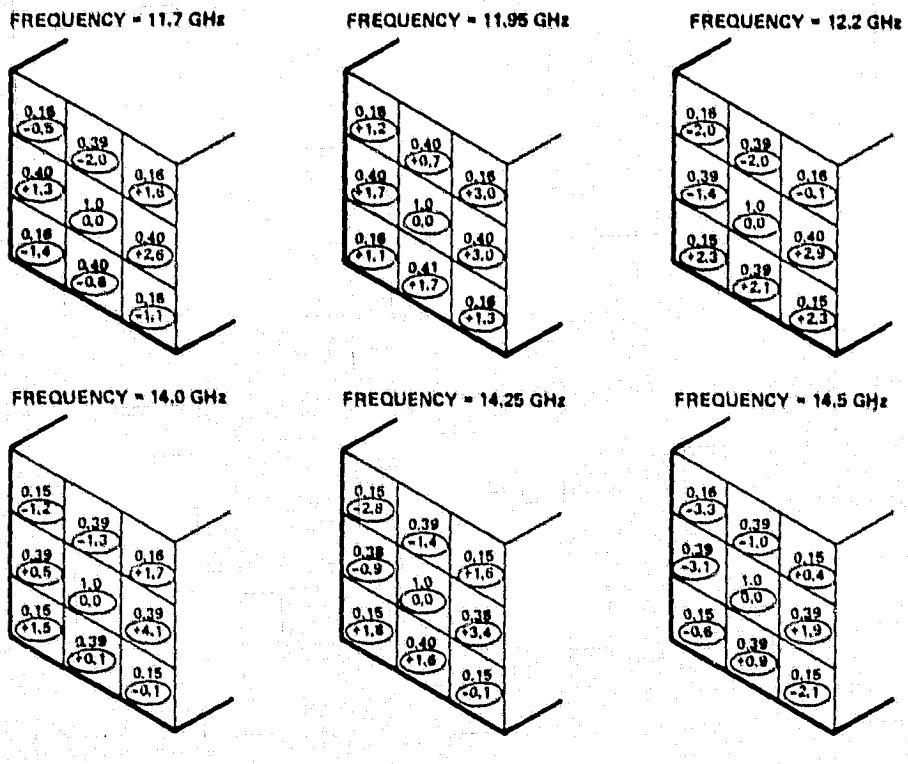

Figure 2.3-15b. Measured Amplitude and Phase (Circled) Distribution to Square Horns

FREQUENCY (GHZ)	FEED CIRCUIT LOSS (DB)
11.7	0.14
11.95	0.19
12.20	0.18
14.0	0.15
14.25	0.11
14.5	0.19

Figure 2.3-15c. Breadboard 9-Horn Cluster Feed Circuit Loss

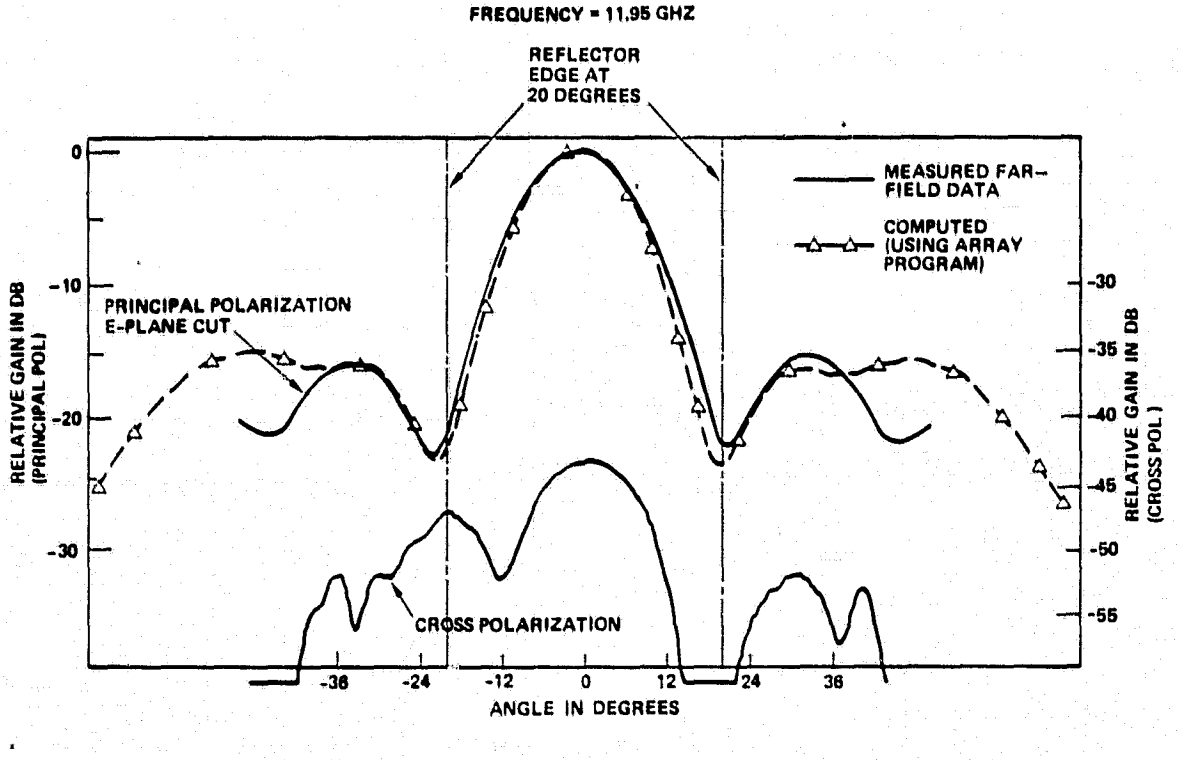

Figure 2.3-16a. Measured and Computed Primary Patterns of Breadboard 9-Horn Cluster Feed

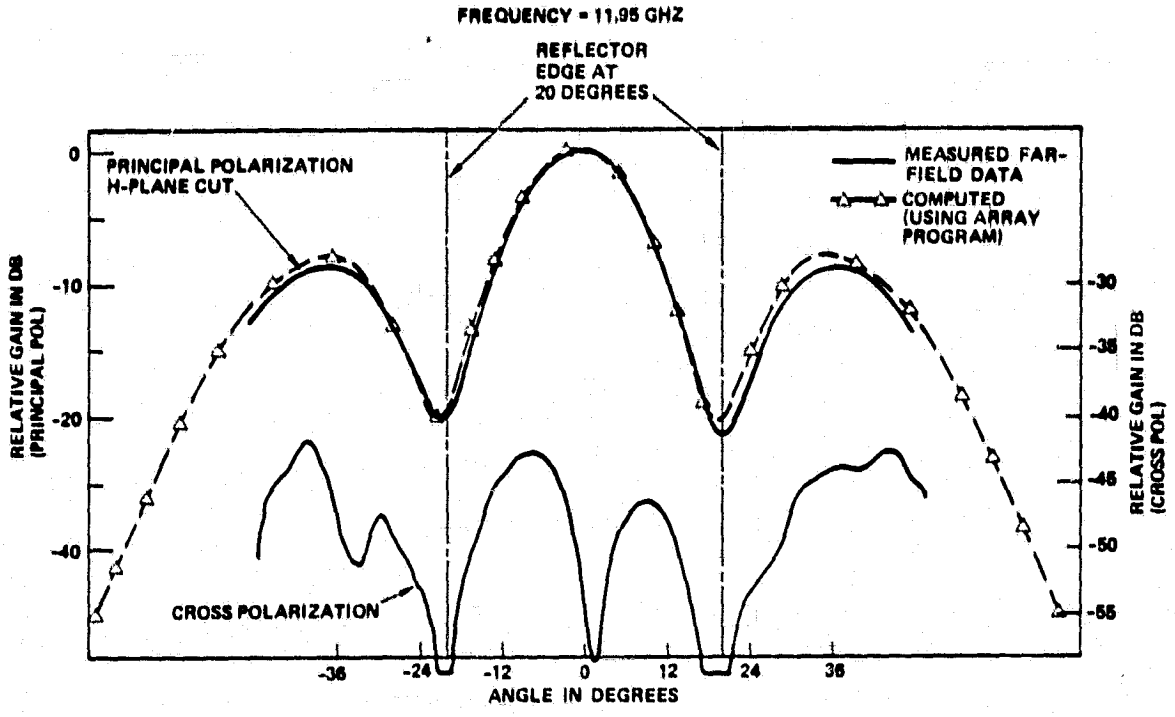

Figure 2.3-16b. Measured and Computed Primary Patterns of Breadboard 9-Horn Cluster Feed

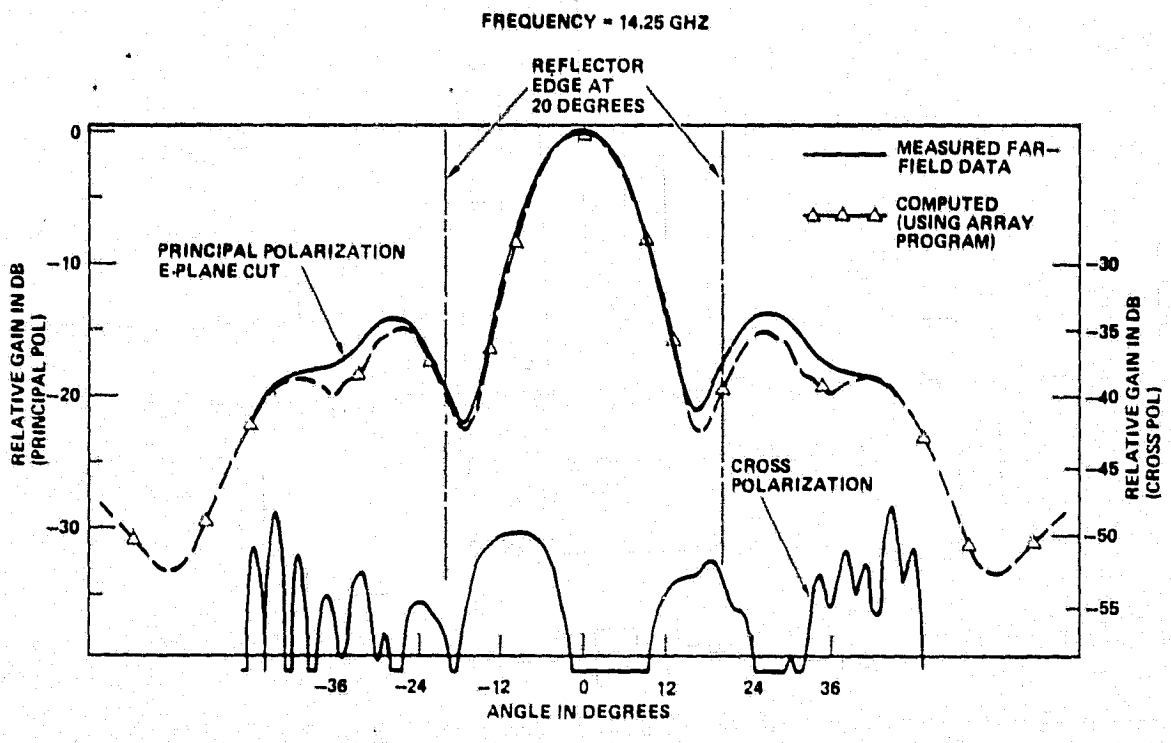

Figure 2.3-16c. Measured and Computed Primary Patterns of Breadboard 9-Horn Cluster Feed

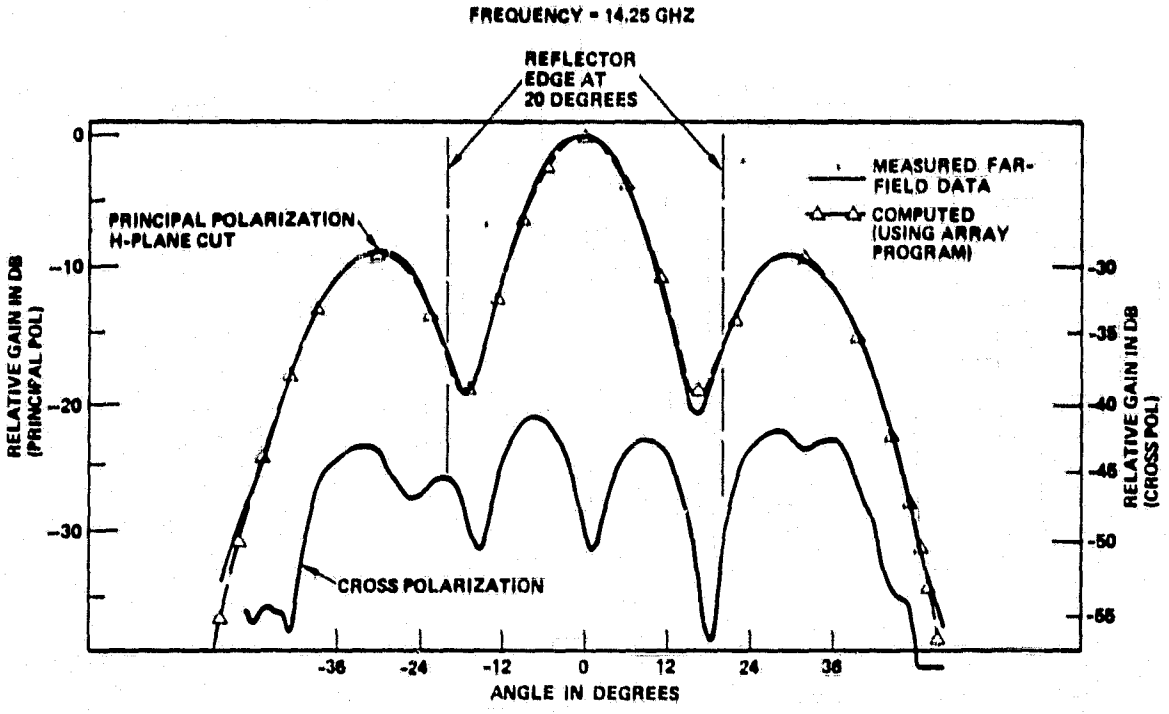

Figure 2.3-16d. Measured and Computed Primary Patterns of Breadboard 9-Horn Cluster Feed

A breadboard elliptical spot beam feed was also assembled and tested. For this feed, the 8 dB input power divider was replaced by a 4 dB divider. Measured VSWR, coupling, insertion loss, and output phase are presented in Figures 2.3-17a and b. The radiation patterns of the elliptical beams are asymmetrical. Two orthogonally polarized beams are achieved by two combinations of these 4 and 8 dB dividers. The first combination consists of one 4 dB input and three 8 dB output dividers to yield a horizontally polarized elliptical beam. The second combination consists of one 8 dB input and three 4 dB output dividers to obtain vertically polarized elliptical beam.

2.3.4 High Power Test

High power tests were conducted on a circular spot beam feed. Transmitted and reflected power was monitored by the setup shown in Figure 2.3-18. Checks were made for the occurrence of high power corona in the feeds by monitoring the return loss and the trasmitted signal while operating in a vacuum. The procedure was: (1) set up the equipment as shown in

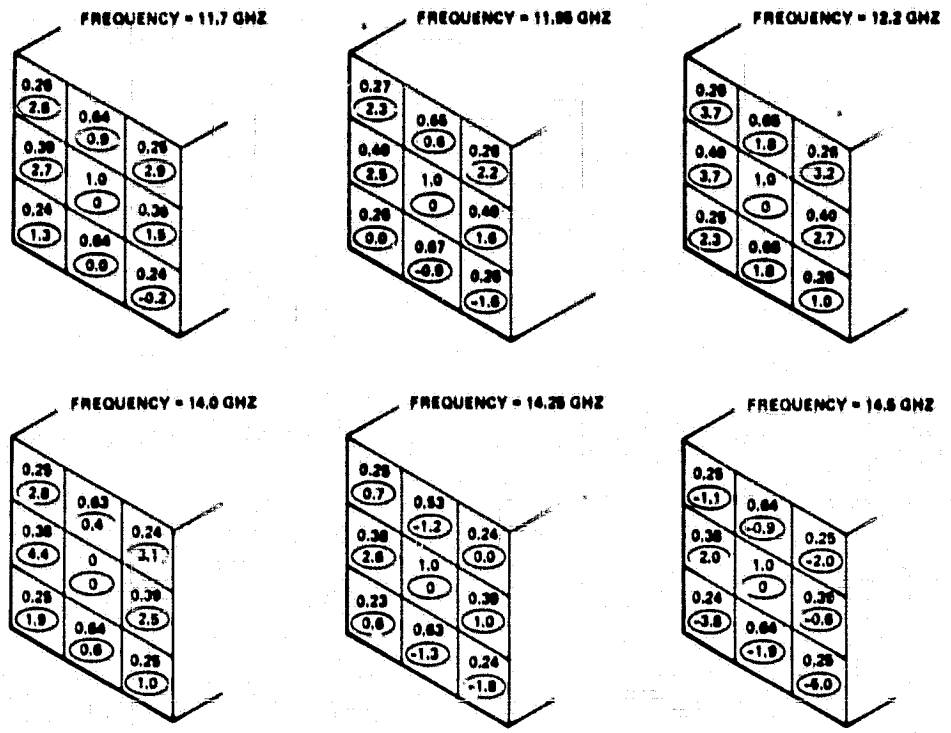

Figure 2.3-17a. Measured Amplitude and Phase (Circled) Distribution of Square Horns for Elliptical Spot Beam Feed

FREQUENCY (GHZ)	FEED CIRCUIT LOSS (DB)
11.7	0.17
11.95	0.23
12.20	0.25
14.0	0.22
14.25	0.17
14.5	0.16

Figure 2.3-17b. Breadboard 9-Horn Cluster Feed Circuit Loss for Elliptical Spot Beam Feed

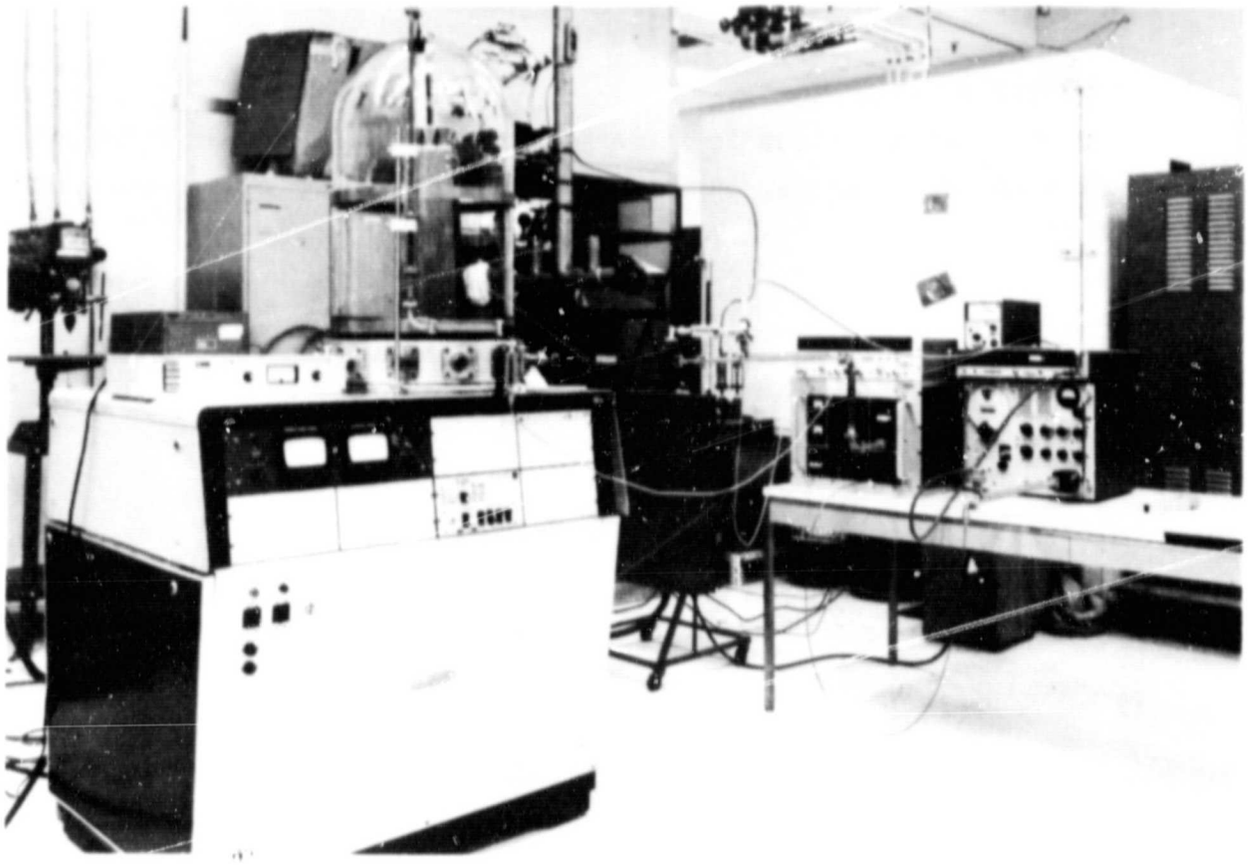

156582-79-22

Figure 2.3-18. High Power Test Setup

Figure 2.3-18; (2) check high power at room pressure (system checkout); (3) pump down vacuum bell jar to 10^{-6} torr; (4) turn on TWT; (5) increase power output on TWT; (6) record reading on reference power meter, reflection power meter, and radiated power meter; and (7) repeat for 11.95 GHz (TX) and 14.25 GHz (RX). The power levels supplied to the feed during the test were as follows:

1) For 11.95 GHz – 32 watts average for 20 minutes at 6.2×10^{-6} to 5.8×10^{-6} torr pressure, 68 watts average for 30 minutes at 5.8×10^{-6} to 5.5×10^{-6} torr pressure.

2) For 14.25 GHz – 46 watts average for 10 minutes at 5.5×10^{-6} to 5.4×10^{-6} torr pressure, 93 watts average for 20 minutes at 5.3×10^{-6} to 5.8×10^{-6} torr pressure.

No arching or distrubance of the operation was observed during the tests.

2.4 MECHANICAL DESIGN AND FABRICATION

2.4.1 Feed Design and Fabrication

The selected spot beam feed configuration shown in Figure 2.4-1 consist of nine square horns, three 90 degree twists, and four 3-way power dividers.

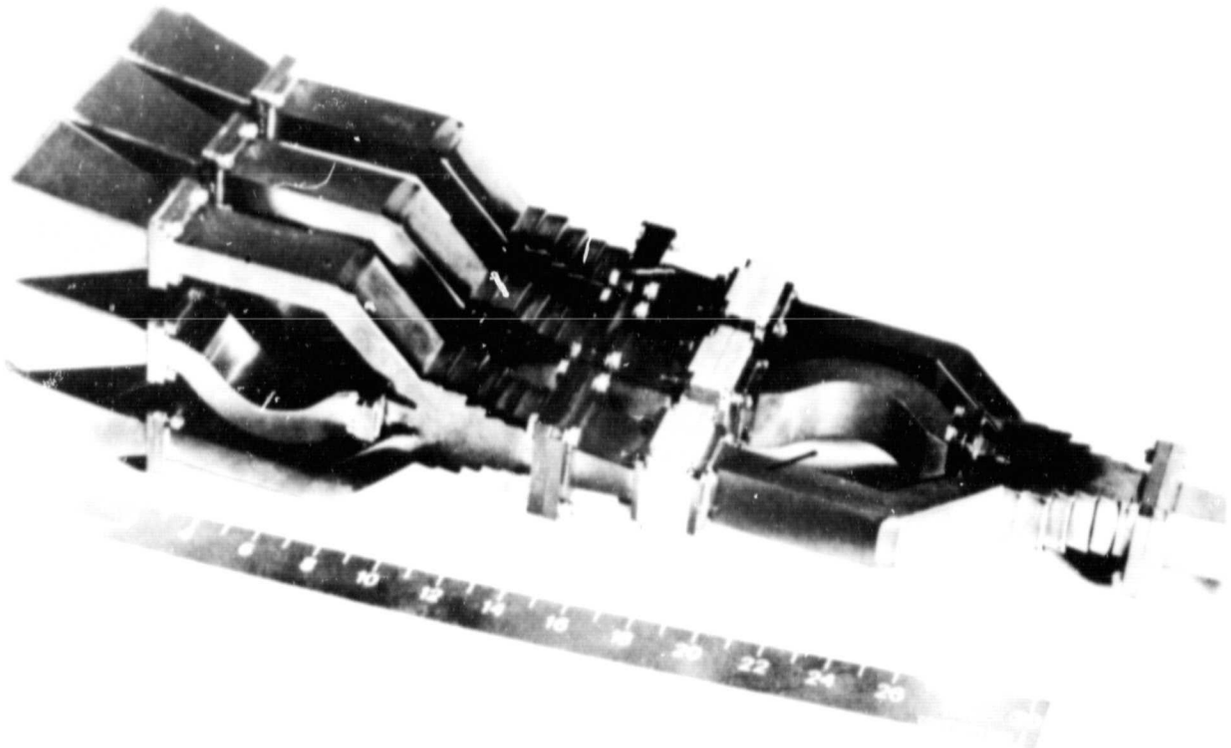

145228-78

Figure 2.4-1. Spot Beam Nine-Horn Array Feed

The square horns are inherently easy to align for good cross-polarization. These horns are relatively short, therefore reducing path length and weight.

There are only two different 3-way power dividers to be developed, 4 and 8 dB power split. These power dividers (4 and 8 dB) have the same basic configuration and the same external dimensions, which permits inter-

changeability and facilitates fabrication. Step transitions and step 90 degree twists are used to reduce total path length, thereby keeping waveguide insertion loss to a minimum. Tight tolerances and identical parts are easily produced making this configuration cost effective.

The square horns were initially fabricated by machining the walls from brass sheet and soldered to assemble. This technique proved difficult to produce identical parts and hold the required tolerance. The electroforming process with permanent mandrels is now utilized to produce the brass board horns. This process produced identical parts with excellent tolerance control at lower cost.

The 90 degree twist consists of two identical parts shown in Figure 2.4-2 doweled together such that the ports are rotated from each other. Each part is machined and broached from brass plate stock.

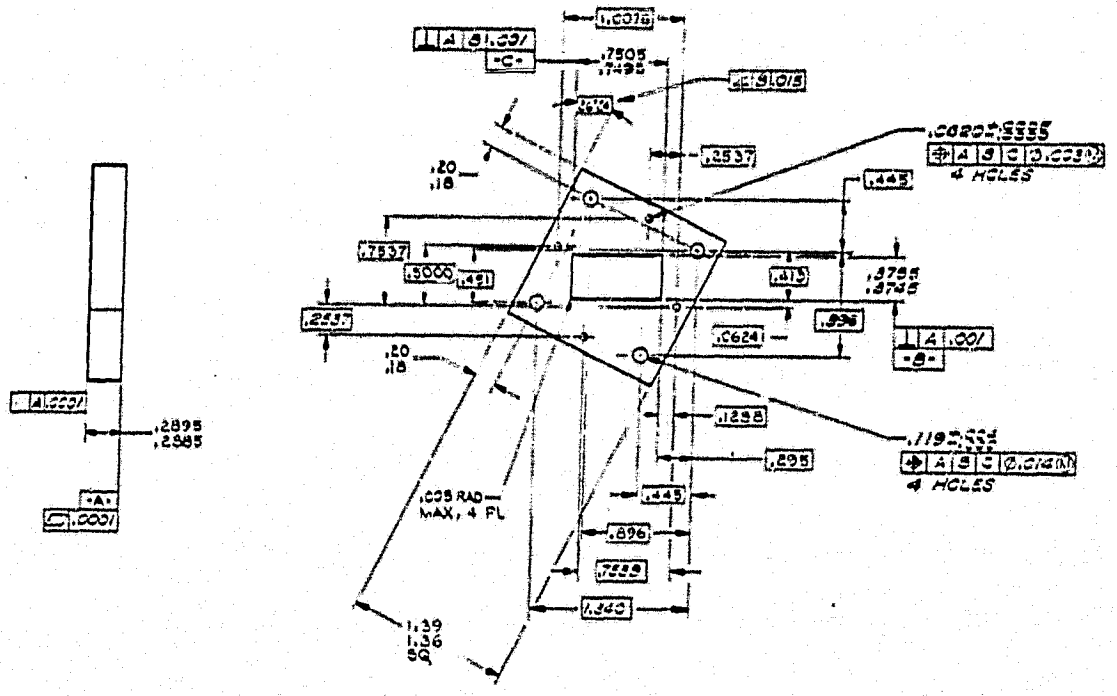

Figure 2.4-2. 90 Degree Waveguide Twist

The initial 3-way power dividers were machined from sections of waveguide and brass sheet stock to form the step transitions, septums, and bends. All these pieces were assembled, fixtured, and soldered together.

This fabrication technique proved too difficult to hold the required tolerance and power split. Insertion loss was marginal. Identical power dividers were impossible to make.

To solve these fabrication problems the electroforming process was implemented. This fabrication process is done in several stages.

The outside port mandrels are machined from a thermally stabilized block of aluminum, approximately 12 inches wide. The "E" plane dimensions including step transitions and bends are machined to finish size shown in Figure 2.4-3. This mandrel is then sliced over-size for the "H" plane dimensions. The adjacent parts are matched to reduce tolerance build-up.

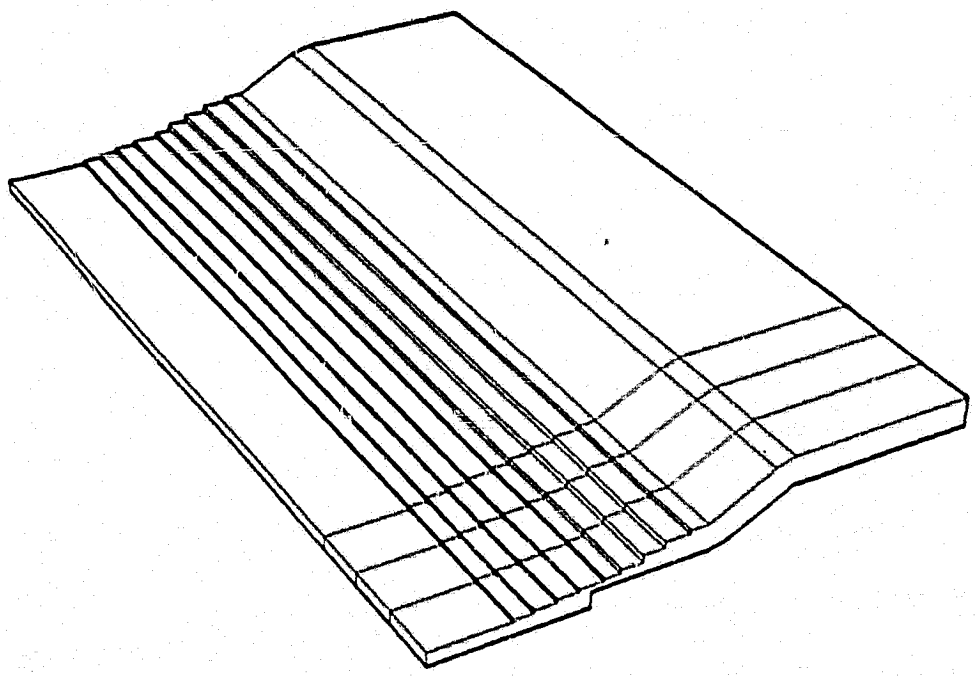

Figure 2.4-3. Mandrel for Step Impedance Transformer

The center port mandrel is designed with a path length compensation loop for correct phasing. This loop is machined from an aluminum tube, sectioned and dowel pinned in the mandrel assembly (Figure 2.4-4). The assembly is then electroformed with copper and machined to acquire the correct thickness for the "E" plane septums. A number of mandrels are cut over sized for the "H" plane dimension from this assembly. Two cut side

"Page missing from available version"

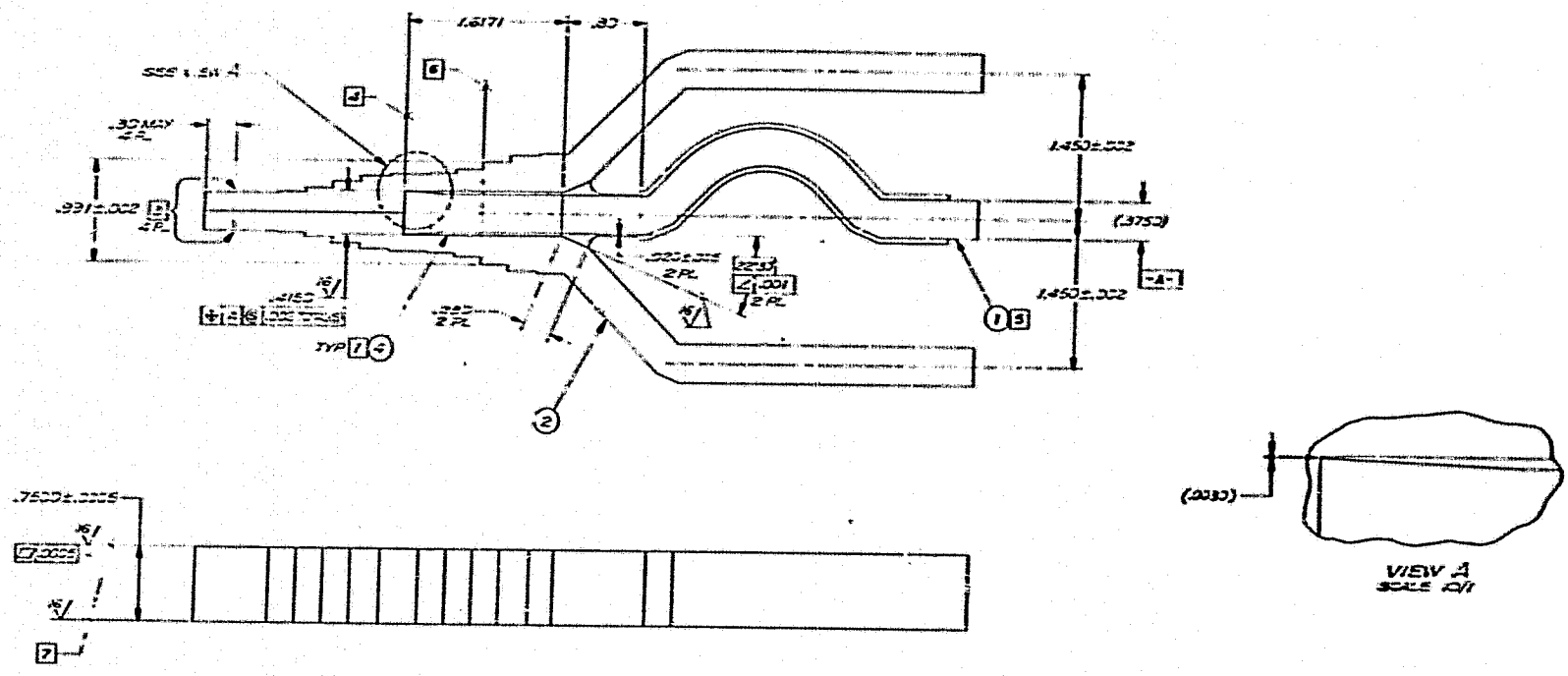

Figure 2.4-5. Complete Mandrel Assembly

material to be used in the double reflector system was tested for phase dispersion and insertion loss. These measurements were used to verify the computed reflectivity of the wire grid surface. Each reflector would be mounted on fiber glass studs attached to a support frame (Figure 2.4-6). They would be aligned by adjustment of the fiber glass studs.

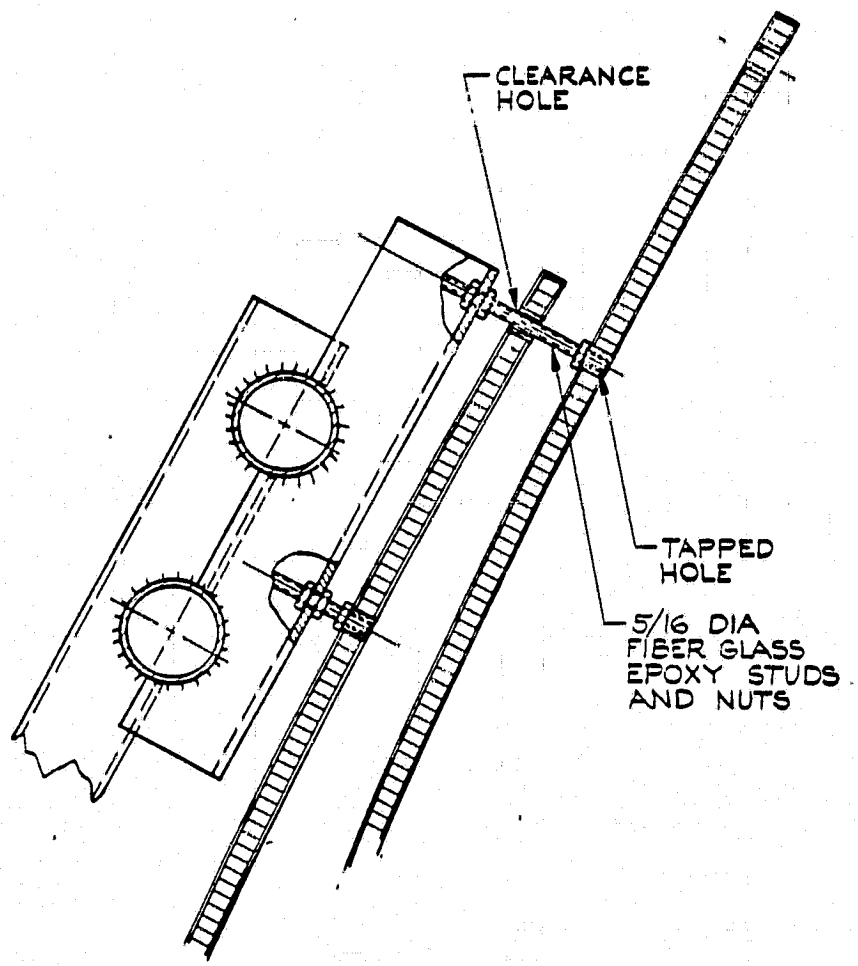

Figure 2.4-6. Dual Reflector Attachment and Mount

Even with the low loss material, the transmission of RF energy through and back out of the front reflector would be a significant loss. Also, a phase change could occur causing more loss. Further degradation of the patterns could be introduced by the variation and misalignment of the wire grid on the parabolic surface due to fabrication tolerance.

A decision was made to investigate the use of a wire grid subreflector approach as a replacement for the double wire grid parabolic reflector system. The wire grid would be used as a flat plate polarization diplexer.

Part of the feeds would see the grid surface as a Cassegrain subreflector. To the remainder of the feeds which operate in a front-fed reflector geometry, the surface would be transparent. The two feed groups would be isolated by orthogonality between their respective polarizations. By being able to set up the feed packages on both sides of the subreflector, the overall antenna geometry would be reduced.

The subreflector was designed with two 0.006 inch thick epoxy glass (G10) laminate face sheets and a 0.25 inch thick polyamid honeycomb core. One side of the panel has copper lines etched 1.4 mil thick, 3 mil wide and spaced 0.030 inch apart. Because of the limited size of the photo etching equipment, four wire grided face sheets were indexed and spliced together with doublers to make the size panel required. A 2 mil polyester film was bonded over the copper lines for protection. The subreflector support structure was designed and fabricated from polycarbonated plastic sheet to keep RF reflections to a minimum.

2.4.3 Offset Reflector Design and Fabrication

The single 2 meter diameter reflector was made up of graphite fiber reinforced plastic (GFRP) face sheets with an aluminum honeycomb core. The GFRP provides the reflective surface, thus, eliminating the need for metallization. Two face sheets, made from four plies of prepregnated GFRP cloth, were separately layed over a steel mold, vacuum bagged, and cured at 360^{o}F for 2 hours. The face sheets were then coated with an adhesive and placed on the mold again with a 1/2 inch thick aluminum honeycomb core placed between them. They were vacuum bagged and cured at room temperature, to reduce thermal distortions.

The offset reflector was assembled to the antenna support structure. The reflector surface was measured with calibrated dial indicators mounted to a metal template machined to the proper parabolic shape. The template was used to sweep the surface about a pivotal line along the reflector's principal axis. Readings taken from the dial indicators were used to align the reflector and to describe surface smoothness. Figure 2.4-7 is a pictorial diagram of the reflector surface contour plotted from measured data. The peak to peak deviations of the surface were about 0.035 inches. This yields a 0.012 inch rms surface error.

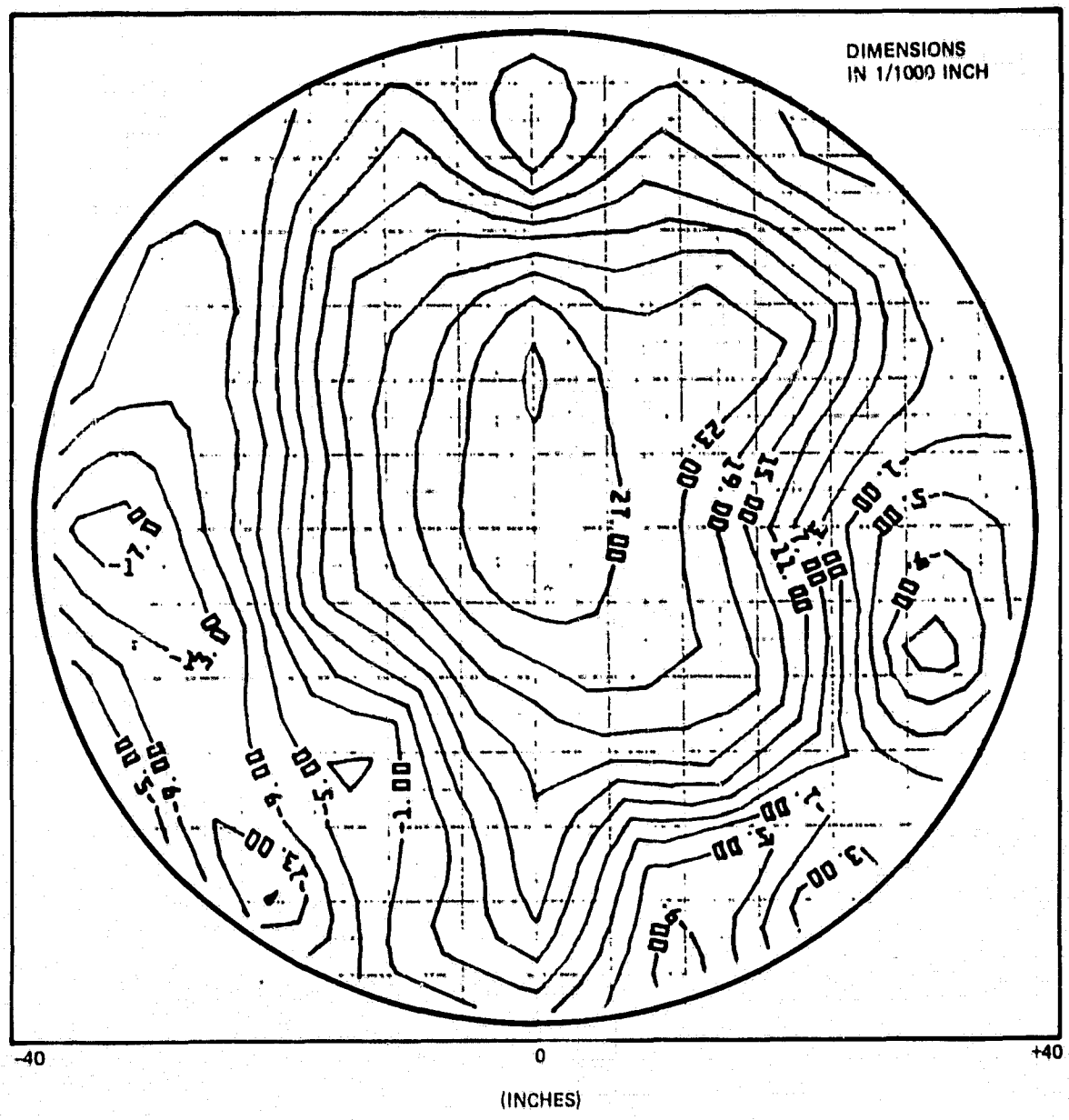

Figure 2.4-7. Measured Reflector Surface Contour

It is suspected that the difference of coefficient of expansion between the GFRP face sheets and the steel mold, caused by the high cure temperature, may have caused the reflector to be larger than the mold after cooling down. This is indicated by the shallow zone in the center of the reflector. The mold could be designed to compensate for this condition in

the future. Also contributing to distortion was the high cure resin used for the face sheets. Lower temperature cure resins would reduce internal stress levels, which in turn would reduce distortion. These lower temperature cure resins are available, but, they have not been qualified for a space environment.

2.5 FAR FIELD PATTERNS AND GAIN CONTOUR MEASUREMENTS

The reflector was separated from the support structure while being transported to the Capistrano Test Range. After arrival, the structure was mounted to the range positioner and the reflector was reattached to the assembly. A picture of this complete reflector feed assembly is shown in Figure 2.5-1. The offset reflector surface was measured with calibrated

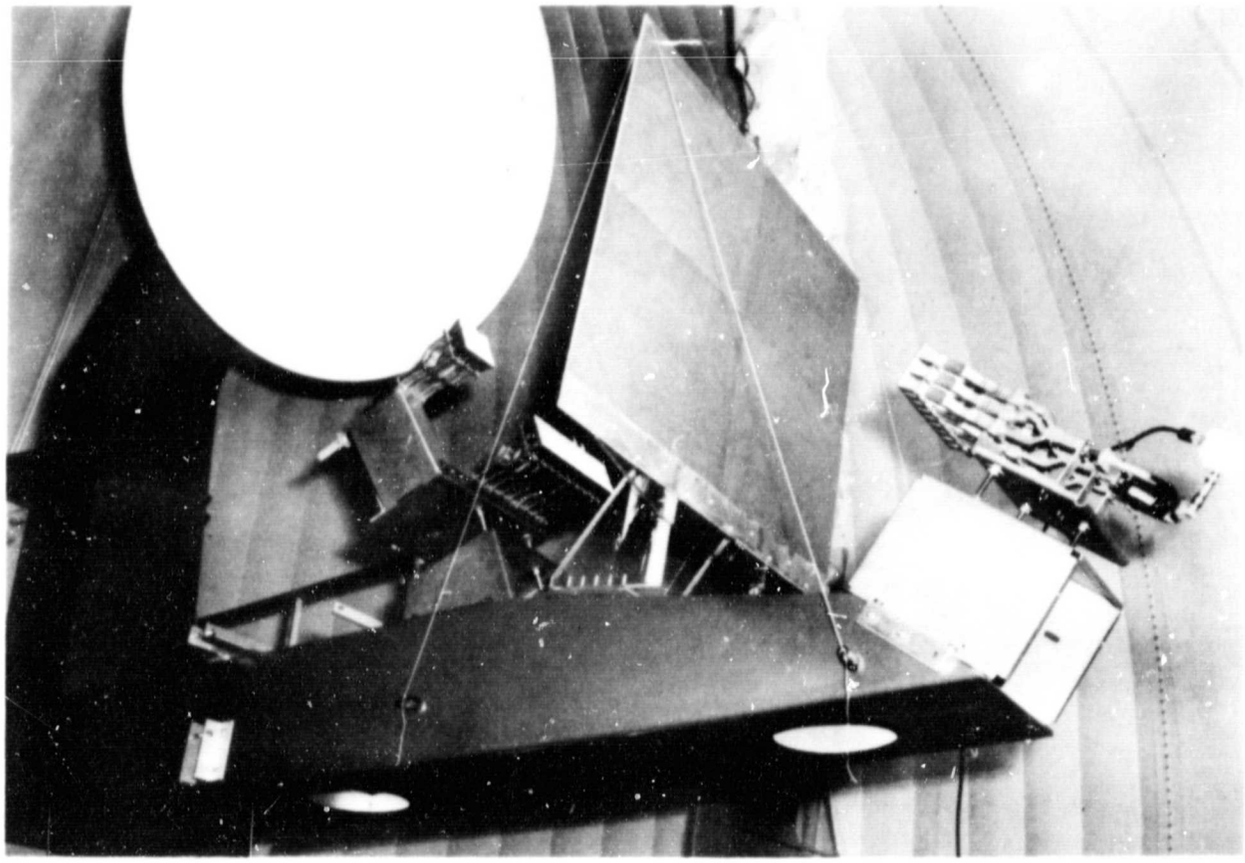

161328-79-03

Figure 2.5-1. Spot Beam Antenna with Polarization Diplexing Feed Assembly

dial indicators mounted to a metal template machined to the proper parabolic shape. The template was used to sweep the surface about a pivotal line along the reflectors principal axis. Readings taken from the dial indicators were used to align the reflector and to describe surface smoothness. A single spot beam feed was attached to an x, y positioner located at the front fed reflector mechanical focal point. The positioner was used for axial and lateral aximuth scanning of the feed. The feed phase center was positioned using a template attached to one end of the arm extended along the pivotal line of the reflector's principal axis, used to support the reflector template. The pivotal arm was removed and radiation patterns were taken with a single feed placed at the focal point. The measured contour pattern as shown in Figure 2.5-2 was distorted from the expected symmetry around the reflector vertical axis. In addition, sidelobe levels were only 34 dB below the main beam peak. Analysis of these patterns using the measured reflector surface data, indicated that errors of this nature could be caused by surface roughness. Therefore the reflector was shiped back to Space Park for refinishing.

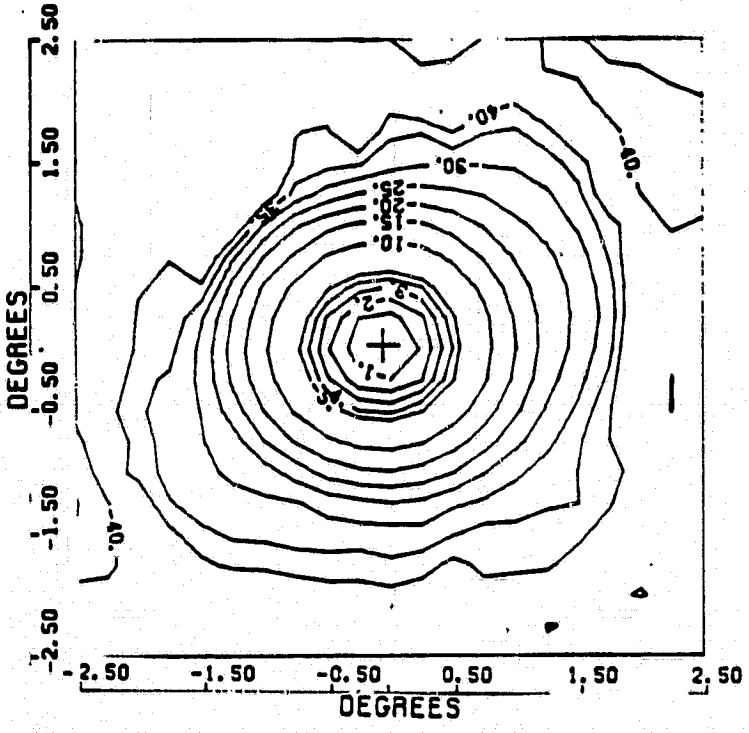

Figure 2.5-2. Single Feed Contour Pattern

A new reflector, of the same geometry, was fabricated. The surface contours for the second reflector are plotted in Figure 2.5-3. Peak surface deviations were on the order of ±0.030 inch with an rms error of 0.010 inch. Preliminary radiation patterns revealed an improvement in pattern symmetry. Sidelobe levels were -36 dB in the elevation plane.

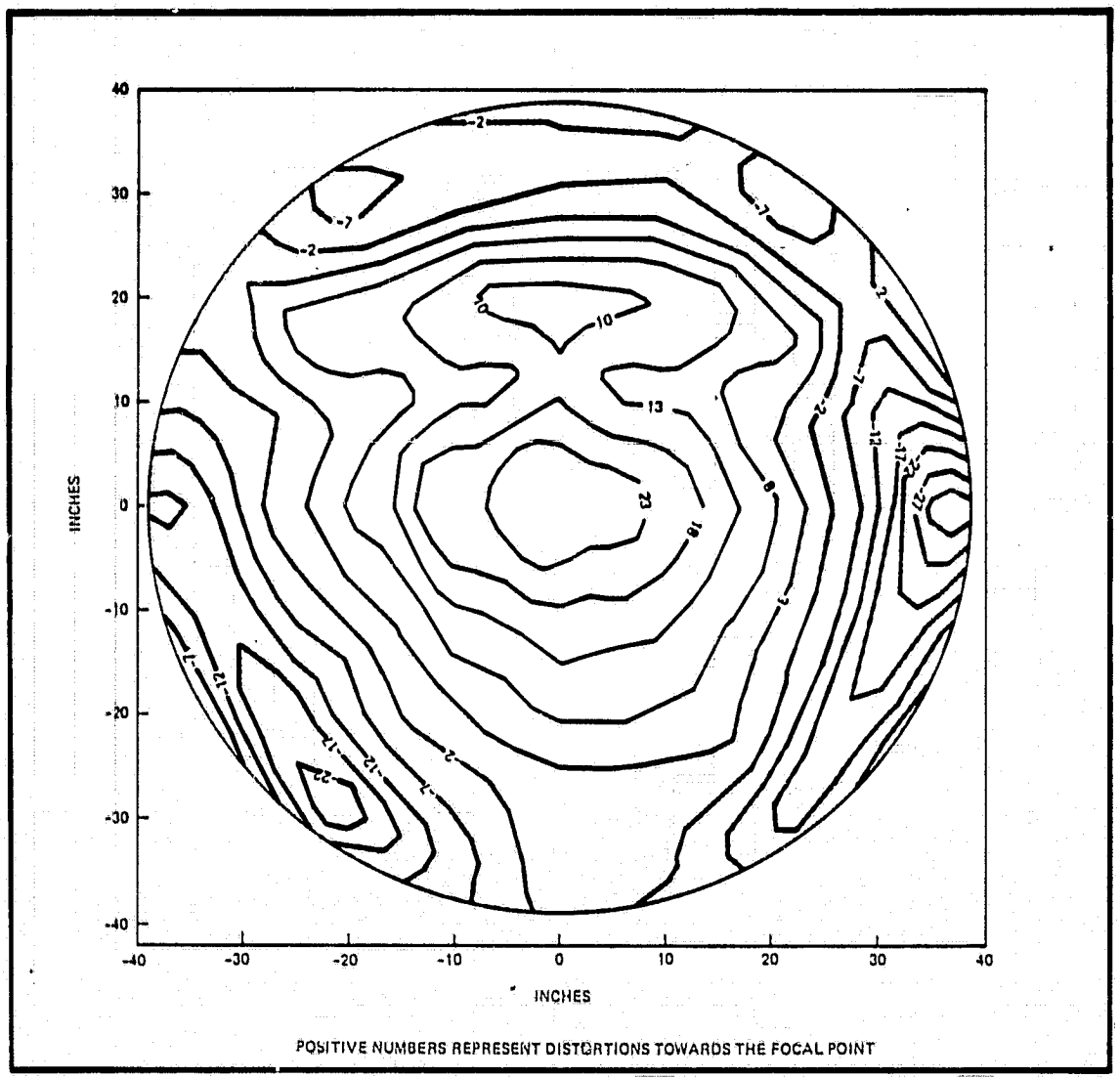

Figure 2.5-3. Measured Surface Error Contour in 1/1000 Inch on 78-Inch Reflector Diameter: 78 inches (200 cm)
Focal Length: 98.04 inches (249 cm)

2.5.1 Reflector with Moveable Feed

A series of laterally displaced single feed patterns was taken on the second reflector before the polarization diplexer was inserted between the reflector and the feed. The procedure was as follows: azimuth scan loss data was obtained by laterally shifting the feed. Scan loss at the beam peak was determined by feed movement in azimuth and elevation.

The wire grid subreflector was then fastened to a fixture that mounted onto machined flats welded to the reflector support structure. The tilt was adjusted by shimming until the proper angle was established (measured with an inclinometer). The single feed was set up along with the x, y positioner to operate in the Cassegrain geometry. Pattern data was taken for the Cassegrain operation. The reason for taking single feed patterns was to verify the mechanical alignment and electrical boresight, and to make preliminary evaluations of antenna performance before inserting the less flexible multiple beam feeds. Azimuth and elevation plane cuts, along with contour patterns, were taken every 2.2 degrees from 0 to 11.0 degrees. Figure 2.5-4 shows the measured boresight as well as scanning beam performance of the CONUS spot beam reflector. It should be noted that as the feed is displaced in the azimuth plane (in the y-axis), the radiation peak moves off the azimuth plane. Therefore the azimuth pattern does not cut through the peak of the radiation pattern.

The next measurement phase was to evaluate the wire grid subreflector. Measurements were made with the subreflector as a vertical grid and as a horizontal grid. For each polarization, the feed was placed in the front fed and cassegrain geometries. Although both grid orientations worked well in the principal polarization, cross-polarization suppression occured only when the grid wires were vertical to the reflector geometry. The measured results are shown in Figures 2.5-5 and 2.5-6. This phenomena is consistant with Chu's analysis[5] except the cross-polarized radiation is only reduced 4 dB with the wire grid.

2.5.2 Reflector Antenna with Alaskan Feed Geometry

After completion of the single feed pattern measurements, the first multiple beam reflector antenna was assembled. This antenna consisted of six vertically polarized circular and three horizontally polarized elliptical spot beam array feeds as shown in Figure 2.5-7. The feed packages

were precisely aligned on flats and then tightened down to maintain proper positioning. One of the nine array feeds was the Alaskan coverage feed, this configuration was designated as the Alaskan feed geometry. The horizontal polarized feeds were placed for front-fed operation, while the vertical polarized feeds were placed for Cassegrain operation. The entire reflector feed assembly is illustrated in Figure 2.5-8.

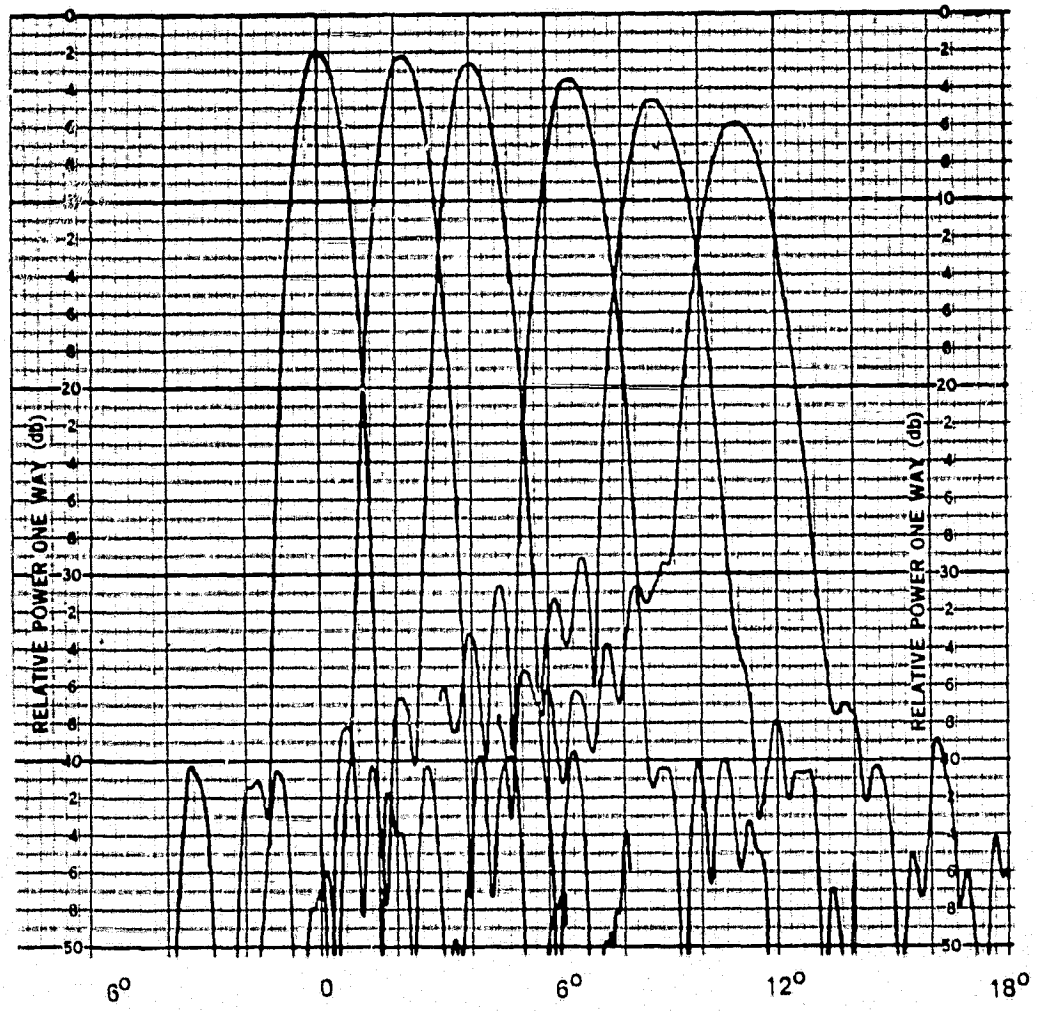

Figure 2.5-4. Measured Scanning Beam Performance, 1.1 Degree Half Power Beamwidth at Boresight, Frequency = 11.95 GHz

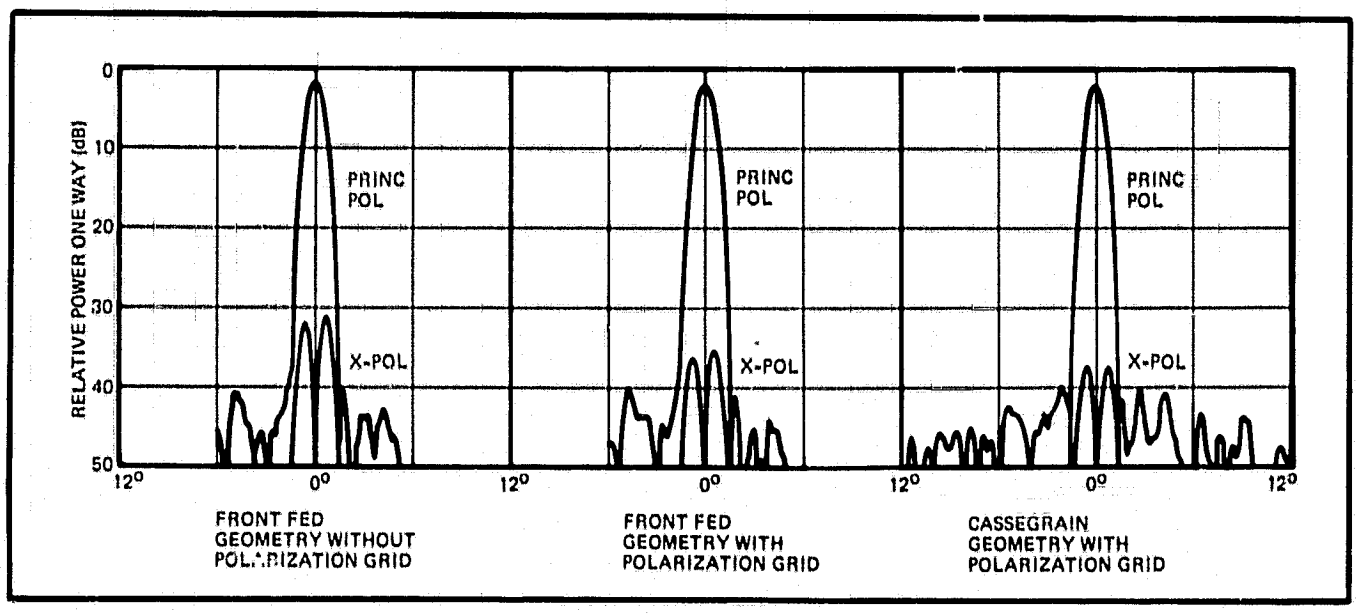

Figure 2.5-5. Measured Principal and Cross Polarization Patterns With and Without Polarization Grid Showing 4 dB Improvement in Cross Polarization

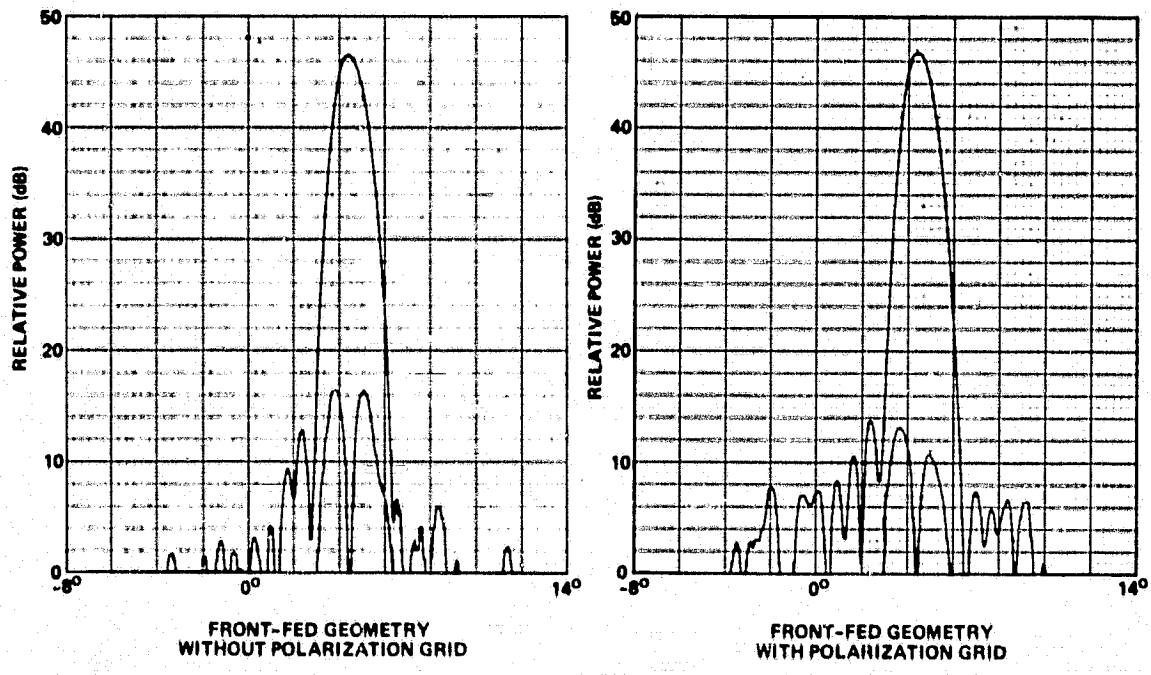

Figure 2.5-6. Measured Principal and Cross Polarization Patterns of a 4.4 Degree Scan Beam

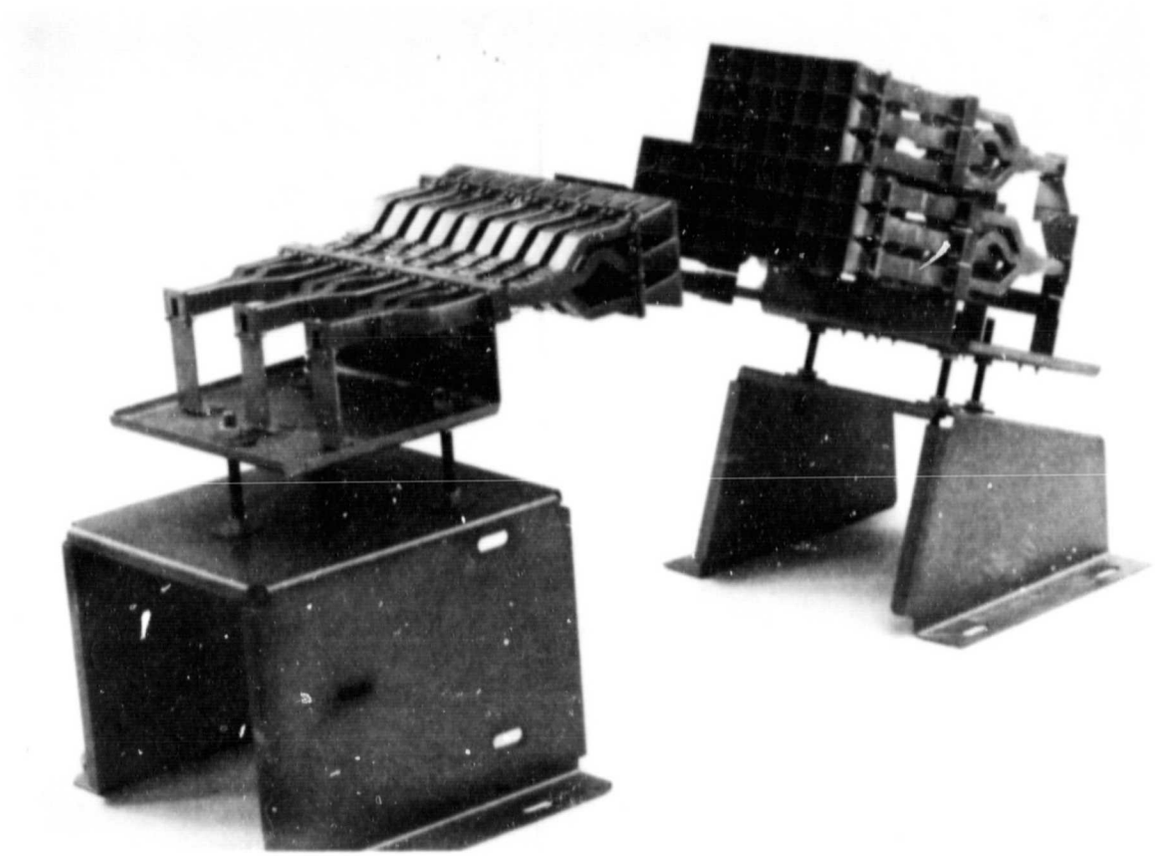

152238-79-3

Figure 2.5-7. Six Vertically Polarized Circular Spot Beam Feeds and Three Horizontally Polarized Elliptical Beam Feeds

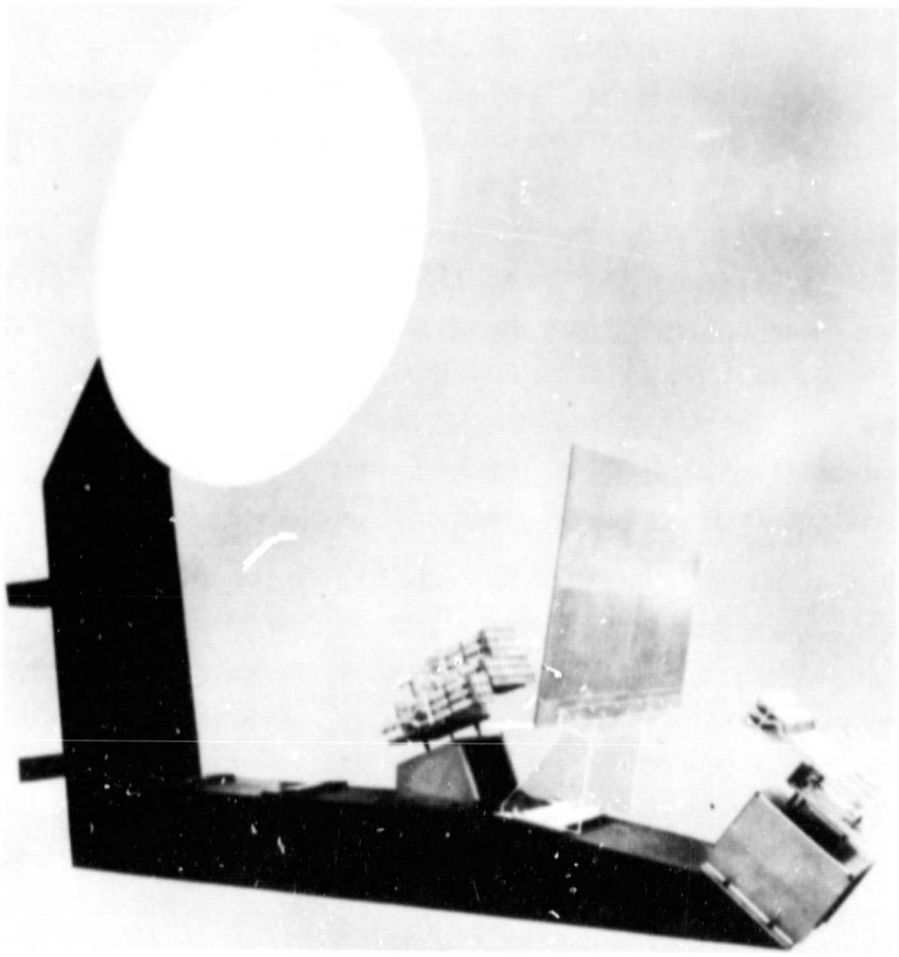

Figure 2.5-8. CONUS Spot Beam Antenna, Providing Six Vertically Polarized Circular Spot Beams and Three Horizontally Polarized Elliptical Beams

The front feeds were located at the focal point by a template attached to the long arm extended along the reflector principal axis pivotal line. The pivotal arm was removed before the Cassegrain fixtures were inserted into position. These feeds were mechanically aligned and their exact location refined by the following procedure: First, a calibrated precision level was placed on the front face of a row of feed elements aligned along

the top edge. This permitted adjustment to eliminate any axial rotation within the antenna geometry. Second, a calibrated inclinometer was rotated 90 degrees to the top and aligned along the side edge. The feeds were then adjusted to the proper reflector vertical bisecting angle. Third, a theodolite was lined up with the azimuth bisecting line of the reflector and the azimuth location of the front feed focal point. The Cassegrain feed package was then optically set using the scope crosshairs to correspond to the correct azimuth location. Fourth, a tooling fixture was used to set the length and vertical location of the focal point with respect to the front feed focal point. Last, several iterations of the above tasks were performed until data from each check coincided.

With the antenna assembly set up in the Alaska geometry, far field measurements were begun. For boresighting, the cluster whose phase center was located on the azimuth axis was used to boresight the antenna in azimuth. Likewise, the elevation boresight was obtained using the appropriate feed cluster. In addition, the feed on the azimuth boresight was used to fine tune the alignment of the polarization tilt angle between the two antennas. This was done by repetatively boresighting to the cross-polarization null until the maximum null depth was achieved. An electrical check on the alignment between the source and test antenna was performed by checking the relative boresights of the adjacent feeds in the Cassegrain and front-fed geometries.

The following sets of patterns were generated for each of the feeds:

1) Principal plane elevation and azimuth rectangular plots
   a) Principal polarization
   b) Cross-polarization
2) Contour plots provided by a series of great circle cuts
   a) Principal polarization
   b) Cross-polarization
3) Frequencies
   a) Transmit - 11.7, 11.95, 12.2 GHz
   b) Receive - 14.0, 14.25, 14.5 GHz.

The principal plane plots were taken in a manual mode and the contour data taken under the control of a PDP 11/780 minicomputer (setup shown in Figure 2.5-9).

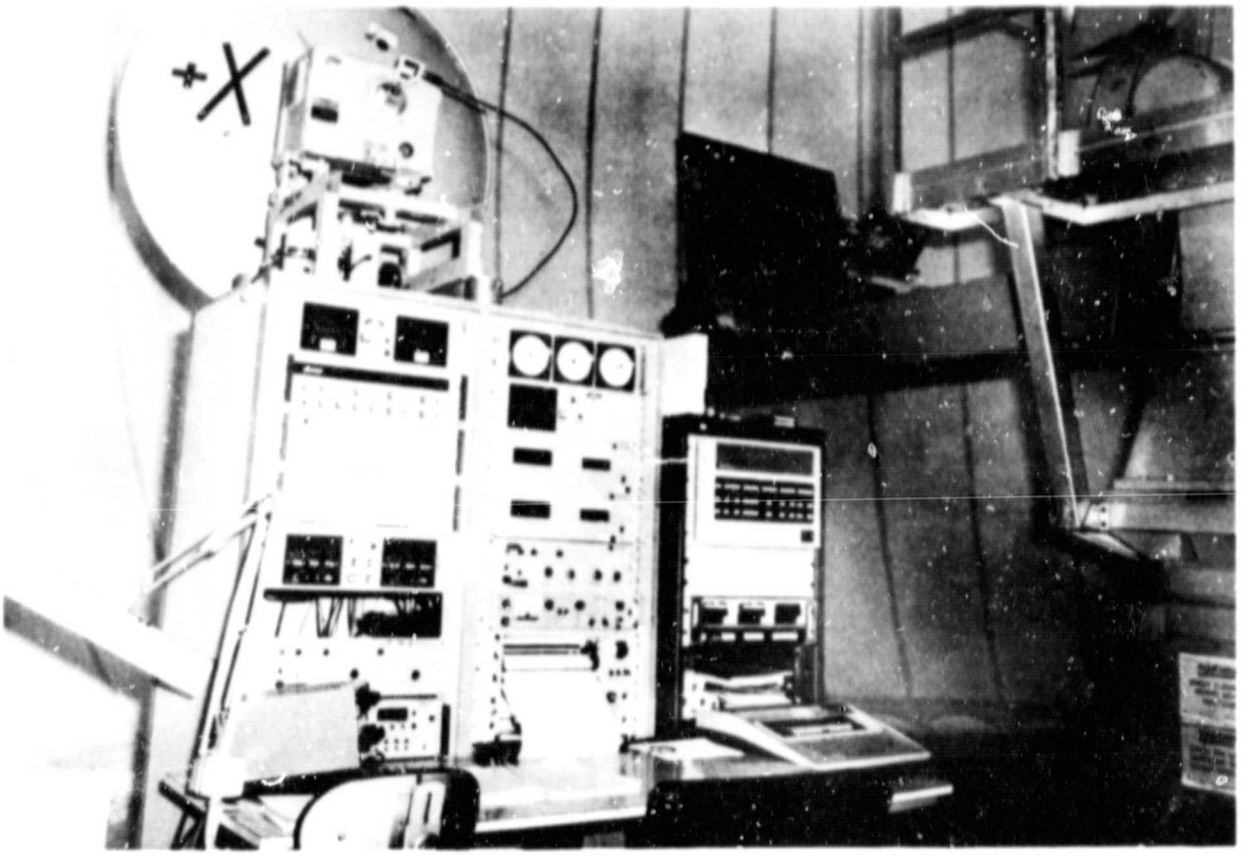

161328-79-7

Figure 2.5-9. Contour Data Measurement Setup

2.5.3 Reflector Antenna with Hawaiian Feed Geometry

After all data pertaining to the Alaska feed geometry was taken, the feed hardware was removed and partially disassembled. A new set of feeds, consisting of five vertically-polarized circular and three horizontally-polarized elliptical spot beam clusters, were packaged, aligned, and locked down. Included in this set was a Hawaii coverage feed. Thus, this feed configuration was designated as the Hawaiian feed geometry. The five circular beams were mounted for Cassegrain operation and the three elliptical beams for front-fed operation. The alignment procedure was identical to that described for the Alaska geometry. A series of contoured beam patterns was taken using the same format as the Alaska feed geometry.

2.5.4 Measured Far Fied Radiation

Figures 2.5-10 and 2.5-11 illustrate four typical calculated and measured gain contours of this 17-beam reflector antenna system. The correlation between the calculated and measured gain contours is, in general, excellent. Minor discrepancies between calculated and measured results, particularly in the -35 dB level or below, are attributed to the fact that the theoretically calculated patterns do not include:

- Alignment of main reflector, subreflector, and feed assemblies
- Amplitude and phase variations of the nine-horn feed vs frequency
- Polarization purity of the source antenna
- Mutual coupling between feed horns
- Scattering by finite grid subreflector
- Scattering from antenna support

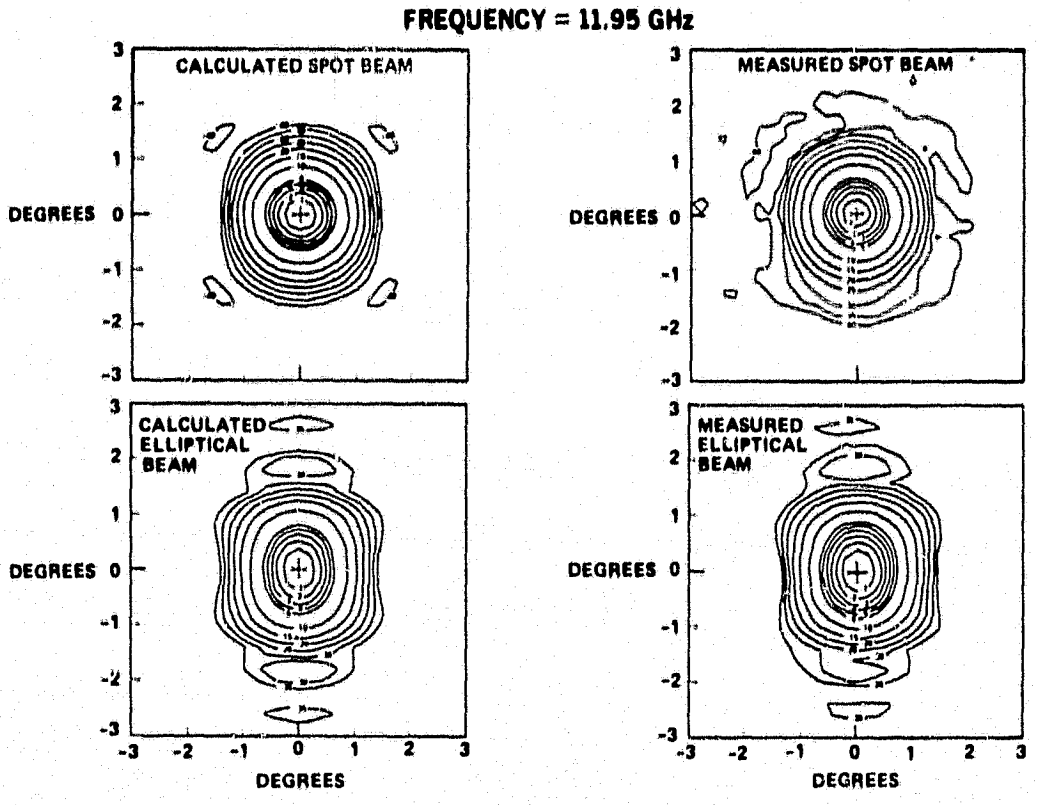

Figure 2.5-10. Comparison of Calculated and Measured Gain Contours

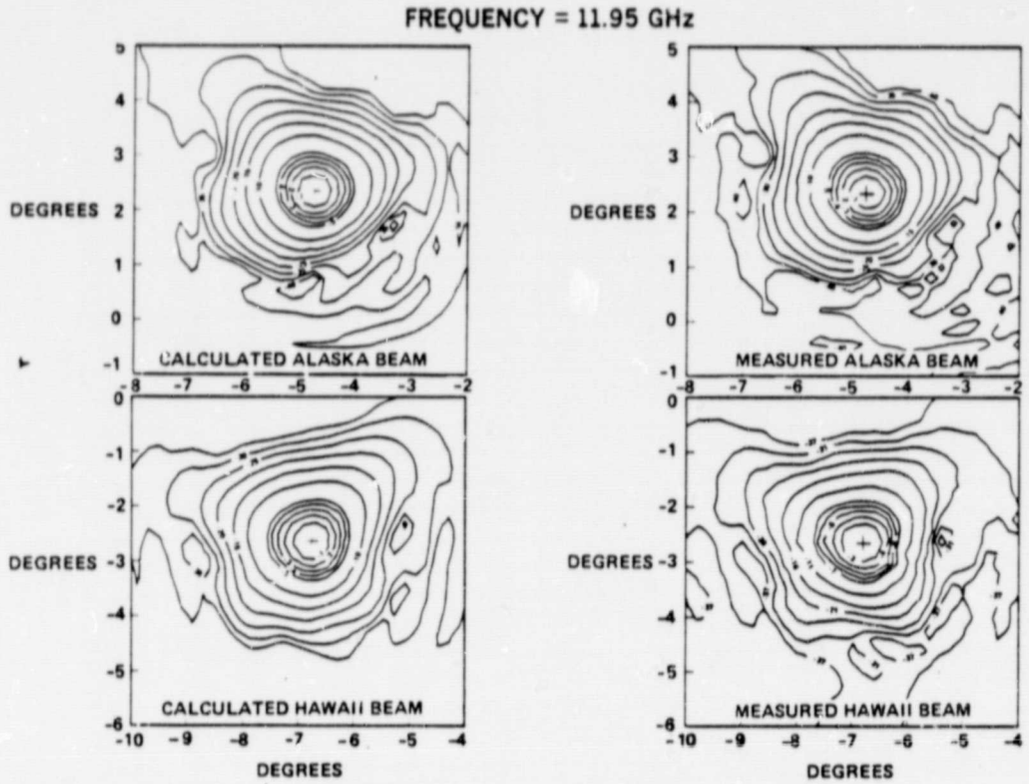

Figure 2.5-11. Comparison of Calculated and Measured Gain Contours

- Direct radiation or diffraction from the feeds
- Reflector surface tolerance
- Insertion of radome curtain in front of test antenna
- Multipath reflection from antenna range.

Figure 2.5-12 shows the measured contiguous spot beam gain contours of CONUS at 11.95 GHz.

A complete set of each individual beam contour and two principal pattern cuts is given in Appendix B.

2.5.5 Beam Isolation Measurements

Figures 2.5-13 through 2.5-16 show the measured -3.5 and -31.5 dB gain contours of all 17 beams at 11.95 GHz. Each plot shows the beam-to-beam isolation of all co-polarized beams which may be operated at the same frequencies.

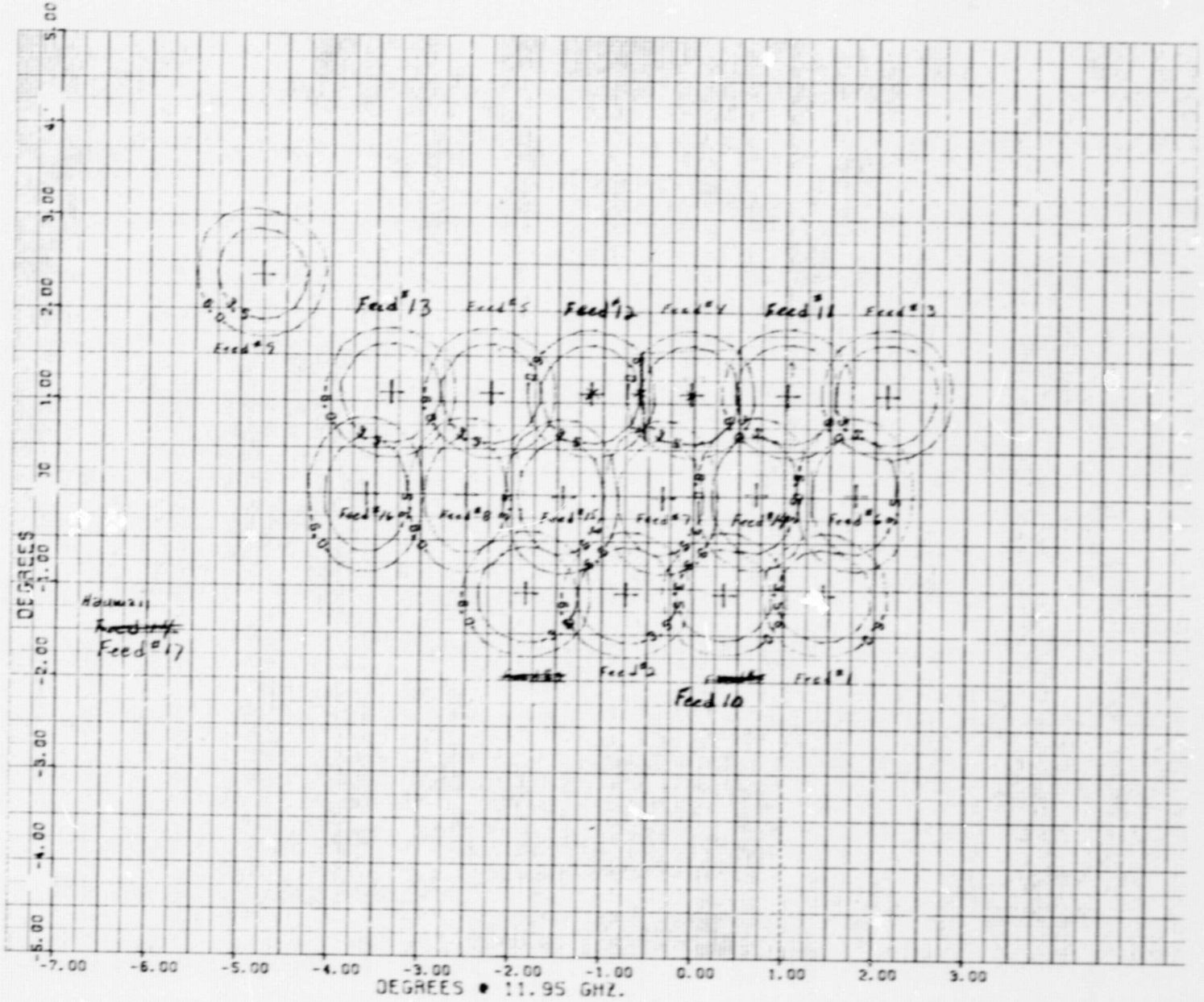

Figure 2.5-12. Measured Spot Beam Gain Contours (-3.5 and -6.0 dB) at 11.95 GHz

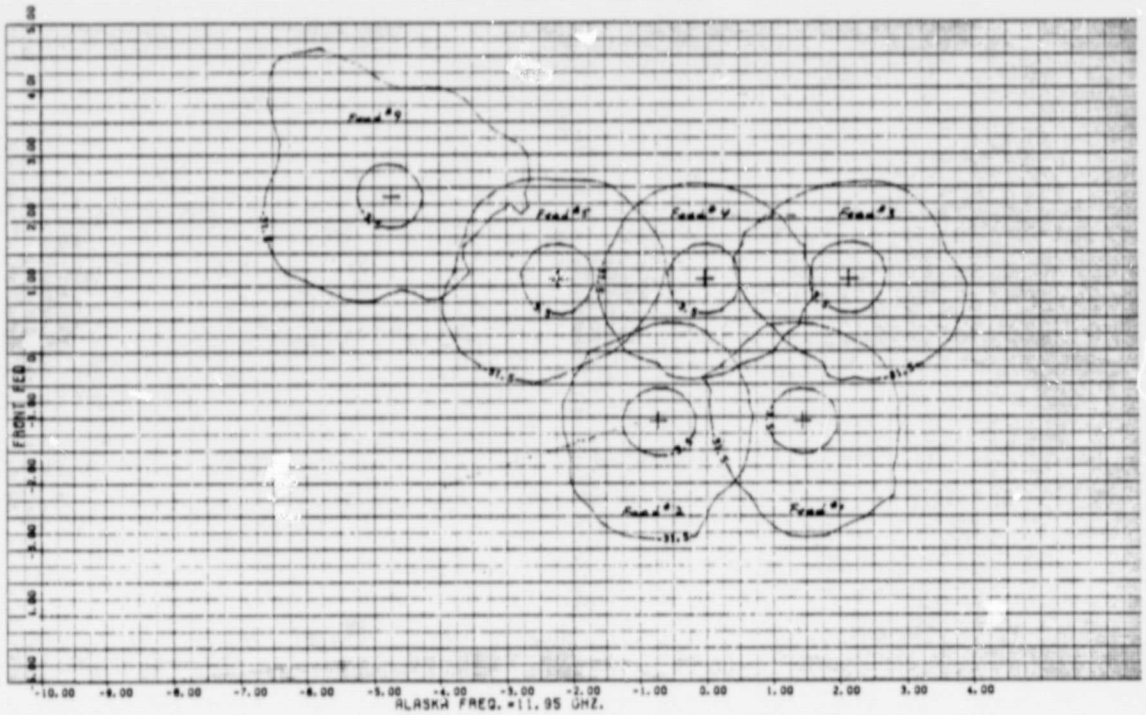

Figure 2.5-13. Measured Co-Polarized Beam Contours Generated by Feed Cluster No. 1, Vertical Polarization Frequency = 11.95 GHz

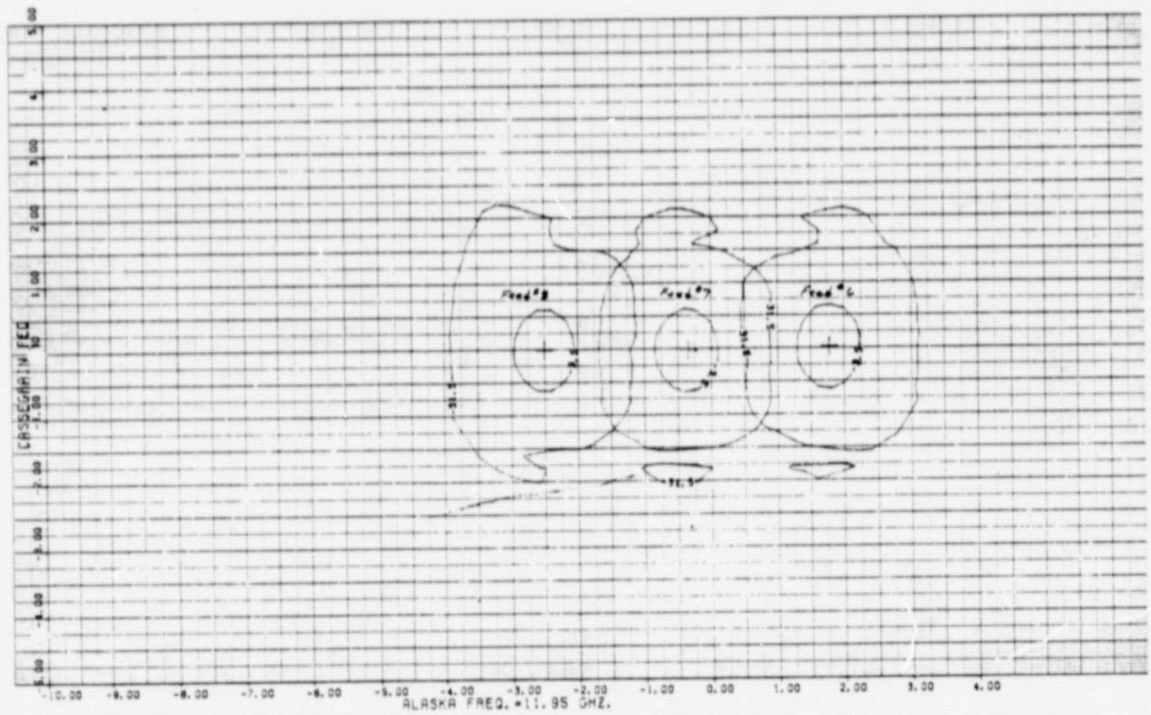

Figure 2.5-14. Measured Co-Polarized Beam Contours Generated by Feed Cluster No. 2, Horizontal Polarization, Frequency = 11.95 GHz

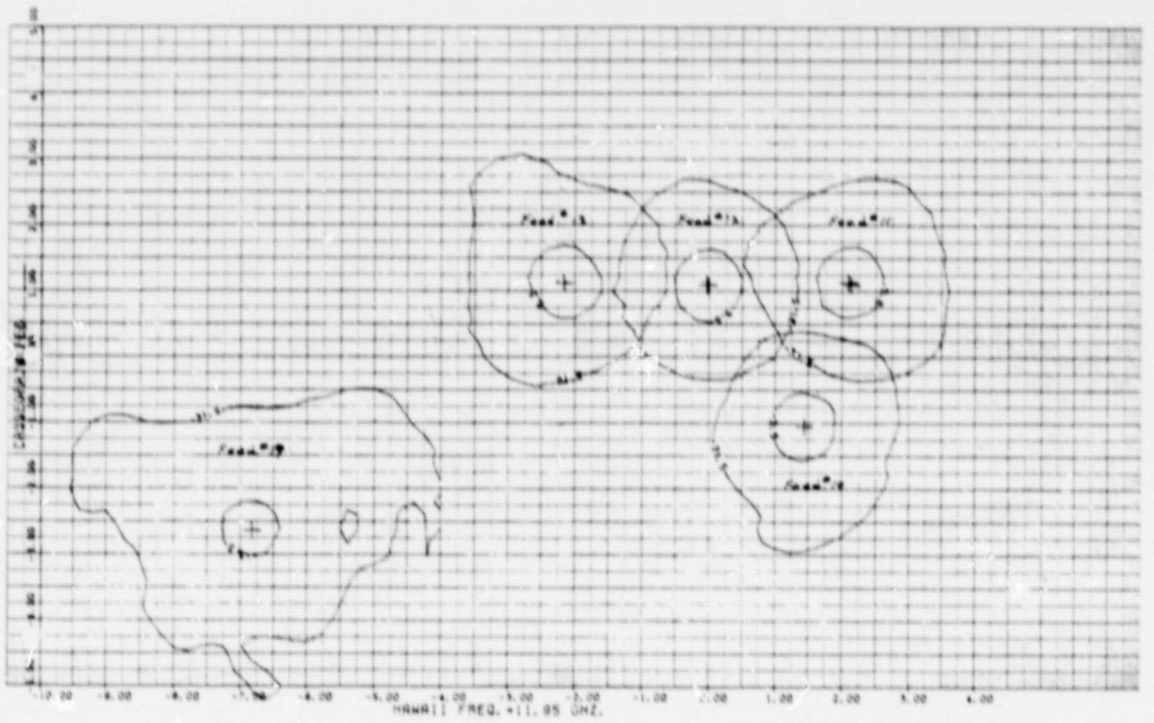

Figure 2.5-15. Measured Co-Polarized Beam Contours Generated by Feed Cluster No. 3, Horizontal Polarization Frequency = 11.95 GHz

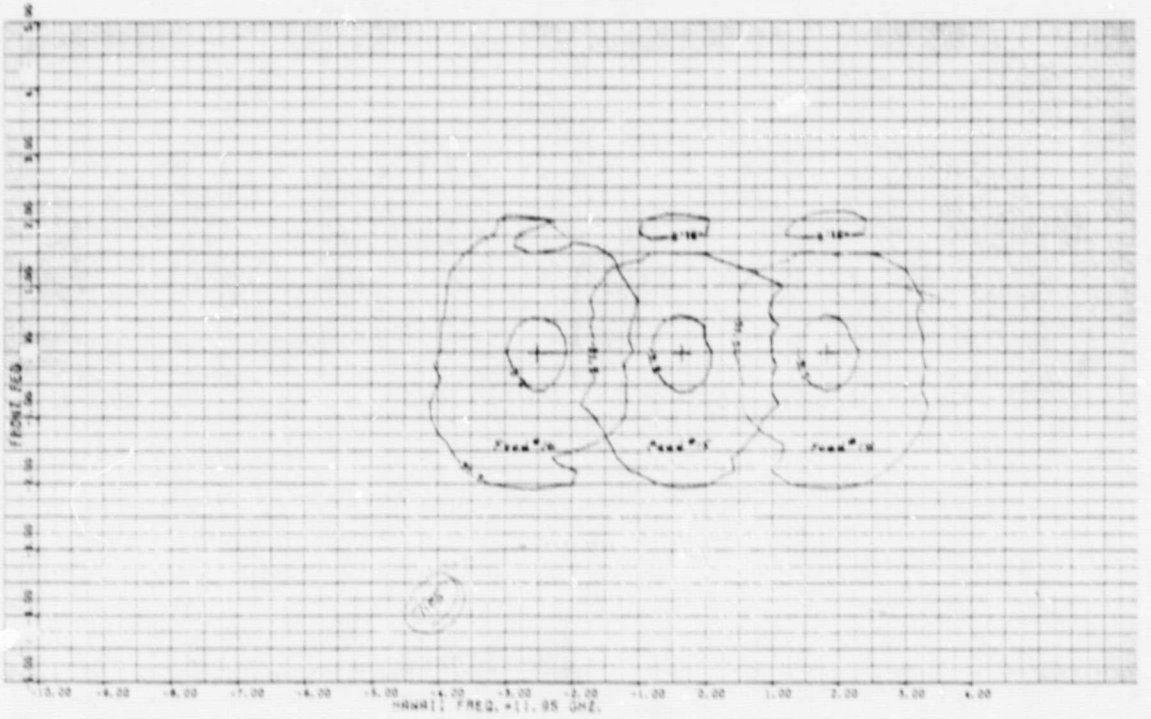

Figure 2.5-16. Measured Co-Polarized Beam Contours Generated by Feed Cluster No. 4, Vertical Polarization, Frequency = 11.95 GHz

The gain contour measurements were performed at six frequencies only. This is not adequate to prove that the 28 dB beam isolation requirements is met throughout the band. Therefore, swept frequency measurements over the 11.7 to 12.2 GHz and 14.0 to 14.5 GHz frequency bands were performed at three representative points within the CONUS area, as shown in Figure 2.5-17.

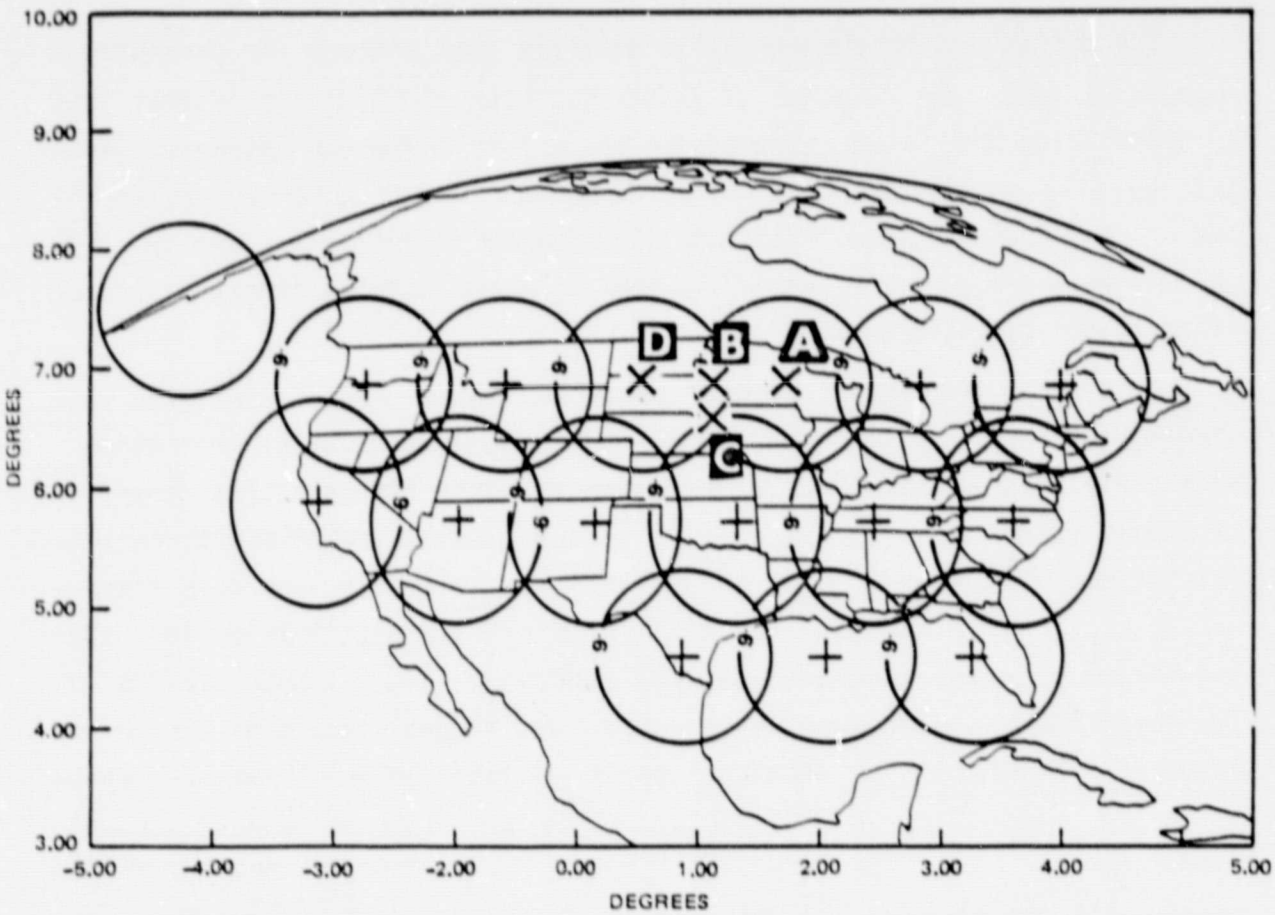

Figure 2.5-17. Swept Frequency Beam Isolation Measurement at Pointing Angles A, B, C, and D

The first point of interest was the peak of a beam at Point A, nested between a cluster of beams. The second, Point B, was at the crossover between the chosen beam and its adjacent beam (double beam center). The third point of interest was the lowest gain at Point C near the center of the three closest beams (triplet beam center). The measurements were performed by rotating the test antenna so that the beam pointing angle which

corresponds to one of the three points of interest is directed toward the source antenna. Signals received at each individual output port of this test antenna were taken via a switching network and added up by the computer with the source antenna first transmitting vertically polarized signals and then horizontally polarized signals.

The results of these measurements are presented in Appendix C.

2.6 SUMMARY AND CONCLUSIONS

The design and development of a multiple beam antenna for providing a contiguous spot beam coverage of CONUS has been successfully accomplished by interlacing the beams produced by two offset reflector antennas placed side by side on a synchronous orbit satellite. Each antenna consists of one offset reflector, one polarization diplexing subreflector, and two sets of nine-horn array feeds; one is placed in the front-fed geometry and the other in the Cassegrain geometry.

A low sidelobe beam synthesis technique for an offset reflector with nine-horn array feeds has been established. Implementation of this nine-horn array feed was achieved by waveguide parallel feed circuits comprised of standarized septum power dividers and 90 degree polarization twists. This standarized nine-horn array feed exhibits broadband, low loss characteristics. A VSWR of less than 1.2:1 with an insertion loss of less than 0.2 dB was obtained over a 25 percent band with steady power division at the output ports. This feed has a compact and rugged mechanical design and features flexibility for arbitrary power division with co-phasal outputs which are needed for low sidelobe operation over a broad band of frequencies. In addition, the feed offers low cost fabrication because of its standarized design. All 17 spot beam feeds are physically identical. They are assembled from three basic building components: square horn, three-way power divider, and 90 degree twist. This design concept can be extended to the 30/20 GHz and even higher frequency bands.

The implementation of a polarization grid subreflector in between the offset reflector and the prime focus not only permits the overlapping of low sidelobe beams without feed interference, but also reduces the cross-polarization radiation. This design offers the advantage of ease in fabrication tolerance required for low sidelobe operation compared to the double-gridded reflector design.

To evaluate antenna performance, extensive tests were carried out. These included VSWR, feed circuit loss, primary pattern, near-field measurement of the feed, far-field measurements of the full scale antenna, and high power test of the feeds. Both principal and cross-polarization pattern cuts and gain contour for all 17 beams at 11.7, 11.95, 12.2, and 14.25 GHz were taken at TRW's 3000 meter antenna range at Capistrano, California. In general, the agreement between the calculated and measured gain contours down to -32 dB is excellent. A comparison of the original design goal and actual measured performance is given in Figure 2.6-1. Minor discrepancies are attributed to the reflector surface tolerance, scattering from the reflector/feed supports, and ground reflection from the antenna range.

	SPECIFICATIONS	MEASURED CAPABILITIES
DOWNLINK FREQUENCY	11.7 TO 12.2 GHz	11.7 TO 12.2 GHz
UPLINK FREQUENCY	14.0 TO 14.5 GHz	14.0 TO 14.5 GHz
POLARIZATION	ORTHOGONAL LINEAR	ORTHOGONAL LINEAR
COVERAGE	CONTIGUOUS CONUS, ALASKA AND HAWAII	CONTIGUOUS CONUS, ALASKA AND HAWAII
NUMBER OF BEAMS	ABOUT 25 BEAMS	17 BEAMS
SIDELOBE LEVEL	-32dB	-36 dB AT BORESIGHT -32 dB OFF BORESIGHT
CROSS POLARIZATION	-28 dB	-32 dB
BEAM CROSS OVER LEVEL	-7 dB FOR DOWNLINK -9 dB FOR UPLINK	-6 dB FOR DOWNLINK -8 dB FOR UPLINK
BEAM ISOLATION	28 dB	TBD
FEED CIRCUIT LOSS	$\leq$ 0.30 dB	$\leq$ 0.20 dB
INPUT VSWR	$\leq$ 1.2:1	$\leq$ 1.2:1
REFLECTOR DIAMETER	200 CM APPROXIMATELY	200 CM
POWER HANDLING CAPACITY	100 WATTS AVERAGE POWER	100 WATTS

Figure 2.6-1. CONUS Spot Beam Antenna Design Specifications and Measured Capabilities

Due to imperfections in the far-field test environments, accurate measurement of the beam isolation among this 17-beam communication system is very difficult to achieve. Nevertheless the results obtained serve as a clear indication that the beam isolation depends greatly upon the reflector surface tolerance and on the total number of beams operated simultaneously at the same frequency.

3. CONTOURED BEAM ANTENNA

3.1 OBJECTIVE

The second objective of the study was to develop a brassboard feed for a shaped contour beam antenna in the 14/12 GHz band for CONUS regional time zone coverage. The four time zones shown in Figure 3.1-1 as viewed from a synchronous orbit satellite located at 98 degrees west longitude are covered by four independently shaped beams produced by an offset paraboloid with a polarization grid. The eastern and mountain time zones are horizontally polarized and fed by two separate array feeds in a front-fed geometry. While the Pacific and Central time zones are vertically polarized

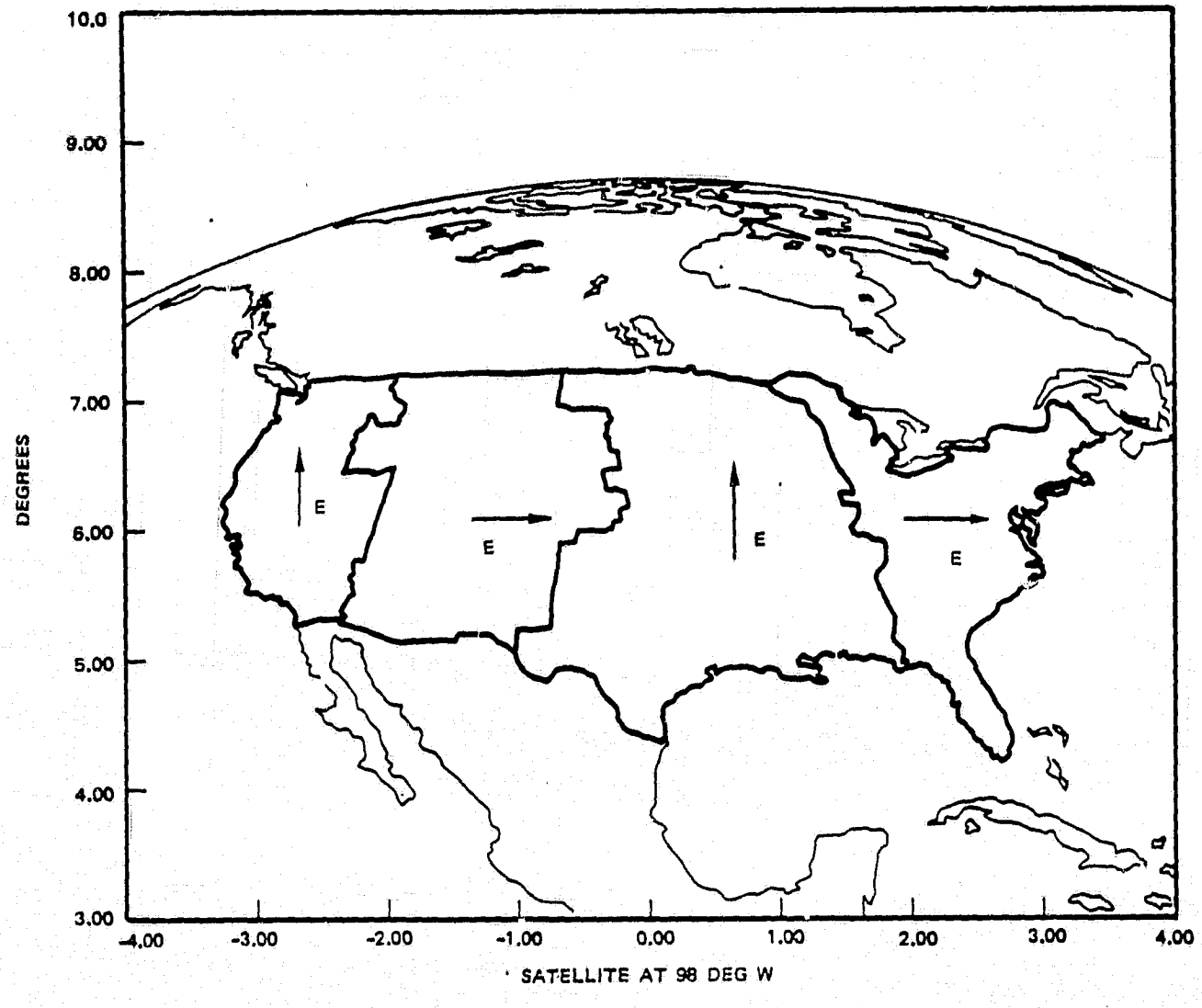

Figure 3.1-1. CONUS Time Zone Map as Viewed from a Synchronous Satellite at 98 Degrees West Longitude

and fed by two array feeds in a Cassegrainian-fed geometry. Beam isolation is obtained by polarization diversity and angular separation of low sidelobe beams. This system will permit a high gain antenna with four times frequency reuse of the full available bandwidth in each time zone. Due to smaller geographical coverage areas in the eastern and pacific time zones, the corresponding beams can produce higher antenna gain in these heavy rainfall areas.

The array feed for the eastern time zone coverage was chosen for development since it appears to be the most difficult task. The design specifications for this feed in the offset reflector are given in Figure 3.1-2.

FREQUENCY	11.7 TO 12.2 GHZ FOR DOWNLINK 14.0 TO 14.5 GHZ FOR UPLINK
POLARIZATION	ORTHOGONAL LINEAR BETWEEN TWO ADJACENT TIME ZONES
COVERAGE AREA	EASTERN TIME ZONE
MINIMUM COVERAGE GAIN	35 DBi
COVERAGE GAIN VARIATION	≤ 4.0 DB WITHIN THE COVERAGE AREA
SIDELOBE LEVEL	≥ 32.0 DB BELOW BEAM PEAK
CROSS POLARIZATION	≥ 28.0 DB BELOW THE PRINCIPAL POLARIZATION
BEAM ISOLATION	≥ 28 DB BETWEEN ANY TWO BEAMS
POWER HANDLING CAPACITY	100 WATTS AVERAGE POWER
FEED CIRCUIT LOSS	≤ .45 DB
VSWR	≤ 1.2:1
REFLECTOR DIAMETER	≤ 400 CM

Figure 3.1-2. Contoured Beam Antenna Design Specifications

The design and development of the eastern time zone feed were performed in four steps:

1) Determination of optimum antenna parameters by analysis and design of the offset reflector system

2) Determination of optimum amplitude and phase excitation of each individual feed in the array by numerical optimization techniques to achieve the desired beam shape

3) Design and implementation of the beam forming network

4) Verification of the design performance by either near field probing techniques or far field gain contour measurements.

3.2 DESIGN ANALYSIS

The purpose of this design analysis was to determine the reflector feed configuration, beam isolation, sidelobes, cross-polarization with and without a gridded subreflector, and method of beam forming.

An offset reflector profile can be deformed to provide a specially shaped or contoured beam. However, in the case of using a single reflector to provide multiple shaped beams for various parts of a country or for specially shaped air traffic corridors, multiple-element feed clusters in an offset reflector are required. The feed elements are combined in amplitude and phase to yield the desired coverage patterns. The success of this multiple contoured beam antenna design depend greatly on the selection of optimum reflector feed dimensions. There are various numerical optimization techniques available in beam shaping. Among these, the direct-pattern search technique has been found the most successful.

3.2.1 Determination of Contoured Beam Antenna Geometry

Selection of the antenna physical dimensions usually imposes constraints on the realizable antenna performance, particularly in the sidelobe region. Suppression of sidelobes in one direction will cause sidelobes to rise in another direction. The physical dimensions of the reflector feed geometry have to be chosen so that the secondary patterns of the individual horns in the array feed cancel in the sidelobe region, according to the rules given in the previous section. A computer-aided optimization process can be extended to include determining these physical parameters as well as shifting the feed to the optimum position. Because of the time consuming process, this optimization is limited to finding a set of optimum amplitude excitation coefficients of this multi-element feed. Therefore, the success of this optimization is greatly dependent upon the designer's judicious selection of these physical parameters.

The physical dimensions of an offset reflector antenna were determined by the following steps:

1) Plot a coverage map as viewed from a synchronous orbit spacecraft, or a composite coverage map including the pointing error and views from different orbit positions.

2) Select a set of contiguous squares or circles which represent the -3 dB beamwidth of each feed in the offset reflector system.

3) Arrange these squares or circles in a rectangular or triangular lattice structure with appropriate scale that best fits the desired coverage area on the map.

4) Add one extra square or circle along the exterior periphery of the desired coverage area. The peripheral horns provide a means for sidelobe suppression. The total number of horns required for the contour beam is the total number of squares or circles.

5) Determine the optimum reflector antenna parameters; the projected reflector diameter D, focal length F, and spacing between feeds or feed diameter are established by the approximate equation

$$d = \frac{1.06\lambda}{D}\left(\frac{2F}{1+\cos\theta_o}\right) \qquad (3.1)$$

where

d = spacing between feed horn or feed diameter

D = projected offset reflector diameter

F = focal length of parent paraboloidal

θ_o = offset angle of the array feed

λ = free space wavelength.

6) Determine the optimum amplitude and phase distribution, for each individual horn by numerical optimization techniques which will be discussed in the following section.

3.2.2 Contoured Beam Synthesis

The synthesis of a low sidelobe contoured beam can be treated as a two-dimensional spatial filter problem. Each feed horn in a multi-element array produces a secondary pattern in the offset reflector system. The gain contours of an offset reflector with a multi-element array feed are a vector superposition of each individual pattern contributed from each horn. This computation is valid based on the assumptions that the offset reflector feed geometry is designed to avoid aperture blockage and the mutual coupling between feed horns is negligibly small.

In the optimization process, the first step is to set up the desired coverage gain $T(\theta,\phi)$ within the desired coverage area, then select a set of initial feed excitation coefficients $a_1, a_2 \ldots a_n$ which specify the state of the antenna gain $D(\theta,\phi)$ over the area of interest. The objective of this optimization problem is to search for a new set of feed excitation coefficients which provide the minimal least-mean-square value of the difference between the desired coverage gain $T(\theta,\phi)$ and the actual computed gain $D(\theta,\phi)$. A more general expression of this objective function may be defined as

$$U = \frac{1}{s} \int_s W(\theta,\phi) |T(\theta,\phi) - D(\theta,\phi)|^2 \, ds \qquad (3.2)$$

where s is the solid spherical angle in the antenna field of view, including the coverage area as well as the sidelobe region; $W(\theta,\phi)$ is a weighting function which is used to assign the order of importance in the desired coverage area. In this formulation, the objective function is an integral of the squared difference between the desired and the actual gain. In numerical computation, the integral is usually evaluated at a few numbers of selected sample angles in the range of interest. Thus the integral equation is reduced to

$$U = \frac{1}{M} \sum_{m=1}^{M} W(\theta_m, \phi_m) \, |T(\theta_m, \phi_m) - D(\theta_m, \phi_m)|^2 \qquad (3.3)$$

where M is the number of points selected for evaluation.

There are a number of numerical optimization techniques available. The one in use for this optimization is the Rosenbrock[8] pattern search method. This technique does not require previous knowledge of the directional derivative of the objective function. The essence of the Rosenbrock method is to increase each of the parameters and move to the new point if the objective function is improved. After all N parameters have been varied several times, a rotation of coordinates is performed in such a way that the first coordinate of the new orthogonal system points in the most successful direction of the previous search cycle. The remaining N-1 new

coordinate vectors are determined by the Gram-Schmidt orthonormalization procedure. Iteration of this optimization process continues until the objective function is minimized to less than the input value, or stops after the preset number of iterations.

3.2.3 East Time Zone Coverage Antenna

An example of this contoured beam antenna design for the eastern time zone (ETZ) of CONUS is illustrated in the following steps:

1) An array of square apertures which represent the image of a multi-element feed shown in Figure 3.2-1 is superimposed on the desired ETZ coverage map. Each square on the map represents roughly the domain of each individual horn in the array. The secondary pattern beamwidth of each horn is approximately 0.65 degree, which is measured by the width of each square

$$D = \frac{58\lambda}{\text{3 dB beamwidth in deg.}} \qquad (3.4)$$

In this case the half-power beamdwidth is about 0.65 degree, thus the projected aperture is about 89 wavelengths.

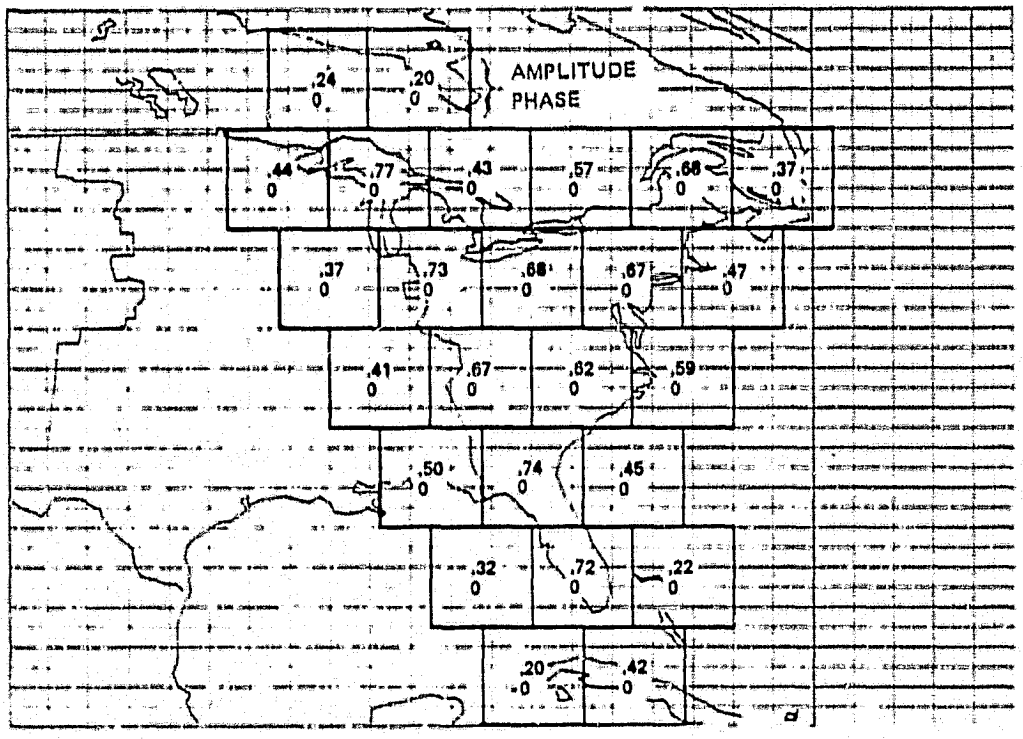

Figure 3.2-1. Reflector Image of ETZ Feed Cluster and its Amplitude and Phase Distribution Overlaid on the ETZ Map

2) A focal length to projected reflector diameter ratio, F/D, of 1.2564 was chosen, so that the contoured beam antenna geometry is similar to that of the spot beam antenna developed in Section 2. Thus, the spot beam reflector can be utilized to evaluate the far field performance of this contoured beam feed. Based on this selection, the rest of the reflector feed parameters was determined by the rules given in Section 3.2.1. The reflector configuration shown in Figure 3.2-2 has the following dimensions:

Aperture diameter	D = 228.6 cm
Focal length	F = 287.33 cm
Feed offset angle	$\theta_o = 40.58^o$
Total number of horns	25
Horn aperture	3.68 x 3.68 cm

A typical secondary pattern of a single horn in the offset reflector is shown in Figure 3.2-3. The extra horns on the periphery of the desired coverage area are used to suppress sidelobes adjacent to the eastern time zone.

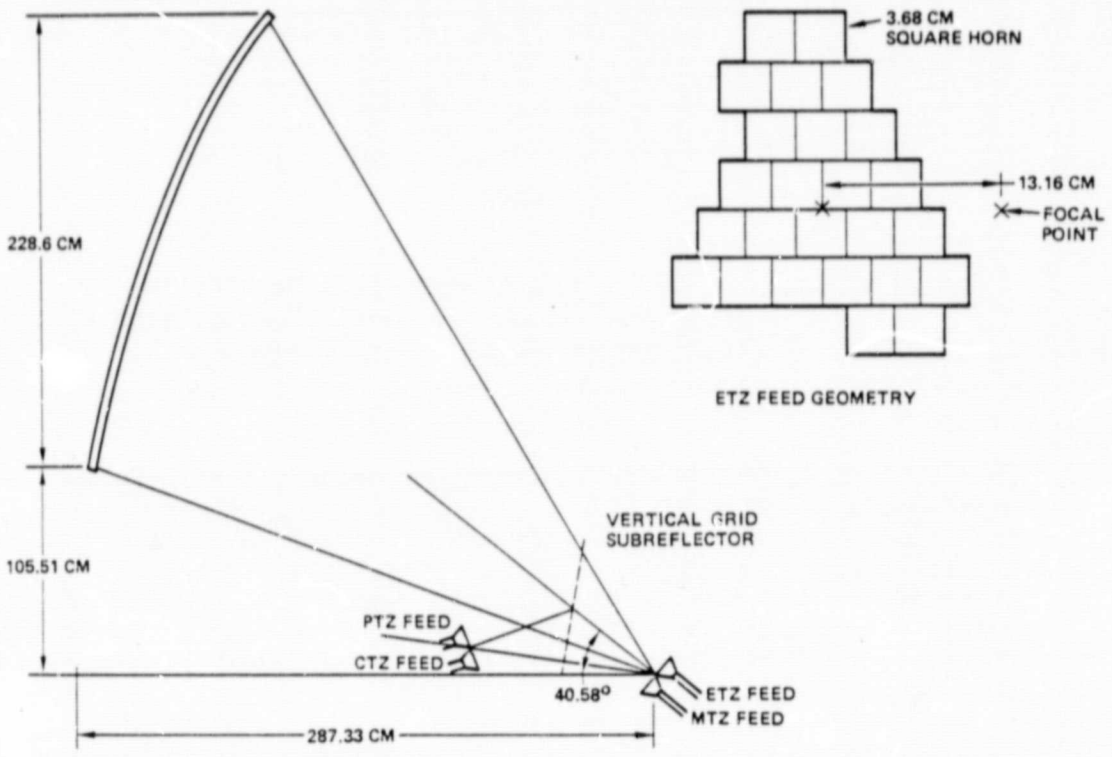

Figure 3.2-2. Contoured Beam Antenna Configuration

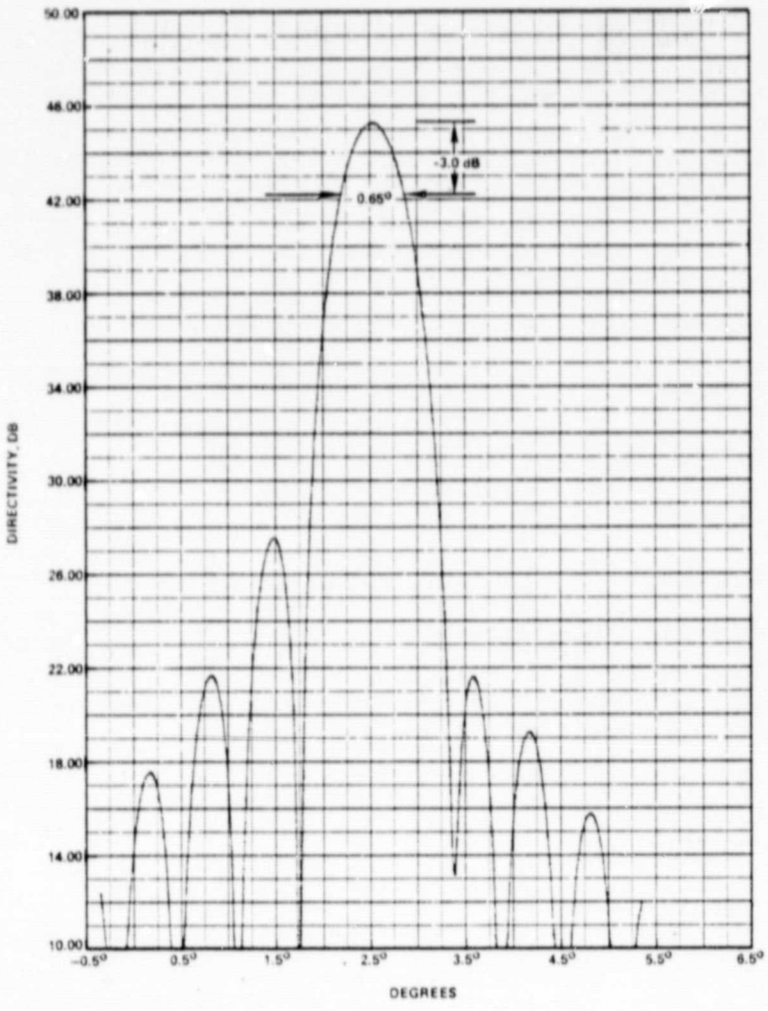

Figure 3.2-3. Typical Single Element Feed Pattern in Horizontal Plane (H-Plane), Feed Located at 14.73 cm Off Focal Point, Frequency = 11.95 GHz

3) Thirty-eight sample points spaced approximately a half beam-width apart as shown in Figure 3.2-4 were selected for numerical evaluation to minimize the objective function U. Selection of these sample points is somewhat arbitrary. Depending on the results of this optimization, the number of sample points and their distribution can be varied to improve the coverage gain during the iteration of this optimization process.

4) The far field response of each horn in the array at the sample points selected in step 4 above were computed and stored in magnetic tape for use in the optimization process.

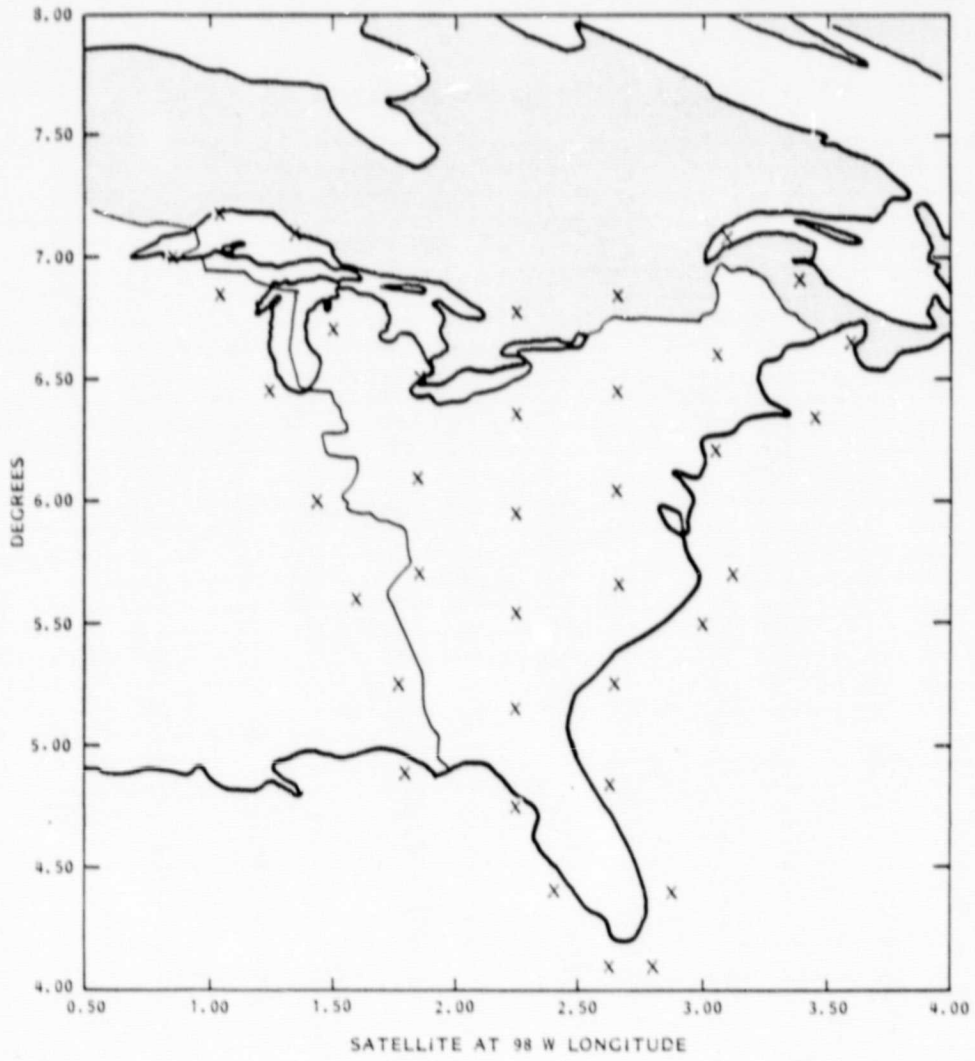

Figure 3.2-4. Selected Sample Points for Gain Optimization

5) The desired coverage gain is set to be 40 dB in this case, and the initial set of feed excitation coefficients is selected to be unity. Use the Rosenbrock optimization routine to search for a new set of feed coefficients which would minimize the objective function U.

6) Calculate and examine the resultant contoured beam coverage, and then select a new set of sample points to be evaluated in the optimization. Repeat steps 5 through 6 until the resultant gain contours are satisfactory.

After a few iterations, the optimum feed excitation of the ETZ array feed at 11.95 GHz is shown in Figure 3.2-1. Predicted principal and cross-polarization gain contours of a solid surface reflector are presented in Figures 3.2-5 through 3.2-8. Even though the feed excitation coefficients

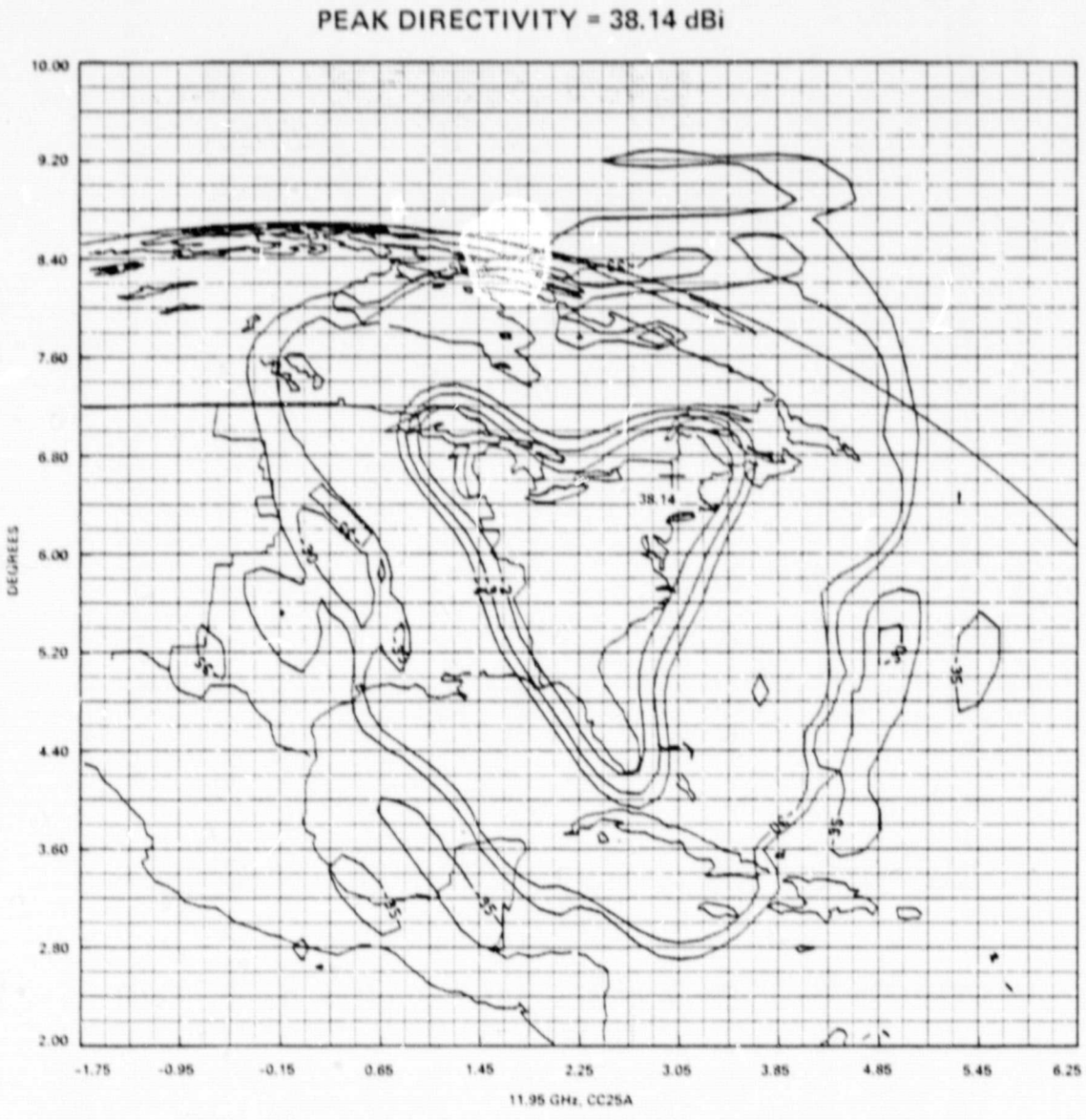

Figure 3.2-5. Downlink Co-Polarized Beam Isolation Contours at 11.95 GHz

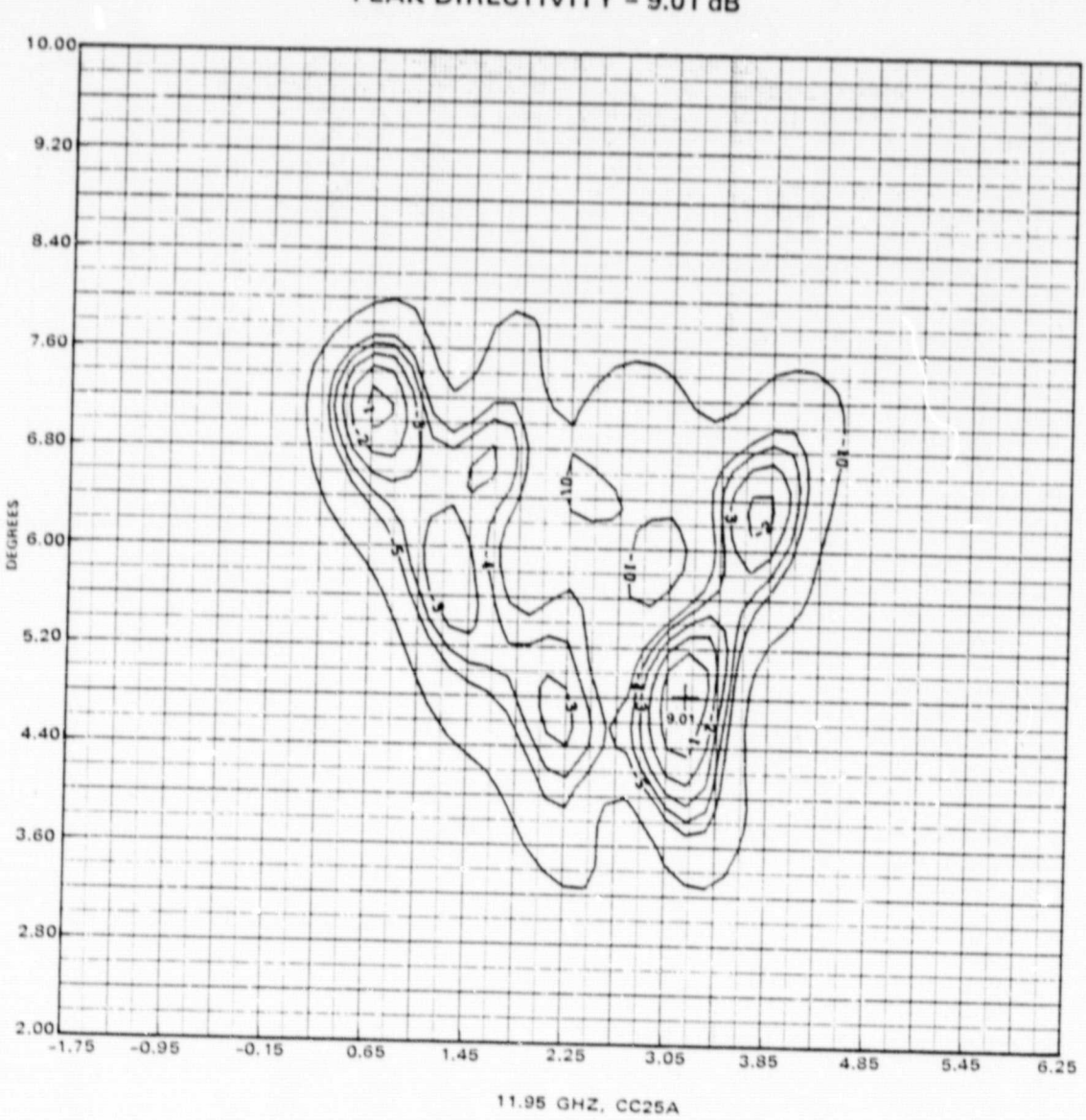

Figure 3.2-6. Downlink Cross-Polarization Gain Contours for ETZ Coverage at 11.95 GHz

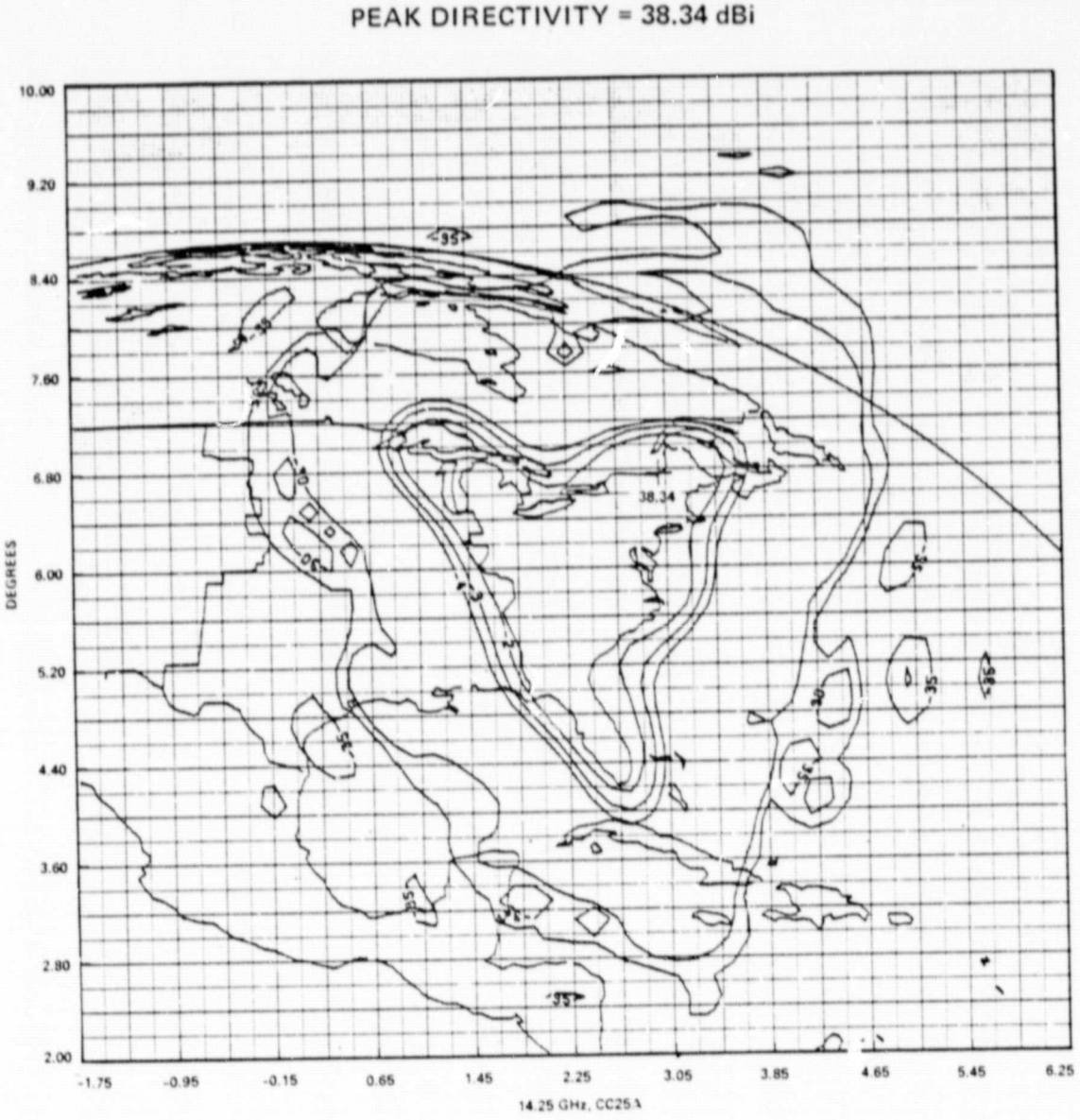

Figure 3.2-7. Uplink Co-Polarized Beam Isolation Contours at 14.25 GHz

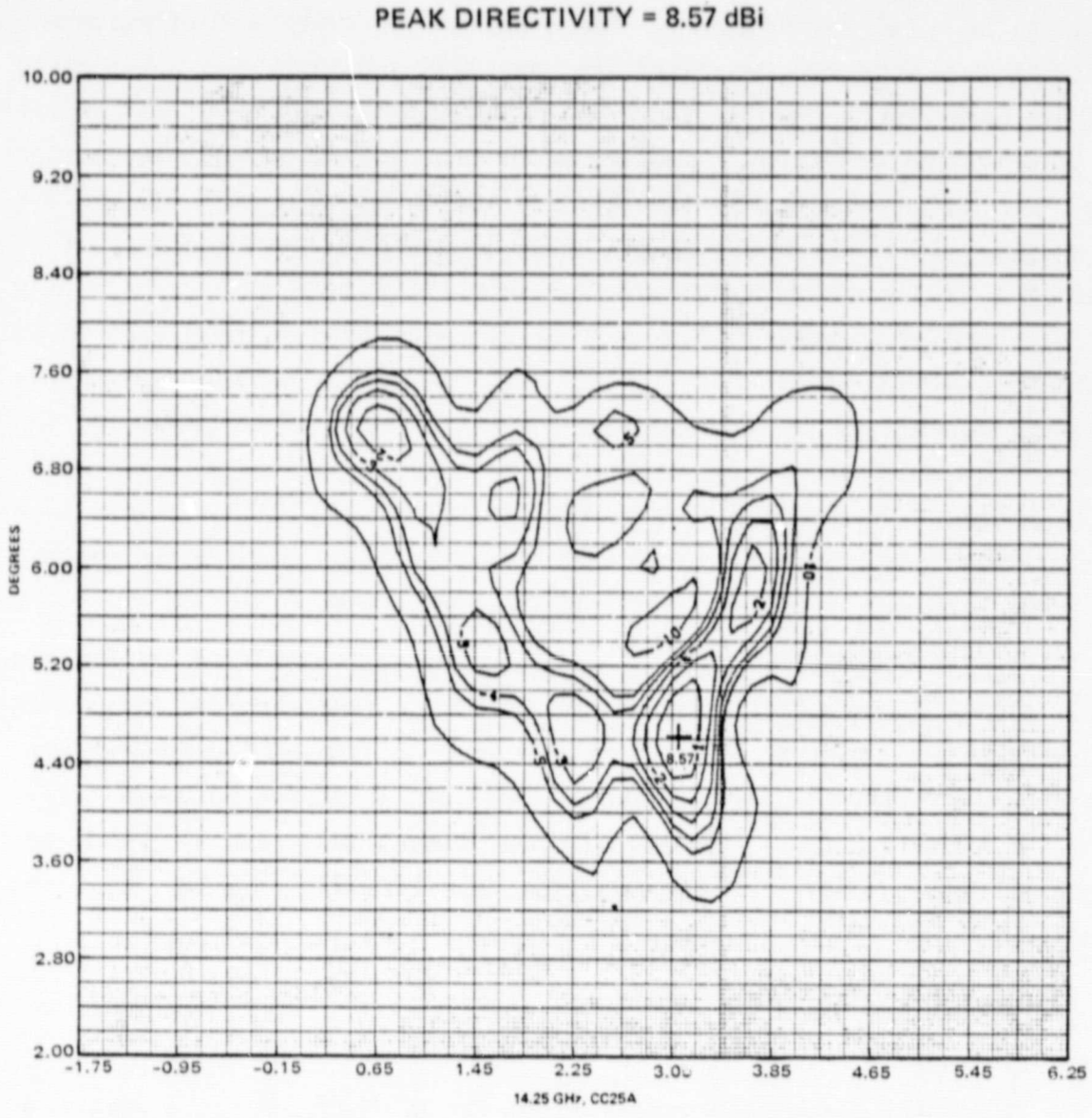

Figure 3.2-8. Uplink Cross-Polarization Gain Contours for ETZ Coverage at 14.25 GHz

were optimized at 11.95 GHz, the calculated gain contours at 14.25 GHz appear to be quite satisfactory. The peaks of the co-polarized radiation are 38.14 and 38.34 dBi, respectively, at 11.95 and 14.25 GHz. The peaks of cross-polarization radiation are about 30 dB below the peaks of principal polarization radiation. A 4 dB improvement in the cross-polarization level is expected when a grid subreflector is incorporated into the reflector system. It is obvious that the -2 dB contour follows the geographical boundaries of the eastern time zone closely. The gain variation at the edge of coverage is about 1.0 dB per 0.2 degree, which is considered to be reasonable, since antenna boresight can be aligned to within 0.05 degree pointing accuracy by using monopulse tracking with a known beacon on the ground. All sidelobes in the mountain time zone are at least 35 dB below the beam peak. This result implies that a 228 cm circular paraboloid with a 25-element array feed is sufficient to effectively illuminate eastern time zone with very little spillover to adjacent areas.

This beam synthesis technique appears to be very effective in that the gain contours fit closely to the desired coverage area, and the gain falls off rapidly with minimal energy spilled over to the adjacent neighbors. The success of this ETZ feed design implies that there should be no difficulty in providing good coverage for the other three zones, since the geographical shape of the eastern time zone is more complex than the others.

3.3 CONTOUR BEAM FEED DEVELOPMENT

3.3.1 Feed Design

A 25-element array feed was selected for development, as a result of the design analysis, to provide the Eastern time zone coverage over the 14/12 GHz band. The desired element excitations are given in Figure 3.3-1.

The design of a corporate feed network to feed a 25-element array with nonuniform power distributions over a 25 percent bandwidth is an extremely difficult task. During the tradeoff of the feed design, two feed circuits were considered. The first was a combination of hybrid couplers and septum power dividers. The desirable feature of this combination was the possibility of minimizing power amplitude variation by terminating the reflected

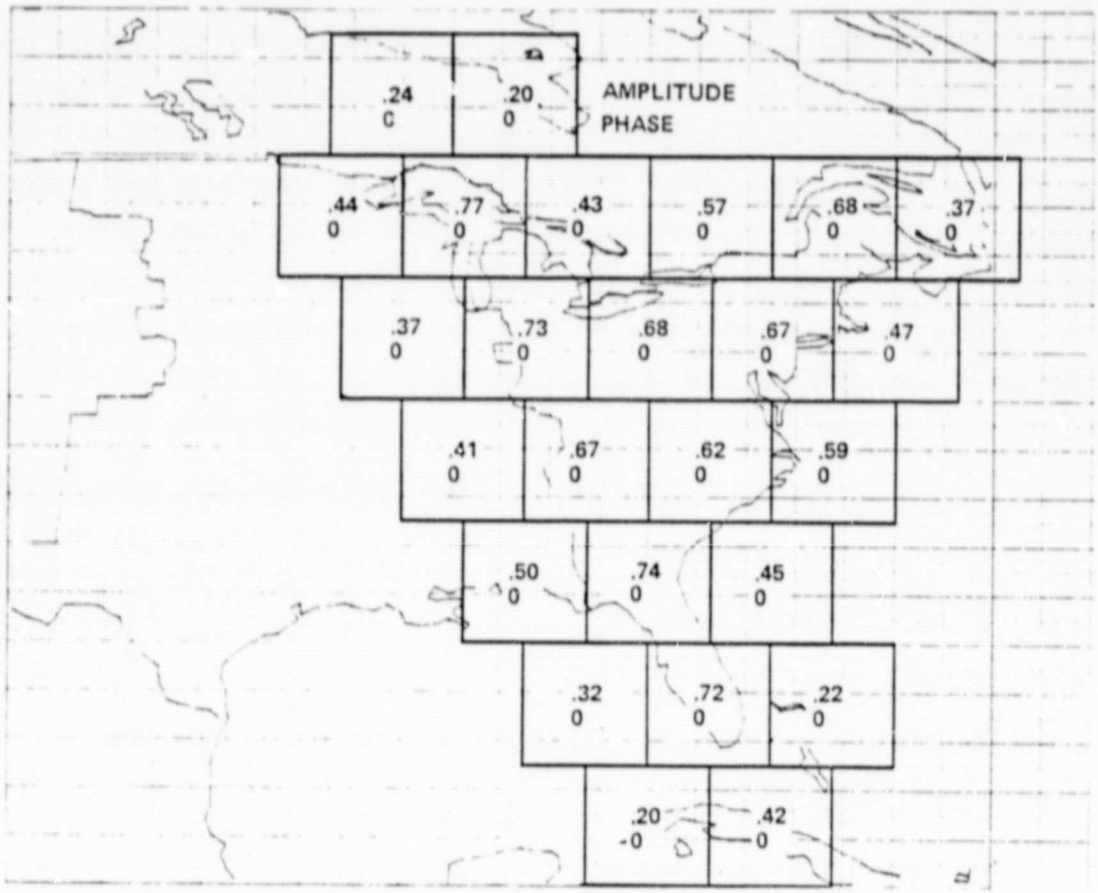

Figure 3.3-1. Reflector Image of ETZ Feed Cluster and its Amplitude and Phase Distribution Overlaid on the ETZ Map

energy into the impedance matched port in the hybrid. The drawbacks are: 1) the mechanical layout becomes complicated due to the large number of junctions required with hybrid devices; 2) the phase differences at the outputs of this corporate feed are difficult to compensate over a wide band of frequencies.

The second approach employs a three-tier cascading of septum power dividers. The septum power dividing technique developed in the nine-horn feed still remained a potentially viable solution to the proper power proportioning of the 25-element array. Because of the increased number of elements, an additional level of power division would be necessary. This additional stage, along with unequal power distribution, would compound the design complexity in maintaining constant power variations with respect to frequency. Nevertheless the operational bandwidth was still broader than the hybrid approach. Also, the mechanical layout was greatly simplified.

The hardware needed to generate the feed configurations above were:

1) Horn (same as nine-horn cluster)
2) 90 degree hybrid coupler
3) 180 degree dual-mode hybrid
4) E-septum power divider multiple power splits in one step
5) Step transformer
6) Reduced height waveguide
   - 1/8 height
   - 1/4 height
   - 1/2 height
7) Semiflex waveguide
8) E-plane and H-plane bends
9) 90 degree waveguide twists.

3.3.2 Feed Hardware Development

The horns and 90 degree waveguide twists were identical to those developed in the nine-horn array feed. An assortment of undersized waveguide bends, twists, and straight sections shown in Figure 3.3-2 was fabricated and tested. The measured insertion losses for 1/8 and 1/4 height

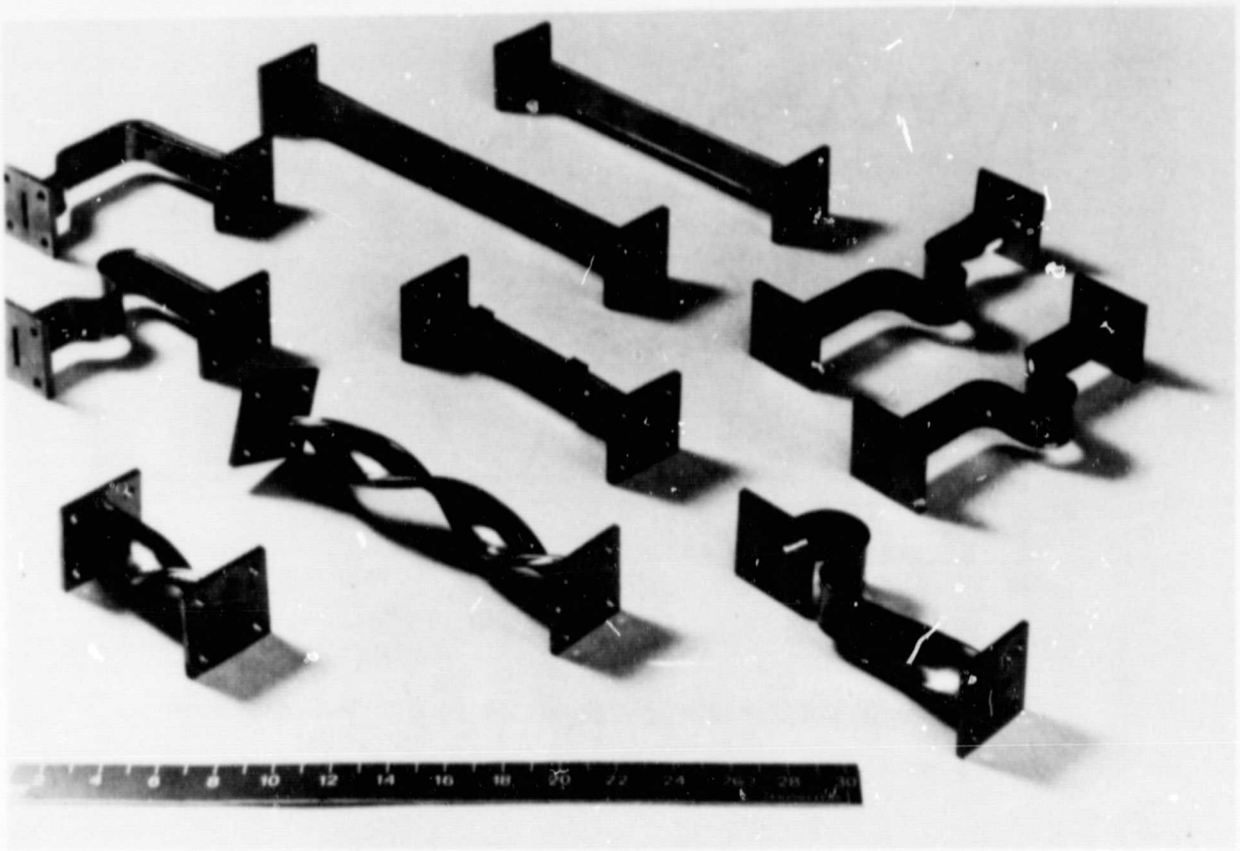

149473-78

Figure 3.3-2. Reduced Height Waveguide Components

waveguide are presented in Figure 3.3-3. The swept frequency VSWR of a typical waveguide H-plane 90-degree bend is presented in Figure 3.3-4. The VSWR of an E-plane bend is usually lower than the H-plane bend. Figure 3.3-5 shows H-bend waveguides.

FREQUENCY (GHZ)	LOSS 1/8 HEIGHT (DB/FT)	LOSS 1/4 HEIGHT (DB/FT)
11.7	0.26	0.21
11.95	0.30	0.17
12.2	0.36	0.16
14.0	0.42	0.16
14.25	0.31	0.18
14.5	0.33	0.18

WR 75 WAVEGUIDE LOSS = 0.04 DB/FT AT 11.8 GHZ

Figure 3.3-3. Measured Insertion Loss of 1/8 and 1/4 Height Waveguide

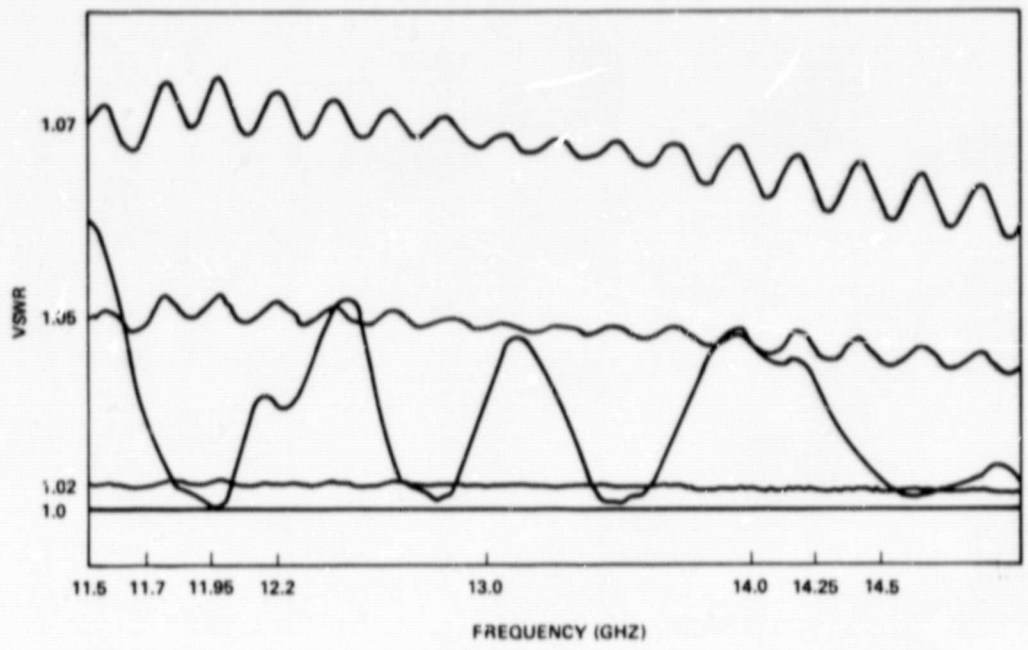

Figure 3.3-4. Reduced Height Waveguide H-Plane Bend
Radius = 1.27 cm (0.500 Inch)

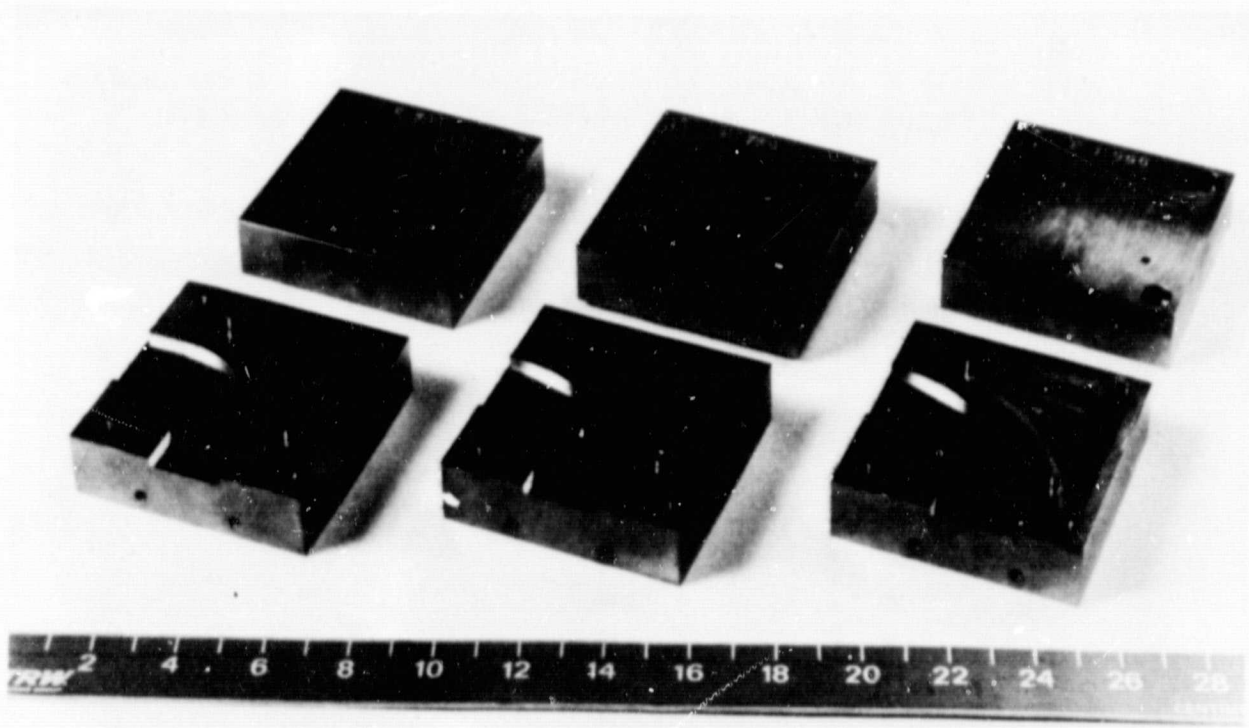

149472-78

Figure 3.3-5. Reduced Weight H-Bend Waveguides

Multiport 90 and 180 degree hybrids were designed and fabricated (Figure 3.3-6). The 180 degree hybrid was designed to operate over two separated frequency bands. The performance is illustrated in Figure 3.3-7. The design of this component becomes a tradeoff between lower frequency bandwidth and frequency separation between two bands; separation can be reduced at the cost of narrowing the low frequency bandwidth. The 90 degree hybrid is much easier to fabricate and can be modified to provide unequal power division. However this device is extremely narrowband.

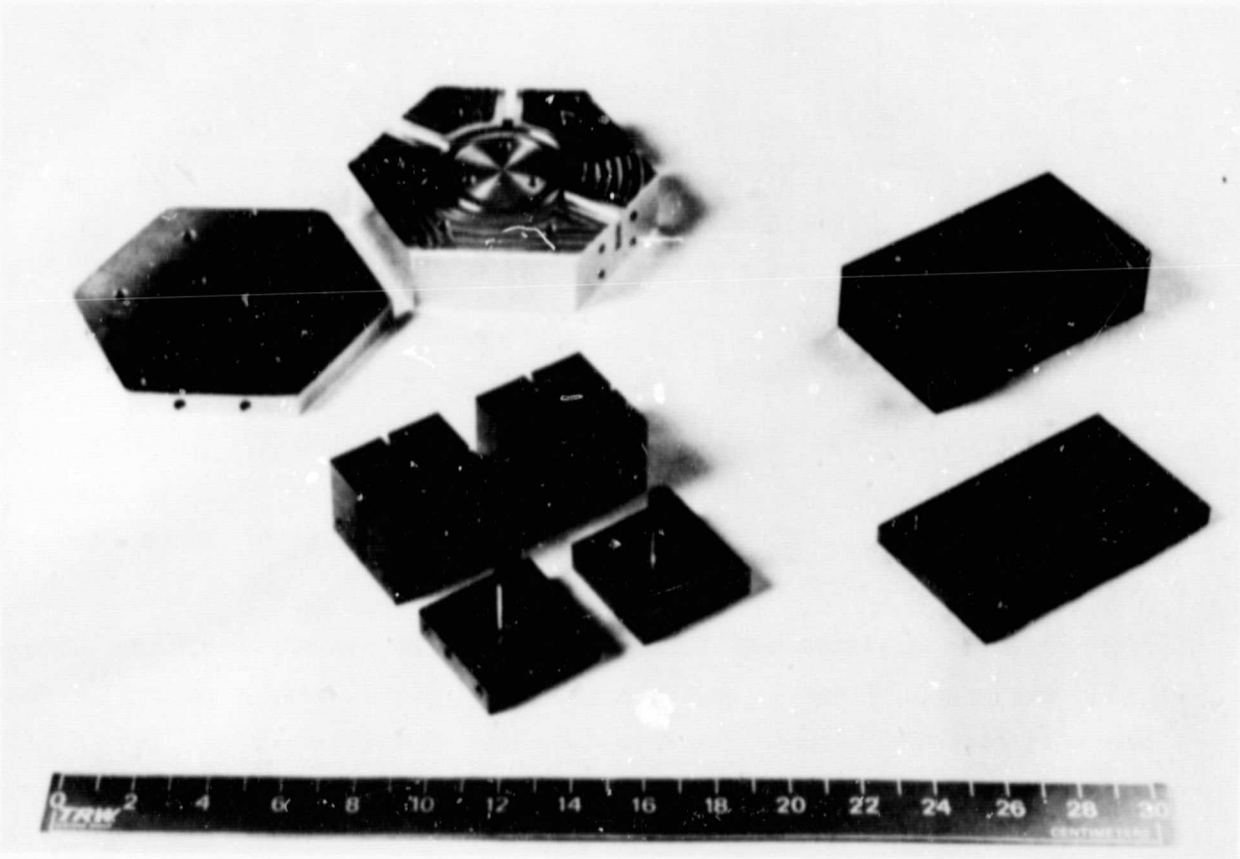

149474-78

Figure 3.3-6. Dual Mode Hybrid Couplers

A revised version of the septum power divider used in the nine-horn array feed was designed and fabricated. Two-, three-, and four-way power splitters were needed to accommodate the feed distribution. Unequal power divisions of up to 10:1 were required to achieve the desired feed aperture distrubition. It was decided to make the power dividers adjustable for fine tuning of the output levels of each port.

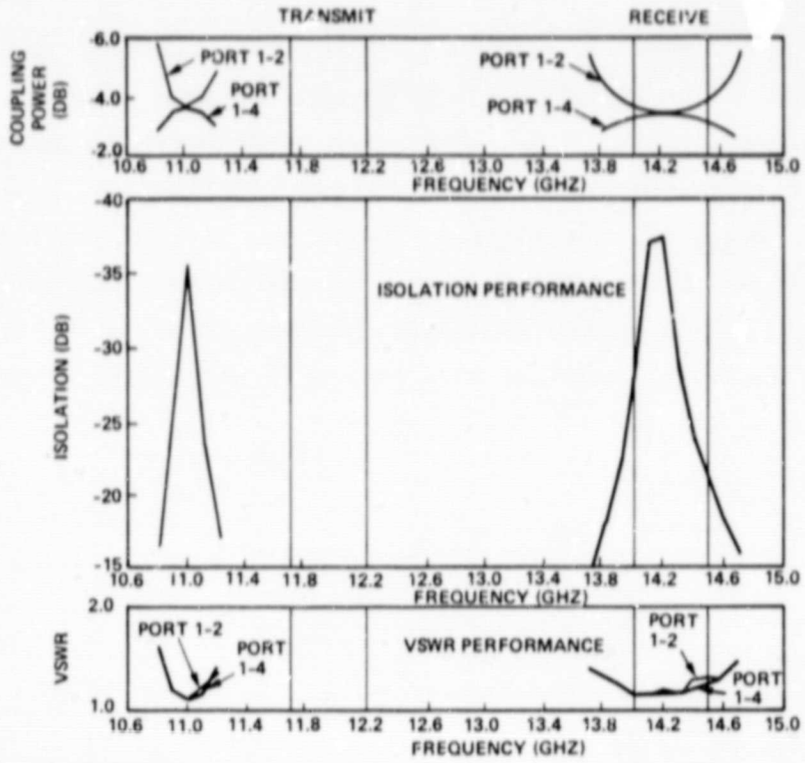

Figure 3.3-7. Performance of Dual Mode Waveguide Hybrid

Evaluation of the above feed components led to the choise of the E-plane septum divider as the sole power distributing element in the feed network. To complete the ETZ feed, three levels of nine, three, and one power dividers each were needed.

Feed power division was accomplished by the process described above. Phasing was accomplished in two steps. First, semiflexible waveguide sections were inserted between the horns and the divider network. The lengths of these sections were varied to equalize the path length differences. Then, reduced height trombone sections were placed between second and third stage dividers to complete the phasing. A photo of the 25-element array feed is shown in Figure 3.3-8. This feed assembly consists of:

1) 25 waveguide horns

2) 25 sections of flexible waveguide

3) 13 power dividers

4) Nine trombone sections

5) Three 90 degree twists.

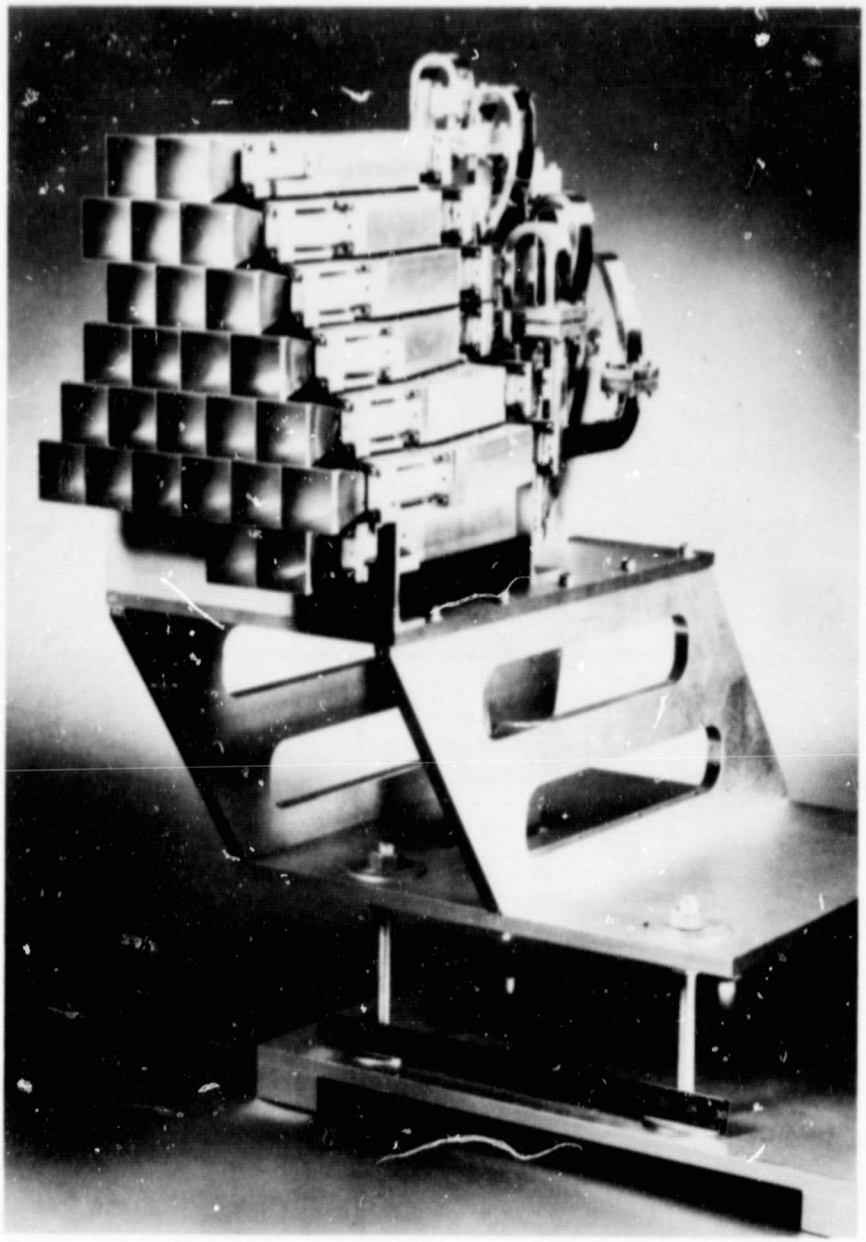

155702-79

Figure 3.3-8. Twenty-Five-Element ETZ Array Feed

The measured in-band VSWR was less than 1.2:1 and the total feed circuit loss was:

Frequency (GHz)	Loss (dB)
11.7	0.56
11.95	0.54
12.2	0.47
14.0	0.54
14.25	0.63
14.5	0.64

Figure 3.3-9 shows the measured amplitude and phase distribution of the 25 horns at 11.95 GHz.

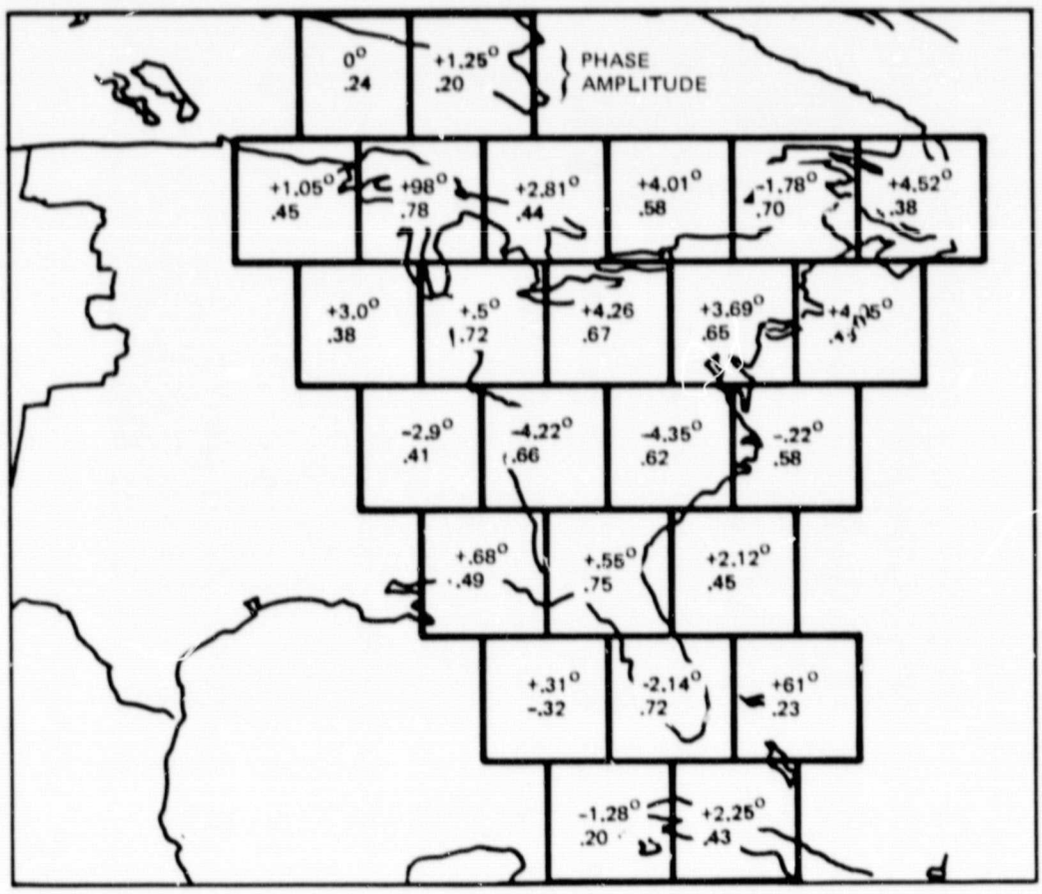

Figure 3.3-9. Measured Amplitude and Phase of ETZ Array Feed at 11.95 GHz

3.3.3 High Power Tests

For the contoured beam feed, the highest level of power is seen by the input power divider. Thus, high power testing of the input divider was performed. Tests were conducted with the same procedure and equipment used for the spot beam feed. The power levels supplied to the feed during the test were as follows:

1) For 11.95 GHz - 68 watts average for 20 minutes at 7.4×10^{-6} to 1.0×10^{-5} torr pressure.

2) For 14.25 GHz - 69 watts average for 20 minutes at 1×10^{-5} torr pressure.

No arcing or disturbance of the operation occurred at any time during the test.

3.4 CONTOURED BEAM FEED FABRICATION

3.4.1 Reduced Height Waveguide

To connect the three levels of divider circuits, an assortment of interconnecting waveguide bends and straight sections were needed. To accommodate the tight feed package needed to minimize insertion losses, flexible and reduced height waveguide sections were fabricated. The flexguide was cut to specified lengths, flanged, and formed on a machine tool. Phase adjustments were made by slightly reforming the flexguide and trimming the flanges. All steps transitions and reduced height sections were made to precise dimensions by fabricating softened aluminum mandrels to be shaped as desired and electroformed with copper. The H-plane bends were machined into the aluminum mandrels. The E-plane bends were formed from annealed aluminum plate material machined to a desired thickness. After forming a 180 degree E-plane bend with a 1/2 inch bend radius, the mandrels were machined to the "H" plane finish dimensions. Final forming of each mandrel was done manually by superimposing on the design layout. Once shaped, the mandrels were electroformed with copper, machined, and flanged with extra thick flanges that were trimmed to phase. The final lengths of these sections were determined by electrical testing of assemblies. All associated brackets were machined and fabricated as required to index, locate, and support the antenna assembly.

3.4.2 Power Dividers

Power dividers were machined from aluminum stock. The septums were machined to standard dimensions. The adjacent wall in each port was tapered from the septum junction to the output port. If the change in impedance between these two junctions exceeded a value that could be matched with a short taper, the taper was terminated at a predetermined impedance. From this point on; a standard step transformer was used to complete the circuit. The taper angles were established by the desired power split and the output port separation. Center port openings were obtained by additional machining on the inner face of the standard septums. Thus, the divider circuit consisted of a standard septum, a standard step transformer, and a standard divider geometry. To satisfy the fine tunning requirement, a screw adjustment mounted in an eccentric slot permitted slight movement of the septums.

3.5 NEAR FIELD MEASUREMENTS

The purpose of this measurement is to assure that the secondary pattern performance can be met before the reflector is assembled and tested in the far field range. A planar near field range was set up as shown in Figure 3.5-1. First a complete electromechanical checkout of the range was performed to verify smooth operation of the probe movement and the stepper motor drive system. A known test aperture, designed to operate in the 10 to 15 GHz range, was placed in the position to be filled by the contoured beam feed. This aperture was mechanically and optically aligned to assure that the aperture plane was parallel to the scanning plane and to establish the boresight coordinates. An open ended waveguide was used as a probe to measure the near field distribution of the feed.

The phase and amplitude distribution of a feed aperture was sampled over a specified scanning plane, a lattice of $\pm$20 inches in the x direction and $\pm$20 inches in the y direction. The vertically polarized field was measured with the probe aligned to the vertical axis. The horizontal field was taken with the probe rotated 90 degrees to the vertical axis. The measured data was computer processed and mathematically transformed to yield far field feed patterns. Measurements were taken at several probe positions off from the feed aperture to establish the proper distance required to minimize the coupling between the probe and feed aperture.

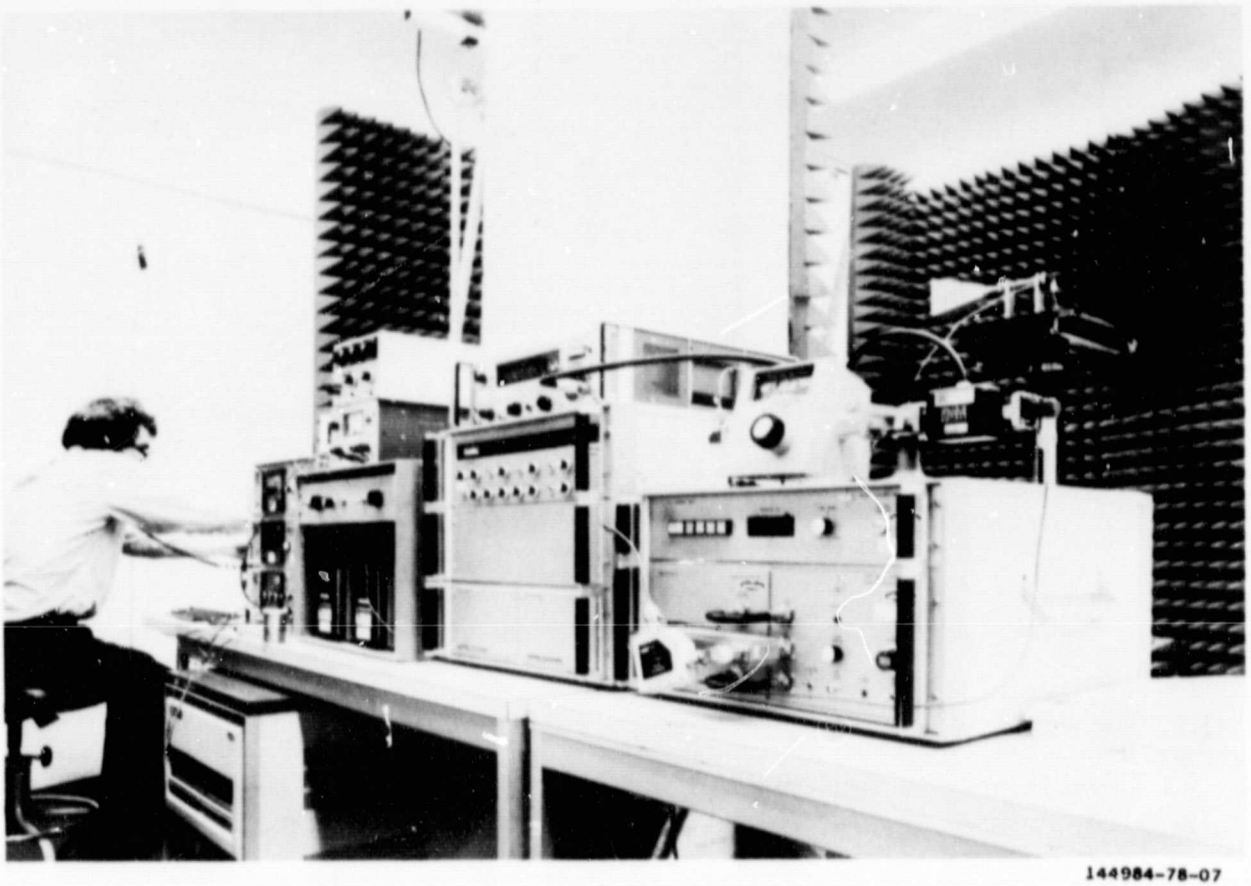

144984-78-07

Figure 3.5-1. Experimental Test Setup for Planar Near-Field Aperture Probing

Comparison between known test aperture patterns and those generated by the near field probing were in agreement. The test aperture was replaced by the breadboard contoured beam feed.

Each contoured beam required two near field measurements, one for vertical and the other for horizontal polarization. The data was used to compute secondary patterns. A secondary contour pattern at 11.95 GHz was computed, using the measured near field data. The results are given in Figure 3.5-2.

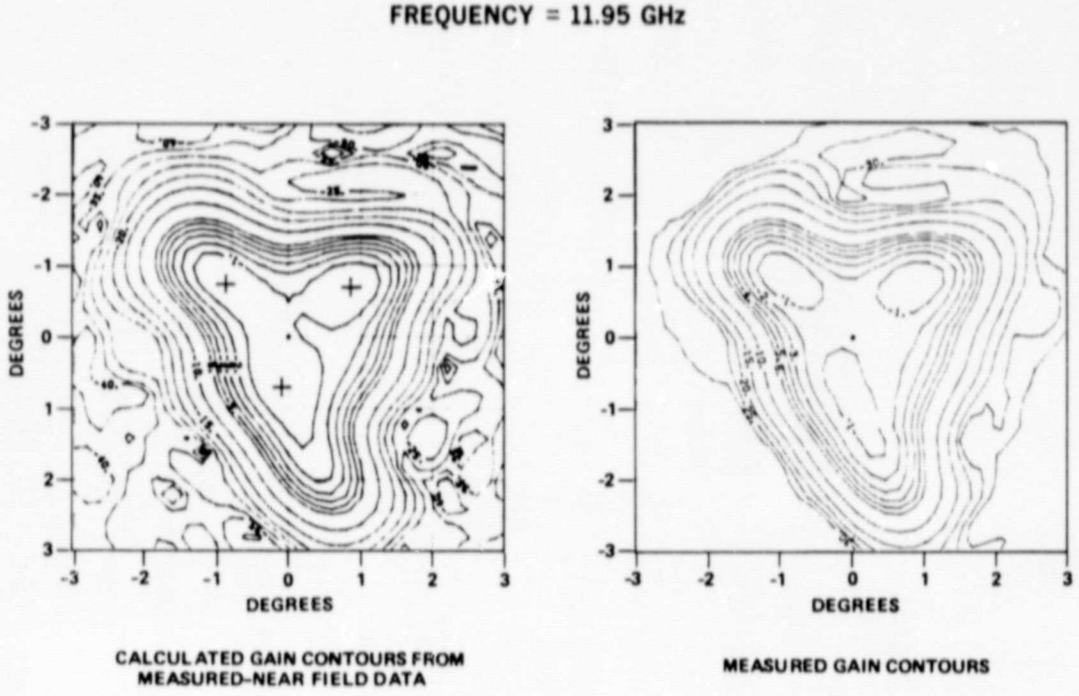

Figure 3.5-2. Calculated and Measured Far-Field Gain Contours

3.6 FAR-FIELD TESTS

A decision was made to test the ETZ feed using the spot beam offset reflector. This reflector configuration is similar to the desired contoured beam reflector configuration except the projected aperture diameter is 200 cm instead of 228.6 cm, corresponding to a 0.875 scale model of the full size reflector. The ETZ contour feed was installed on the fixture in the front fed position as shown in Figure 3.6-1. The alignment of the feed was the same as that used for the spot beam antenna. After the feed was aligned to the focal point of the reflector it was repositioned to an azimuth offset by restraining movement in all other coordinate directions while sliding the feed along the azimuth axis to a premarked position. The purpose of the offset was to allow room for the addition of a Central time zone feed. Since the feed was placed in a 200 cm rather than 228.6 cm offset reflector, the lateral displacement was 11.4 cm from the focal point in azimuth. A wire grid subreflector was inserted between the reflector and the ETZ feed in order to simulate the actual polarization diplexing conditions.

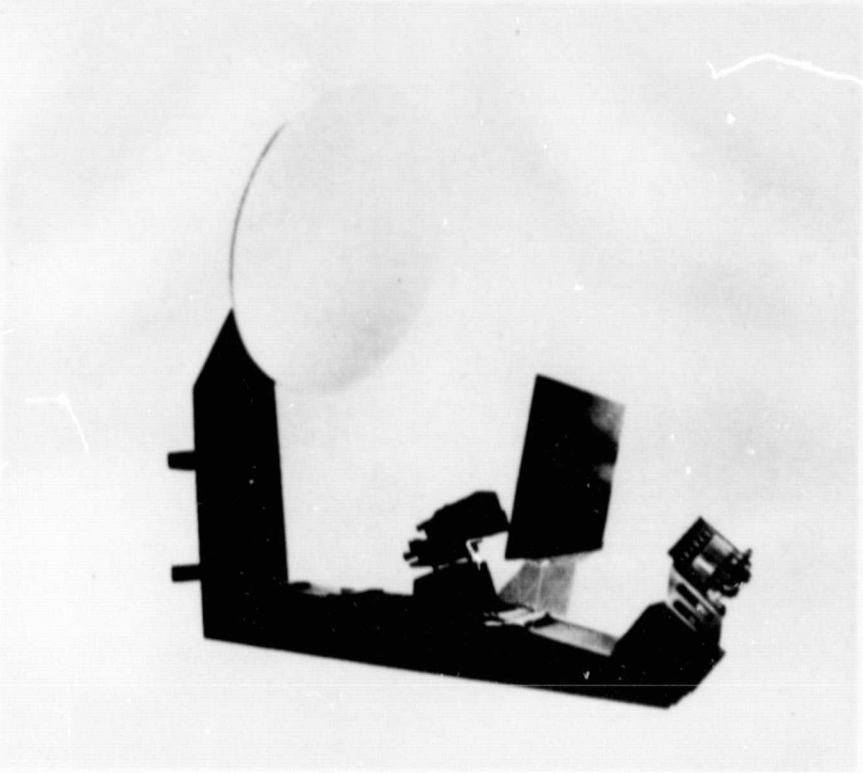

152865-79R

Figure 3.6-1. Contoured Beam Antenna, Reflector/ Feed Assembly

Principal and cross polarization contour plots were generated for the following frequencies: 11.7, 11.95, 12.2, 13.0, 14.0, 14.25, and 14.5 GHz. Figures 3.6-2 through 3.6-4 show the comparisons of calculated and measured gain contours at three representative frequencies 11.7, 11.95, and 14.5 GHz. Figure 3.6-5 shows a three dimensional plot of both calculated and measured gain contours at 11.95 GHz. It is noted that correlation between the calculated and measured gain contours is excellent down to the -35 dB level below the peak of the beam. The minor difference in the -40 dB level may be attributed to the imperfect antenna range and test environment, such as transmission through the radome curtain and scattering from reflector supports etc.

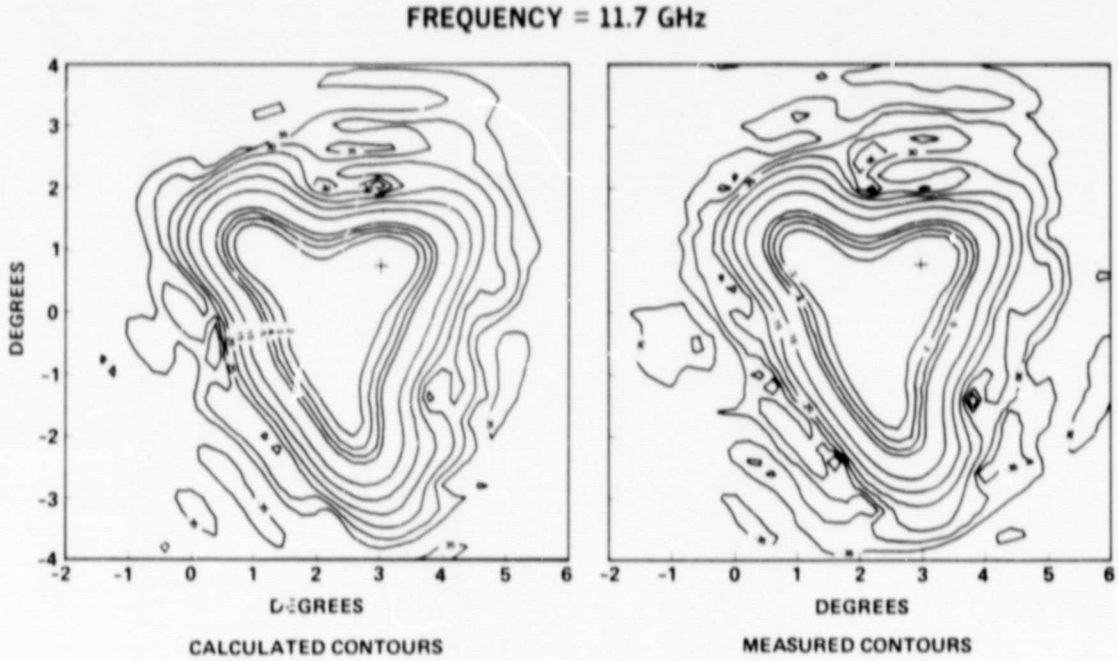

Figure 3.6-2. Comparison of Calculated and Measured Gain Contours

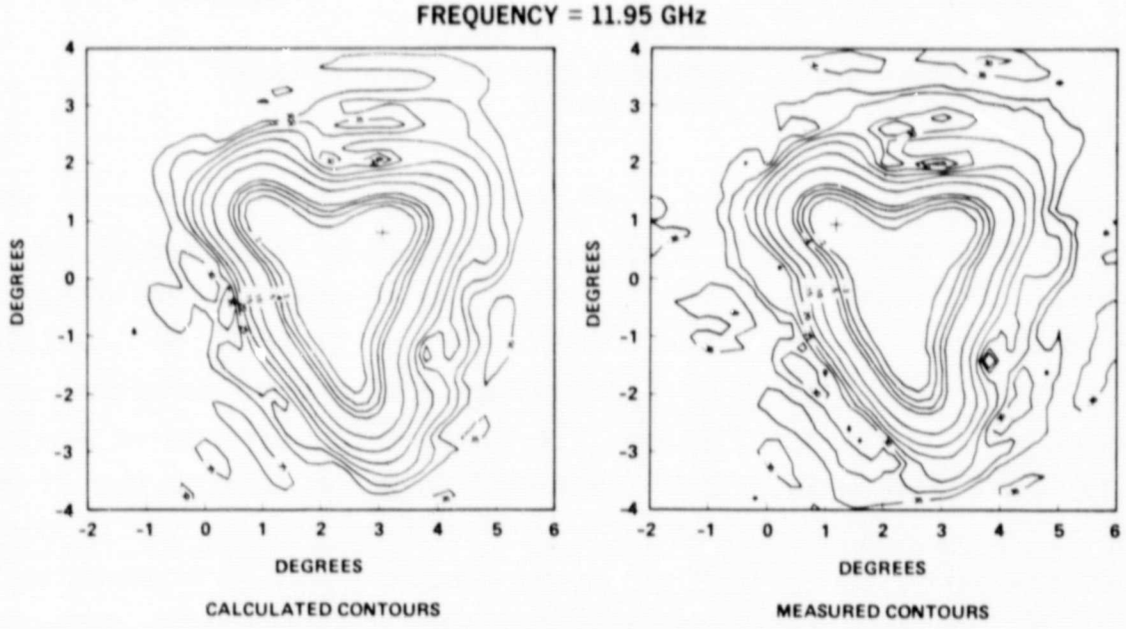

Figure 3.6-3. Comparison of Calculated and Measured Gain Contours

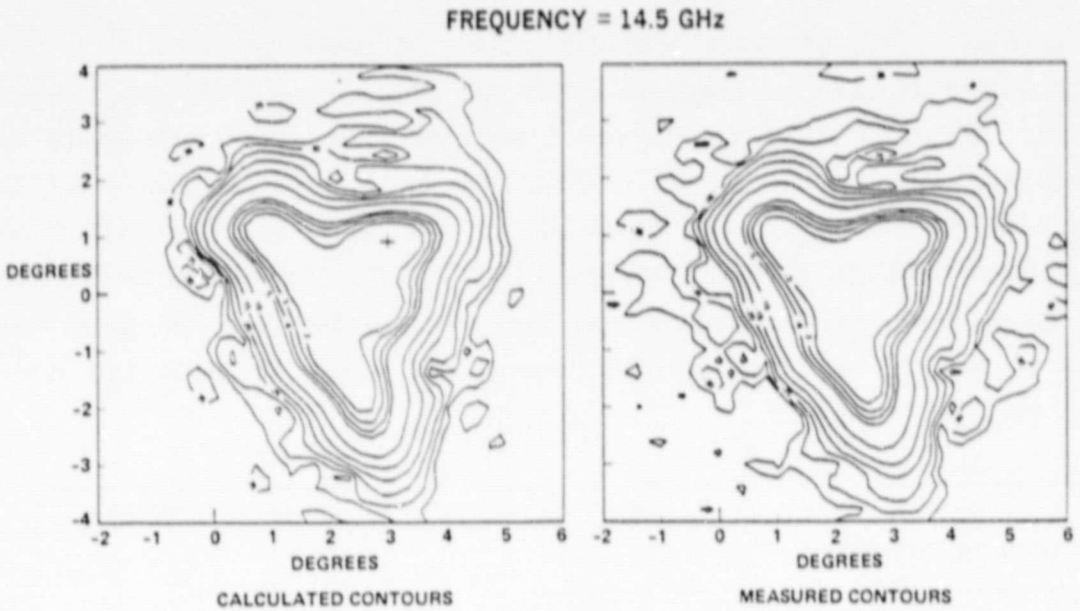

Figure 3.6-4. Comparison of Calculated and Measured Gain Contours

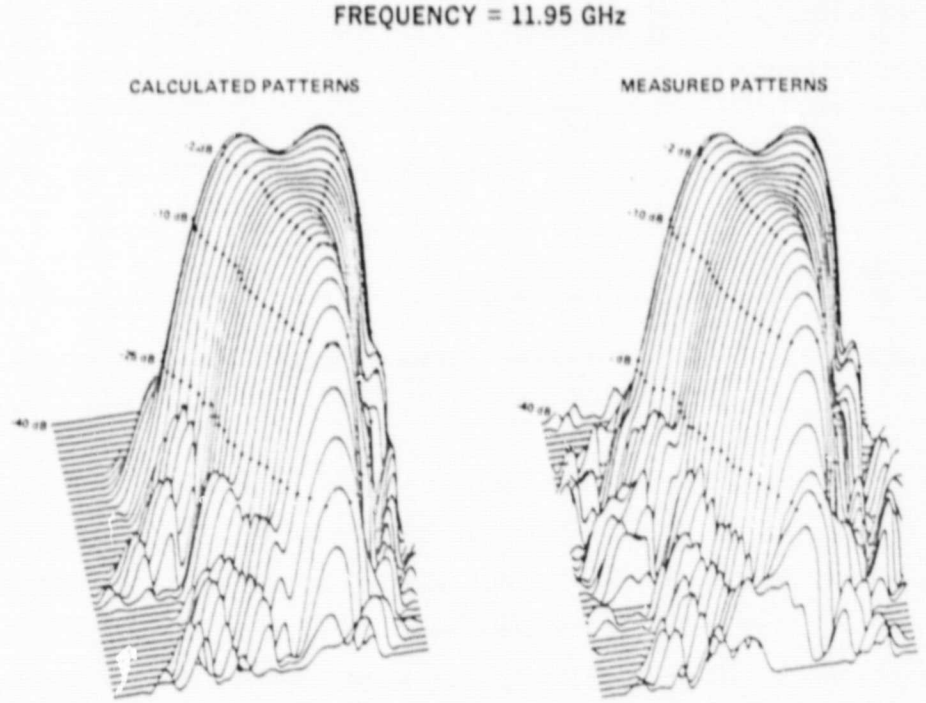

Figure 3.6-5. Comparison of Calculated and Measured Radiation Patterns

3.7 CONCLUSIONS

The feasibility of using a single offset reflector antenna to provide a contiguous time zone coverage of CONUS has been fully established by the design and development of an Eastern time zone feed which represents the most complicated feed in the four time zone beams. A comparison of the design specifications and the measured capabilities is given in Figure 3.7-1. Both sidelobe and cross-polarization levels, and consequently beam isolation performance, are better than orginally expected. The beam shape as well as antenna peak gain remains roughly the same throughout the entire 11.7 to 14.5 GHz bandwidth.

	SPECIFICATIONS	MEASURED CAPABILITY
DOWNLINK FREQUENCY	11.7 TO 12.2 GHz	11.7 TO 12.2 GHz
UPLINK FREQUENCY	14.0 TO 14.5 GHz	14.0 TO 14.5 GHz
POLARIZATION	ORTHOGONAL LINEAR	ORTHOGONAL LINEAR
COVERAGE AREA	EASTERN TIME ZONE	EASTERN TIME ZONE
MINIMUM COVERAGE GAIN	35 dBI	35 dBI
COVERAGE GAIN VARIATION	$\leq$ 4.0 dB WITHIN COVERAGE AREA	$\leq$ 2.5 dB FOR DOWNLINK $\leq$ 3.0 dB FOR UPLINK
SIDELOBE LEVEL	-32.0 dB IN MOUNTAIN TIME ZONE	-34.0 dB
CROSS POLARIZATION	-28.0 dB	-32.0 dB
BEAM ISOLATION	$\geq$ 28 dB BETWEEN ANY TWO BEAMS	$\geq$ 30 dB
POWER HANDLING CAPACITY	100 WATTS AVERAGE POWER	100 WATTS
FEED CIRCUIT LOSS	$\leq$ 0.45 dB	$\leq$ 0.56 dB
VSWR	$\leq$ 1.2:1	$\leq$ 1.2:1
REFLECTOR DIAMETER	$\leq$ 400 CM	230 CM

Figure 3.7-1. Contoured Beam Antenna Design Specifications and Measured Capabilities

The feed circuit loss is slightly higher than the estimated value which is attributed to the long waveguide run and the flex waveguide sections used for equalizing the output phases in the breadboard model. In the flight hardware the flex waveguide section will be completely eliminated and the overall waveguide run can be made shorter to reduce the feed circuit loss.

The contoured beam synthesis technique has been fully established and verified by actual measurements. The experience gained in fabricating and testing a wideband contoured beam feed is invaluable.

REFERENCES

1. W.C. Wong, "TRW Reflector Software," TRW Internal Memo, October, 1979.

2. A.W. Rudge and N.A. Adatia "Offset-Parabolic — Reflector Antennas: A Review," Proceedings of the IEEE, Vol. 66, No. 12, December 1978.

3. E.J. Wilkinson," A Dual-Polarized, Cylindrical-Reflector Antenna for Communication Satellites," Microwave Journal, December 1973, pp. 27-30.

4. C. Dragone, "New Grids for Improved Polarization Diplexing of Microwaves in Reflector Antennas," IEEE Trans. Antennas and Propagation, Vol. 26, No. 3, May 1978, pp. 459-463.

5. T.S. Chu, "Cancellation of Polarization Rotation in an Offset Paraboloid by a Polarization Grid," Bell System Technical Journal, Vol. 56, No. 6, July-August 1977.

6. C.C. Chen, "Scattering from Parallel Plate or Strip Grating," TRW Internal Memo No. 77-7320.17-238, September 16, 1977.

7. J. Ruze, "Antenna Tolerance Tehory — A Review," Proceedings of the IEEE, Vol. 54, April 1966, pp. 633-640.

8. H.H. Rosenbrock, "An Automatic Method for Finding the Greatest or Least Value of a Function," Computer Journal, October 1960.

APPENDIX A
ANTENNA FAR FIELD PATTERN TEST FACILITIES

A.1 RANGE SETUP

Secondary pattern measurements were performed at a 10,000 foot range located at TRW's San Juan Capistrano Test Site. The transmit and receive sites were located on hills separated by a canyon. A profile of this range is shown in Figure A-1. The test equipment setup is shown in Figure A-2.

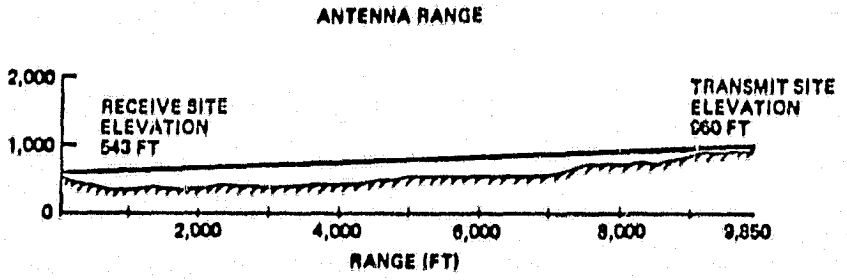

Figure A-1. Capistrano Test Site Range 1 Profile

Equipment performance was calibrated by the TRW Metrology Laboratory. The source antenna shown in Figure A-3 used for CONUS beam pattern tests was a 152 cm diameter low sidelobe offset paraboloid fed by a nine-horn array feed similar to the one described in Section 2.3. It was designed to provide a 1.3 degree half power beamwidth pencil beam, at 11.95 GHz, with all sidelobes below the -40 dB level from the peak of the main beam. This antenna was made up of three sections:

- A rotatable polarization feed
- A deployable support structure (stowed when not in use)
- Offset parabolic reflector.

The reflector was mounted to the antenna support structure. The alignment procedure was the same one used for the CONUS antenna: a template rotated about a principal axis pivotal line. The feed was attached to a polarization positioner and collimated on a machine shop flat. It was dowl pinned so it could be removed when necessary. The positioner was attached to the support, after which the feed was replaced by a collimated light source. The positioner was adjusted until the light beam coincided

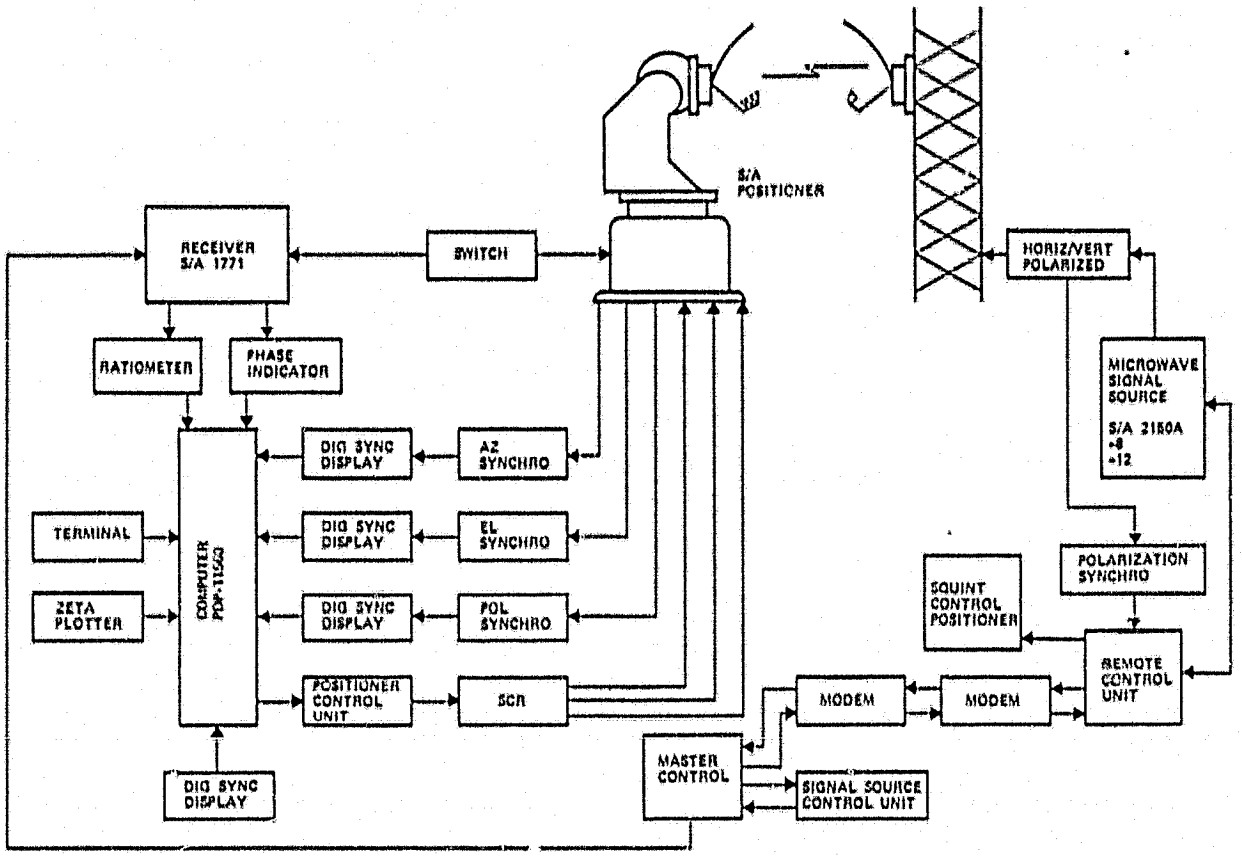

Figure A-2. Equipment Setup at 3000 Meter (10,000 Foot) Antenna Range

with the reflector geometry feed axis. It was then locked down and the feed reinserted into position. A Scientific Atlanta center fed parabolic reflector, calibrated by the National Bureau of Standards in Boulder, Colorado, was used as a transmit antenna when evaluating the source antenna and test antenna in the range checkout.

The reflector antenna under test was about 2 meters in diameter. The 10,000 foot antenna range is about $19D^2/$, at 11.95 GHz, which limits the phase variation over the test aperture to less than 3 degrees. This phase variation ensures that signal levels on the order of 36 dB below the beam peak are accurately measured.

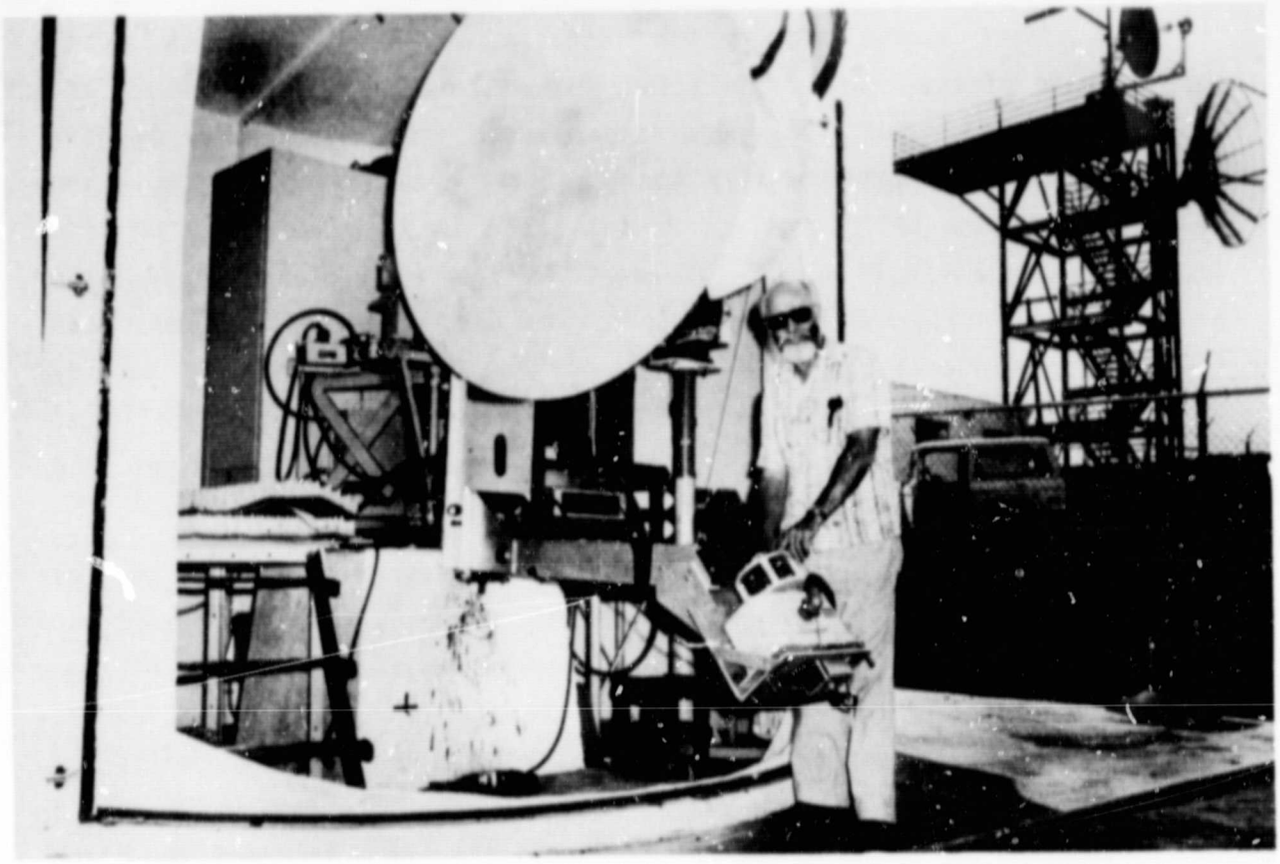

161327-79-3

Figure A-3. Transmit Antenna Setup, 150 cm Diameter Offset Reflector with Nine-Horn Array Feed

Range evaluation was undertaken after the test facility was set up. During this process, proof of adequate instrumentation and the test environment needed to be established. Sources of measurement variations occuring during the far field test were divided into the following catagories:

- Antenna alignment
- Extraneous reflections
- Radome curtain interference
- Measurement stability.

A.2 ANTENNA ALIGNMENT

The offset source antenna was installed as a test antenna on the receive side of the range. The Scientific Atlanta reflector was used as a transmit antenna. Position coordinates, known from previous range work, were used to yield approximately correct boresight between the two antennas. Each of the reflectors was installed on an x, y polarization positioner which provided lateral movement in the x, y-plane and rotation around a roll axis. A boresight scope was used to align the roll axis. The scope was placed in front of and looking into the transmit antenna. The antenna location on the positioner was adjusted until its roll axis coincided with the crosshairs of the boresight scope. The boresight scope was then removed.

The equipment was turned on and the RF link established with the test antenna held fixed. The Scientific Atlanta source antenna was moved in x and y, to the beam peak, in the plane perpendicular to the line-of-sight direction. This was followed by fixing the source antenna at the coordinates of the peak of its main beam and moving the test antenna to its main beam peak. This process was repeated until the two main beam peaks were in line. Each of the antennas was rotated in polarization to check the alignment of the polarization axis by comparing the peak-to-peak axial ratio of 0 to 180 degree rotation to the 180 to 360 degree rotation. Any change made in the axis position required a realignment of the main beam peaks. These two processes were iterated until the two main beam peaks and the rotational axis were electrically aligned. Increased alignment accuracy was obtained by cross-polarizing the two antennas, once they were boresighted, and repeating the above procedure using the cross-polarization null. Remaining differences in principal and cross polarization alignment appeared as slight assymetrics in the cross-polarization patterns. These were attributed to feed displacement in the reflector geometry.

A.3 EXTRANEOUS REFLECTIONS

Extraneous reflections of the transmitted wavefront can significantly distort the free space radiation patterns. The field at a point in the test aperture is the sum of the principal and extraneous radiating fields. The phases and amplitudes of these field components vary over the aperture surface. This causes variations in the illuminating wavefront. A major contributor to these error components is source antenna sidelobes.

A low sidelobe antenna was designed to be used as the source antenna. Figure A-4 illustrates the feed assembly. Radiation patterns were measured with the range setup as described above. Pattern data revealed a 33 dB shoulder in the field emanating from the upper hemisphere region of the reflector. This presented no potential ground reflection problems. Measured patterns shown in Figure A-5 show sidelobes to be below 35 dB in all other regions. No range evaluation was completed prior to these measurements. It was assumed that any existing extraneous signals would have no impact on final CONUS beam patterns since a final range checkout was to be accomplished using the source antenna at the transmit post.

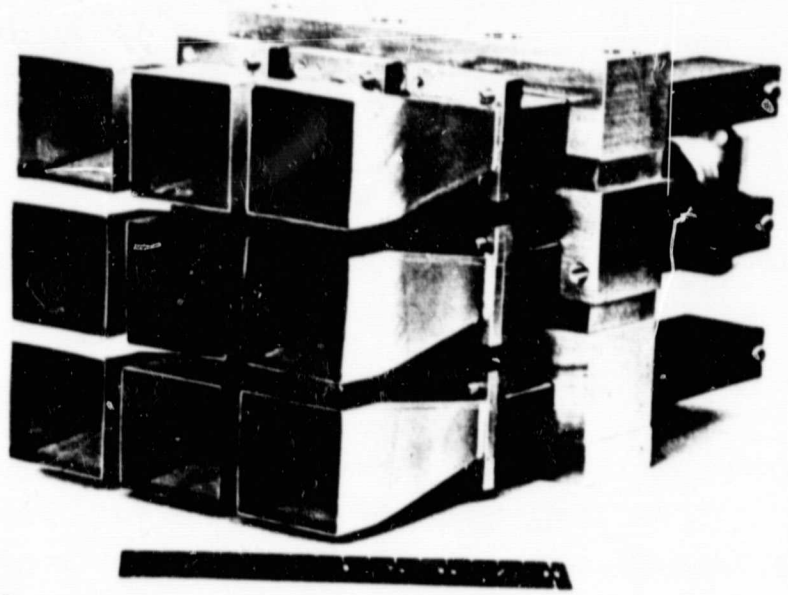

141876-77

Figure A-4. Feed Assembly

After the source patterns were taken, the low sidelobe and Scientific Atlanta antennas were interchanged. The two antennas were aligned as previously described. Range reflection interference levels were examined by pattern comparison measurements. This consisted of comparing two

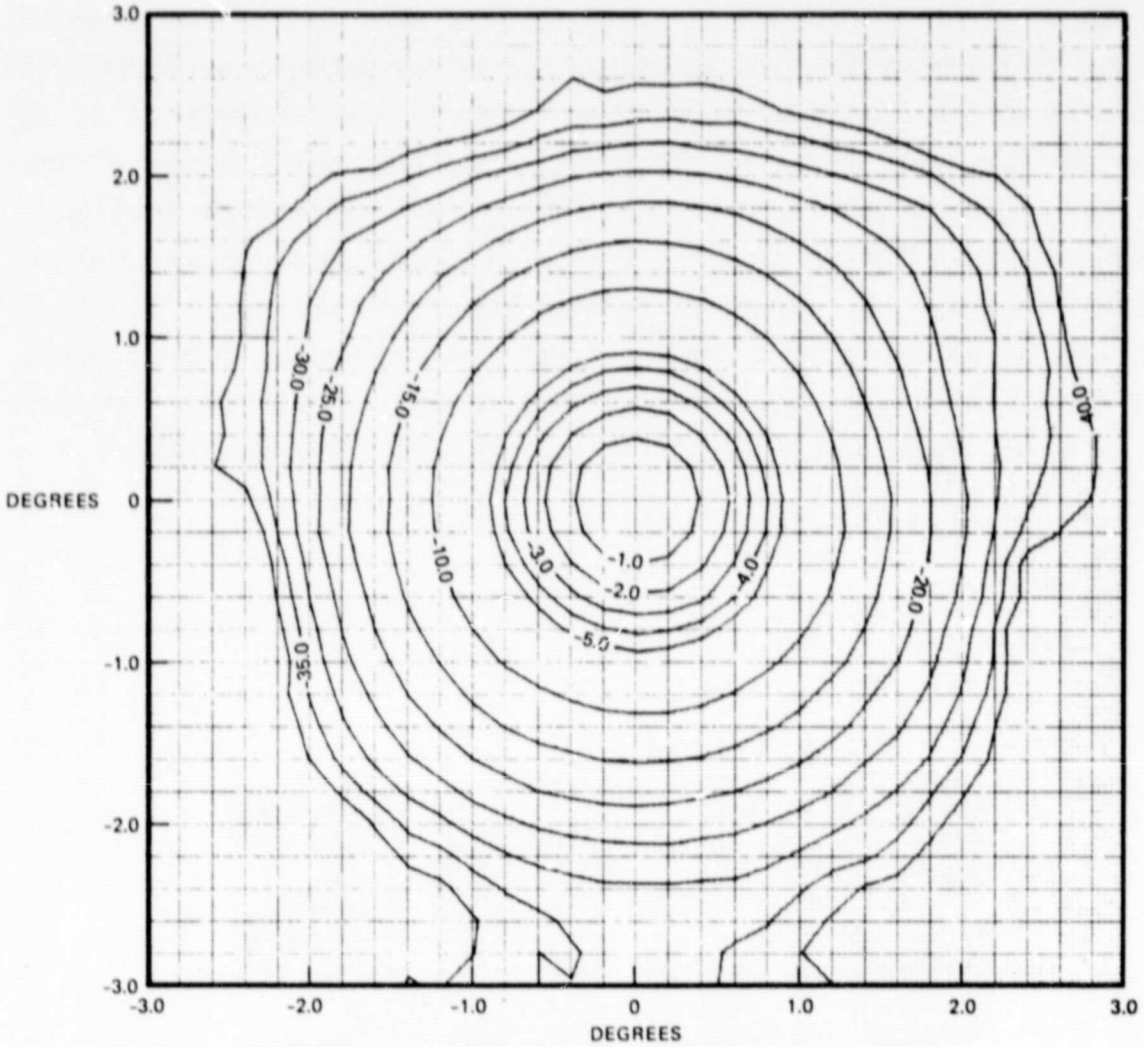

Figure A-5. Measured Transmit Antenna Pattern

patterns recorded with the same geometrical relationship between the incident field and the receiving antenna. The primary purpose of this method was to identify extraneous signal interference levels along the transmission path and at the wide angle minor lobe regions of the field. The level of the extraneous signals was determined by noting variations in principal signal amplitude with respect to changes in phase. Elevation and azimuth patterns were taken with the polarization vectors of the transmit and receive antennas pointing perpendicular to the range ground. The test antenna was moved vertically, only, in a plane perpendicular to the line-of-sight. Again, elevation and azimuth patterns were taken. Vertical movement altered the phase relationships between desired and undesired

signals. Additional changes in test height were made until a full period of destructive and constructive phase conditions had been traversed. The maximum peak-to-peak deviations of the main beam and minor lobe amplitudes were recorded.

The two antennas were rotated until their polarization vectors were horizontal to the range ground. As in the preceding case, the peak-to-peak deviation of major and minor lobe amplitudes were determined over the field region of interest. For vertical polarization, the minimum ratio of reflected signal to direct signal strength was -45 dB. This was determined from the 0.1 dB ripple of the 27 dB minor lobe level. The horizontal polarization ratio was -39 dB, determined from the 0.2 dB ripple of the -31 dB minor lobe. Additional evaluation was possible by comparing patterns taken when the antennas were orientated in like geometrical relationships, but differing in polarization. A third check was to compare the measured data with that produced by the National Bureau of Standards. At their facility, planar near field measurements were performed on the Scientific Atlanta reflector. The data was then reprocessed by computer to obtain the far field pattern. Deviations in amplitude between this data and that taken at the Capistrano Test Site were consistent with the data presented above. Maximum field strength deviations encountered during the interference test indicate that when patterns are taken, signal level perturbation errors, due to range reflections, fall in the less than or equal to 1 dB range.

A.4 RADOME CURTAIN INTERFERENCE

At the Capistrano range, tests were conducted within a pressurized weather proofed radome. The front surface of this dome was constructed of two separate curtain layers of vinyl coated nylon material. During testing, the inner layer was raised above the test aperture. The outer layer (used to enclose the radome in order to maintain a clean room environment) was designed to be opened only occasionally to permit moving large items in and out of the dome. The thickness of this outer curtain was 0.020 inches. Pattern comparison measurements were used to determine the degree of pattern degradation caused by outer curtain interference.

Elevation and azimuth pattern cuts (shown in Figure A-6) were made with the curtain raised out of the illuminating wavefront path and then with the curtain in its normally closed and inflated position. Elevation cuts show no change when measured with and without the curtain interference. A 3 dB increase in sidelobes was generated in the azimuth plane in the presence of by the curtain. Additional tests demonstrated that the interference would always be constructive. To summarize, a signal level measured in the azimuth plane, 40 dB below the beam peak, is increased by approximately 3 dB.

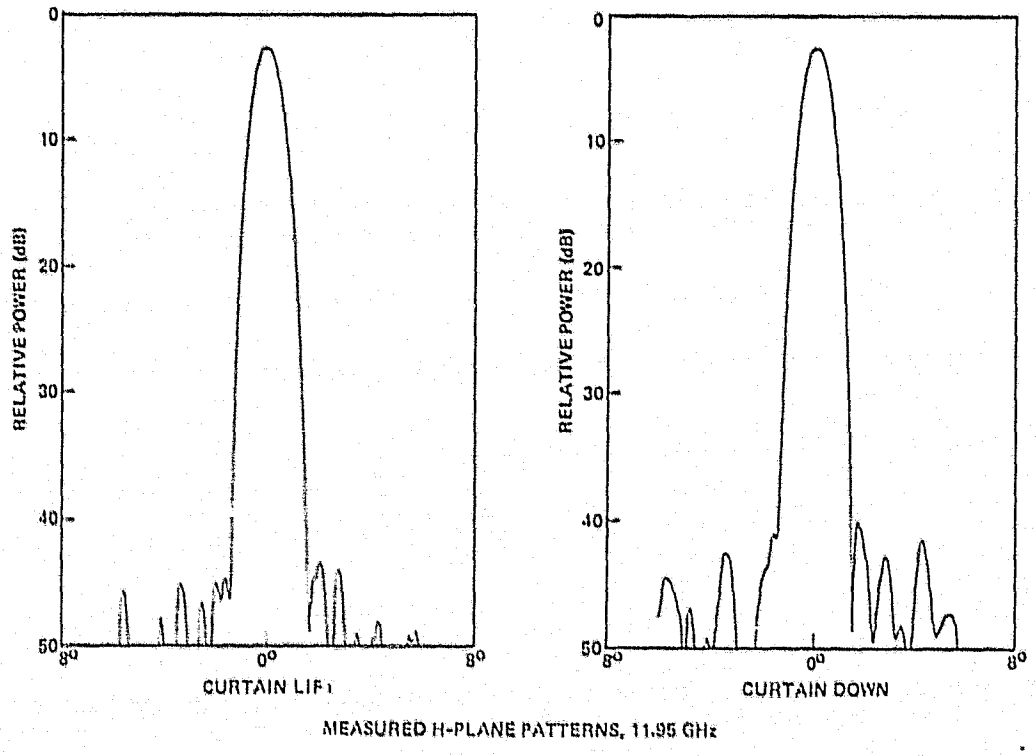

Figure A-6. Effect of Randome Curtain on Sidelobe Level

A.5 MEASUREMENT STABILITY

A remaining question, in the topic of range evaluation, was how much uncertainty is contributed by measurement instability. This includes mechanical vibration, equipment signal drift, and atmospheric conditions. Measurements were conducted to determine the test range system amplitude stability. These measurements consisted of pointing the test antenna in the main beam boresight direction and connecting all the test equipment,

including the computer, to its operating mode. The peak field point was monitored for approximately 5 minutes. Both analog and digital sampling was recorded. The peak-to-peak variation is typically less than 0.1 dB.

A.6 SUMMARY OF RANGE EVALUATION PROCESS

To summarize the range evaluation process:

- Range was set up for manual and automated pattern taking
- Both test and low sidelobe source antennas were mechanically and electrically aligned
- Maximum amplitude error measurements:
  - Phase variation over test aperture = ±0.2 dB at -40 dB relative to beam peak
  - Extraneous reflections = 1 dB at -40 dB relative to beam peak
  - Outer radome curtain interference = +3 dB at -40 dB relative to beam peak
  - Measurement stability (at beam peak) = ±0.1 dB.

APPENDIX B
MEASURED BEAM CONTOUR DATA

Pattern plots are representative of all data taken. Additional plots are available upon request.

B.1 BEAM CONTOUR SCAN DATA

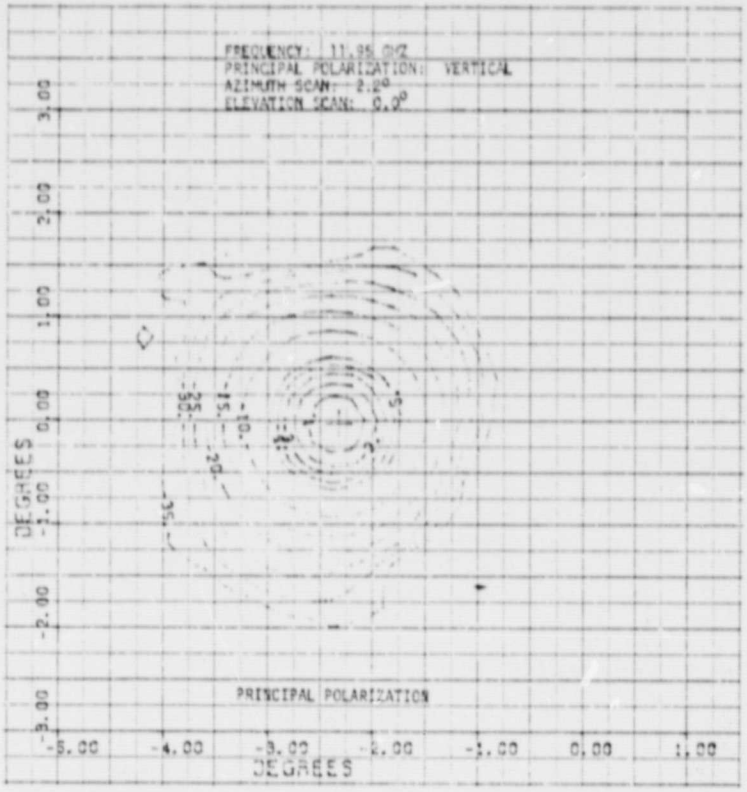

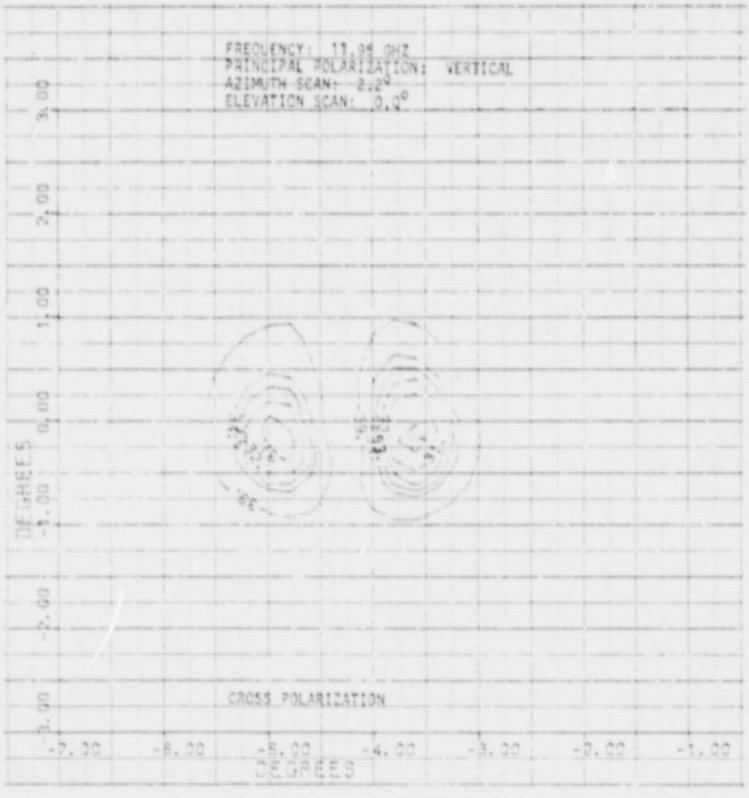

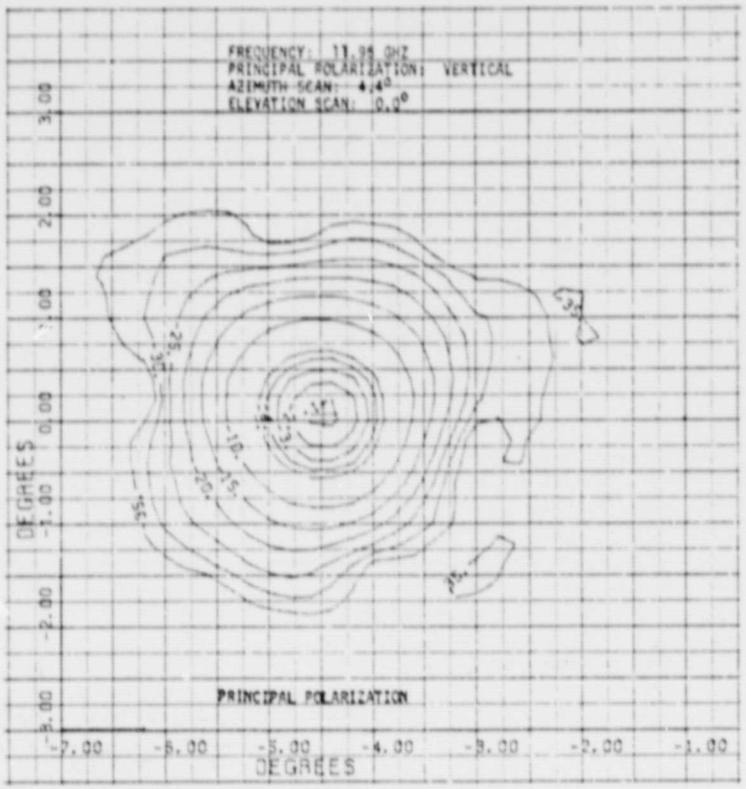

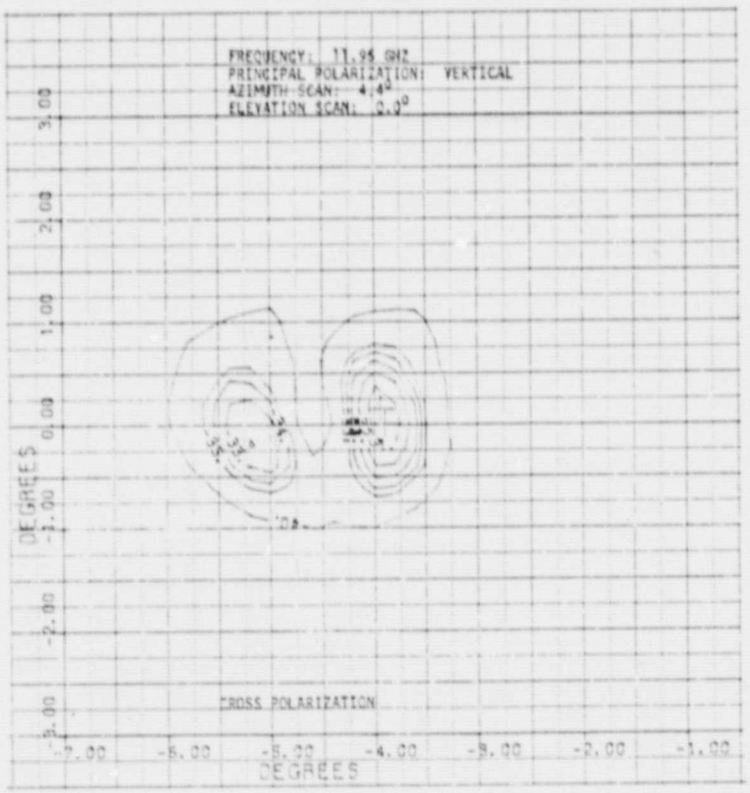

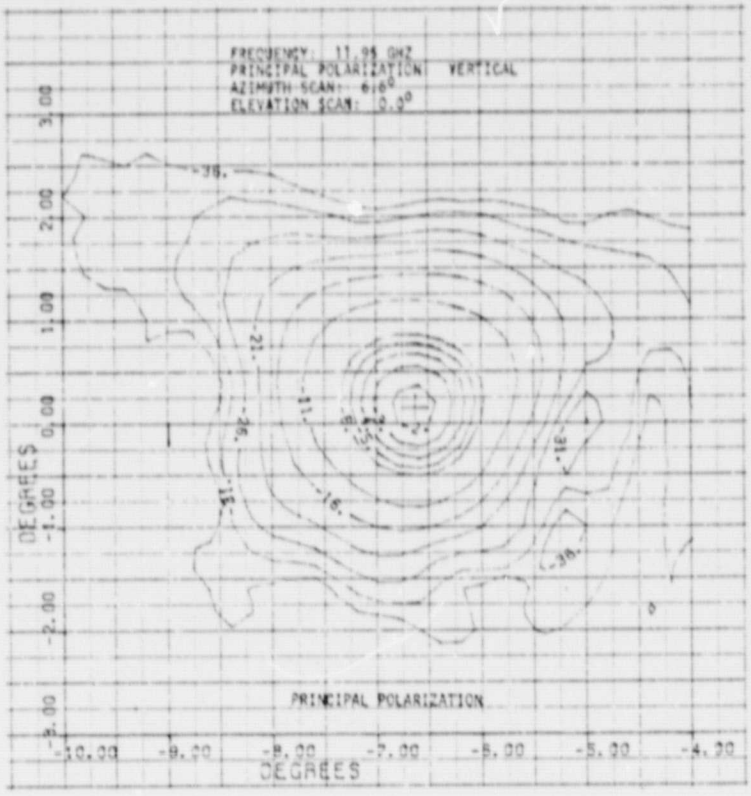
FREQUENCY: 11.95 GHZ
PRINCIPAL POLARIZATION: VERTICAL
AZIMUTH SCAN: 0.0°
ELEVATION SCAN: 0.0°
-36.
-21.
-11.
-26.
-15.
-18.
-18.
-30.
3.00
2.00
1.00
0.00
-1.00
-2.00
-3.00
DEGREES
PRINCIPAL POLARIZATION
-10.00
-9.00
-8.00
-7.00
-6.00
-5.00
-4.00
DEGREES

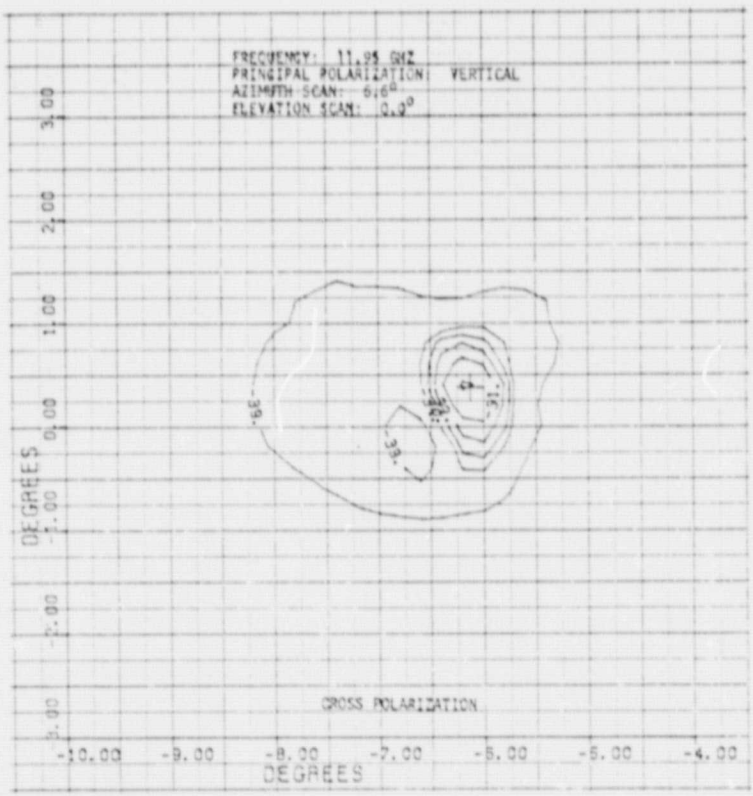
FREQUENCY: 11.95 GHZ
PRINCIPAL POLARIZATION: VERTICAL
AZIMUTH SCAN: 0.0°
ELEVATION SCAN: 0.0°
-39.
-31.
-33.
3.00
2.00
1.00
0.00
-1.00
-2.00
-3.00
DEGREES
CROSS POLARIZATION
-10.00
-9.00
-8.00
-7.00
-6.00
-5.00
-4.00
DEGREES

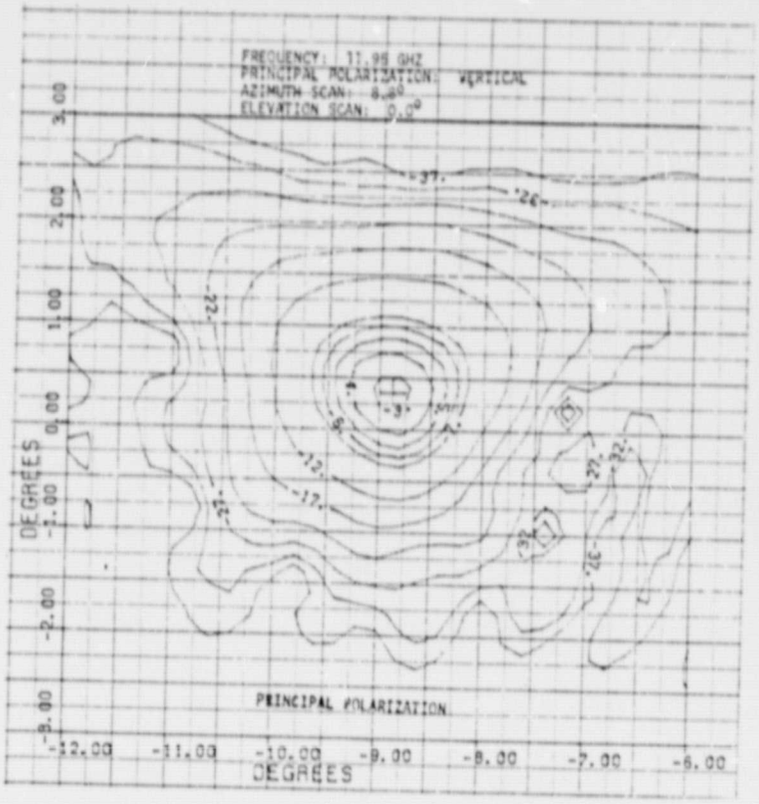

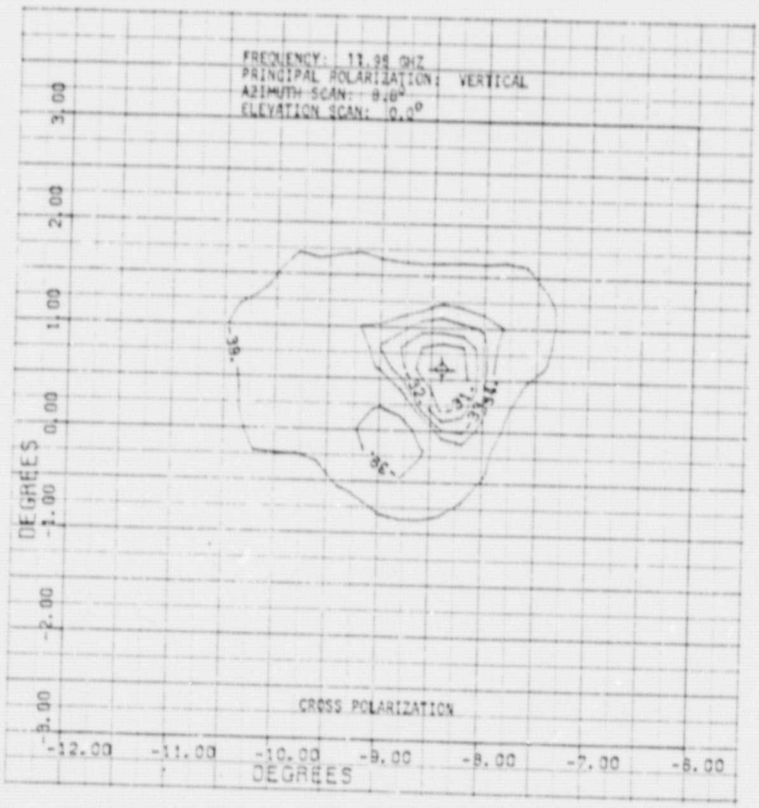

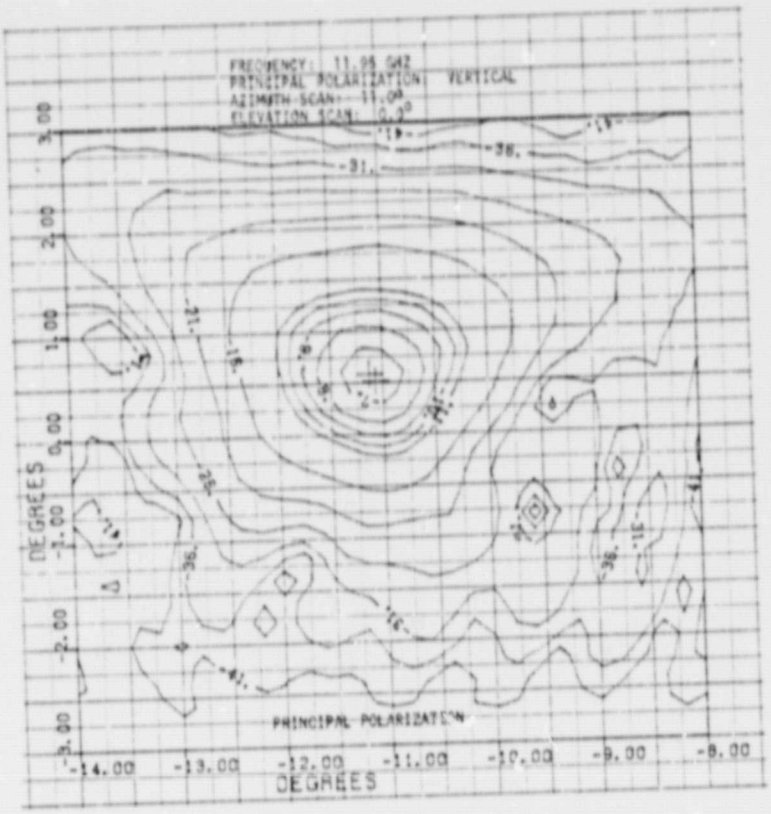
FREQUENCY: 11.95 GHZ
PRINCIPAL POLARIZATION: VERTICAL
AZIMUTH SCAN: 11.0°
ELEVATION SCAN: 0.0°
-1.
-31.
-36.
-41.
PRINCIPAL POLARIZATION
3.00
2.00
1.00
0.00
-1.00
-2.00
-3.00
DEGREES
-14.00
-13.00
-12.00
-11.00
-10.00
-9.00
-8.00
DEGREES

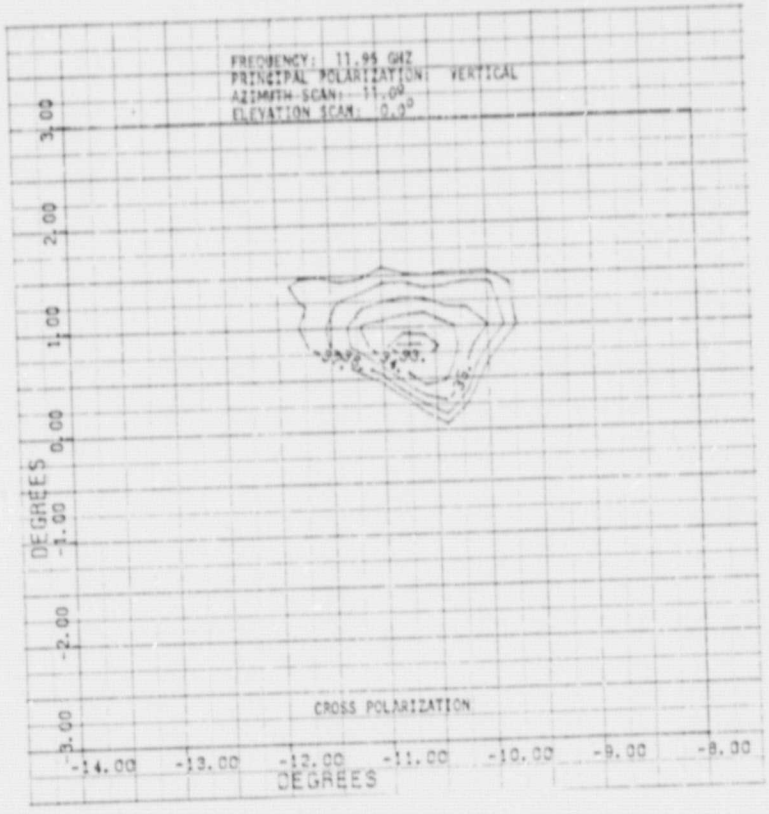
FREQUENCY: 11.95 GHZ
PRINCIPAL POLARIZATION: VERTICAL
AZIMUTH SCAN: 11.0°
ELEVATION SCAN: 0.0°
-31.
CROSS POLARIZATION
3.00
2.00
1.00
0.00
-1.00
-2.00
-3.00
DEGREES
-14.00
-13.00
-12.00
-11.00
-10.00
-9.00
-8.00
DEGREES

B.2 BEAM CONTOUR PATTERN CUTS

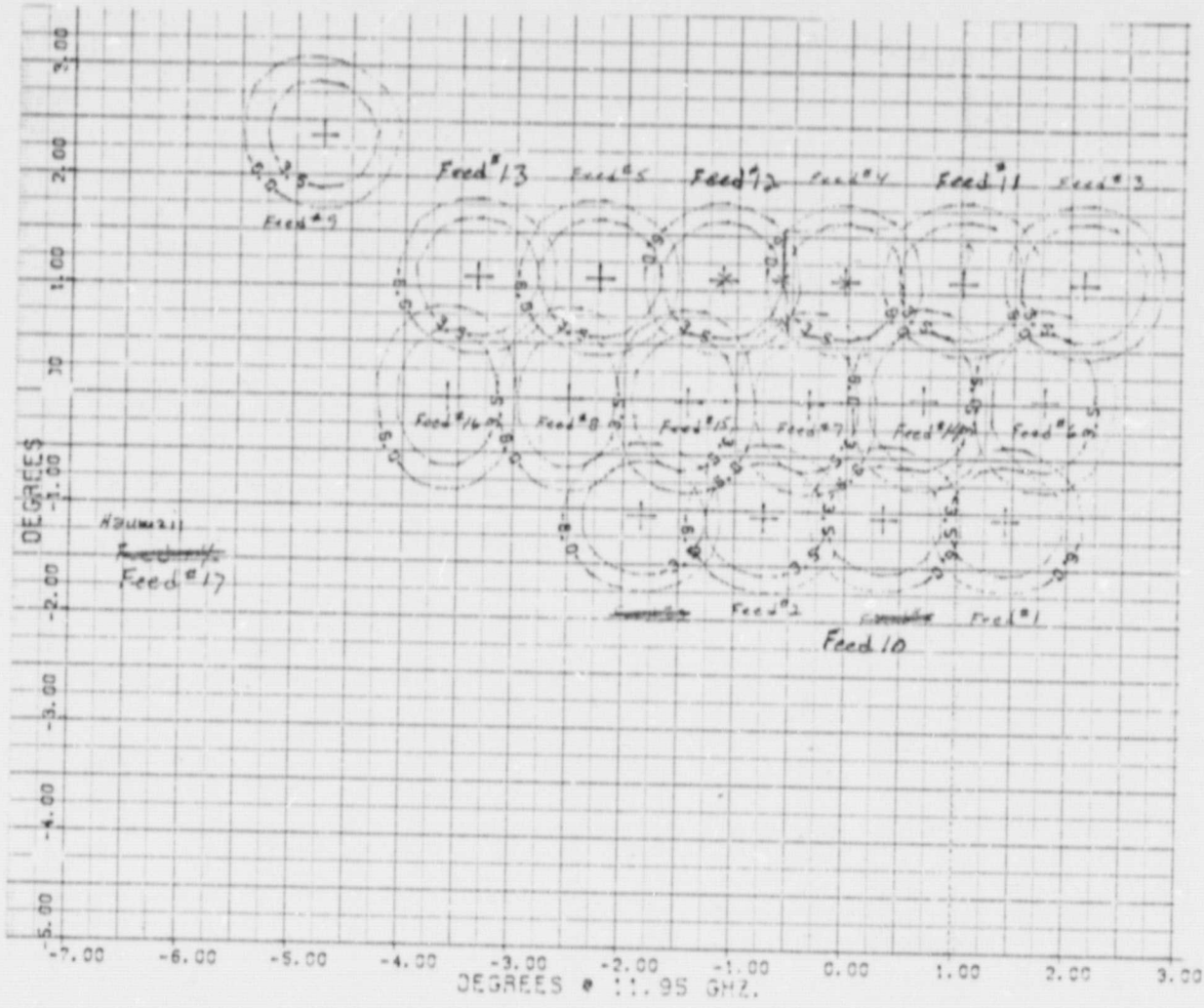

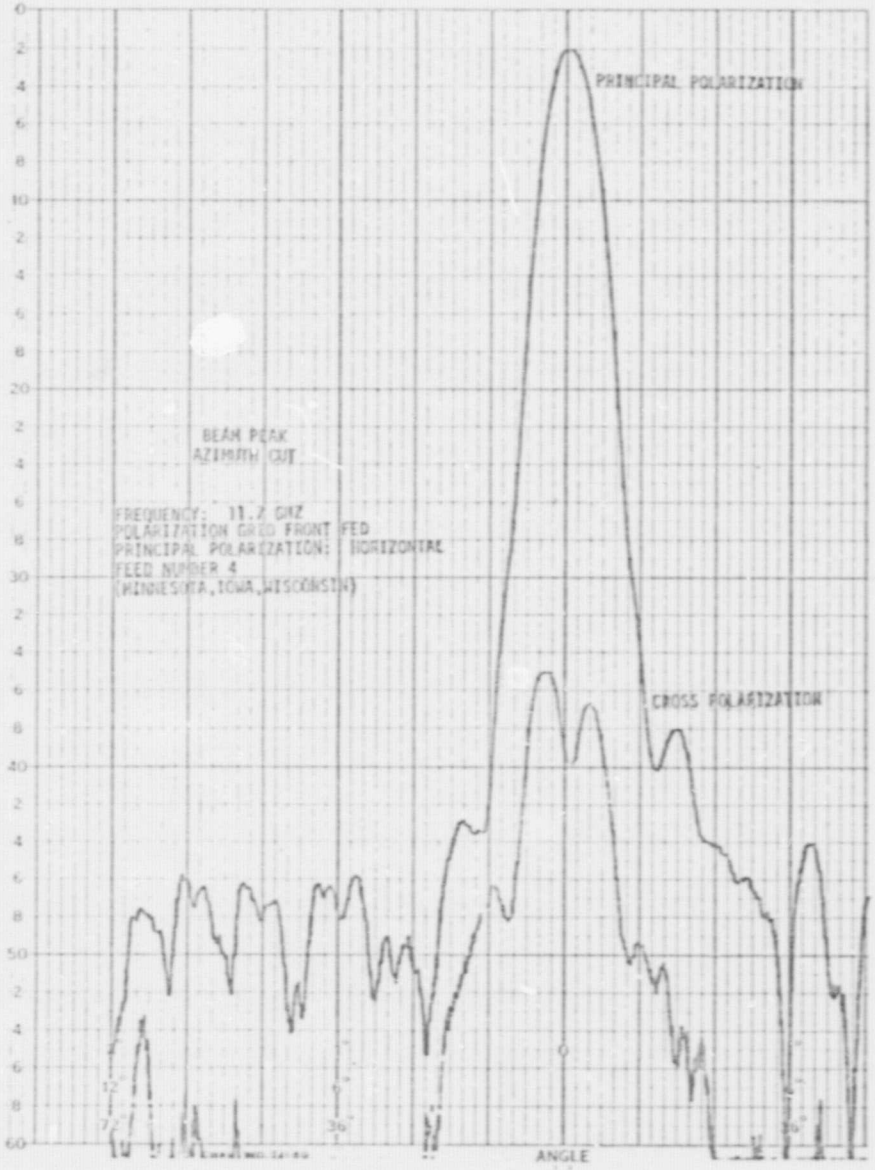
PRINCIPAL POLARIZATION
CROSS POLARIZATION
BEAM PEAK
AZIMUTH CUT
FREQUENCY: 11.7 GHZ
POLARIZATION GRID FRONT FED
PRINCIPAL POLARIZATION: HORIZONTAL
FEED NUMBER 4
(MINNESOTA, IOWA, WISCONSIN)
ANGLE

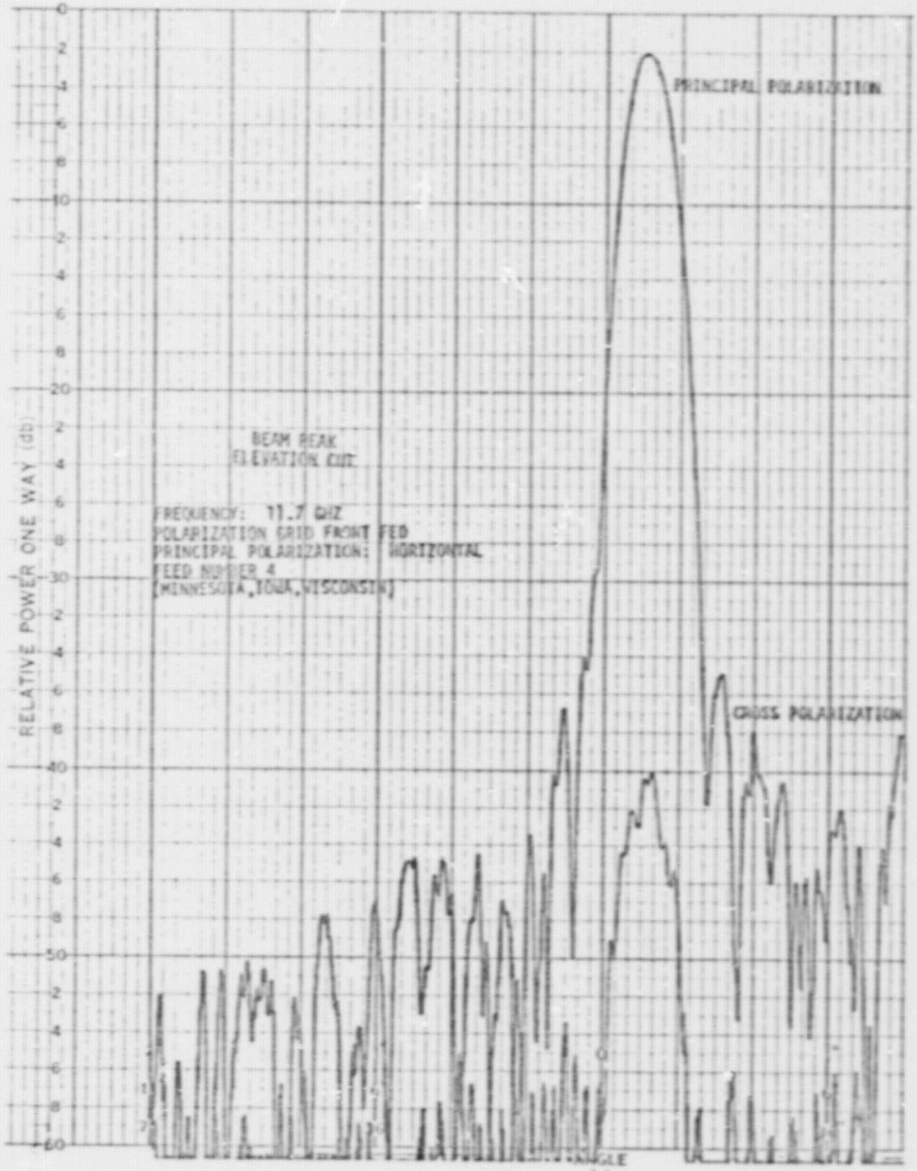
RELATIVE POWER ONE WAY (dB)
PRINCIPAL POLARIZATION
CROSS POLARIZATION
BEAM PEAK
ELEVATION CUT
FREQUENCY: 11.7 GHZ
POLARIZATION GRID FRONT FED
PRINCIPAL POLARIZATION: HORIZONTAL
FEED NUMBER 4
(MINNESOTA, IOWA, WISCONSIN)

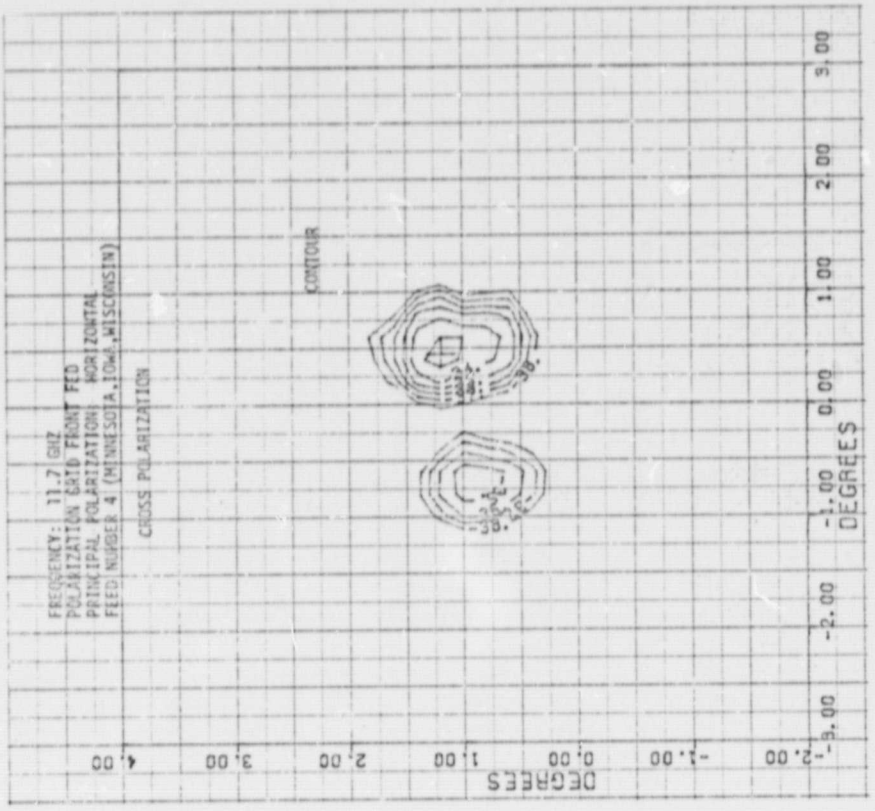
FREQUENCY: 11.7 GHZ
POLARIZATION GRID FRONT FED
PRINCIPAL POLARIZATION: HORIZONTAL
FEED NUMBER 4 (MINNESOTA,IOWA,WISCONSIN)
CROSS POLARIZATION
CONTOUR
-30.
-36.
-36.
DEGREES
DEGREES
3.00
2.00
1.00
0.00
-1.00
-2.00
-3.00
4.00
3.00
2.00
1.00
0.00
-1.00
-2.00

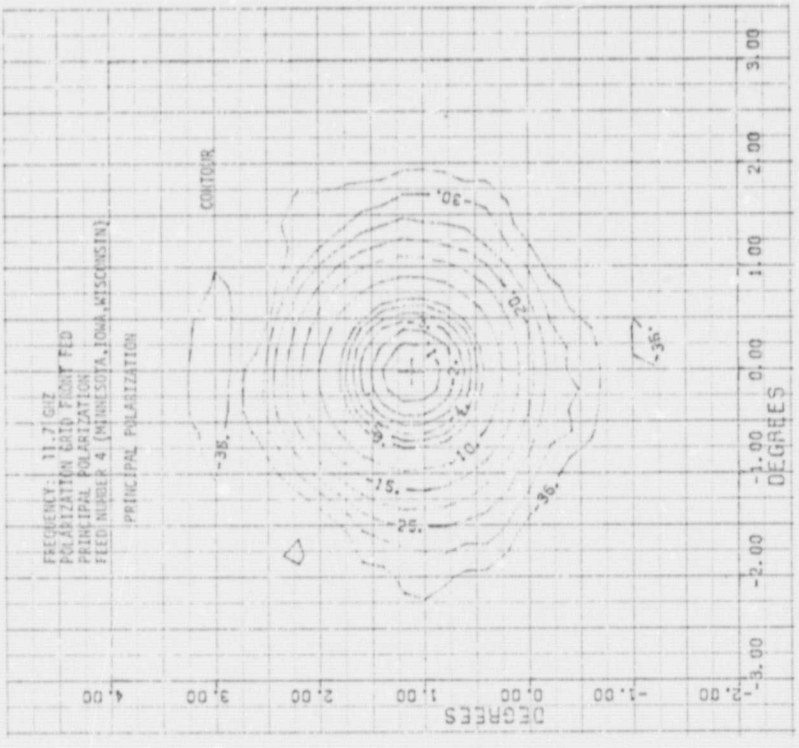
FREQUENCY: 11.7 GHZ
POLARIZATION GRID FRONT FED
PRINCIPAL POLARIZATION
FEED NUMBER 4 (MINNESOTA,IOWA,WISCONSIN)
PRINCIPAL POLARIZATION
CONTOUR
-30.
-36.
-36.
DEGREES
DEGREES
3.00
2.00
1.00
0.00
-1.00
-2.00
-3.00
4.00
3.00
2.00
1.00
0.00
-1.00
-2.00

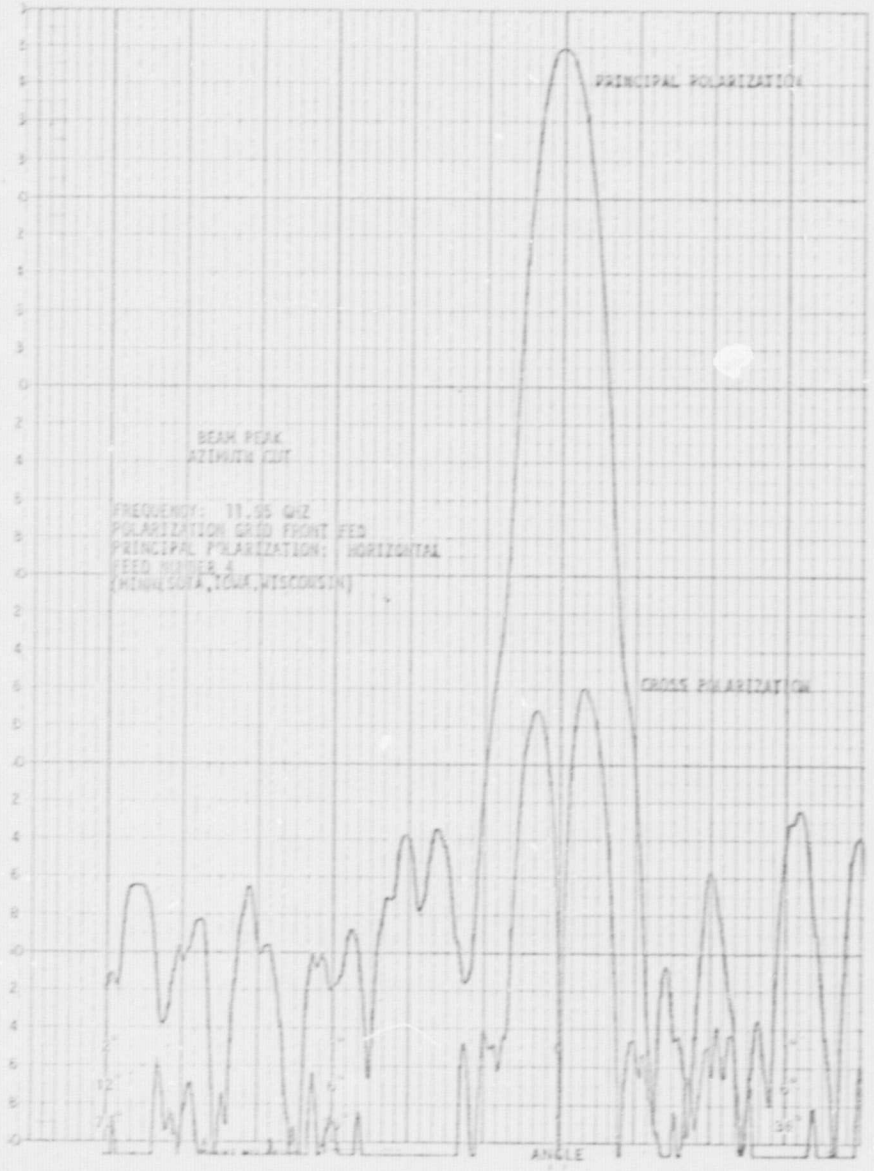
PRINCIPAL POLARIZATION
BEAM PEAK
AZIMUTH CUT
FREQUENCY: 11.95 GHZ
POLARIZATION GRID FRONT FED
PRINCIPAL POLARIZATION: HORIZONTAL
FEED NUMBER 4
(MINNESOTA,IOWA,WISCONSIN)
CROSS POLARIZATION
ANGLE

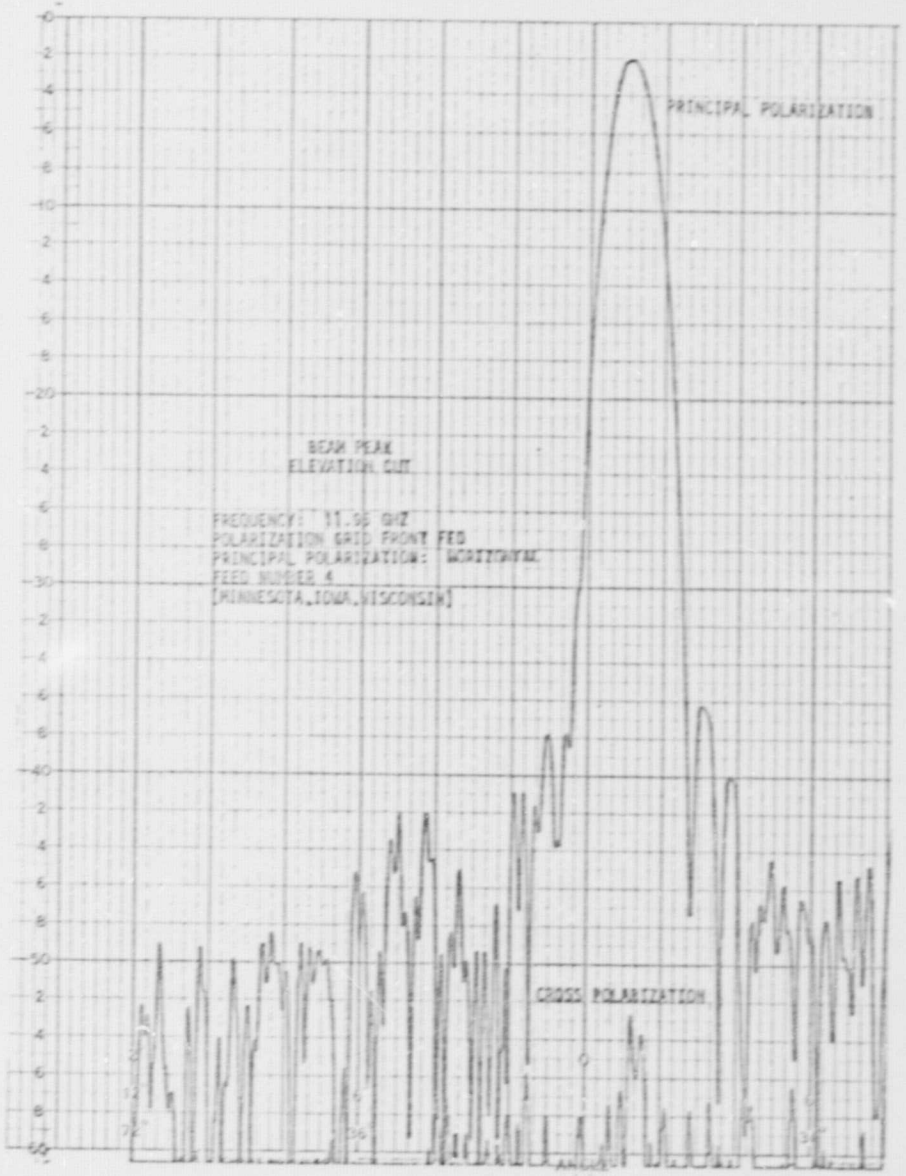
PRINCIPAL POLARIZATION
BEAM PEAK
ELEVATION CUT
FREQUENCY: 11.95 GHZ
POLARIZATION GRID FRONT FED
PRINCIPAL POLARIZATION: HORIZONTAL
FEED NUMBER 4
(MINNESOTA,IOWA,WISCONSIN)
CROSS POLARIZATION

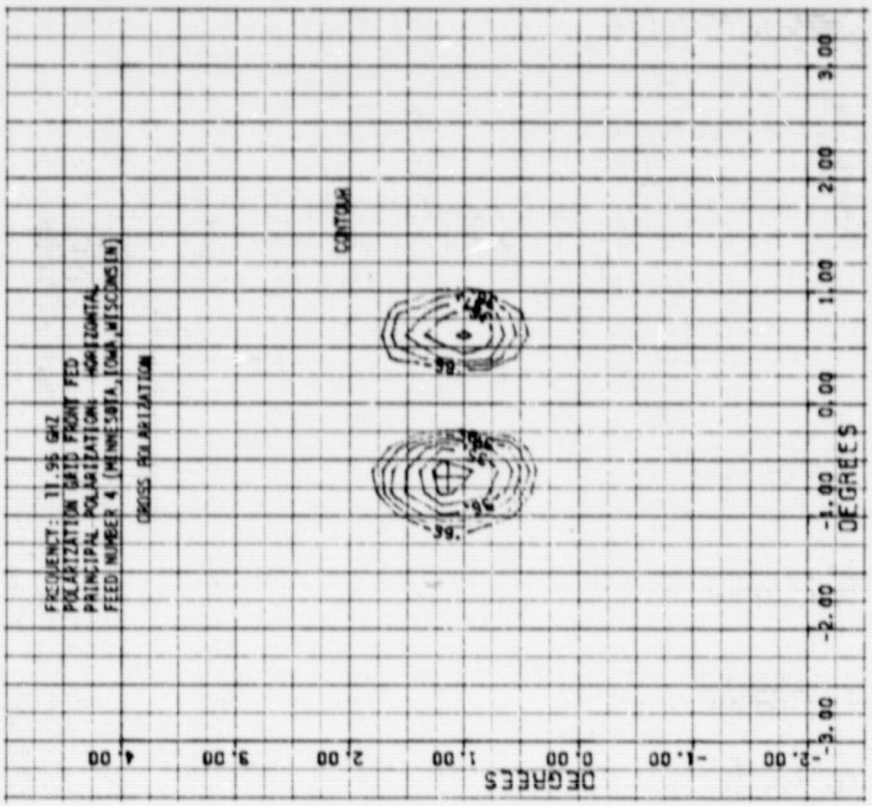

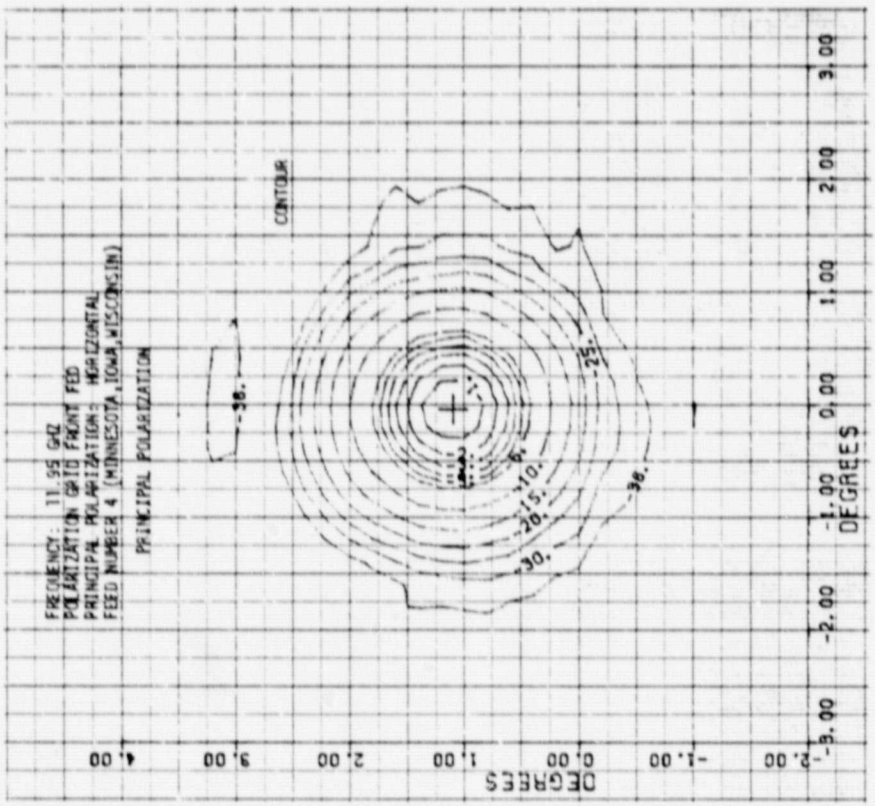

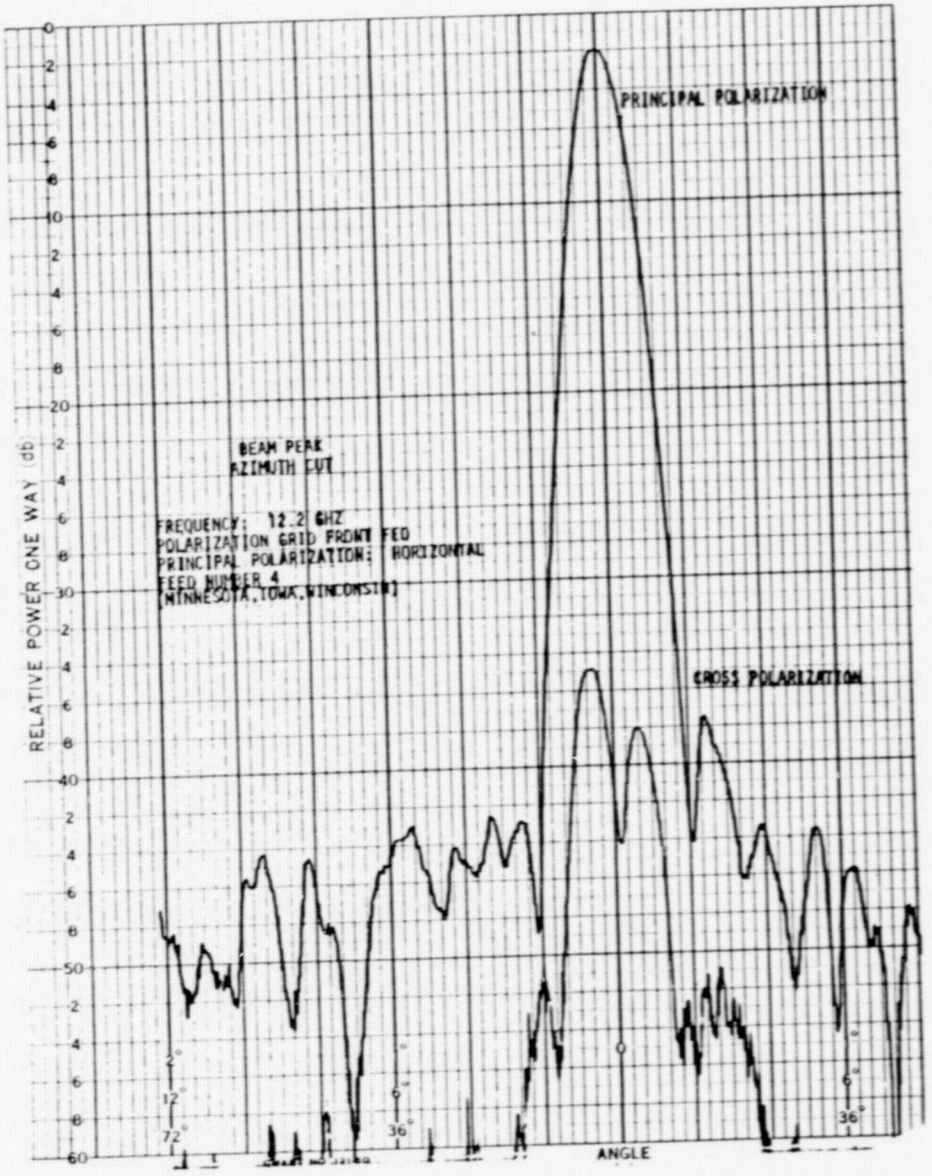
PRINCIPAL POLARIZATION
CROSS POLARIZATION
BEAM PEAK
AZIMUTH CUT
FREQUENCY: 12.2 GHZ
POLARIZATION GRID FRONT FED
PRINCIPAL POLARIZATION: HORIZONTAL
FEED NUMBER 4
(MINNESOTA, IOWA, WISCONSIN)
RELATIVE POWER ONE WAY (db)
ANGLE
2°
12°
72°
36°
6°
36°

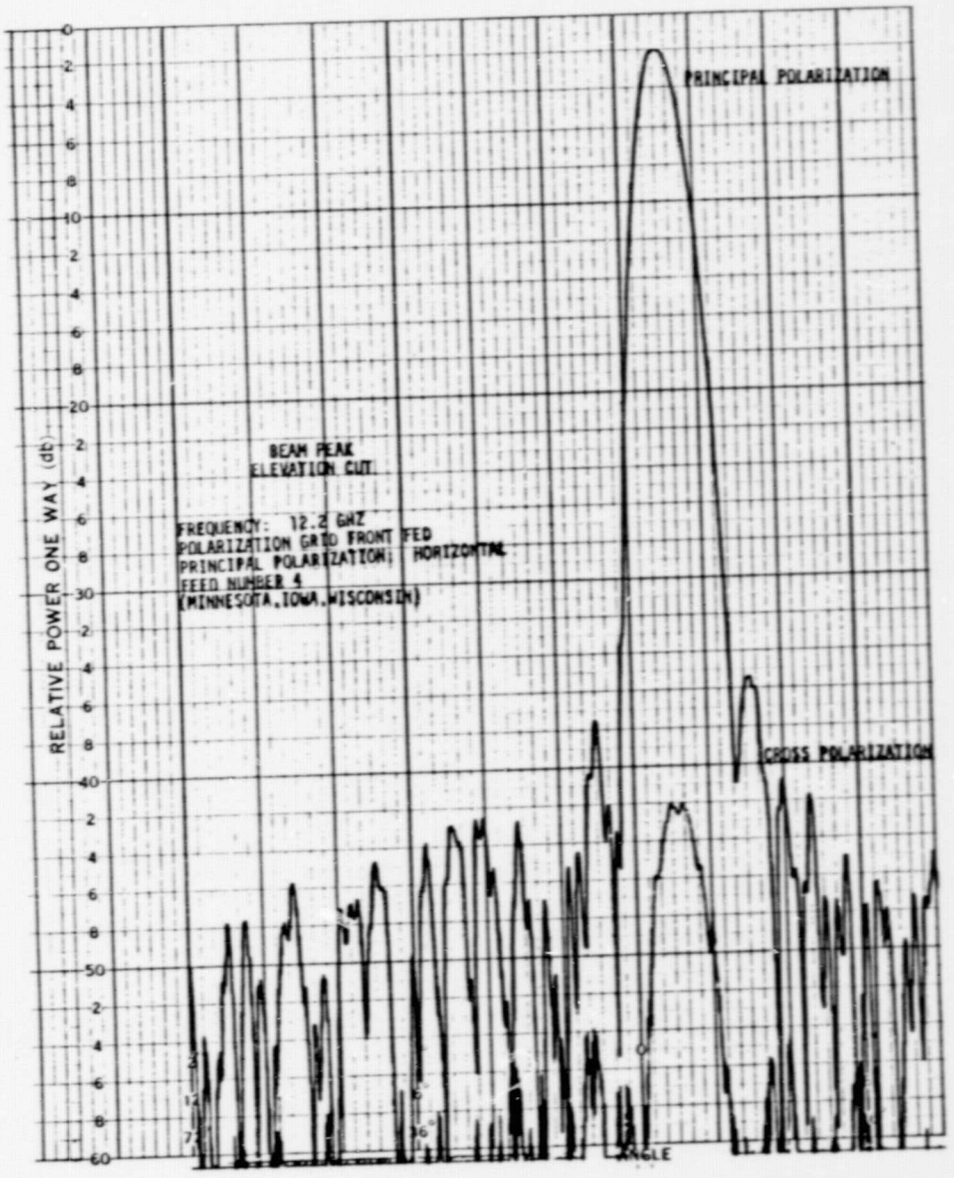
PRINCIPAL POLARIZATION
CROSS POLARIZATION
BEAM PEAK
ELEVATION CUT
FREQUENCY: 12.2 GHZ
POLARIZATION GRID FRONT FED
PRINCIPAL POLARIZATION: HORIZONTAL
FEED NUMBER 4
(MINNESOTA, IOWA, WISCONSIN)
RELATIVE POWER ONE WAY (db)
ANGLE

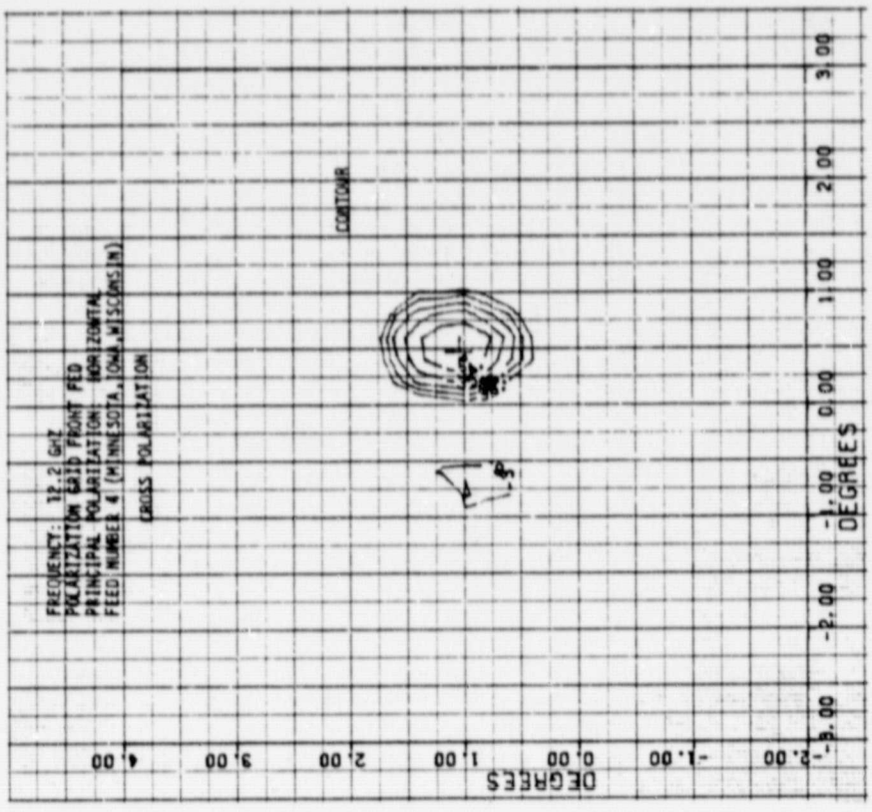
FREQUENCY: 12.2 GHZ
POLARIZATION BAID FRONT FED
PRINCIPAL POLARIZATION: HORIZONTAL
FEED NUMBER 4 (MINNESOTA,IOWA,WISCONSIN)
CROSS POLARIZATION
CONTOUR
DEGREES
DEGREES

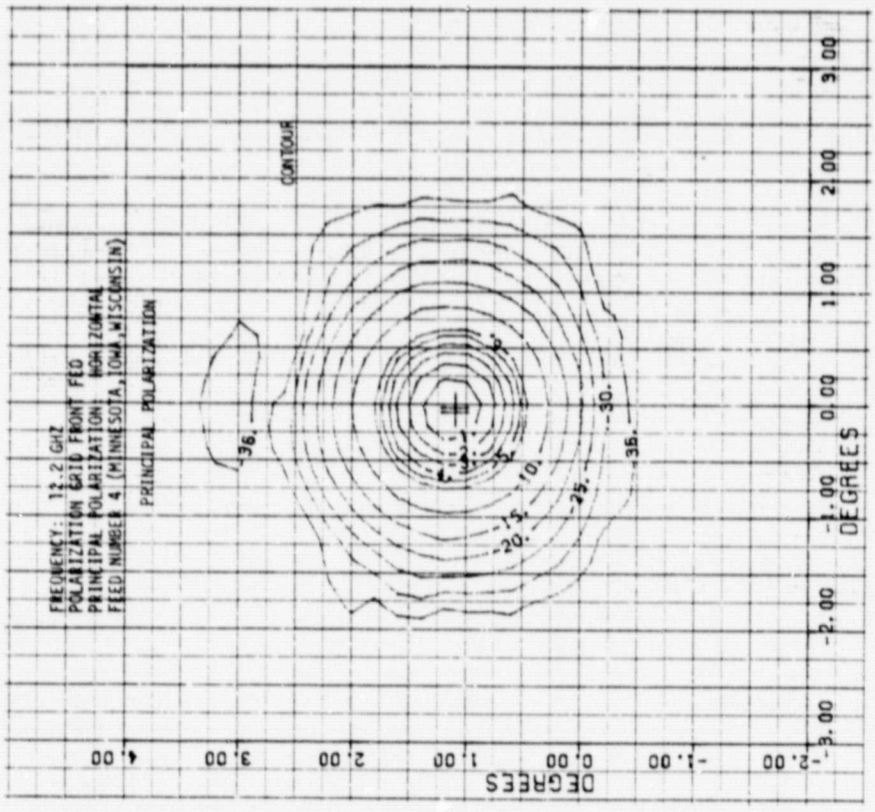
FREQUENCY: 12.2 GHZ
POLARIZATION BAID FRONT FED
PRINCIPAL POLARIZATION: HORIZONTAL
FEED NUMBER 4 (MINNESOTA,IOWA,WISCONSIN)
PRINCIPAL POLARIZATION
CONTOUR
-36.
-30.
-25.
-20.
-15.
-10.
-5.
-2.
DEGREES
DEGREES

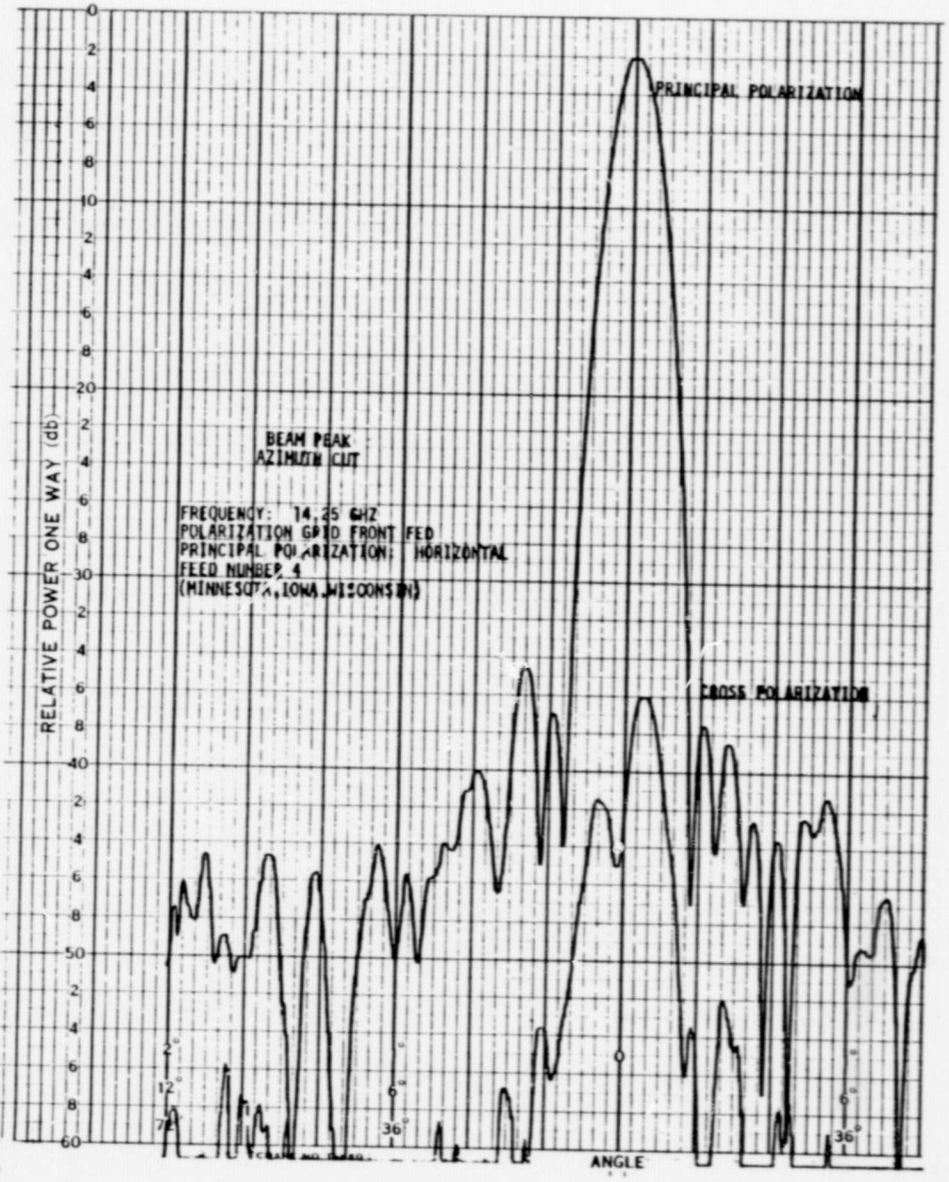

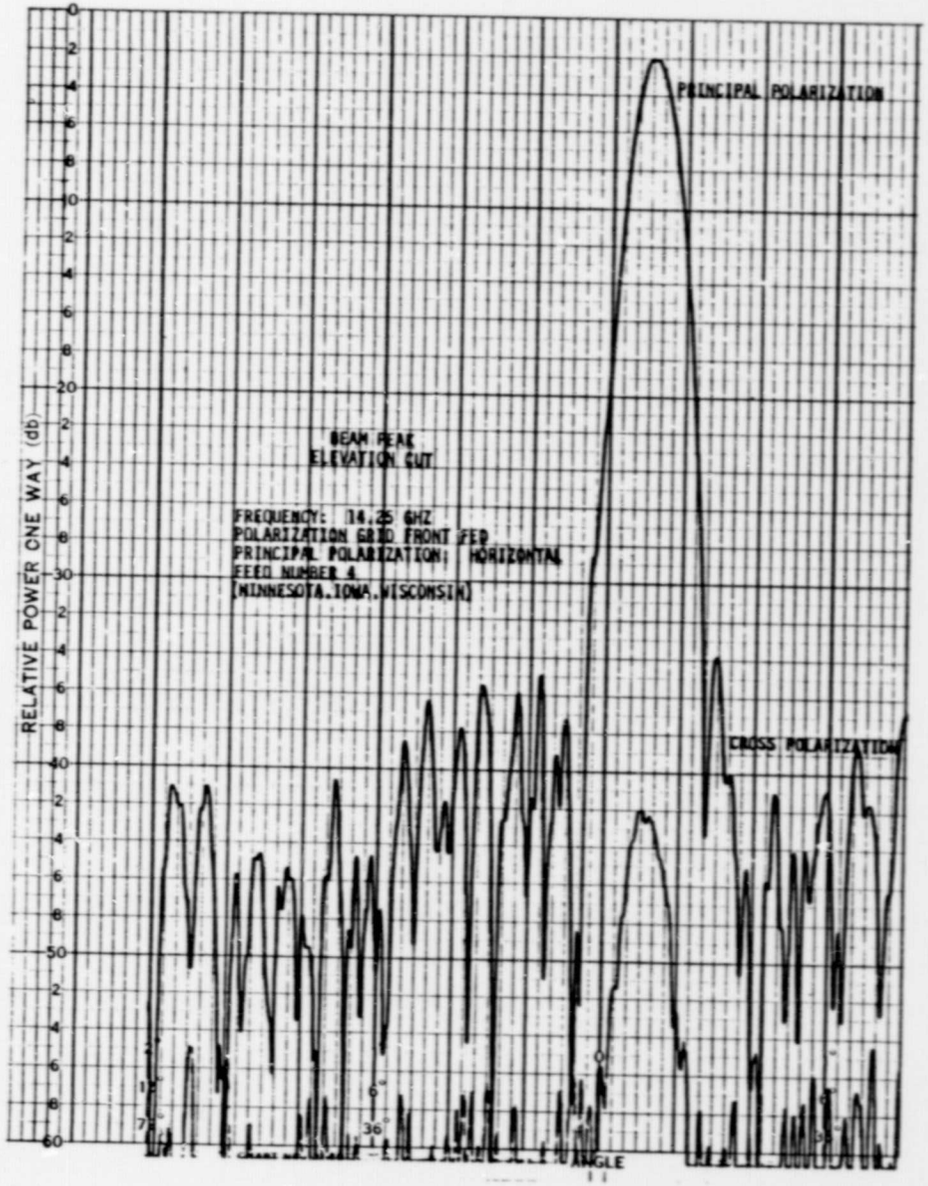

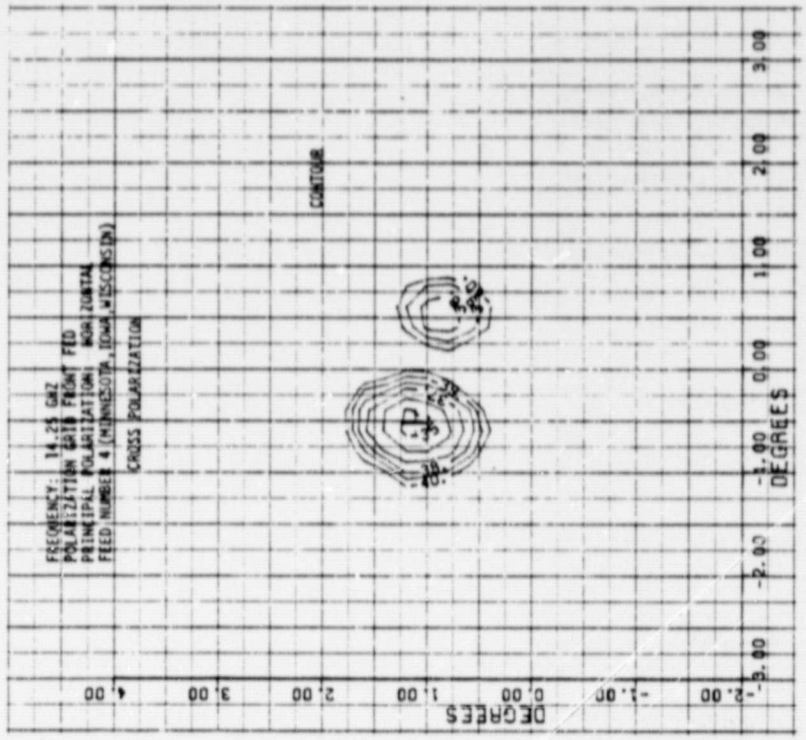
FREQUENCY: 14.25 GHZ
POLARIZATION GRID FRONT FED
PRINCIPAL POLARIZATION: HORIZONTAL
FEED NUMBER 4 (MINNESOTA,IOWA,WISCONSIN)
CROSS POLARIZATION
CONTOUR
DEGREES
DEGREES

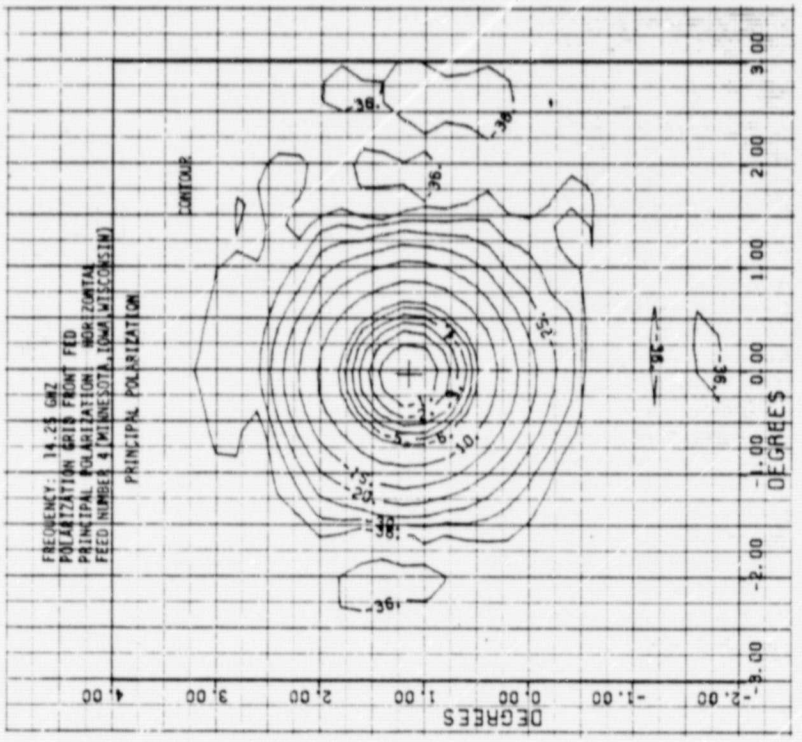
FREQUENCY: 14.25 GHZ
POLARIZATION GRID FRONT FED
PRINCIPAL POLARIZATION: HORIZONTAL
FEED NUMBER 4 (MINNESOTA,IOWA,WISCONSIN)
PRINCIPAL POLARIZATION
CONTOUR
DEGREES
DEGREES

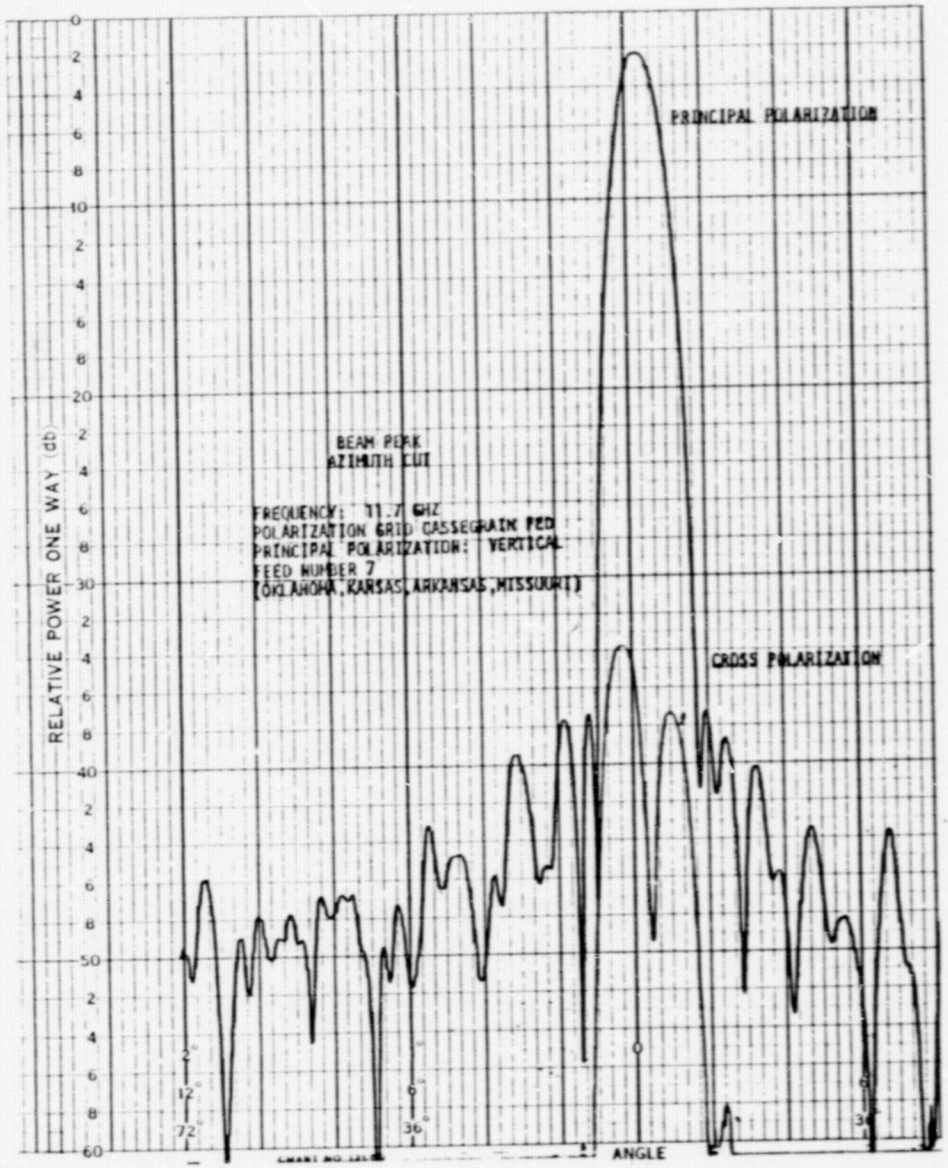
PRINCIPAL POLARIZATION
CROSS POLARIZATION
BEAM PEAK
AZIMUTH CUT
FREQUENCY: 11.7 GHZ
POLARIZATION GRID CASSEGRAIN FED
PRINCIPAL POLARIZATION: VERTICAL
FEED NUMBER 7
(OKLAHOMA, KANSAS, ARKANSAS, MISSOURI)
RELATIVE POWER ONE WAY (db)
ANGLE

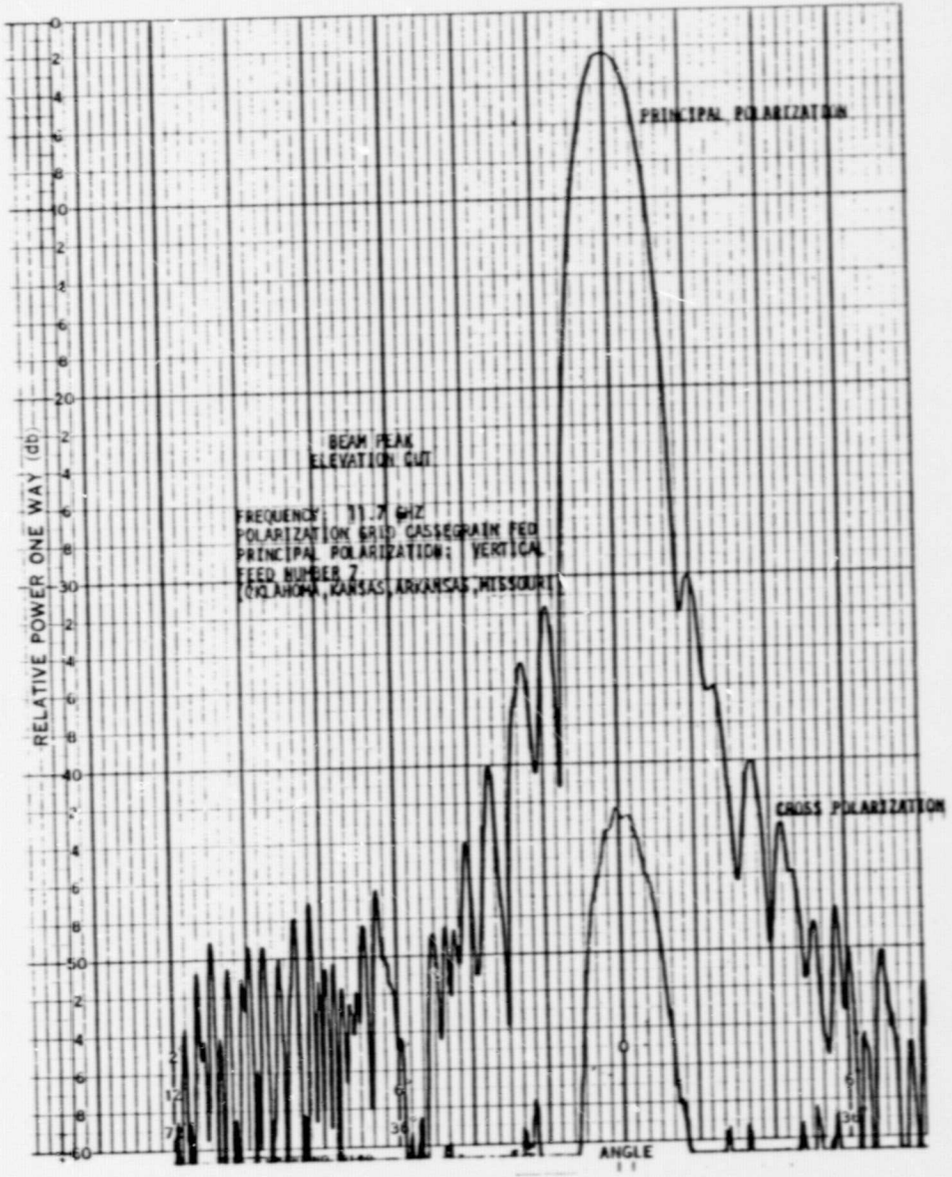
PRINCIPAL POLARIZATION
CROSS POLARIZATION
BEAM PEAK
ELEVATION CUT
FREQUENCY: 11.7 GHZ
POLARIZATION GRID CASSEGRAIN FED
PRINCIPAL POLARIZATION: VERTICAL
FEED NUMBER 7
(OKLAHOMA, KANSAS, ARKANSAS, MISSOURI)
RELATIVE POWER ONE WAY (db)
ANGLE

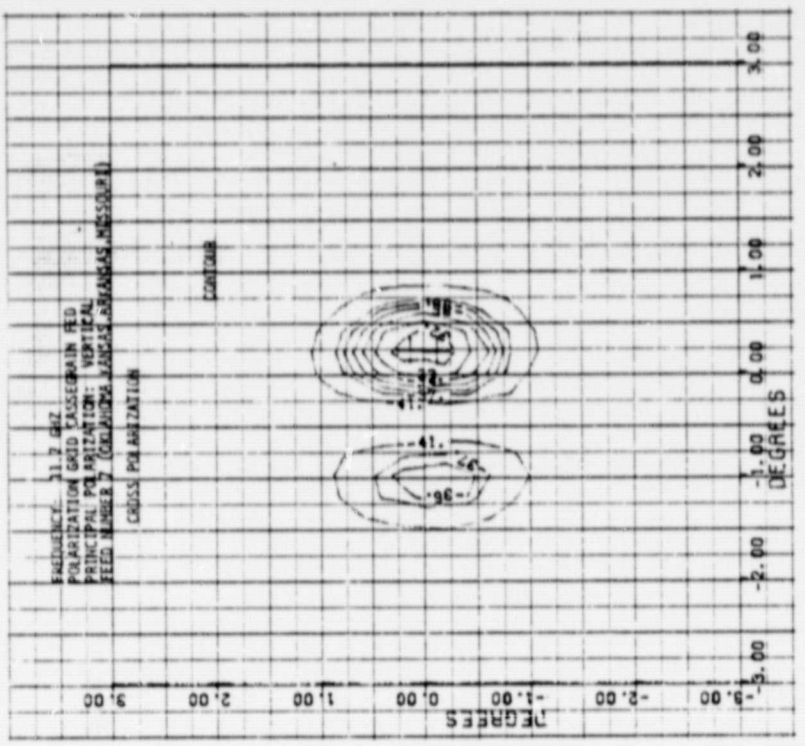
FREQUENCY 11.7 GHZ
POLARIZATION GRID CASSEGRAIN FED
PRINCIPAL POLARIZATION: VERTICAL
FEED NUMBER 7 (OKLAHOMA,KANSAS,ARKANSAS,MISSOURI)
CROSS POLARIZATION
CONTOUR
-41.
-36.
DEGREES
3.00
2.00
1.00
0.00
-1.00
-2.00
-3.00
-3.00
-2.00
-1.00
0.00
1.00
2.00
3.00

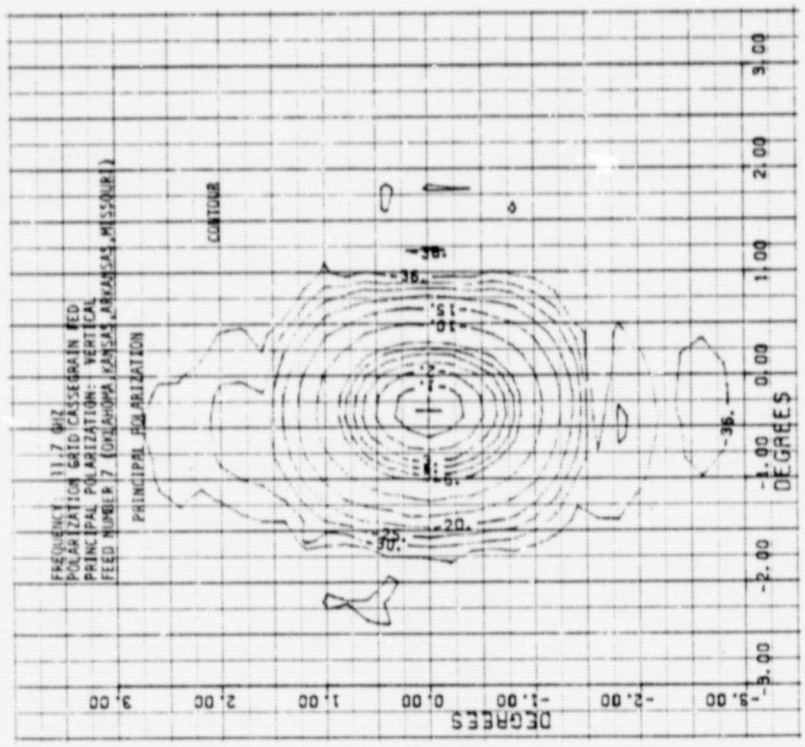
FREQUENCY 11.7 GHZ
POLARIZATION GRID CASSEGRAIN FED
PRINCIPAL POLARIZATION: VERTICAL
FEED NUMBER 7 (OKLAHOMA,KANSAS,ARKANSAS,MISSOURI)
PRINCIPAL POLARIZATION
CONTOUR
-36.
-15.
-10.
-5.
-2.
-20.
-30.
DEGREES
3.00
2.00
1.00
0.00
-1.00
-2.00
-3.00
-3.00
-2.00
-1.00
0.00
1.00
2.00
3.00

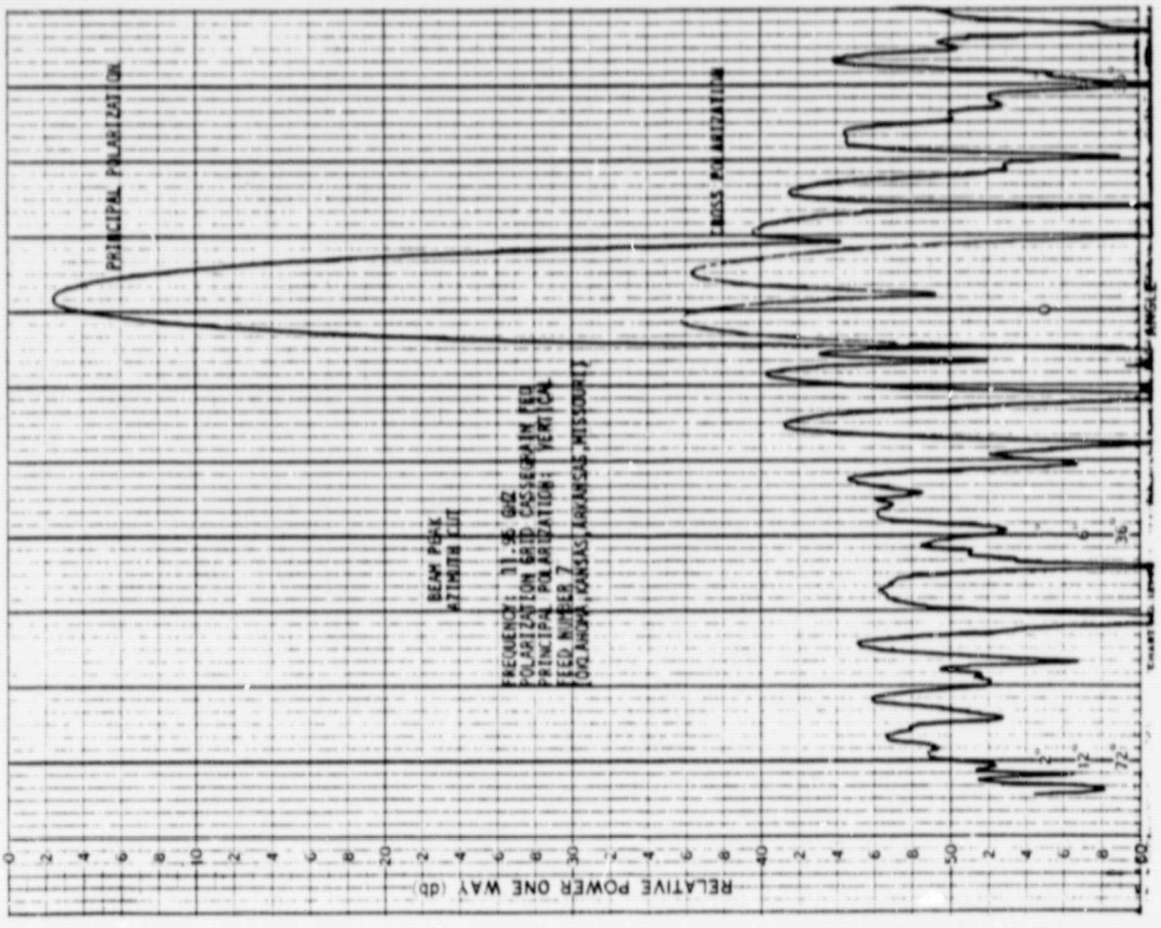
PRINCIPAL POLARIZATION
CROSS POLARIZATION
BEAM PEAK
ELEVATION CUT
FREQUENCY: 11.95 GHz
POLARIZATION GRID CASSEGRAIN FED
PRINCIPAL POLARIZATION: VERTICAL
FEED NUMBER 7
(OKLAHOMA, KANSAS, ARKANSAS, MISSOURI)
RELATIVE POWER ONE WAY (db)
ANGLE

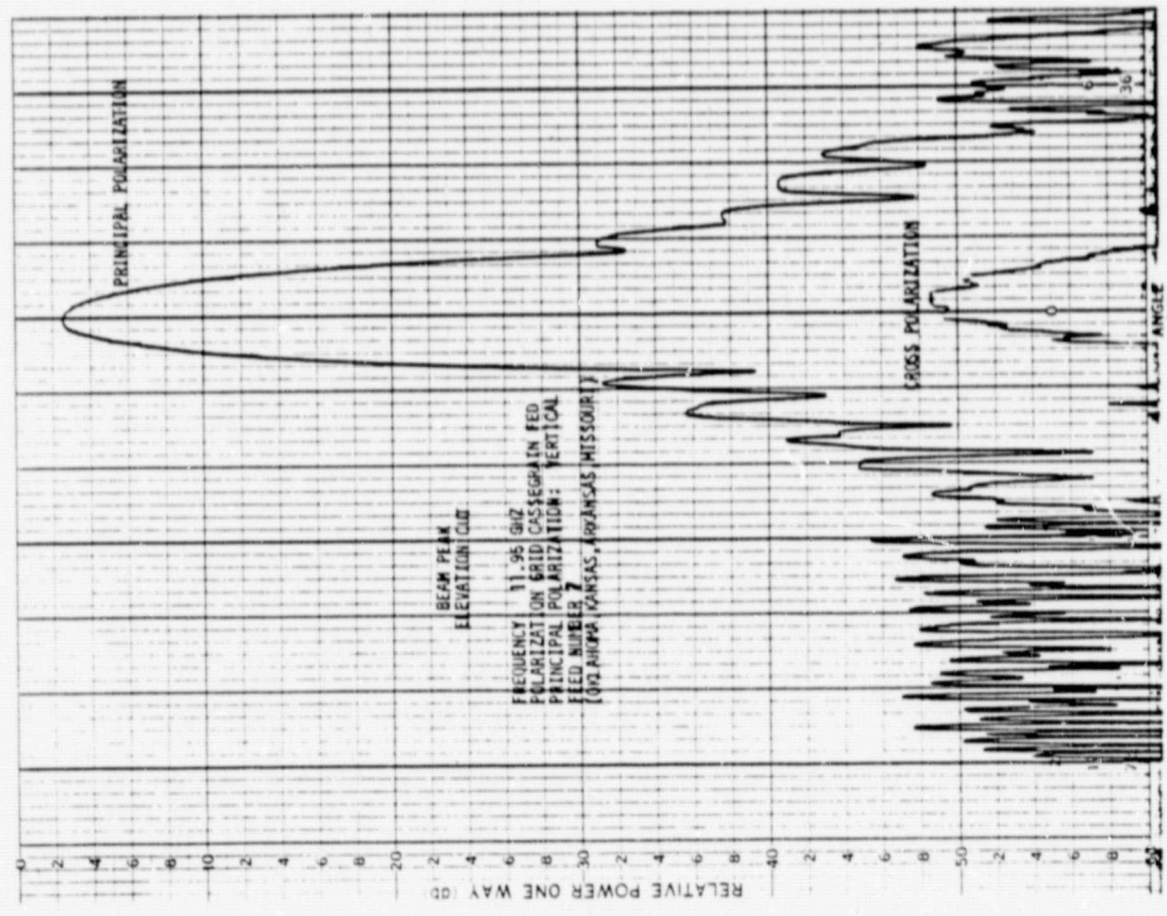
PRINCIPAL POLARIZATION
CROSS POLARIZATION
BEAM PEAK
ELEVATION CUT
FREQUENCY 11.95 GHz
POLARIZATION GRID CASSEGRAIN FED
PRINCIPAL POLARIZATION: VERTICAL
FEED NUMBER 7
(OKLAHOMA, KANSAS, ARKANSAS, MISSOURI)
RELATIVE POWER ONE WAY (db)
ANGLE

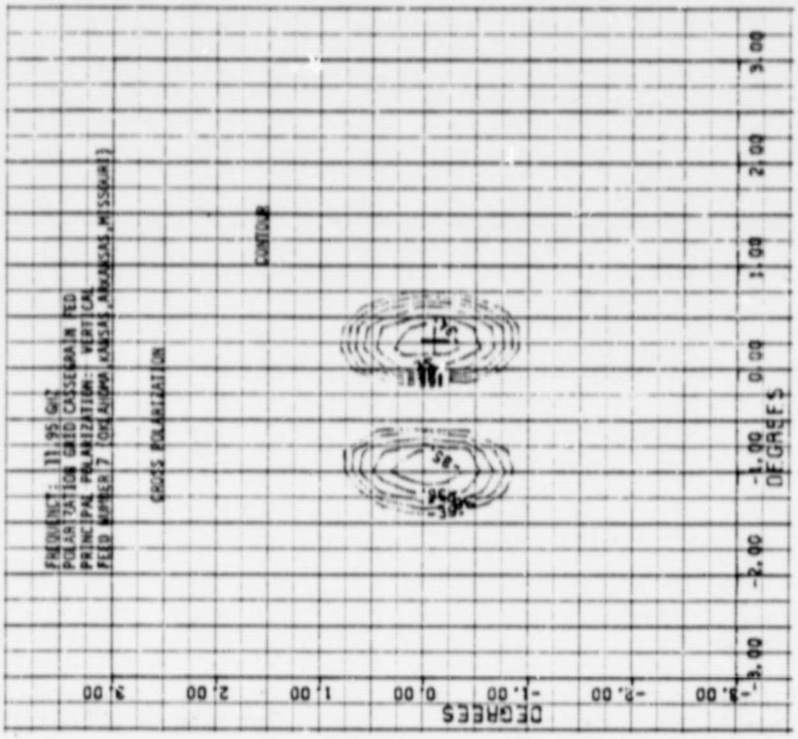

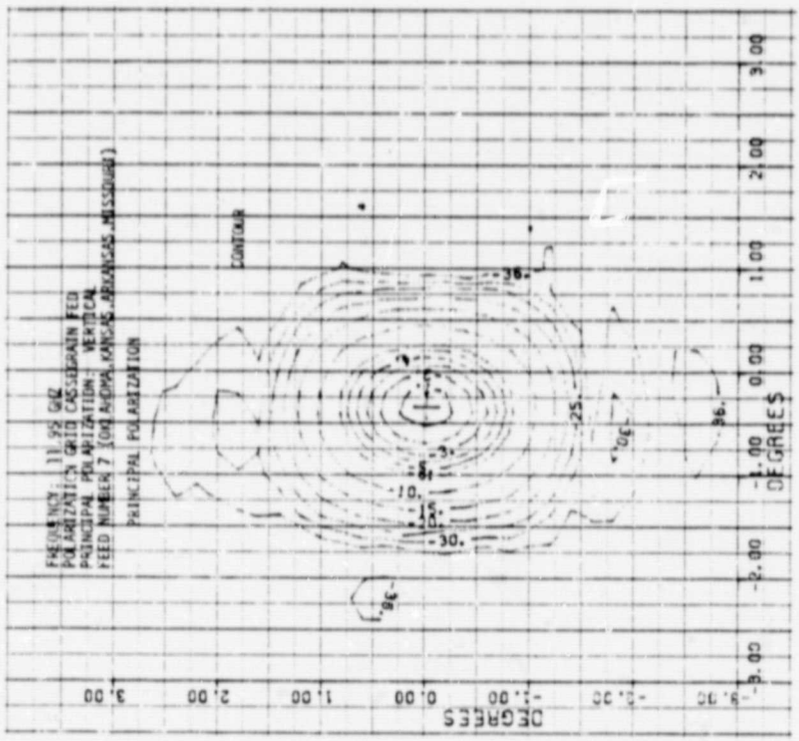

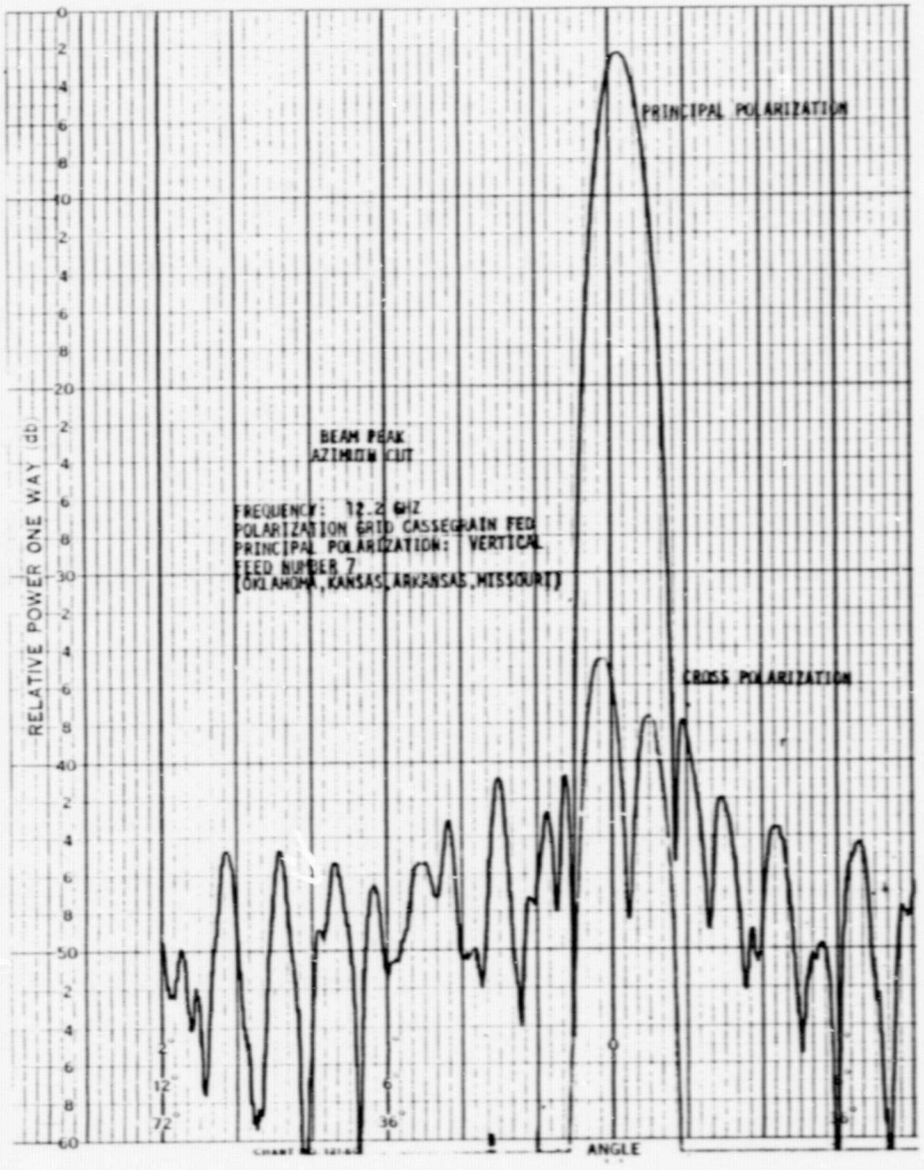
PRINCIPAL POLARIZATION
CROSS POLARIZATION
BEAM PEAK
AZIMUTH CUT
FREQUENCY: 12.2 GHZ
POLARIZATION GRID CASSEGRAIN FED
PRINCIPAL POLARIZATION: VERTICAL
FEED NUMBER 7
(OKLAHOMA, KANSAS, ARKANSAS, MISSOURI)
RELATIVE POWER ONE WAY (db)
ANGLE

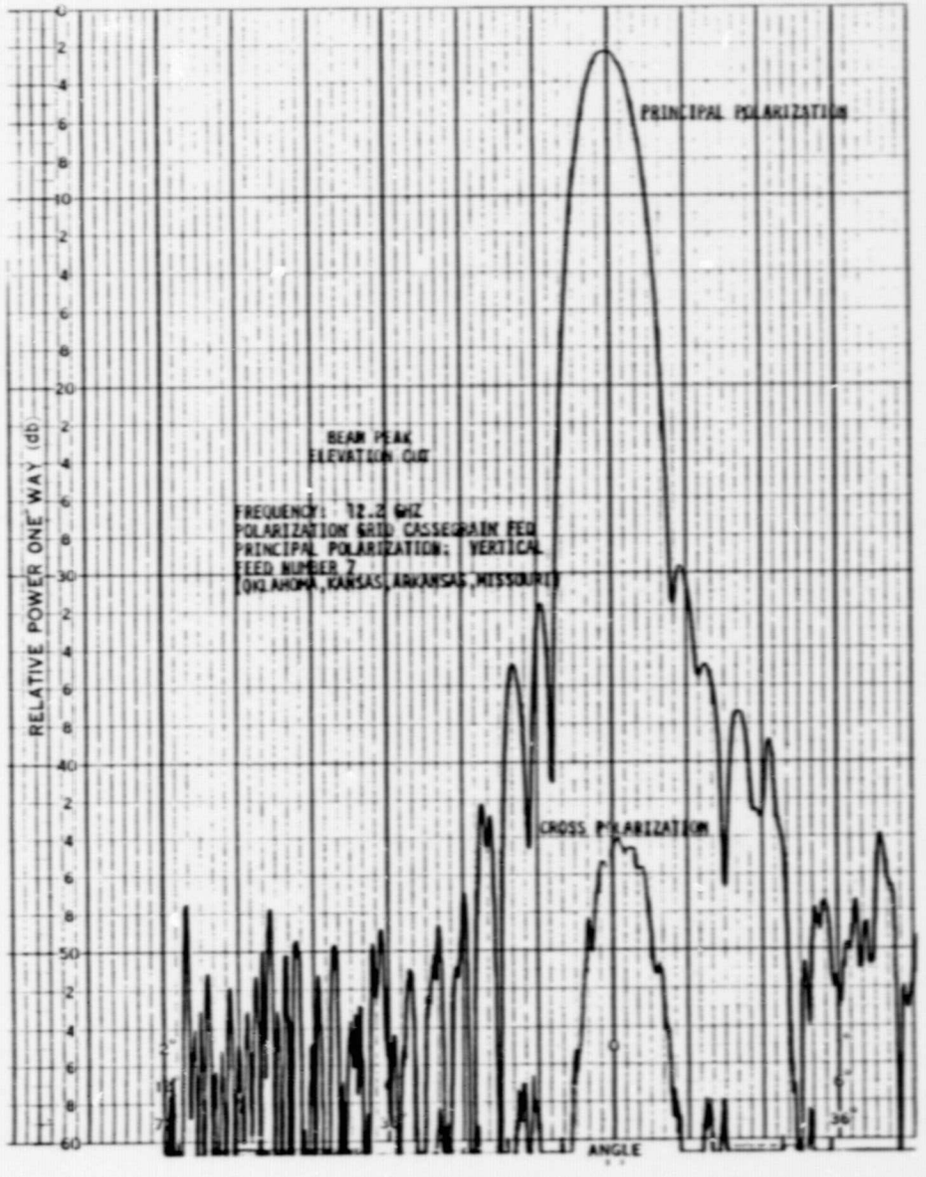
PRINCIPAL POLARIZATION
CROSS POLARIZATION
BEAM PEAK
ELEVATION CUT
FREQUENCY: 12.2 GHZ
POLARIZATION GRID CASSEGRAIN FED
PRINCIPAL POLARIZATION: VERTICAL
FEED NUMBER 7
(OKLAHOMA, KANSAS, ARKANSAS, MISSOURI)
RELATIVE POWER ONE WAY (db)
ANGLE

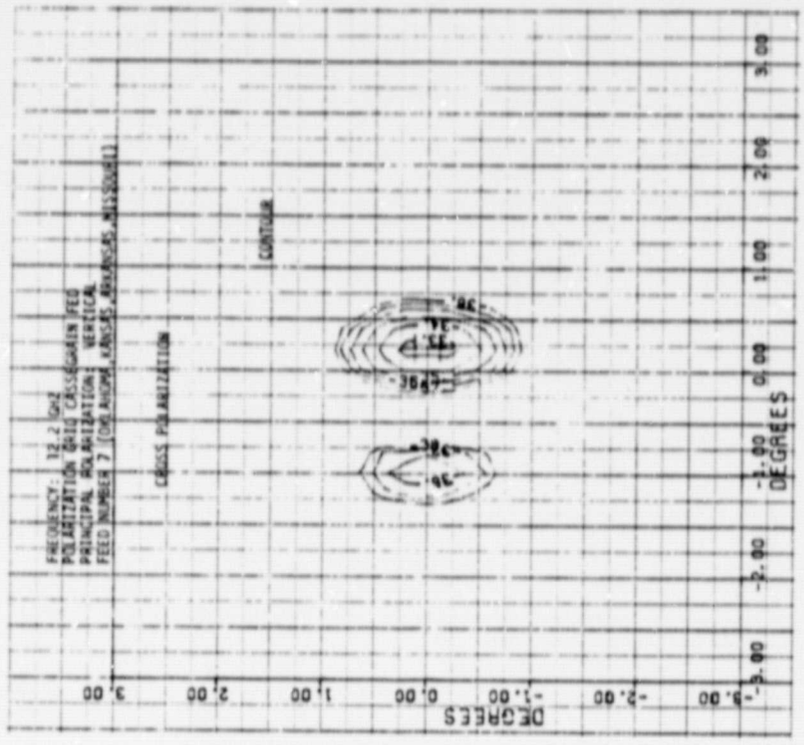
FREQUENCY: 12.2 GHz
POLARIZATION GRID CASSEGRAIN FED
PRINCIPAL POLARIZATION: VERTICAL
FEED NUMBER 7 (OKLAHOMA,KANSAS,ARKANSAS,MISSOURI)
CROSS POLARIZATION
CONTOUR
-35.
-36.
-38.
DEGREES
DEGREES
3.00
2.00
1.00
0.00
-1.00
-2.00
-3.00

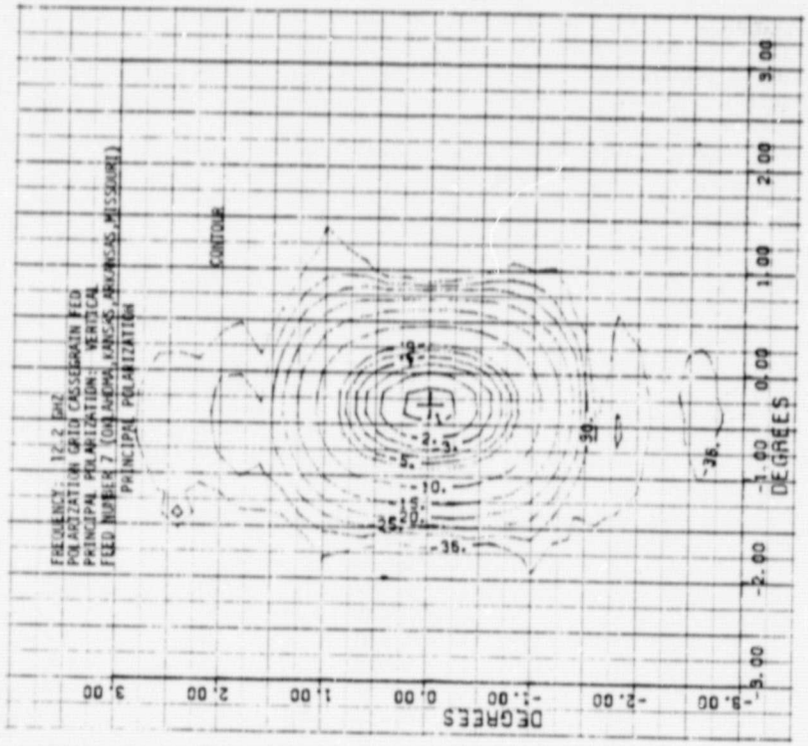
FREQUENCY: 12.2 GHz
POLARIZATION GRID CASSEGRAIN FED
PRINCIPAL POLARIZATION: VERTICAL
FEED NUMBER 7 (OKLAHOMA,KANSAS,ARKANSAS,MISSOURI)
PRINCIPAL POLARIZATION
CONTOUR
-2.
-3.
-5.
-10.
-20.
-35.
-36.
-39.
DEGREES
DEGREES
3.00
2.00
1.00
0.00
-1.00
-2.00
-3.00

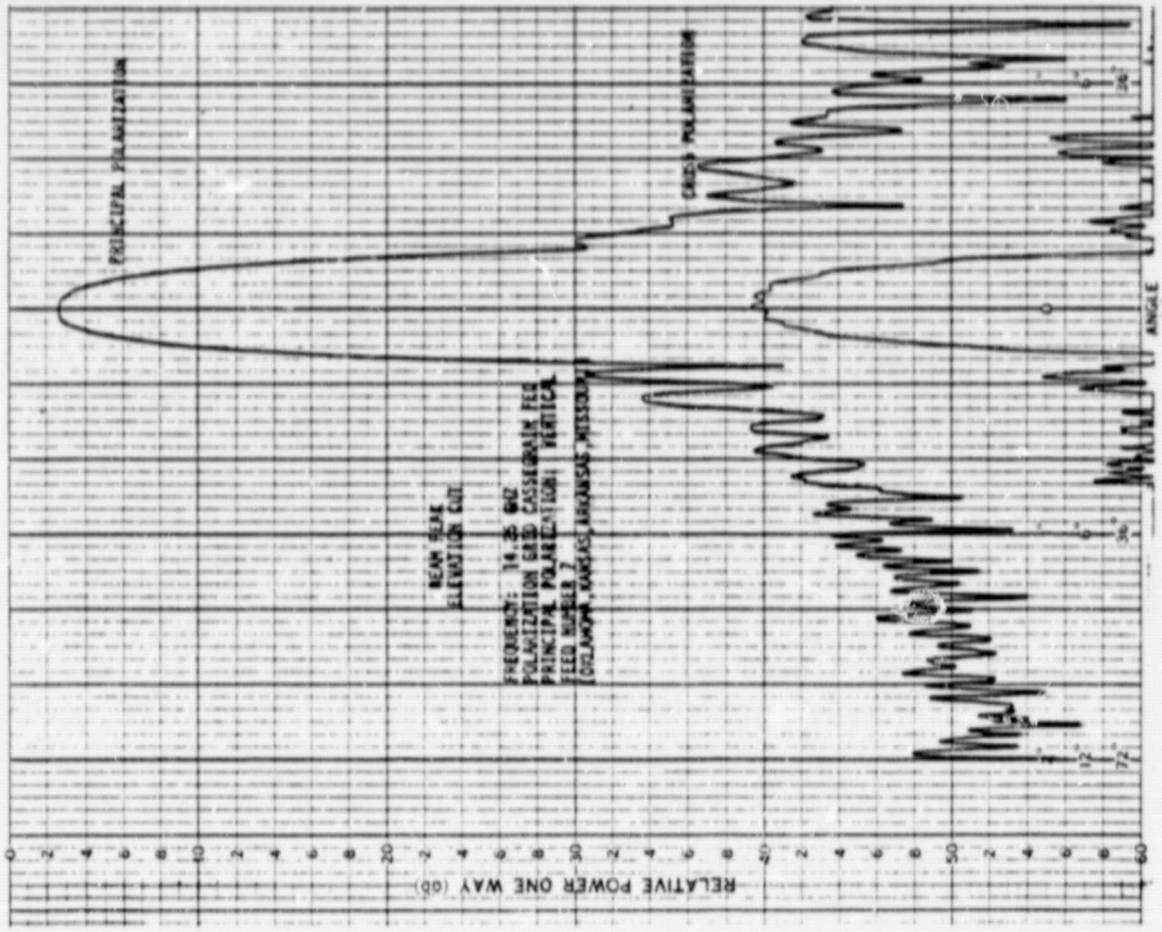
PRINCIPAL POLARIZATION
CROSS POLARIZATION
BEAM PEAK
ELEVATION CUT
FREQUENCY: 14.25 GHZ
POLARIZATION GRID CASSEGRAIN FED
PRINCIPAL POLARIZATION: VERTICAL
FEED NUMBER 7
(OKLAHOMA, KANSAS, ARKANSAS, MISSOURI)
RELATIVE POWER ONE WAY (dB)
ANGLE

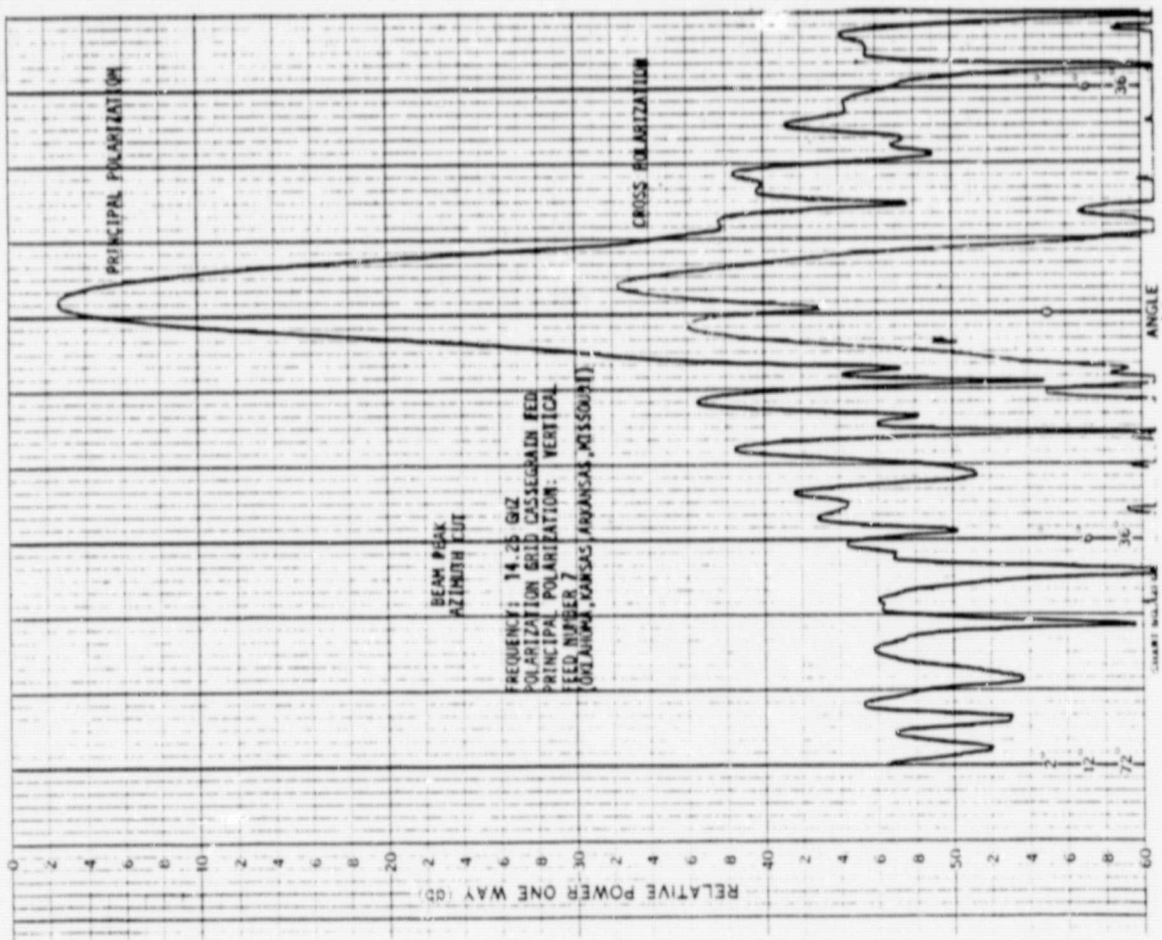
PRINCIPAL POLARIZATION
CROSS POLARIZATION
BEAM PEAK
AZIMUTH CUT
FREQUENCY: 14.25 GHZ
POLARIZATION GRID CASSEGRAIN FED
PRINCIPAL POLARIZATION: VERTICAL
FEED NUMBER 7
(OKLAHOMA, KANSAS, ARKANSAS, MISSOURI)
RELATIVE POWER ONE WAY (dB)
ANGLE

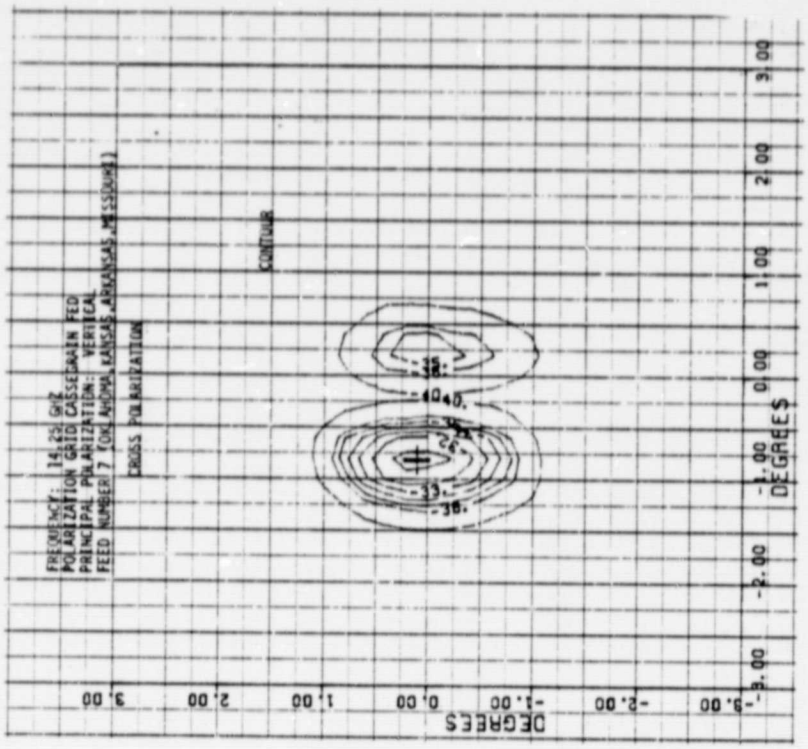
FREQUENCY: 14.25 GHz
POLARIZATION GRID CASSEGRAIN FED
PRINCIPAL POLARIZATION: VERTICAL
FEED NUMBER 7 (OKLAHOMA,KANSAS,ARKANSAS,MISSOURI)
CROSS POLARIZATION
CONTOUR
-35.
-40.
-45.
-25.
-30.
-35.
DEGREES
DEGREES
3.00
2.00
1.00
0.00
-1.00
-2.00
-3.00

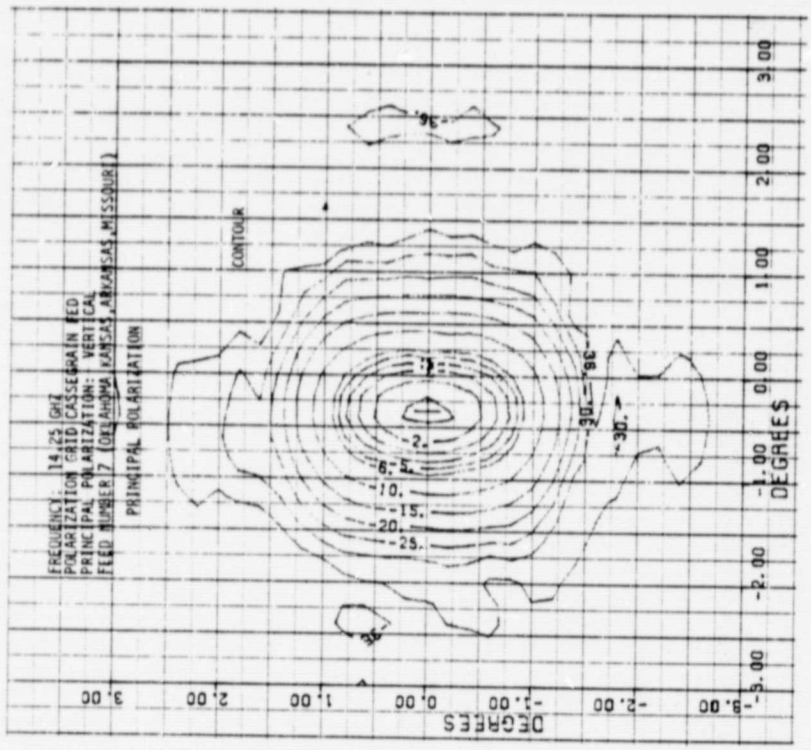
FREQUENCY: 14.25 GHz
POLARIZATION GRID CASSEGRAIN FED
PRINCIPAL POLARIZATION: VERTICAL
FEED NUMBER 7 (OKLAHOMA,KANSAS,ARKANSAS,MISSOURI)
PRINCIPAL POLARIZATION
CONTOUR
-35.
-30.
-2.
-6.
-10.
-15.
-20.
-25.
-30.
-35.
DEGREES
DEGREES
3.00
2.00
1.00
0.00
-1.00
-2.00
-3.00

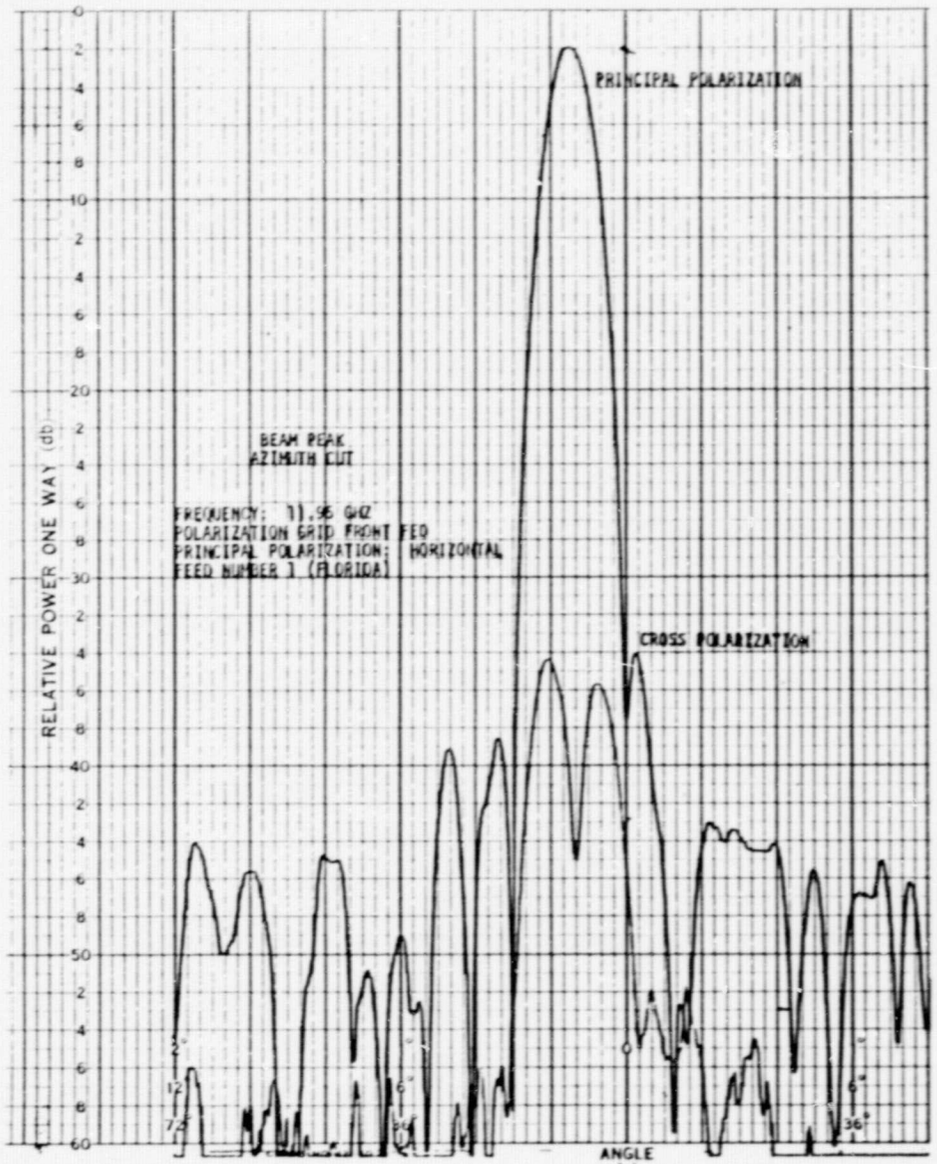
PRINCIPAL POLARIZATION
BEAM PEAK
AZIMUTH CUT
FREQUENCY: 11.96 GHZ
POLARIZATION GRID FRONT FED
PRINCIPAL POLARIZATION: HORIZONTAL
FEED NUMBER 1 (FLORIDA)
CROSS POLARIZATION
RELATIVE POWER ONE WAY (db)
ANGLE

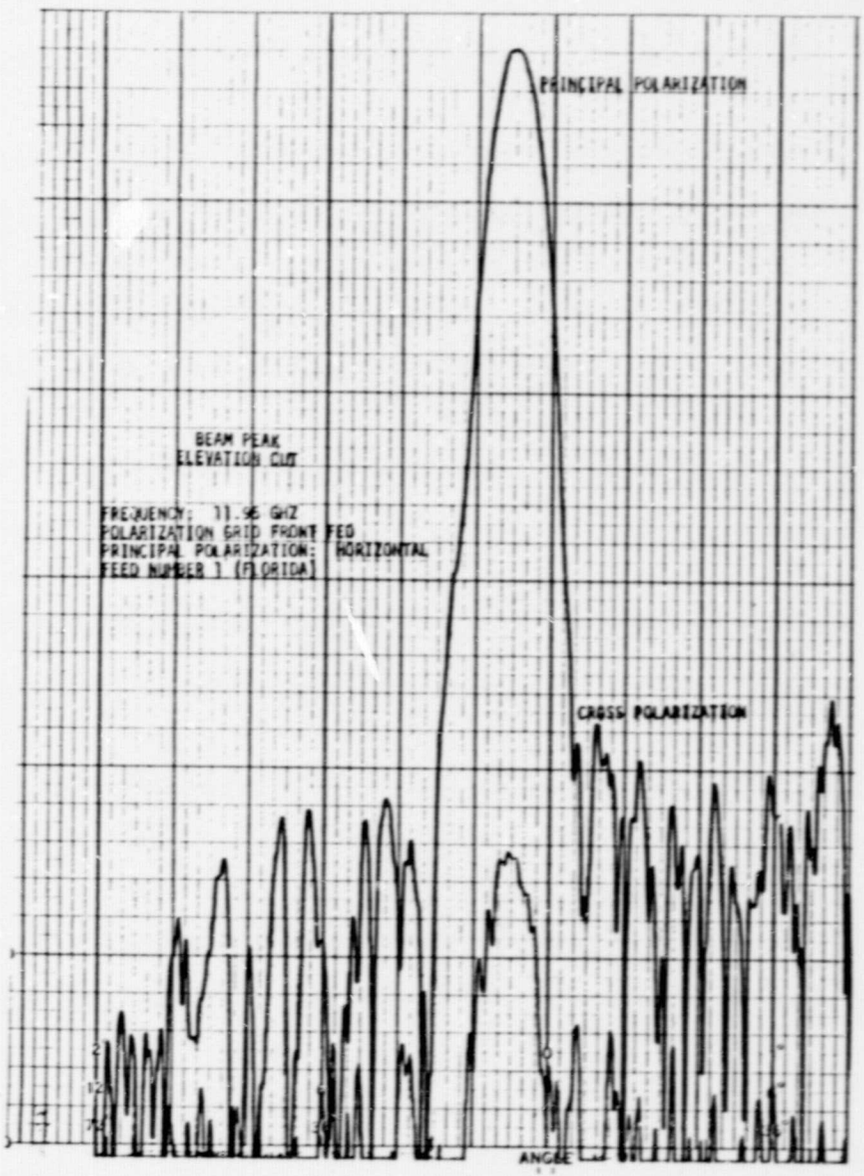
PRINCIPAL POLARIZATION
BEAM PEAK
ELEVATION CUT
FREQUENCY: 11.96 GHZ
POLARIZATION GRID FRONT FED
PRINCIPAL POLARIZATION: HORIZONTAL
FEED NUMBER 1 (FLORIDA)
CROSS POLARIZATION
ANGLE

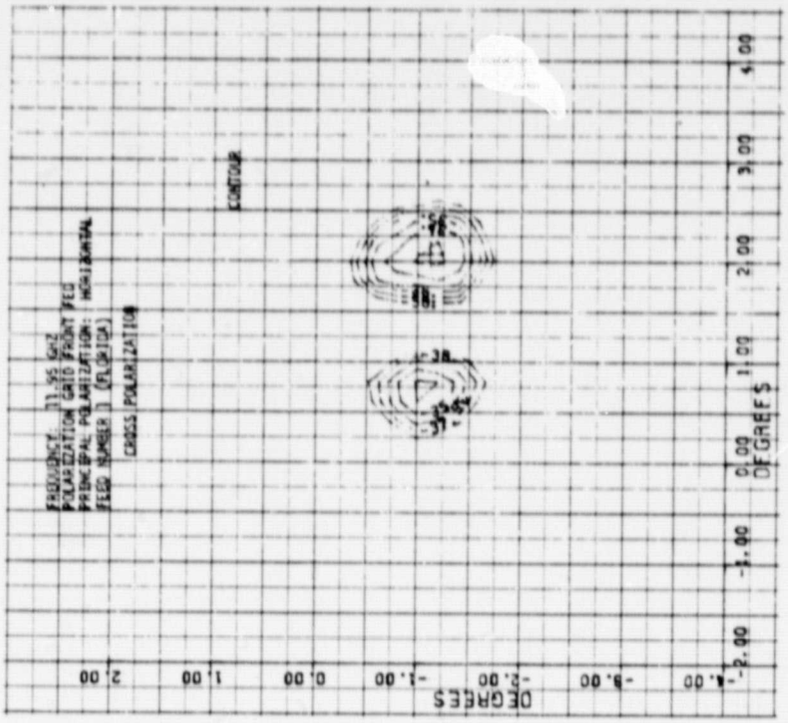

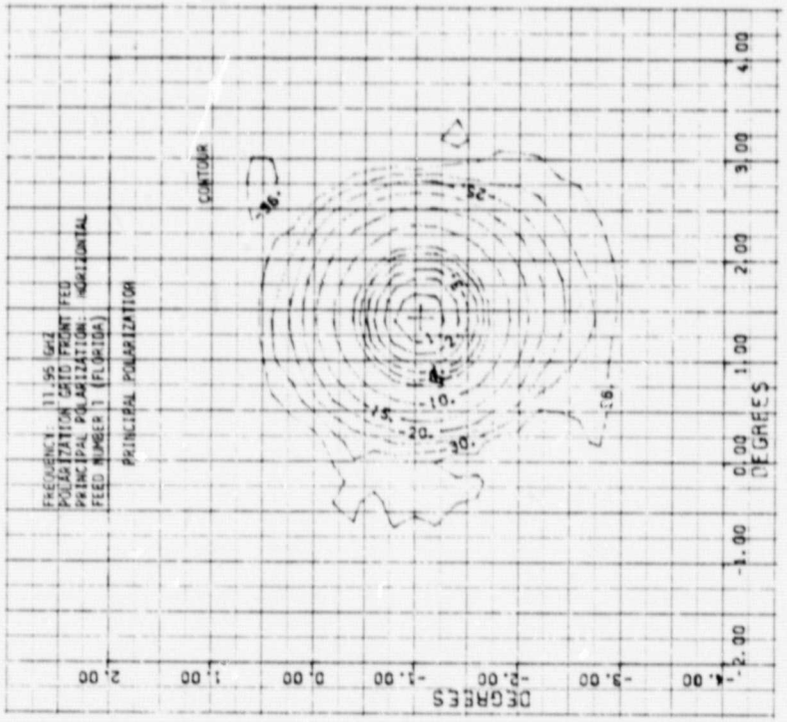

APPENDIX C
SWEPT FREQUENCY BEAM ISOLATION MEASUREMENTS

Swept frequency beam isolation measurements were made for the following cases:

1) Point A

   a) Summation of the signals received from two adjacent feeds energized in a row

   b) Summation of all signals from co-polarized beams operated at the same frequency

2) Point B

   a) Single adjacent feed energized

   b) All feeds energized

3) Point C

   a) Two adjacent feeds energized

   b) All feeds energized.

Both principal polarization and cross-polarization coupling components were derived from the above procedure.

The Alaska configuration was replaced by the Hawaii feed geometry. Assembly and alignment, as mentioned above, was identical to the Alaska configuration procedure. Antenna boresighting and electrical alignment were as previously discussed. Swept frequency techniques were again used to provide complete isolation data. Point D (the peak of the nestled beam in the Hawaii group) was added. Locations of the remaining representative points were chosen to coincide with the interlaced points of the Alaska beams. The swept frequency beam isolation measurement was again made of the following cases:

1) Point D received power

   a) Adjacent feed energized

   b) All feeds energized

2) Point B received power

   a) Single adjacent feed energized

   b) All feeds energized

3) Point C received power

   a) Two adjacent feeds energized

   b) All feeds energized.

As before, both principal polarization and cross-polarization were measured. Results of these measurements are presented in the following graphs. Differences in insertion losses of the switching circuits associated with each feed, introduced a 2 dB power amplitude uncertainty into the data recording.

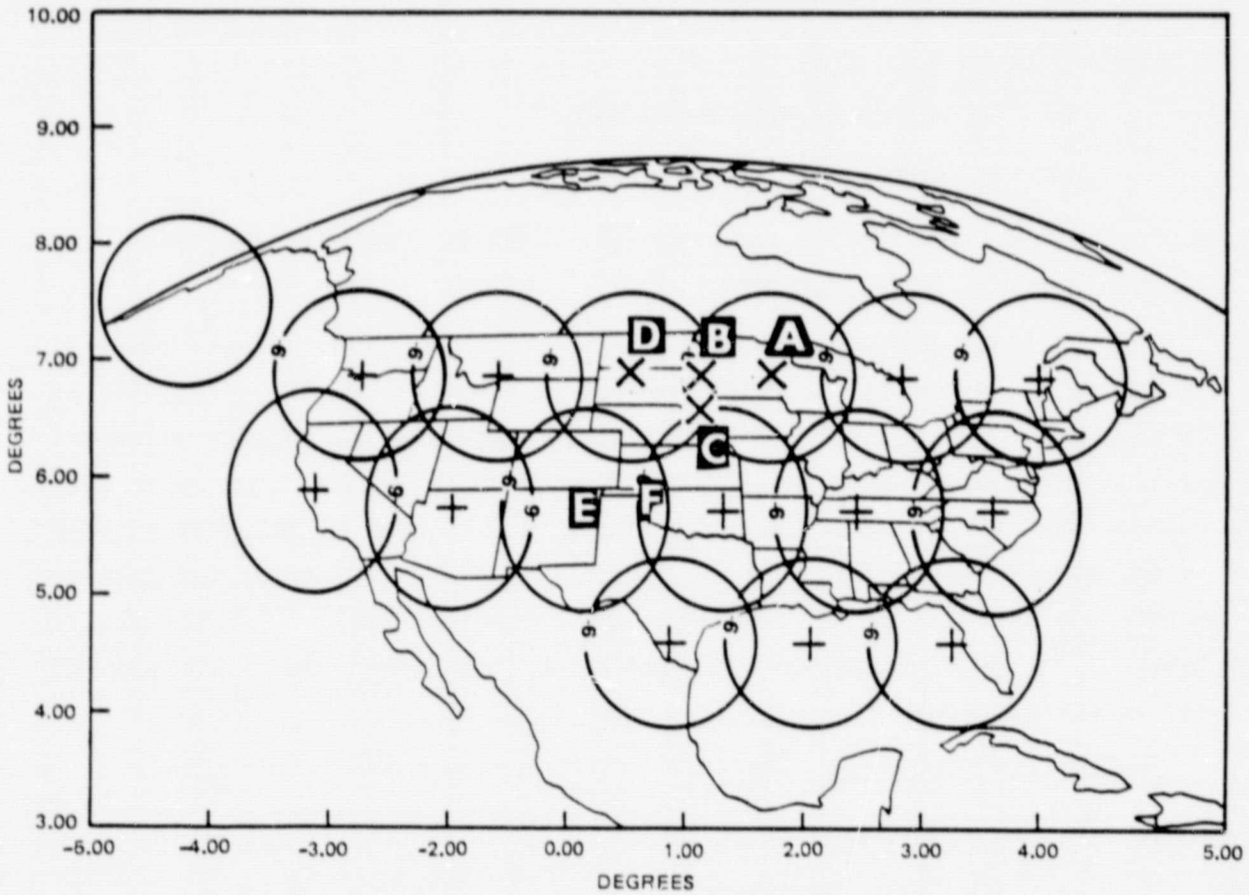

Source Antenna Pointing Locations

SPOT BEAM MEASURED DATA

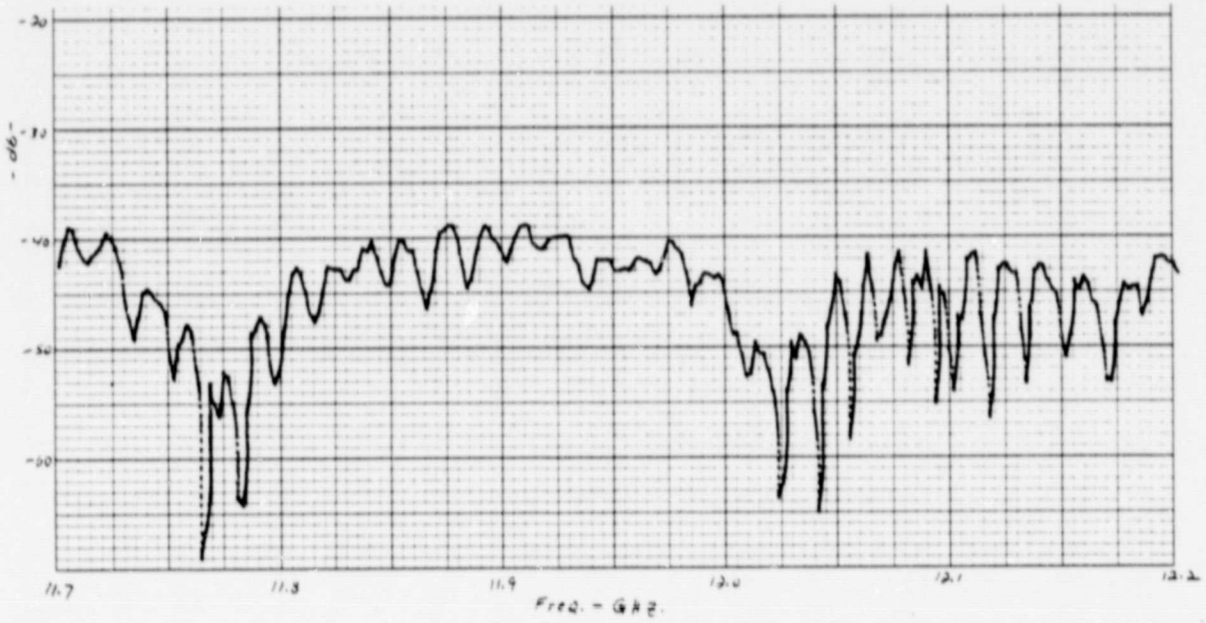

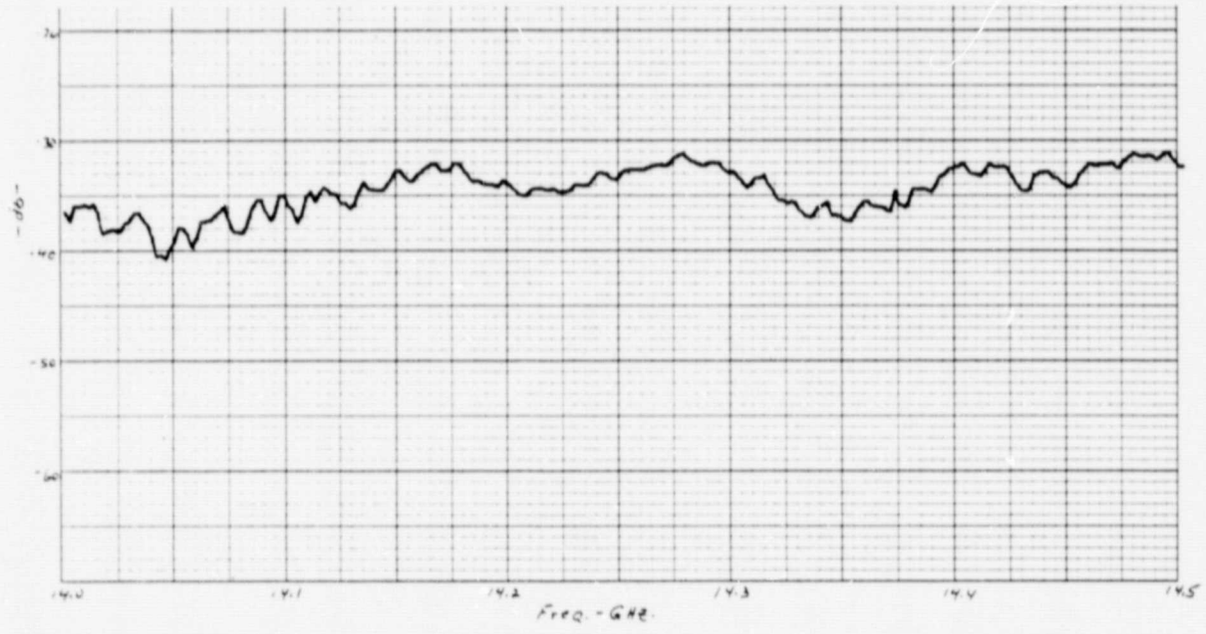

Isolation of Feed 12 With the Source Antenna Pointed to Peak of Beam 12 (Point D) and Feed 11 Energized

SPOT BEAM MEASURED DATA

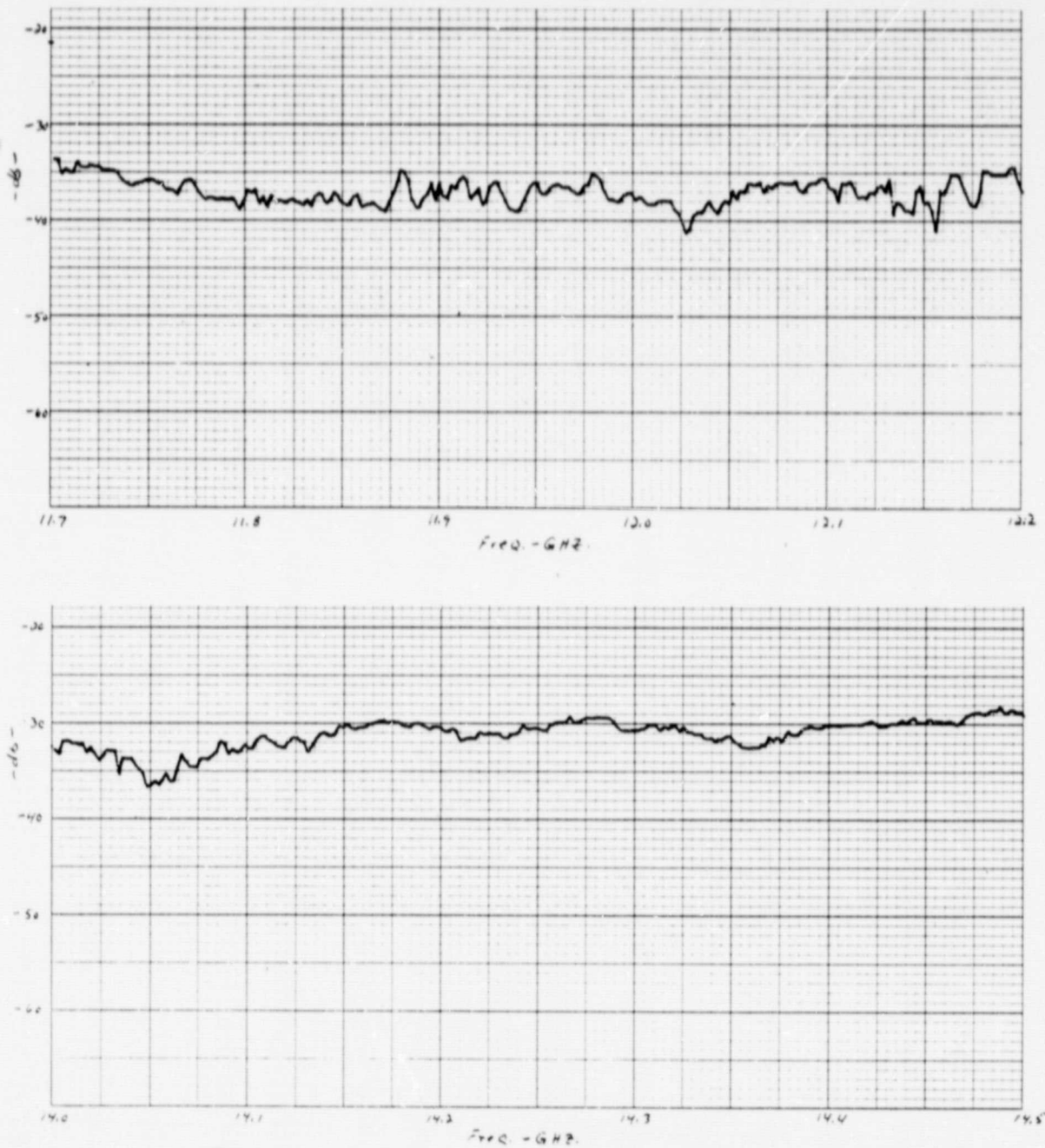

Isolation of Feed 12 With the Source Antenna Pointed to Peak of Beam 12 (Point D) and Feeds 10, 11, 13, 17 Energized

SPOT BEAM MEASURED DATA

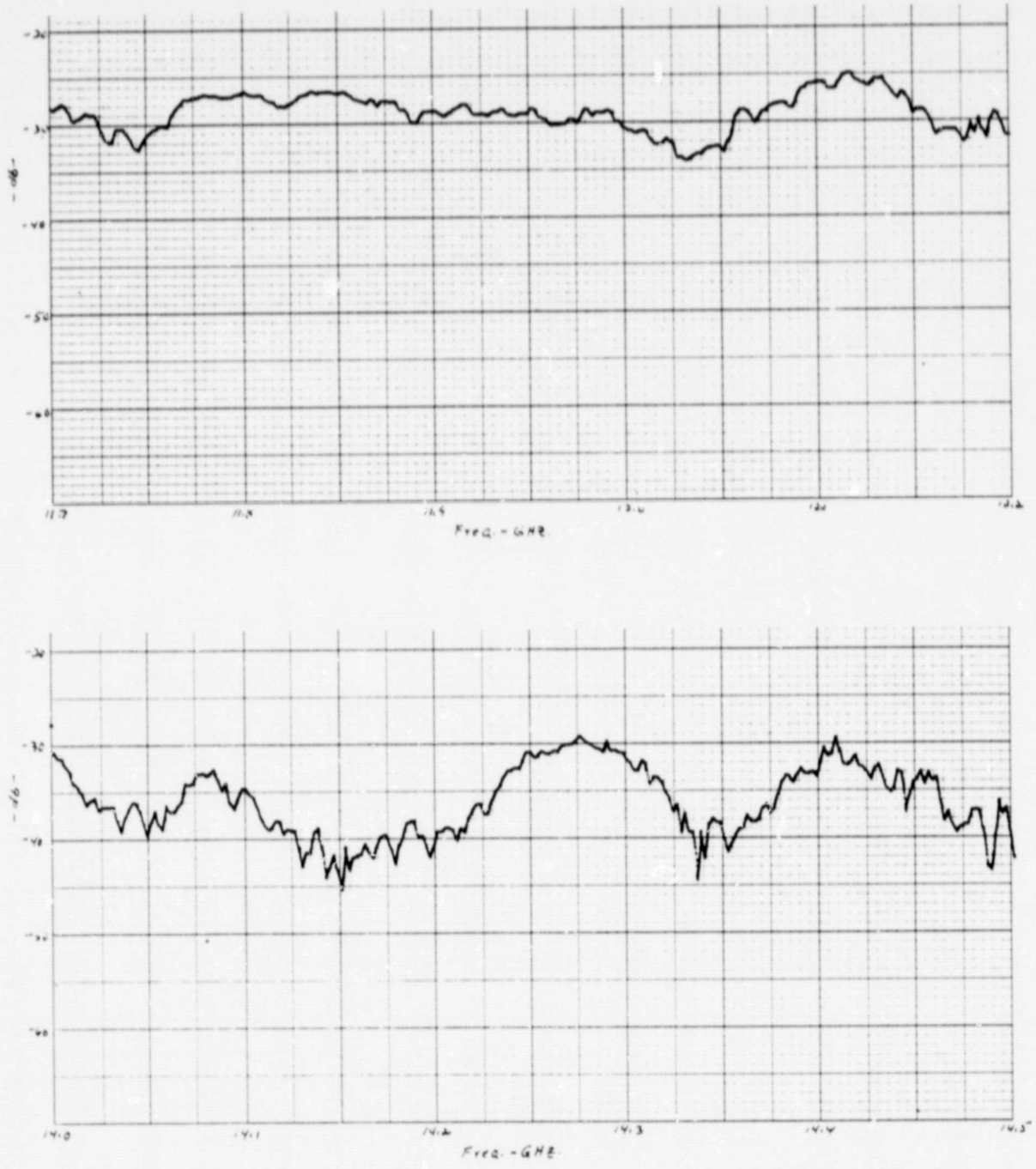

Isolation of Feed 12 With Source Antenna Pointed to the Doublet Beam Center Location Between Feed 11 and 12 (Point B) and Feeds 10, 11, 13, 17 Energized

SPOT BEAM MEASURED DATA

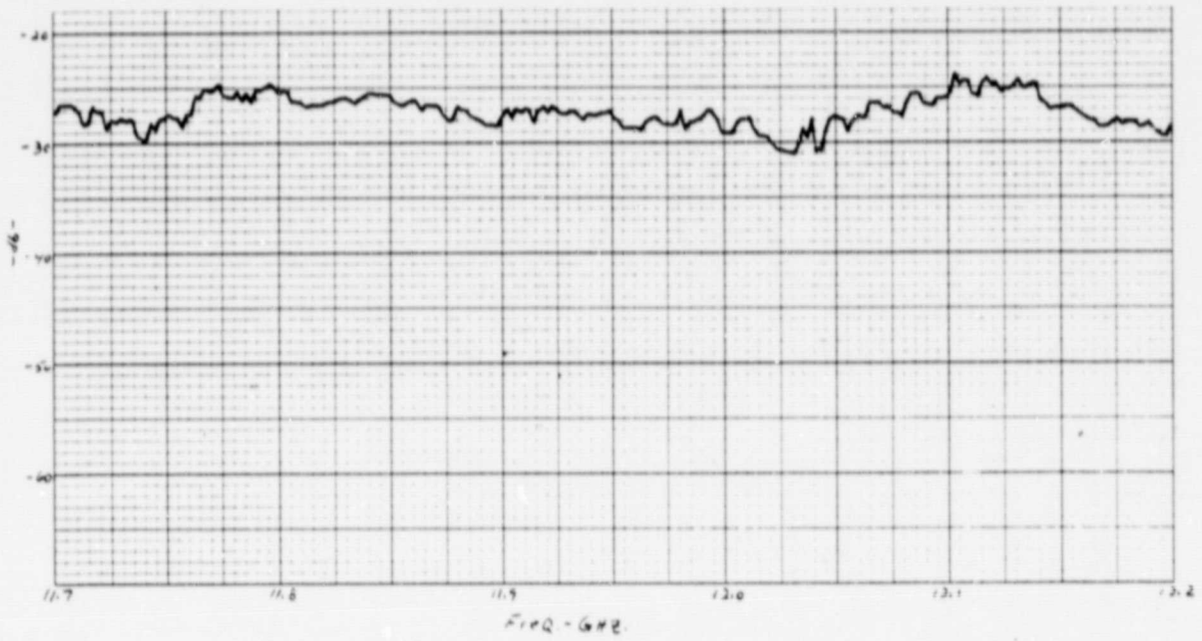

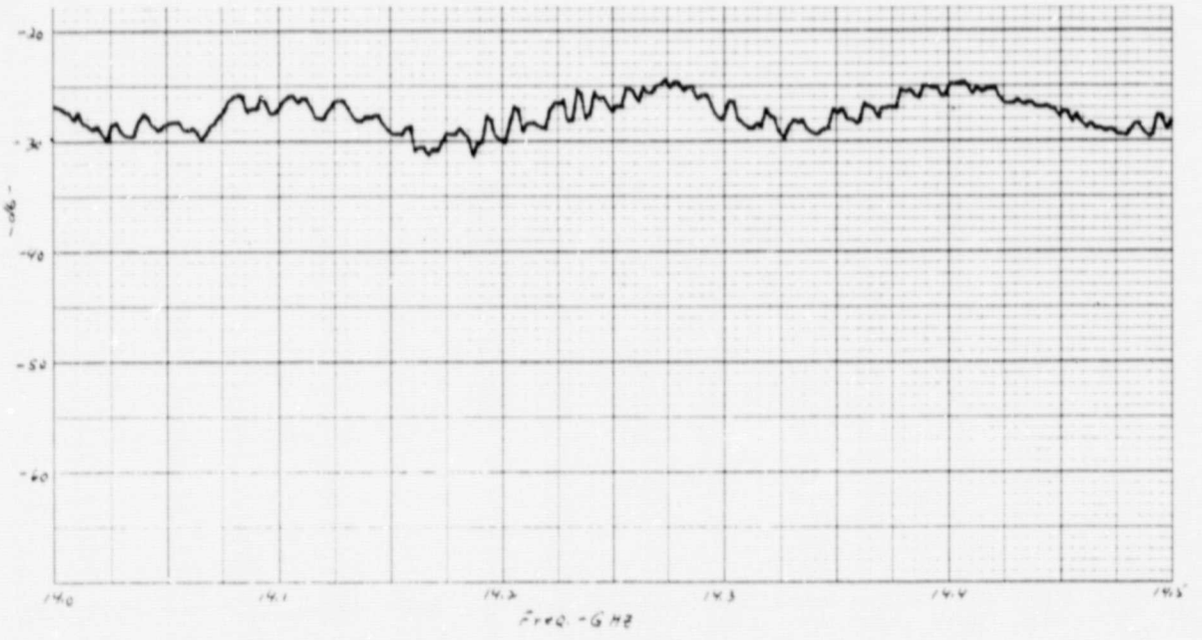

Isolation of Feed 12 With Source Antenna Pointed to the Doublet Beam Center Location Between Feed 11 and 12 (Point B) and Feeds 10, 11, 13, 17 Energized

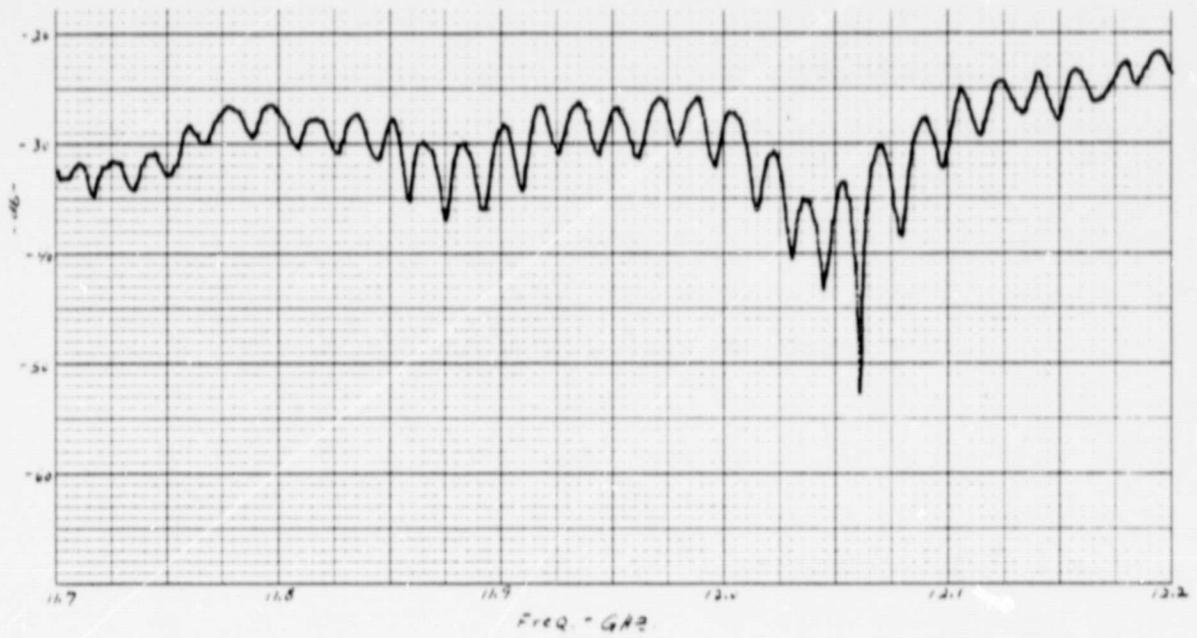

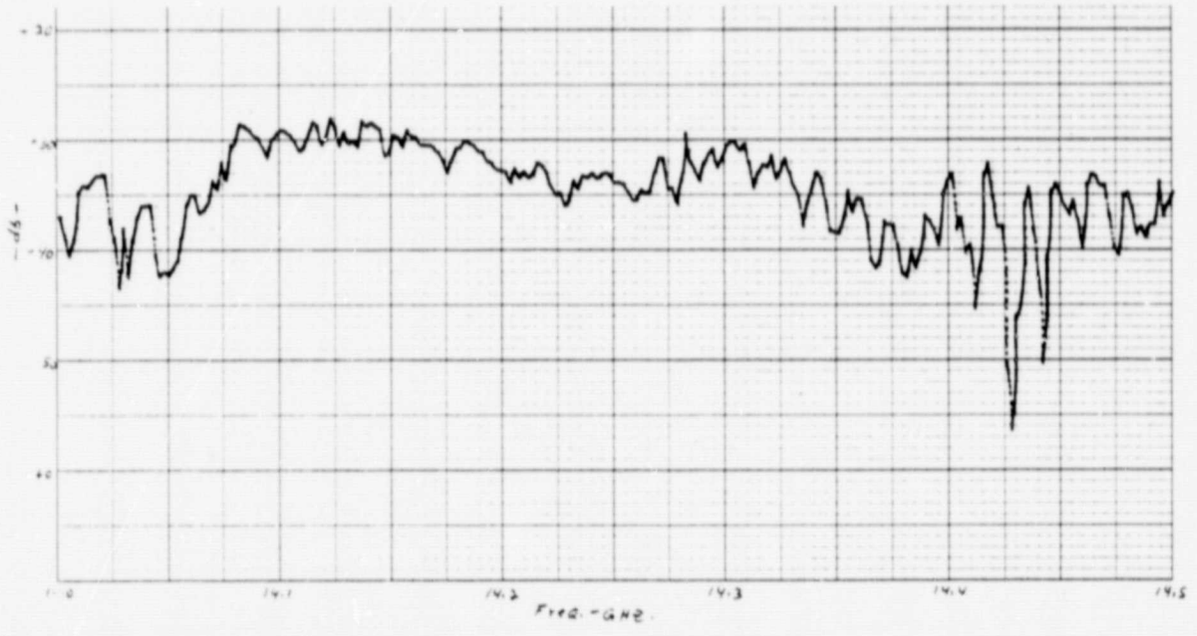

Isolation of Feed 12 With Source Antenna Pointed to the Triplet Beam Center Location Between Feeds 10, 11, 12 (Point C) and Feed 10 and 11 Energized

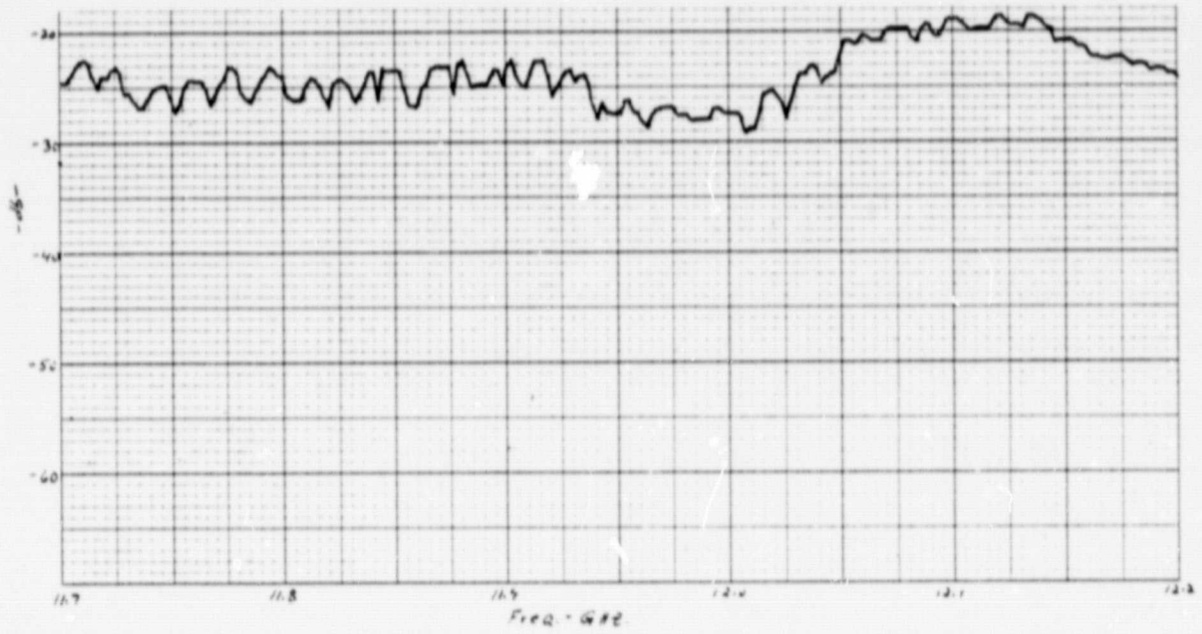

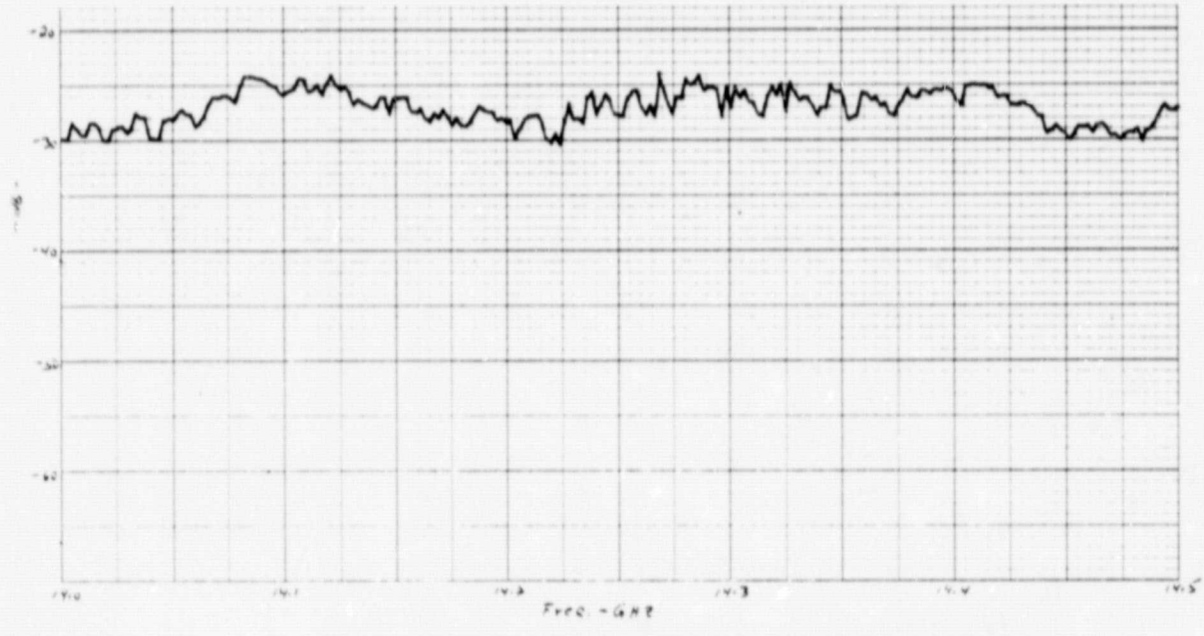

Isolation of Feed 12 With Source Antenna Pointed to the Triplet Beam Center Location Between Feeds 10, 11, 12 (Point C) and Feeds 10, 11, 13, 17 Energized

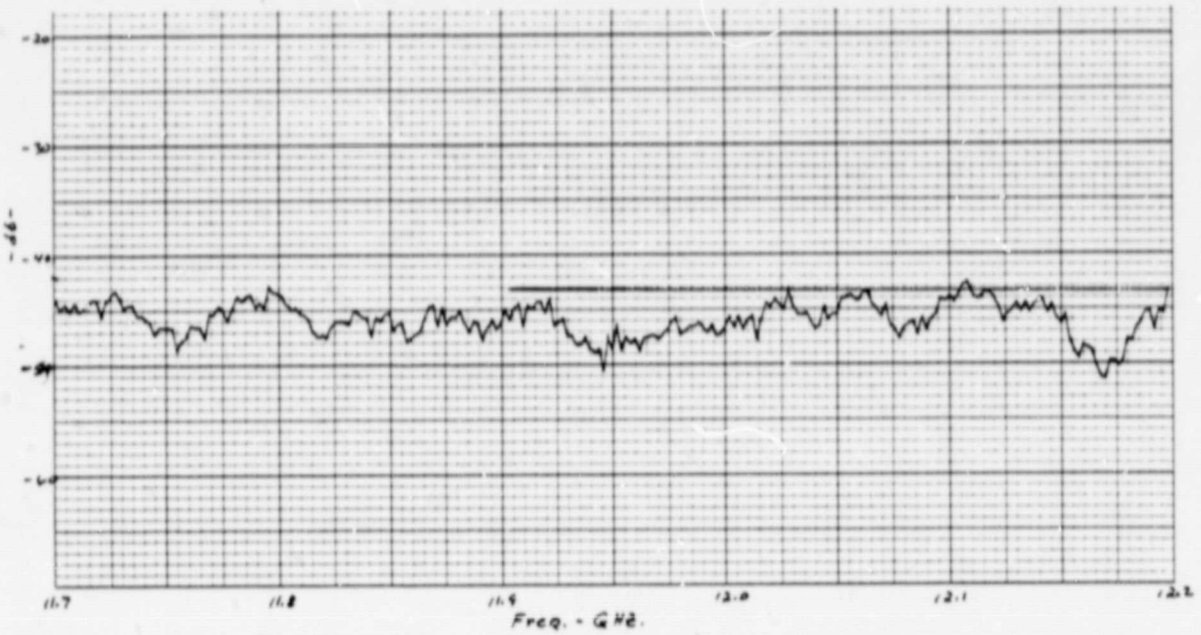

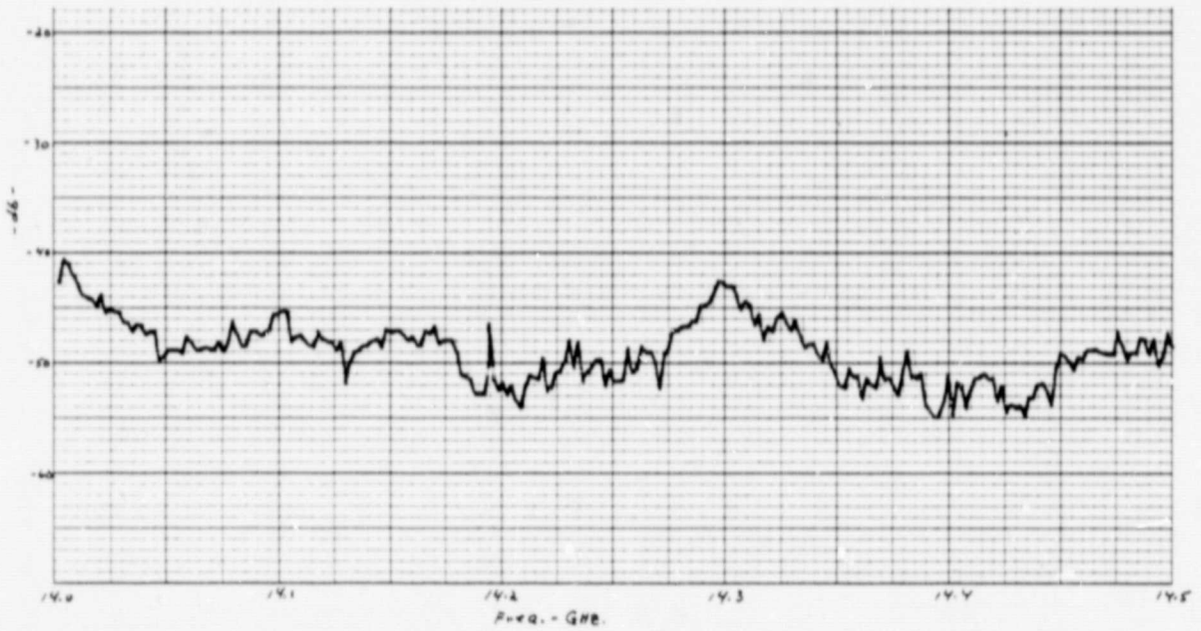

Isolation of Feed 4 With the Source Antenna Cross Polarized
to Feed 4 and Pointed to its Peak (Point A)
With Feeds 1, 2, 3, 5 Energized

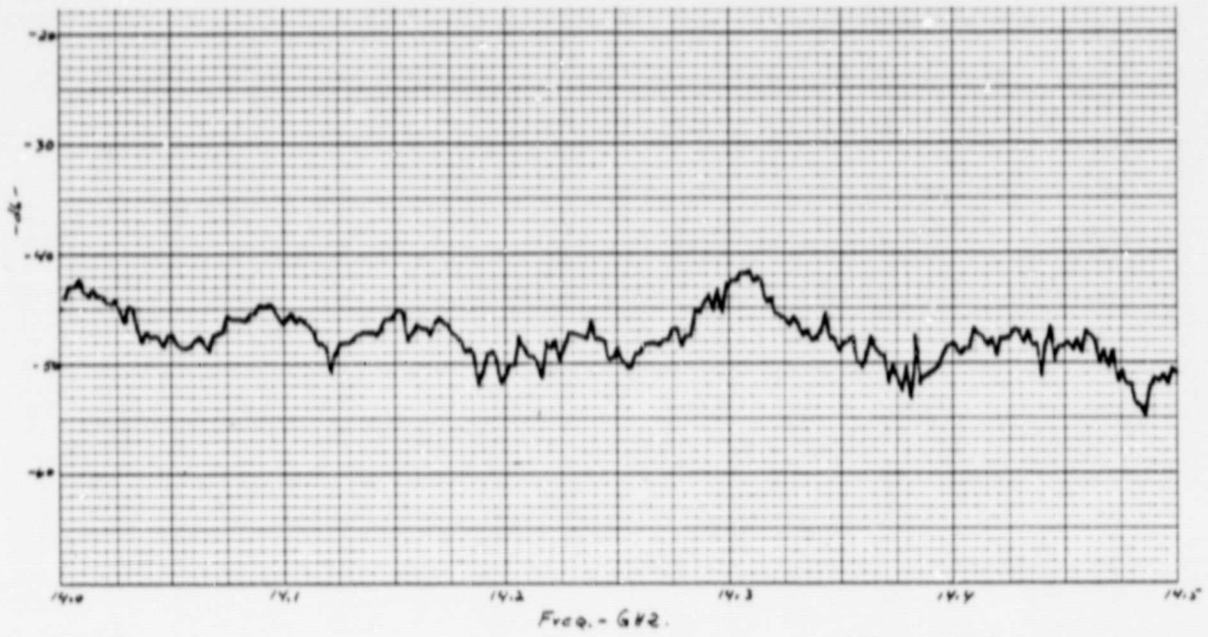

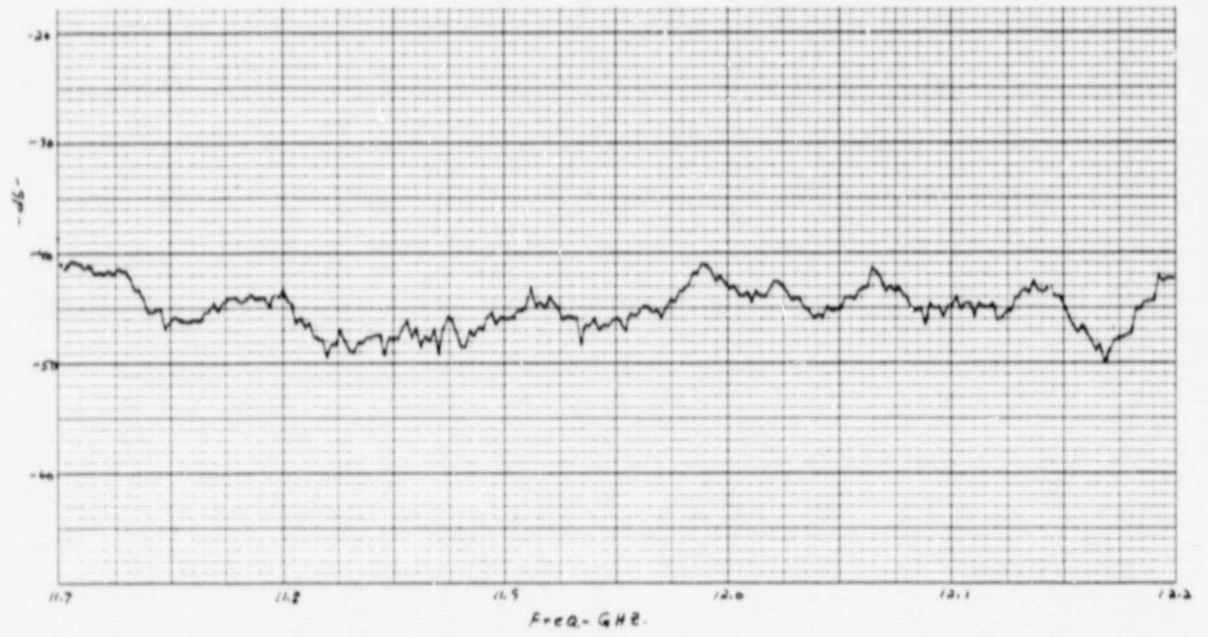

Isolation of Feed 4 With the Source Antenna Cross Polarized to Feed 4 and Pointed to the Doublet Beam Center Location Between Feeds 4 and 5 (Point B) With Feeds 1, 2, 3, 5 Energized

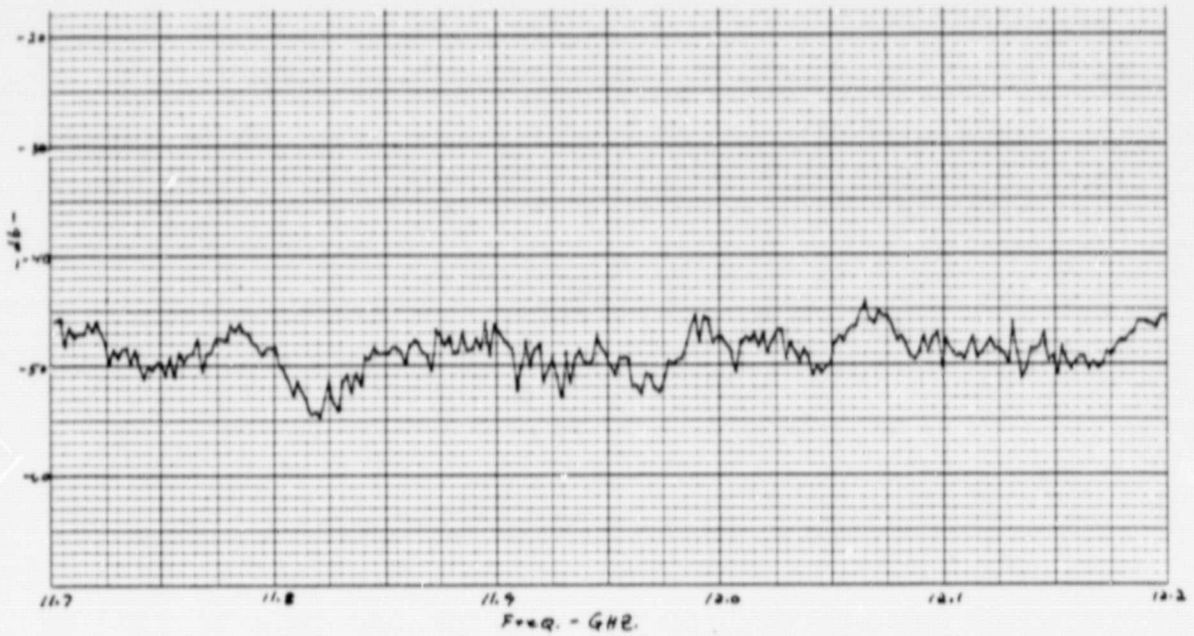

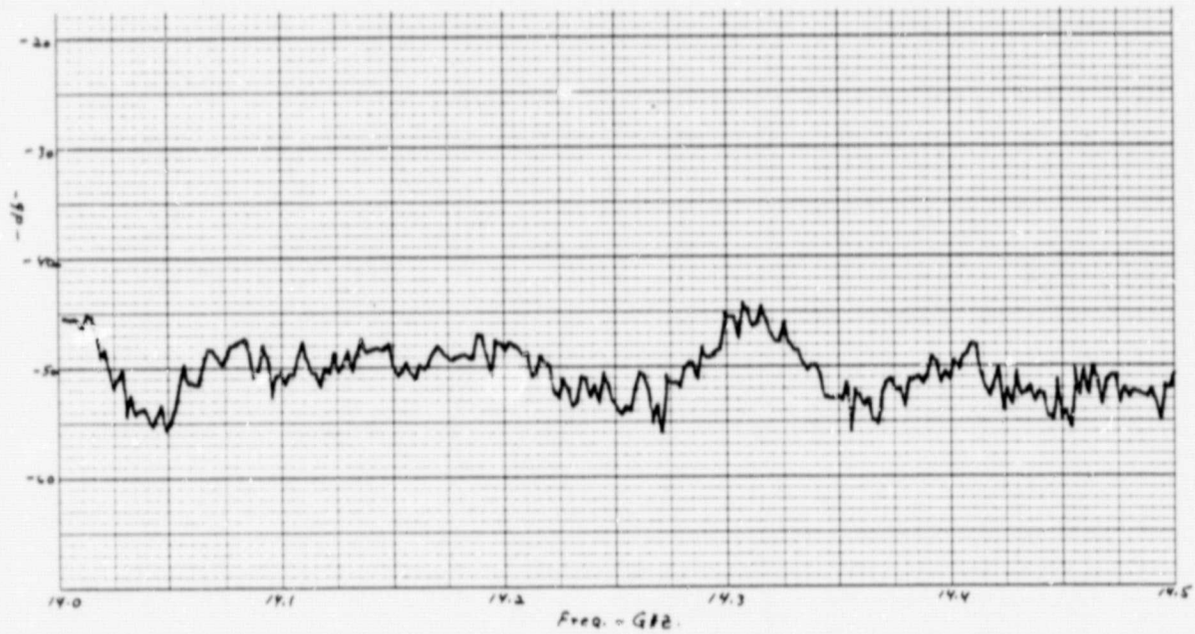

Isolation of Feed 4 With the Source Antenna Cross Polarized to Feed 4 and Pointed to the Triplet Beam Center Location Between Feeds 2, 4, and 5 (Point C) With Feeds 1, 2, 3, 5 Energized

SPOT BEAM MEASURED DATA

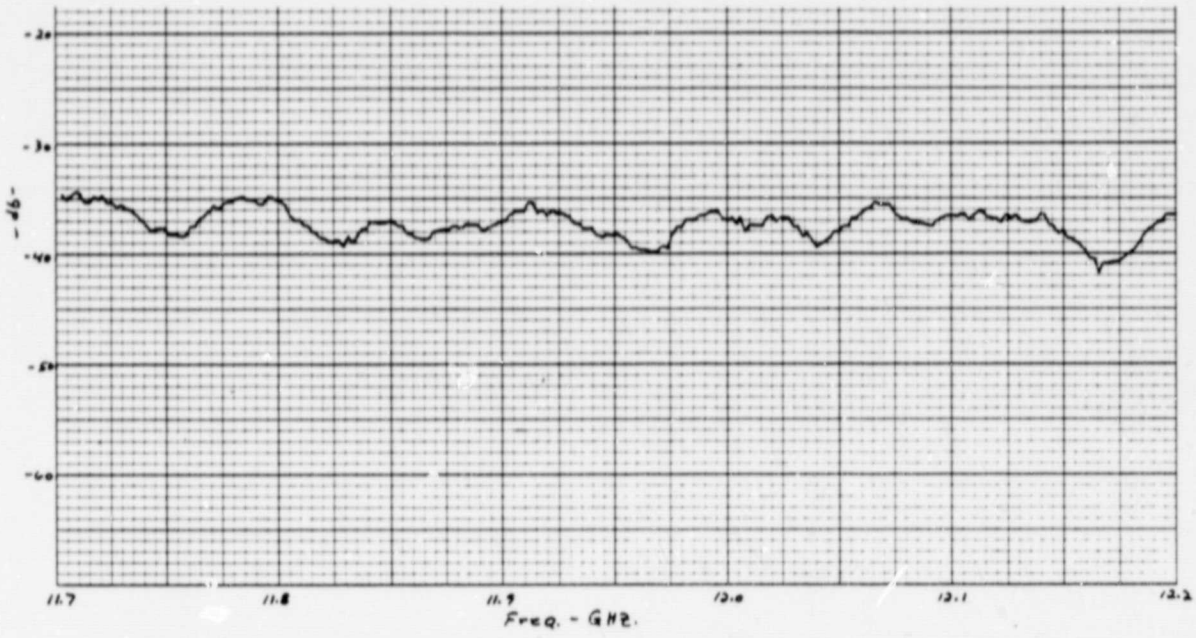

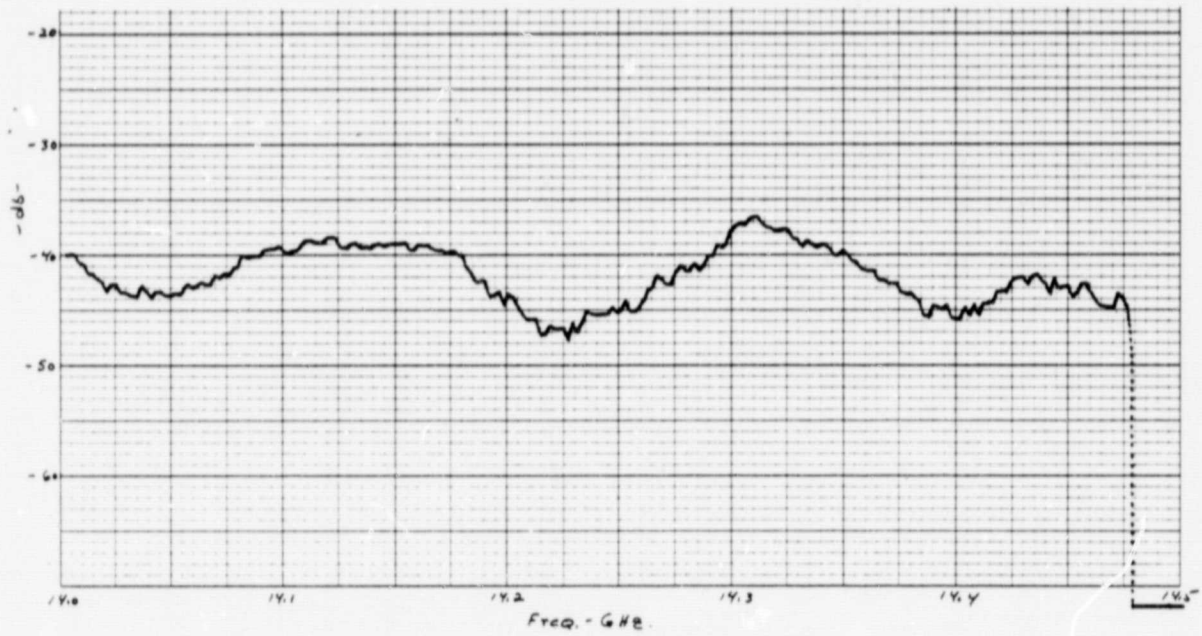

Isolation of Feed 4 With the Source Antenna Cross Polarized to Feed 4 and Pointed to the A Location 1.10 in Azimuth From Feed 4 Toward Feed 5 (Point D). Feeds 1, 2, 3, 5 Were Energized

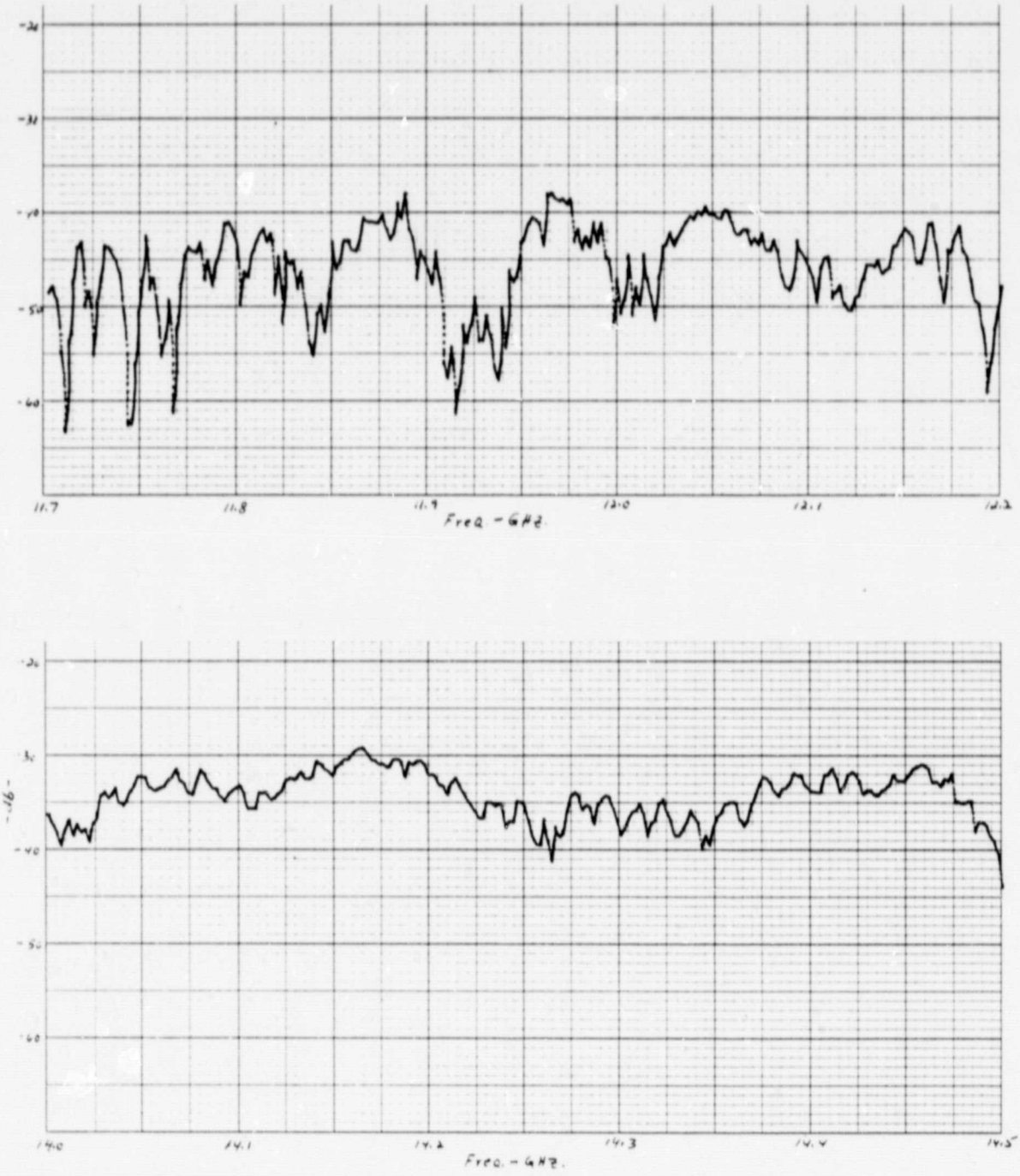

Isolation of Feed 15 With the Source Antenna Pointed to the Peak of Beam 15 (Point E) and Feed 14 Energized

ELLIPTICAL BEAM MEASURED DATA

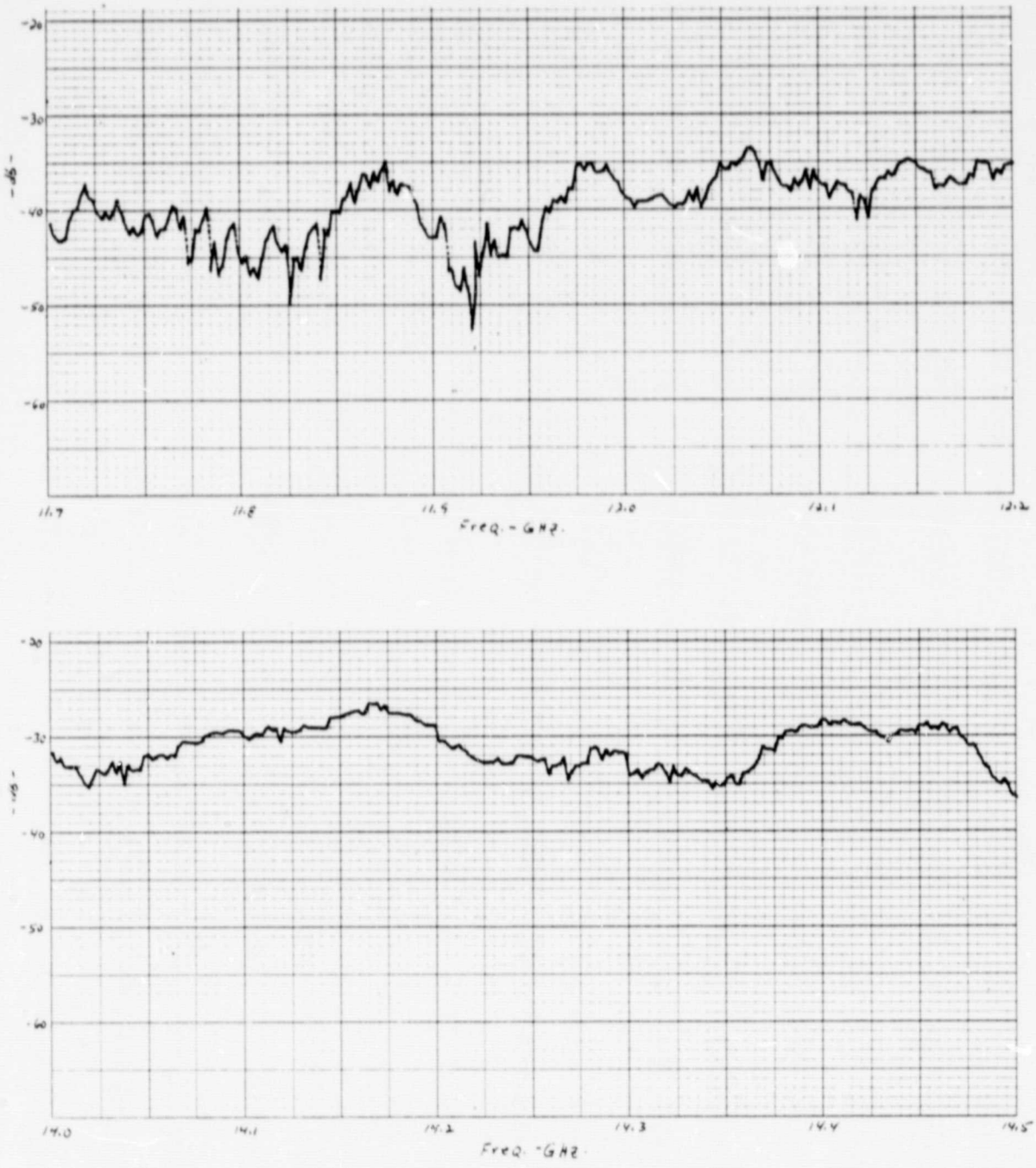

Isolation of Feed 15 With the Source Antenna Pointed to the Peak of Beam 15 (Point E) and Feeds 14, 16 Energized

ELLIPTICAL BEAM MEASURED DATA

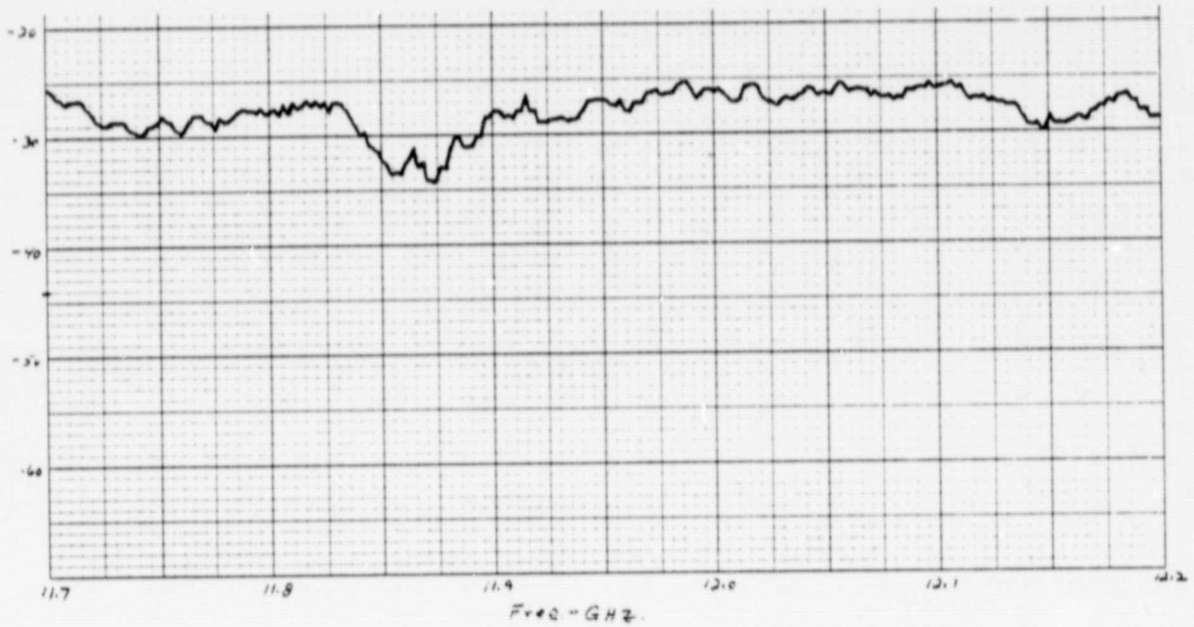

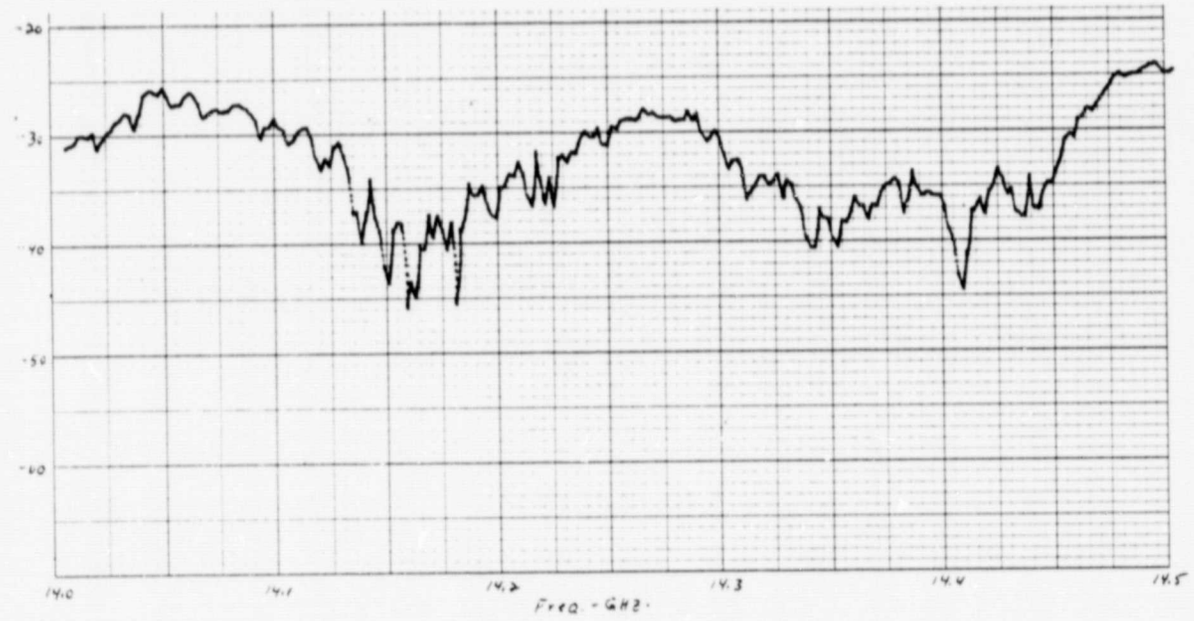

Isolation of Feed 15 With the Source Antenna Pointed to the Doublet Beam Center Location Between Feed 11 and 12 (Point F) and Feed 14 Energized

ELLIPTICAL BEAM MEASURED DATA

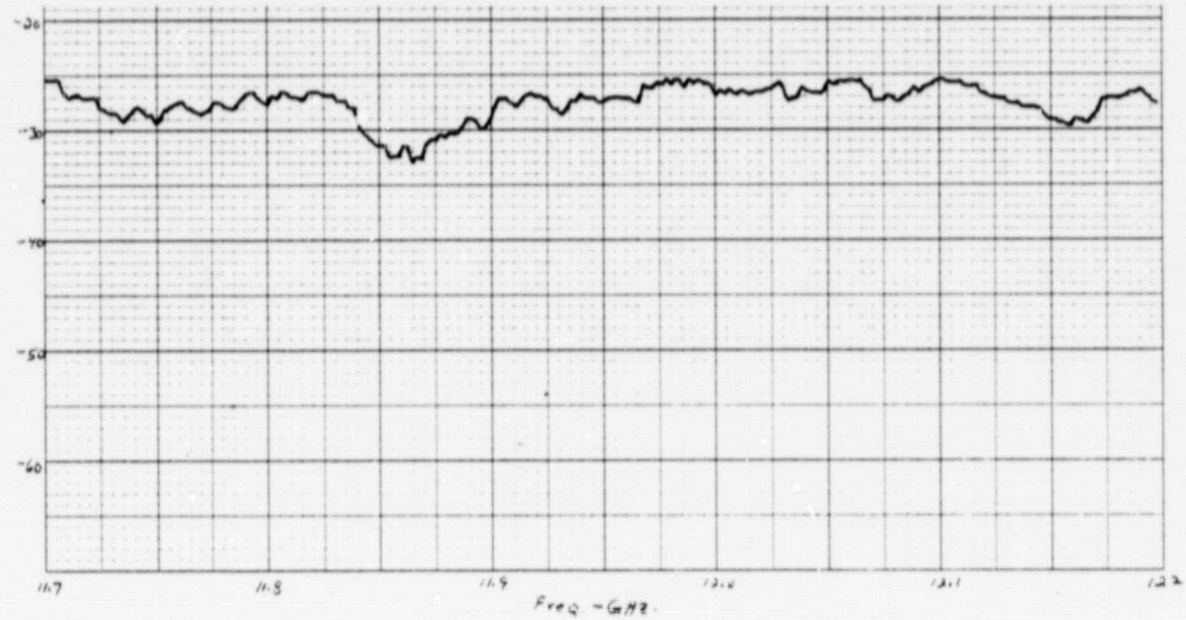

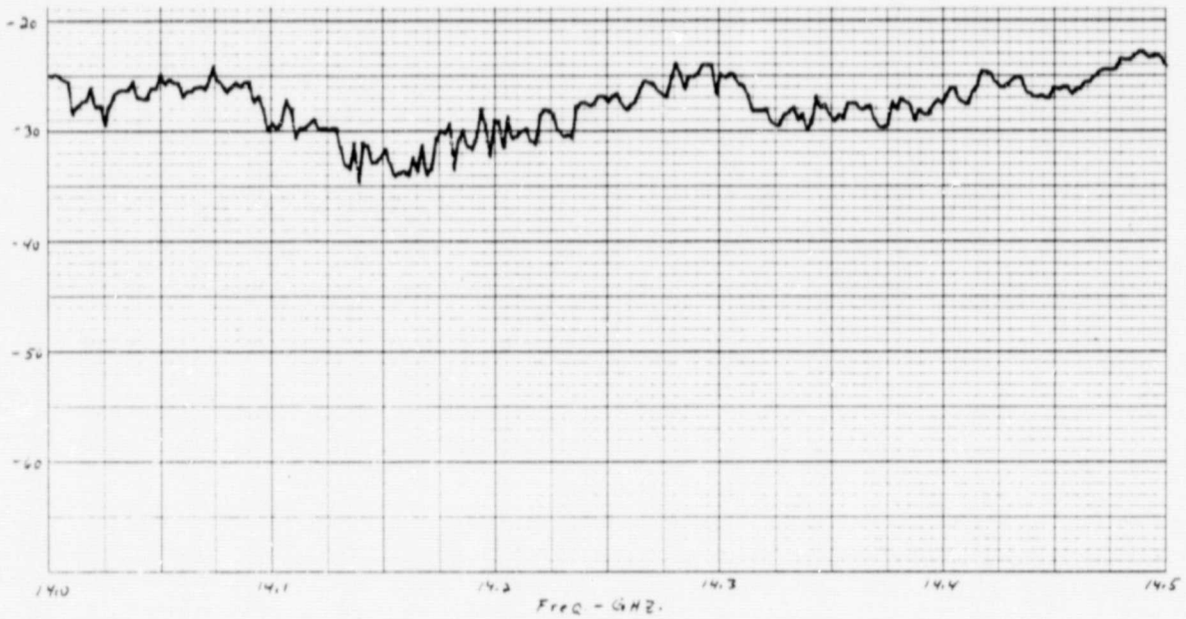

Isolation of Feed 15 With the Source Antenna Pointed to the Doublet Beam Center Location Between Feed 11 and 12 (Point F) and Feed 14, 16 Energized